



Polymérisation topochimique de macrocycles rigides : nouvelle stratégie pour l'obtention de nanotubes organiques

Thèse

Simon Rondeau-Gagné

Doctorat en Chimie
Philosophiae Doctor (Ph.D.)

Québec, Canada

© Simon Rondeau-Gagné, 2014

Résumé

Les travaux présentés dans cette thèse concernent principalement la mise en place d'une stratégie visant à obtenir de nouvelles nano-architectures moléculaires à partir de composés ayant une réactivité et une structure bien définies. Ainsi, par l'utilisation de macrocycles rigides de type phénylacétylène, il a été possible d'obtenir des nanotubes entièrement organiques, et ce, de façon plus rapide et contrôlée.

Dans le chapitre 1, une revue de la littérature scientifique actuelle sera présentée en mettant l'accent particulièrement sur l'obtention de nano-objets à partir de précurseurs moléculaires bien définis. Par la suite, dans le chapitre 2, une étude détaillée sur l'empilement supramoléculaire des macrocycles rigides de type phénylacétylène à l'état gel sera présentée en mettant en lumière l'influence des différents paramètres structuraux sur la réactivité de ces précurseurs. Dans le troisième chapitre, il sera question de la photopolymérisation topochemique à l'état gel des unités diynes contenues dans les macrocycles de type phénylacétylène vers l'obtention de nanobâtonnets rigides. Une caractérisation détaillée par spectroscopie Raman et par microscopie électronique sera présentée dans le but de confirmer les structures attendues. Dans le chapitre 4, il sera question de la photopolymérisation topochemique de macrocycles plus larges de type phénylènebutadiynylène dans le but de contrôler la largeur de la cavité interne des nouvelles nano-architectures tubulaires. L'utilisation de ces précurseurs montrant la polyvalence de notre approche hybride pour le contrôle des nanostructures finales. Le chapitre 5 comprendra une étude de la pyrolyse des nanotubes décrits dans les chapitres précédents dans le but d'aller vers des nanotubes riches en carbone. L'obtention de tels matériaux est particulièrement intéressante vu l'utilisation des plus en plus répandue des nanotubes de carbone, souvent difficile d'obtention avec de bonnes puretés. Dans le chapitre 6, il sera question de nos récentes tentatives afin d'augmenter la réactivité des macrocycles à la réaction de polymérisation topochemique par la modification des chaînes périphériques. Finalement, une conclusion et une synthèse des résultats ainsi qu'une mise en contexte des travaux futurs seront présentées dans le chapitre 7.

Abstract

The work presented in this thesis mainly concerns the establishment of a novel strategy to obtain new molecular nanoarchitectures from molecular precursors having a precise reactivity and a well-defined structure. Thus, by the use of shape-persistent phenylacetylene macrocycles, it has been possible to obtain discrete organic nanotubes in a more rapid and controlled fashion.

In chapter 1, a review of the recent literature will be presented focusing particularly on synthesis of nanomaterials from well-defined molecular precursors. Subsequently, in the second chapter, a detailed study on the supramolecular stacking of rigid phenylacetylene macrocycles in a gel state will be presented highlighting the influence of different structural parameters on the reactivity of these precursors.

In the third chapter, the topochemical photopolymerization in the gel state of diynes containing phenylacetylene macrocycles to obtain well-defined organic nanorods will be presented. A detailed characterization by Raman spectroscopy and electron microscopy will be presented in order to confirm the expected structures.

The chapter 4 will present the topochemical photopolymerization of larger phenylenebutadiynylene macrocycles in order to control the width of the inner cavity of the new tubular nanoarchitectures. By using these precursors, the versatility of our approach by a hybrid method will be discussed to exemplify the control over the final nanostructures.

Chapter 5 will present a study on the pyrolysis of the previously obtained organic nanorods toward carbon-rich nanotubes. The production of such materials is particularly interesting given the large use of carbon nanotubes, often difficult to obtain with good purities. Chapter 6 will present our recent strategy to improve the reactivity of the macrocycles toward topochemical polymerization by side-chains modification.

Finally, chapter 7 will present a conclusion and future work.

Table des matières

Résumé.....	III
Abstract.....	V
Liste des tableaux.....	XI
Listes des figures	XIII
Liste des schémas.....	XVII
Remerciements.....	XXIII
Chapitre 1. Introduction.....	1
1.1 Préambule.....	2
1.2 Résumé.....	2
1.3 Abstract.....	2
1.4 Introduction.....	3
1.5 Solid-State Polymerization of Oligoynes.....	6
1.6 Carbon-Rich Materials from Topochemical Polymerization.....	9
1.6.1 Carbon-Rich Materials From Non-Organized Oligoynes.....	9
1.6.2 Carbon-Rich Materials From Self-Assembled Oligoynes.....	14
1.7 Carbon-Rich Nanomaterials from Organometallic Precursors.....	23
1.7.1 Carbon-rich Nanomaterials From Cobalt-Encapsulated Dehydroannulene.....	23
1.7.2 Carbon-rich materials from organometallic complexes of hexabenzocoronene and related structures.....	24
1.7.3 Carbon-rich materials from polymeric organometallic precursors.....	26
1.8 Carbon-Rich Materials from Hexabenzocoronene (HBC) and Polymer Precursors.....	29
1.9 Objectifs des travaux.....	33
1.10. Références.....	38
Chapitre 2.....	43
2.1 Préambule.....	44
2.2 Résumé.....	44
2.3 Abstract.....	44
2.4 Introduction.....	45
2.5 Results and Discussion.....	48
2.5.1 Synthesis.....	48
2.5.2 Characterization.....	50
2.5.3 Theoretical Calculations.....	55
2.6 Conclusions.....	62

2.7 Supporting Information	62
2.7.1 General	62
2.7.2 Synthetic procedure	64
2.7.3 MALDI-ToF analysis	70
2.7.4 XRD analysis	72
2.7.5 Raman spectroscopy	75
2.8 Références	76
Chapitre 3	79
3.1 Préambule	80
3.2 Résumé	80
3.3 Abstract	80
3.4 Introduction	80
3.5 Results and Discussion	82
3.6 Conclusion	89
3.7 Supporting Information	89
3.7.1 General	89
3.7.2 Synthetic procedure	91
3.7.3 Gelation Properties	96
3.7.4 XRD analysis	97
3.7.5. UV Visible spectroscopy	99
3.7.6. SEC chromatography	99
3.7.7. Theoretical representation	100
3.8. Références	100
Chapitre 4	103
4.1 Préambule	104
4.2 Résumé	104
4.3 Abstract	104
4.4 Introduction	104
4.5 Results and discussion	106
4.6. Conclusion	112
4.7 Supporting information	112
4.7.1 General	112
4.7.2 Synthetic procedure	114
4.7.3. Scanning-electron microscopy (SEM) imaging	120

4.7.4. Powder X-rays diffraction analysis.....	120
4.7.5. UV-visible spectroscopy.....	121
4.7.6 Raman spectroscopy	122
4.7.7. TEM images of the nanotubes	123
4.8 Références	123
Chapitre 5.....	125
5.1. Préambule.....	126
5.2. Résumé.....	126
5.3. Abstract	126
5.4 Introduction	127
5.5 Experimental	129
5.5.1 Sample preparation	129
5.5.2 Characterization	130
5.6. Results and discussion.....	130
5.7 Conclusion.....	137
5.8. Références	137
Chapitre 6.....	141
6.1 Préambule.....	142
6.2. Résumé.....	142
6.3. Abstract	142
6.4 Introduction	142
6.5. Results.....	145
6.6. Conclusion.....	150
6.7. Supporting Information.....	150
6.7.1. General.....	150
6.7.2 Synthetic pathway.....	151
6.7.3. Experimental procedure.....	153
6.7.4. Gelation properties.....	160
6.7.5. Powder X-Ray diffraction (PXRD)	161
6.7.6. Differential scanning calorimetry (DSC).....	161
6.7.7. Transmission electron microscopy (TEM)	162
6.8 Références	163
Conclusion et perspectives.....	167

Liste des tableaux

Table 2.1 Gelation properties of amide-containing PAMs at 1.0 w/v %.....	51
Table 2.2. Conformation of minimum energy for molecules of series 1 and 2 , see text for details.	59
Table 3.1. Gelation properties of PAM 2 at 1.0 w/v %	96
Table 5.1. Carbon-rich features observed by HRTEM after pyrolysis of PDA-walled nanorods.....	135
Table 6.1. Gelation properties of monomers where G = gel; PG= partial gelification, S = solution, I = insoluble, a= previously reported.....	160

Listes des figures

Figure 1.1 Schematic overview of the drawbacks associated with both the physical and all-organic methods to prepare carbon nanomaterials; hybrid methods could be the best of both worlds	5
Figure 1.2. Possible addition pathways in topochemical polymerizations of oligoynes.	8
Figure 1.3. Preparation of graphitic materials from diphenylacetylene under elevated temperature and high pressure. ¹³	10
Figure 1.4. Possible pathway proposed by Kojima and coworkers for the formation of amorphous cross-linked carbon from PPBs upon heat treatment. ¹⁴	10
Figure 1.5. Suggested “one-dimensional” and “two-dimensional” mechanisms for the solid-state polymerization of 1-iodohexa-1,3,5-triyne at room temperature. ¹⁸	13
Figure 1.6. The “molecular dumbbell” used as starting materials for the preparation of carbon nanospheres (above) and AFM images of the “molecular dumbbell” before (a) and after (b) thermal annealing at 160°C for 1h. ¹⁶ Copyright 2005 American Chemical Society	14
Figure 1.7. Preparation of graphitic carbon from readily accessible poly(diiododiacetylene) (PIDA). ^{18,19}	15
Figure 1.8. CMA and DBAs prepared by Baughman and Swager, respectively. ²¹	16
Figure 1.9. Vollhardt’s DBAs and TEM image of the carbon materials obtained after their thermal decomposition. ²⁴ Copyright 1997 American Chemical Society	17
Figure 1.10. Structures of non-benzoannulated dehydroannulenes (a), schematic of a stack of the same macrocycle undergoing a topochemical polymerization (b) and the packing diagram of macrocycles where R = CH ₂ OH (c). ²⁷ Copyright 2010 American Chemical Society	19
Figure 1.11. Structures (a) and X-ray crystal structure (b and c) of the butadiyne-containing macrocycle prepared by Shimizu and coworkers. ²⁸ Copyright 2010 American Chemical Society	20
Figure 1.12. Preparation of hollow carbon nanospheres with controlled morphology through topochemical polymerization of an amphiphilic hexayne derivative. ³⁴ Copyright 2012 American Chemical Society	22
Figure 1.13. TEM images of CNTs containing crystalline cobalt from dehydroannulene cobalt complexes. ³⁵ Copyright 1999 American Chemical Society.....	25
Figure 1.14. HBC-Co complex leading to carbon nanomaterials upon pyrolysis. ³⁸	26
Figure 1.15. Cobalt-containing graphene layer to graphene/CNTs composite film. ⁴⁶	29
Figure 1.16. SEM images of a) carbon nanospheres (scale bar 5µm) b) carbon microfibers (scale bar 100 µm) and c) bundles of carbon nanowires (scale bar 200 nm) formed after pyrolysis at 800°C of HBCs precursors in an ordered mesophase. ⁴⁷ Copyright 2002 American Chemical Society	30
Figure 1.17. Synthesis of chiral polypyrrole nanotubes and CNTs. a) polypyrrole nanotubes prepared by self-assembly of C18-d-Glu (template) with ammonium persulfate (APS) as initiator and b) carbonaceous CNTs prepared by carbonization of polymeric nanotubes under an Ar atmosphere. ⁵⁰ Copyright 2013 Wiley	31
Figure 1.18. Approche générale proposée vers l’obtention de matériaux riches en carbones	35
Figure 2.1 Structure of PAMs 1a , 1b , 2a and 2b	47

Figure 2.2. SEM images of a) dried gel of PAM 1a in toluene (10 mg/mL), and b) dried gel of PAM 2a in toluene (10 mg/mL). Scale bars of 0.5 μm for a) and b).	52
Figure 2.3 Two different amide configurations studied.....	56
Figure 2.4. Potential energy, red (■) and blue (●) for molecules of series 1 and 2 respectively, with respect of the dihedral angle, \square , associated to the bond linking the amide function to the phenyl group (Figure 2.3).....	58
Figure 2.5. Potential energy with respect to the rotation angle between the cores.....	60
Figure 2.6. Schematic representation of the translation of one core in relation to the other core.....	61
Figure 2.7. Isoenergetic plot with x and y displacement corresponding to translation shown in figure 2.6.....	61
Figure 2.8. MALDI-ToF spectrum of PAM 1a	70
Figure 2.9. MALDI-ToF spectrum of PAM 1b	70
Figure 2.10. MALDI-ToF spectrum of PAM 2a	71
Figure 2.11. MALDI-ToF spectrum of PAM 2b	71
Figure 2.12. X-ray diffraction spectrum of gel of PAM 1a in toluene (10 mg/mL).....	72
Figure 2.13. X-ray diffraction spectrum of PAM 1b in toluene (10 mg/mL).....	72
Figure 2.14. X-ray diffraction spectrum of PAM 2a in cyclohexane (10 mg/mL).....	73
Figure 2.15. X-ray diffraction spectrum of PAM 2a in ethyl acetate (10 mg/mL).....	73
Figure 2.16. X-ray diffraction spectrum of PAM 2b in ethyl acetate (10 mg/mL)	74
Figure 2.17. X-ray diffraction spectrum of PAM 2b in cyclohexane (10 mg/mL)	74
Figure 2.18. Raman spectra of Poly-2a	75
Figure 2.19. Raman spectra of Poly- 2b	75
Figure 3.1. Phenylacetylene macrocycles 1 and 2	82
Figure 3.2. SEM images of dried ethyl acetate organogel from PAM2 (10 mg/mL). Scale bars are (a) 2 μm and (b) 0.2 μm	84
Figure 3.3. Raman spectra of PAM 2 (red) and SEC-purified blue material (black).	87
Figure 3.4. HRTEM images of the nanorods. Scale bars are 200 nm (a) and 20 nm (b).....	88
Figure 3.5. Proposed mechanism for the topochemical polymerization between macrocycles in the dried gel state.	89
Figure 3.6. a) Organogel of PAM 2 in ethyl acetate (10 mg/mL) before and after the topochemical polymerization, b) Solution of PAM 2 organogel in CHCl_3 after the topochemical polymerization.....	97
Figure 3.7. X-ray diffraction spectrum of PAM 2 gel in ethyl acetate (10 mg/mL).....	98
Figure 3.8. X-Ray diffraction spectrum of SEC-purified PDA	98
Figure 3.9. UV Visible spectrum of PAM 2 and SEC-purified PDA in CHCl_3	99
Figure 3.10. SEC chromatograms of PAM 2 before (black) and after (blue) UV irradiation. The red trace corresponds to the SEC-purified blue material.	99
Figure 3.11. Models of side view (a) and front view (b) of the nanotube after the topochemical polymerizations. Red spheres on (a) are the alkyne carbon atoms of the PDA chains. Peripheral groups have been omitted for clarity.....	100
Figure 4.1. Structure of PBM1 and PBM2	106
Figure 4.2. Structure and PDA1 in front and side views. Side groups and hydrogen atoms have been omitted for clarity. The red and blue carbon atoms represent the PDA chains and the phenyl groups, respectively.....	111

Figure 4.3. TEM (a) and HRTEM (b) images of the nanotubes. Scale bars are 500 nm (a) and 20 nm (b).	112
Figure 4.4. SEM images of dried gel of PBM1 in cyclohexane (10 mg/mL)	120
Figure 4.5. X-rays diffractogram for PBM1 gel in cyclohexane (10 mg/mL).	121
Figure 4.6. UV visible spectra of PBM1 and PDA1 in CHCl ₃	122
Figure 4.7. Raman spectra of PBM1 (red) and PDA1 (black).	122
Figure 4.8. TEM image of a single nanotube. The channel inside the nanotube can be clearly differentiate, especially on the right side of the nanotube.	123
Figure 5.1. Pathway toward carbon-rich material from organic PDA nanorods [38]	129
Figure 5.2. Thermogravimetric analysis (TGA) of pyrolysed PDA-walled nanorods	131
Figure 5.3. UV-visible spectra of PDA-walled nanorods (black line) and pyrolyzed nanorods (red line) in CHCl ₃ .	132
Figure 5.4. Raman spectrum of a) pyrolysed nanorods and b) PDA-walled nanorods, ($\lambda = 514$ nm)	133
Figure 5.5. HRTEM image of PDA-walled nanorods a) before [38] (Copyright 2013 American Chemical Society) and b) to d) after pyrolysis and TEM images of PDA walled-nanorods e) and f) after pyrolysis. Scale bars are a) 200 nm, b) and c) 1 μ m, d) and e) 20 nm, f) 50 nm, g) 200 nm, h) 50 nm, i) 100 nm, j) 1 μ m, k) 0.2 μ m and l) 100 nm	134
Figure 5.6. TEM imaging of pyrolyzed cobalt-containing PDA-walled nanorods. Scale are a) 100 nm and b) 20 nm.	136
Figure 6.1. Structures of PAM1-PAM3	144
Figure 6.2. Scanning electron microscopy (SEM) images of PAM2 xerogel in cyclohexane (10 mg/mL). Scales are a) 1 μ m and b) 0.5 μ m.	147
Figure 6.3. UV Visible spectrum of PAM2 before (black) and after (red) polymerization (PDA).	149
Figure 6.4. Background-corrected Raman spectra of PAM2 (red) and the blue material obtained after UV irradiation (black).	149
Figure 6.5. Powder X-Ray diffraction (PXRD) spectrum of a 10 mg/mL xerogel of PAM2 in cyclohexane	161
Figure 6.6. DSC curves of a gel (10 mg/mL) of PAM1 in cyclohexane, 10°C/min.	161
Figure 6.7. DSC curves of a gel (10 mg/mL) of PAM2 in cyclohexane, 10°C/min	162
Figure 6.8. TEM imaging of PDA on carbon-coated copper grid. Scale bars are a) 100 nm and b) to d) 50 nm.	163
Figure 7.1. Molécules modèles inspirées des motifs de base d'un polydiacétylène pour étude de cycloaromatisation.	170
Figure 7.2. Photopolymérisation d'un précurseur tétrayne pour l'obtention de nanoparticules de carbone.	172

Liste des schémas

Scheme 2.1. Synthetic pathway to PAMs 1a and 1b	49
Scheme 3.1. Synthesis of PAM2	83
Scheme 4.1. Synthesis of PBM1 and PBM2	108
Scheme 6.1. Synthetic pathway to PAM2 and PAM3	152

Liste des abréviations

6-Chloro-HOBt	=	6-Chloro-1-hydroxybenzotriazole
Å	=	angström
ACN	=	Acétonitrile
AFM	=	Microscopie à force atomique
al.	=	collaborateurs
APPI	=	Atmospheric pressure photoionization
Ar	=	Atmosphère d'argon
ATR	=	Attenuated Total Reflexion
CC	=	Chromatographie sur colonne
CCM	=	Chromatographie sur Couche Mince
CNT	=	Nanotubes de carbone
CVD	=	Déposition chimique en phase vapeur
d	=	doublet
DA	=	Diacétylène
DBA	=	Dehydrobenzoannulène
DCC	=	<i>N,N'</i> -dicyclohexylcarbodiimide
DCE	=	Dichloroéthane
DCM	=	Dichlorométhane
dd	=	Doublet de doublets
DMAP	=	<i>N,N'</i> -diméthylaminopyridine
DMF	=	Diméthylformamide
DMSO	=	Diméthylsulfoxyde
DSC	=	Calorimétrie différentielle à balayage
EDC	=	1-Éthyl-3-(3-diméthylaminopropyle)carbodiimide
EDLC	=	Capaciteur électrochimique à double couche
Et₂O	=	Éther diéthylique
Eg	=	Largeur de bande interdite
FTIR	=	Fourier Transform Infrared Spectroscopy
GPC	=	Gas Permeation Chromatography
h	=	Heure
HBC	=	Hexa- <i>peri</i> -hexabenzocorrone
HOBt	=	1-Hydroxybenzotriazole
HRMS	=	Spectrométrie de Masse Haute Résolution
HRTEM	=	Microscopie Électronique à Transmission Haute Résolution
m	=	Multiplet
MeOH	=	Méthanol
MHz	=	mégahertz
min	=	minute
mmol	=	Milimole
MPa	=	Méga Pascals
mPPB	=	<i>mé</i> ta-poly(phénylène butynylène)
mPPE	=	<i>mé</i> ta-poly(phénylène éthynylène)
nm	=	Nanomètre

NRG	= Nanoruban de graphène
NTC	= Nanotube de carbone
OFET	= Transistor organique à effet de champ
OPV	= Cellule photovoltaïque
PBM	= Macrocycle de type phénylènebutadiynylène
PDA	= Polydiacétylène
PIDA	= Poly(iodoacétylène)
PPB	Poly(phénylène-butadiynylène)
PPh₃	= Triphénylphosphine
PXRD	= Diffraction des rayons X de poudres
RMN	= Résonance magnétique nucléaire
s	= Singulet
SEC	= Chromatographie d'exclusion stérique
SEM (MEB)	= Microscope électronique à balayage
t	= triplet
t.a.	= Température ambiante
TBAF	= Fluorure de tetrabutylammonium
TBDMS-Cl	= Chlorure de <i>tert</i> -butyldiméthylsilyle
TBS ou TBDMS	= <i>tert</i> -Butyldiméthylsilyle
TEA	= Triéthylamine
TEM (MET)	= Microscope électronique à transmission
TGA	= Analyse thermogravimétrique
THF	= Tétrahydrofurane
TIPS	= Triisopropylsilyle
TIPSA	= (Triisopropylsilyl)acétylène
TMS	= Triméthylsilyle
TMSA	= (triméthylsilyl)acétylène
u.a. ou a.u.	= unité arbitraire
UV-Vis	= Ultra-violet et Visible

À mes parents, Louise et Marc

« You will still be here tomorrow, but your dreams may not »

-Cat Stevens

Remerciements

J'aimerais tout d'abord remercier mon directeur de thèse, le professeur Jean-François Morin, pour m'avoir confié cet ambitieux projet et pour m'avoir donné toutes les ressources nécessaires pour son accomplissement. Le professeur Morin, de par sa générosité, ses conseils judicieux, ses encouragements, sa disponibilité et son sens critique a une grande part dans la réussite de ce projet. Le côtoyer tous les jours fut pour moi source d'inspiration, de motivation et un immense privilège. Le Dr Morin m'a permis des apprentissages incommensurables dans le domaine scientifique et humain qui me permettront de faire face aux futurs défis. Merci pour tout.

J'aimerais également remercier mon collègue et ami, le Dr Jules Roméo Néabo pour son appui et son aide tout au long de ces années de recherche. Jules m'a été d'une aide précieuse et a été un élément clé dans la réussite de ce projet et de toutes mes ambitions.

Je me dois de remercier M. Phillippe Dufour pour son aide et son écoute. Phil, dès le début de ma carrière, s'est avéré être une aide précieuse et une source de motivation infinie. Son aide et ses conseils, particulièrement dans les moments difficiles, m'ont été salutaires et j'apprécie encore toutes les discussions avec ce brillant chercheur devenu, au fil des années, un ami cher. Je ne peux passer sous silence la précieuse aide du Dr Dominic Thibault qui m'a aidé tout au long de ma carrière et qui est devenu également un ami. Le Dr Thibault a été, et est pour moi, un modèle de rigueur et de travail.

J'aimerais remercier grandement mes collègues Isabelle Levesque, Maxime Daigle, Maude Desroches, Katy Cantin et Jérémie Larouche pour leur précieuse aide lors de la réalisation de ce projet. Ces jeunes chercheurs m'ont grandement impressionné de par leur talent et leurs ambitions. Ils formeront, sans aucun doute, une brillante relève au sein de la communauté scientifique mondiale. Je leur lève mon chapeau!

J'aimerais, finalement, remercier tous les autres membres, présents et anciens, du groupe Morin pour leur aide quotidienne et pour leur écoute. Travailler avec eux tout au long de mes années d'études graduées fut un grand plaisir et un honneur. Je leur souhaite la meilleure chance dans leurs projets futurs. Merci aux professionnels de recherche, Rodica

Pleasu, Jean-François Rioux-Dubé, Richard Janvier, Bi Wenhua pour leur apport respectif dans l'avancement de ce projet.

D'un point de vue plus personnel, j'aimerais remercier mes parents Louise et Marc pour leur aide, leur soutien et leur compréhension tout au long de ces longues années de recherches. Leur encouragement, leur fierté et leur présence à mes côtés sont une source de bonheur et de surpassement. J'espère ne jamais les décevoir et je me dois de leur mentionner que sans eux, rien de cela n'aurait été possible. Merci d'avoir cru en moi et d'être encore là!

J'aimerais remercier ma conjointe, Émilie, pour être à mes côtés et pour me suivre dans tous mes projets. Émilie m'a toujours appuyé et cru en moi ce qui me donne le courage d'avancer. Merci pour le soutien dans les moments difficiles, merci pour les sourires et pour les encouragements quotidiens. Émilie est ma source de bonheur et sa présence est partie intégrante de la réussite de ces travaux. Merci d'être mon ange gardien.

J'aimerais remercier M. Pierre-Luc Dallaire et M. Sébastien Laberge, deux amis précieux, pour leur écoute et pour leur appui. J'ai bien apprécié leur aide, particulièrement pour m'aider à me changer les idées dans les moments difficiles. Ils feront, sans aucun doute, une brillante carrière dans leurs domaines respectifs et j'espère les avoir près de moi pour plusieurs années encore. J'en profite également pour remercier tous mes amis de la ZV8 et de Chicoutimi-Nord qui m'ont, depuis toujours, soutenu et appuyé.

Finalement, j'aimerais remercier ma famille pour leur appui et leur soutien. Particulièrement, merci à ma grand-mère Gemma, ma tante Louise et mon oncle Guy pour leur appui et leurs encouragements.

Chapitre 1. Introduction

Préparation de nanomatériaux de carbone à partir de précurseurs moléculaires

Preparation of carbon nanomaterials from molecular precursors

Simon Rondeau-Gagné and Jean-François Morin*

*Département de Chimie and Centre de recherche sur les matériaux avancés (CERMA),
1045 Ave. de la médecine, Université Laval, Québec, Canada G1V 0A6.*

Publié dans la revue *Chemical Society Reviews*, **2014**, *43*, 85-98.

1.1 Préambule

Cette revue de la littérature portant sur la synthèse de nanomatériaux à partir de précurseurs moléculaires représente une introduction aux travaux présentés dans la présente thèse. Cet article résume et précise les différentes méthodes de synthèse de nanomatériaux à partir de composés structurellement bien définis. L'approche hybride y est également mise en perspective par rapport aux approches plus conventionnelles (méthodes physiques et chimiques). Ma contribution à cette revue de la littérature est majeure. J'ai effectué la recherche bibliographique ainsi que la rédaction de la majeure partie de l'article. J'ai également travaillé à la conception du plan de l'article et à sa mise en œuvre.

1.2 Résumé

La préparation de nanomatériaux de carbone a fait l'objet de nombreuses recherches parmi plusieurs groupes au cours des vingt dernières années. Traditionnellement, la synthèse de ces matériaux a été réalisée en utilisant des méthodes physiques impliquant des conditions difficiles, ce qui limite leur utilisation dans de nombreux domaines d'applications. Ainsi, les chercheurs ont travaillé en permanence à développer de nouvelles méthodes impliquant des molécules organiques possédant des groupes fonctionnels réactifs qui peuvent être graphitisés et réticulés dans des conditions douces. Dans cette revue de littérature, nous soulignons les récentes approches pour la préparation de divers nanomatériaux de carbone en utilisant divers stimuli physiques (chaleur et/ou lumière) pour déclencher la graphitisation de précurseurs moléculaires autoassemblés ou non organisés. Une attention particulière est consacrée à la préparation de nanomatériaux de carbone à partir de molécules contenant des fonctionnalités alcyne et diacétylène.

1.3 Abstract

The preparation of carbon nanomaterials has been the focus of many research groups over the last twenty years. Traditionally, the synthesis of these materials has been accomplished using physical methods involving harsh conditions, limiting their applicability in numerous technological areas. Thus, researchers have been constantly working at developing new methods involving organic molecules possessing highly reactive functional groups that can be graphitized under mild conditions. In coming pages, we highlight recent approaches for the preparation of various carbon nanomaterials using physical stimuli (heat and/or light) to

trigger graphitization of both non-organized and self-assembled molecular precursors. A special attention is devoted to the preparation of carbon nanomaterials from alkyne-containing molecules.

1.4 Introduction

Since the discovery of fullerenes, carbon nanotubes (CNTs) and, more recently, graphene, carbon nanomaterials have emerged amongst the most promising materials for various types of applications owing to their outstanding electronic and optical properties.¹ The high number of scientific articles published annually in this area (more than 100,000 articles overall having either graphene, carbon nanotube or fullerene in the article title according to SciFinder[®]) is a direct measure of the popularity of these materials. Despite the success story of modern carbon-rich materials, a lot of new researches are performed to modulate the structures, shapes and properties of these nanomaterials. Thus, it is not surprising that novel structures appeared in the recent years for more and more applications, such as nanoelectronics, nanomedicine and so on.

Historically, carbon materials have been obtained by top-down approaches. Despite the effectiveness of these methods, obtaining new structures with interesting properties and with good purities is particularly difficult. Moreover, structural defects can sometimes be observed, which is still a major issue. Thus, materials science focused on some bottom-up approaches. These new methods recently allowed formation of new nanoarchitectures with interesting properties that can be directly related to the nanostructures. However, these new "all-organic" approaches still has some limitations that have to be addressed. The synthesis of novel nanostructured carbon-rich materials remains a hot field in materials sciences, particularly stimulated by these new materials and their applications. Despite the enthusiasm within the scientific community, many challenges still have to be solved. Is it possible to rationally predict the structural parameters required for the nanostructure depending on the desired optical and electronic properties? How to obtain different nanoarchitectures by careful design of molecular precursors? How carbon materials can be obtained without defects and what is the best way to modulate their properties? Here are just a few questions that remain to be answered by developing new methodologies and new materials.

The interest for the carbon-rich nanostructured materials comes in major part from their unique network of sp^2 carbon atoms that allow electron delocalization all over the molecules, either in one or two dimensions. Depending on different structural parameters, these nanomaterials can be semiconducting or metallic, which make them potentially useful in a wide range of electronic applications such as transistors, supercapacitors, batteries, transparent electrodes, sensors, solar cells, and so on. As most materials, the properties and functions of carbon nanomaterials can be tuned by changing their size, shape and dimensionality. For example, graphene, which is a two-dimensional zero-gap material, could be transformed into a one-dimensional, nonzero gap semiconducting CNT just by folding the graphene sheet on itself following a precise vector.² Thus, the control of these structural parameters is of utmost importance when specific applications are targeted. The best way to obtain high level of preciseness for these parameters remains the modulation of the reaction conditions used to prepare carbon nanomaterials. For instance, synthetic methods that use carbon feedstock (gas, graphite, amorphous carbon, solvents, etc.) to prepare carbon nanomaterials such as laser ablation, arc discharge and hydrocarbon combustion are all methods in which reaction conditions can be adjusted to give preferentially one specific carbon nanomaterial.³ Although very valuable, these synthetic methods, called “physical methods”, possess serious disadvantages regarding materials purity, uniformity, batch-to-batch consistency and industrial applicability.⁴ Because physical methods often involved elevated temperature processes, the control over the structural parameters is possible, but rather limited in large-scale production of well-defined carbon nanomaterials.

To circumvent the lack of control inherent to the physical methods, chemists and materials scientists proposed fancier alternatives that rely on synthetic organic chemistry strategies. With the help of modern and classical synthetic tools, total synthesis of carbon nanomaterials can be achieved, although these methods are far from being efficient to prepare large quantities of materials. Beautiful examples of synthesis of fullerenes, CNT fragments, nanographene and graphene nanoribbons have been published in the last twenty years and works toward more efficient synthetic paths are still underway in many research groups.⁵ A mid-point strategy between the physical and all-organic methods, called the “hybrid method”, is to use a mix of both in which reactive, carbon-rich precursors are

synthesized in few synthetic steps and exposed to physical stimuli such as heat or light. Depending on their organization in solution, solid or thin-film state, these precursors can be transformed into graphitic carbon materials of various sizes, shapes and functions. Although this method is not perfect and effective for routine production of materials yet, it could provide the best long-term alternative to overcome some major disadvantages of both physical and all-organic methods. One of the major benefits of this method is the possibility of preparing carbon nanomaterials under very mild conditions (with temperature usually below 250°C) without any complex experimental setup. Mild conditions are particularly important for the growth or preparation of carbon nanomaterials directly on sensitive substrates such as silicon and semiconducting electrodes used by the electronics industry. Nevertheless, more research must be conducted to evaluate the real potential of this increasingly popular alternative in large-scale materials production.

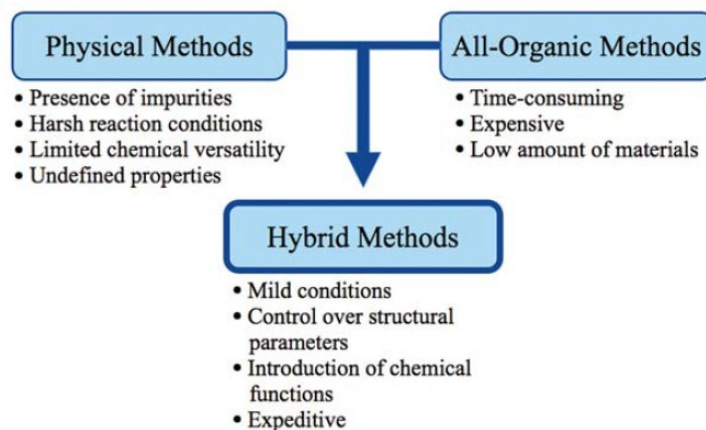


Figure 1.1 Schematic overview of the drawbacks associated with both the physical and all-organic methods to prepare carbon nanomaterials; hybrid methods could be the best of both worlds

To be transformed under physical stimuli, organic molecules have to be reactive in some way under these stimuli, meaning that the molecules, or building blocks, should possess metastable, carbon-rich functional groups. A good balance between stability under standard organic reaction conditions, allowing the synthesis of complex building blocks, and reactivity under specific physical stimuli has thus to be reached. Unfortunately, the number

of functional groups fitting this category is quite low. As proof of this, the vast majority of carbon nanomaterial syntheses reported in the literature rely on the preparation of [n]yne derivatives as reactive precursors. Upon irradiation or heating, self-assembled [n]yne derivatives can undergo topochemical polymerization to give polydiacetylenes (PDAs) (when $n = 2$) or other carbon-rich, less-defined materials (when $n \geq 3$), which can be further transformed, graphitized in most cases, to give carbon nanomaterials. Although the addition mechanism is well understood in the case of buta-1,3-diyne, it is a bit more complicated in the cases of higher oligoyne homologues, especially for [n]ynes where $n \geq 4$ which often lead directly to amorphous graphitic carbon upon irradiation or heating.

In the next pages, the strategies developed in the past twenty years or so to prepare carbon nanomaterials using reactive, carbon-rich precursors are surveyed. A particular emphasis will be put on reactive precursors that contain alkyne moieties, especially oligoynes, although other carbon-rich molecules will also be covered.

1.5 Solid-State Polymerization of Oligoynes

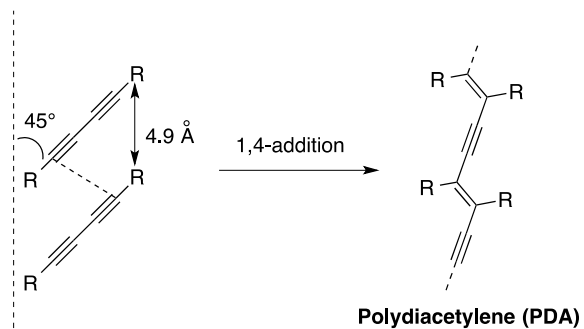
In order to prepare thermodynamically stable carbon nanomaterials under mild conditions and low temperatures, carbon-rich precursors with reactive functional groups that can be transformed without the use of excessive energy input have to be used. Unfortunately, very few functional groups fit that category and the one that has been studied the most is undoubtedly the alkyne. In fact, alkyne, or carbon-carbon triple bond, is a reactive functional group owing to its two π -bonds that provide intrinsic thermodynamic instability. On one hand, this reactivity enables, among others, hydrogenation, electrophilic additions, hydroboration and oxidation reactions that are very precious to the organic chemists' toolbox. On the other hand, alkyne is sufficiently stable to be prepared and handled without significant decomposition. Moreover, alkynes can be installed on organic substrates using different, very versatile set of reactions⁶ and coupled together in various conditions to give oligoynes and polyynes.⁷

Considering its relative thermodynamic instability and ease of preparation using common organic transformations, alkyne is definitely the ideal functional group for the preparation

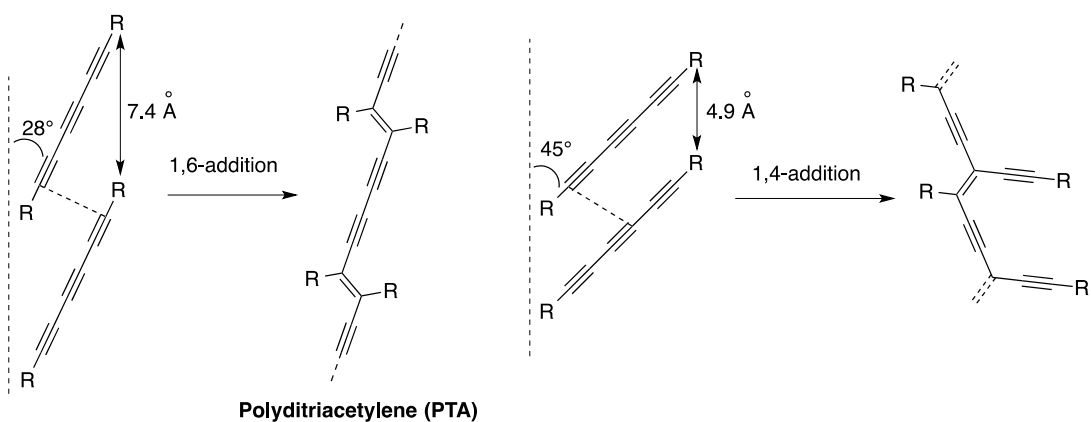
of carbon nanomaterials under mild conditions, especially in the solid state. One of the most exploited reactions for the transformation of alkyne in the solid state is undoubtedly the 1,4-addition of 1,3-butadiynes, called topochemical polymerization, to give polydiacetylene (PDA, Figure 1.2). Gerhard Wegner whose goal was to prepare highly crystalline polymers in the solid state discovered this reaction in 1969⁸ and since then, thousands of articles have been published on this topic, mostly because of the excellent chromic properties of PDAs that could potentially be used in sensor devices.

However, not all oligoyne-embedded compounds can react to give PDAs and eventually carbon nanomaterials. For the reaction to occur, rigorous structural parameters including intermolecular distance and tilt angle have to be respected. For the 1,3-butadiyne derivatives, an intermolecular distance of 4.9Å and a tilt angle of 45° are required in the solid state. These strict prerequisites mean that proper elements of design that will orient the molecules properly in the solid state must be embedded within their scaffold. Usually, H-bonding, π - π and, at a lesser extent, van der Waals interactions can be very efficient to organize molecules in a particular orientation to allow topochemical polymerization. Over the years, the scope of this reaction has been extended to longer oligoynes,⁹ giving new sets of conjugated polymers. The topochemical polymerizations of different oligoynes and their structural requirements are summarized in Figure 1.2. It is noteworthy that oligoynes polymerization mechanism is still under debate.

1,3-butadiyne



1,3,5-hexatriyne



1,3,5,7-octatetrayne

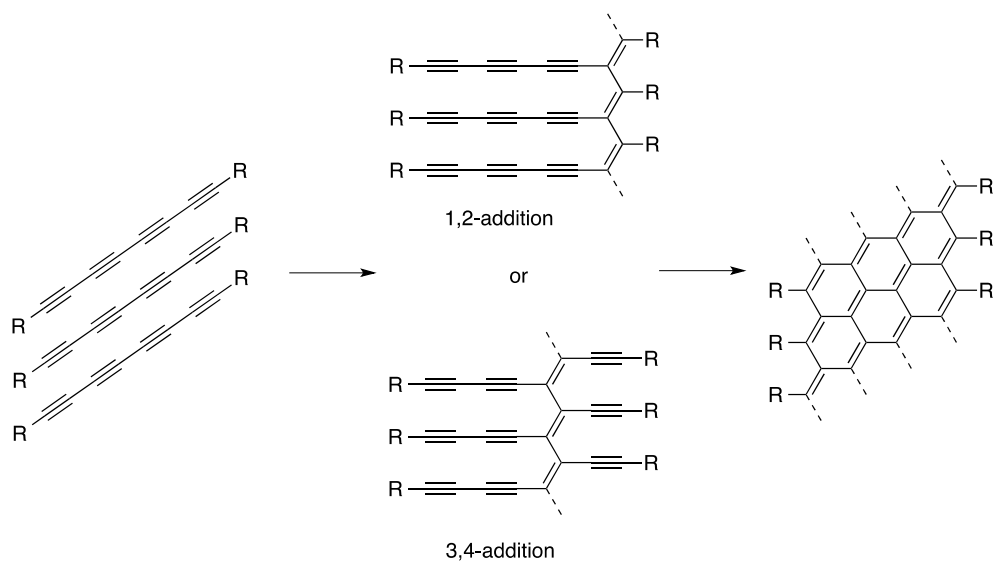


Figure 1.2. Possible addition pathways in topochemical polymerizations of oligoynes.

1.6 Carbon-Rich Materials from Topochemical Polymerization

1.6.1 Carbon-Rich Materials From Non-Organized Oligoynes

Beside the preparation of chromic materials, the topochemical polymerization of oligoynes can also be used to prepare carbon-rich materials with amorphous graphitic structure. The first example of preparation of graphitic materials from alkyne precursors involved the pyrolysis of poly(diethynylbenzene). In 1992, Economy and coworkers showed that poly(1,3-diethynylbenzene) underwent crosslinking reactions to form condensed aromatic structures, or amorphous graphitic carbon, that could be transformed into carbon-fiber-carbon-matrix composites.¹⁰ The authors associated the formation of amorphous graphitic carbon to multiple Diels-Alder reactions between two 1,3-butadiynes in adjacent polymer chains, although this hypothesis was not demonstrated experimentally. It is worth mentioning that this particular Diels-Alder reaction would be very difficult to drive because of the high rigidity of the alkyne. To the best of our knowledge, no such reaction has been ever reported in the literature.

Few years after the Economy's report, Kijima and coworkers reported the carbonization reaction of poly(phenylenebutadiynylene)s (PPBs) at 900°C to give amorphous graphitic carbon in very high yields.¹¹ Interestingly, differential scanning calorimetry (DSC) analysis on powder sample of PPBs suggested that an exothermic reaction occurred at 200°C with enthalpy change (ΔH) values of approximately -100 kJ/mol, which is in perfect agreement with the enthalpy change observed during the 1,4-additions of 1,3-butadiyne units to form PDAs.¹² This result indicates that graphitization reaction at higher temperature is attributable to the formation of a pre-carbon material (PDA) that undergoes a cycloaromatization reaction upon further heating.

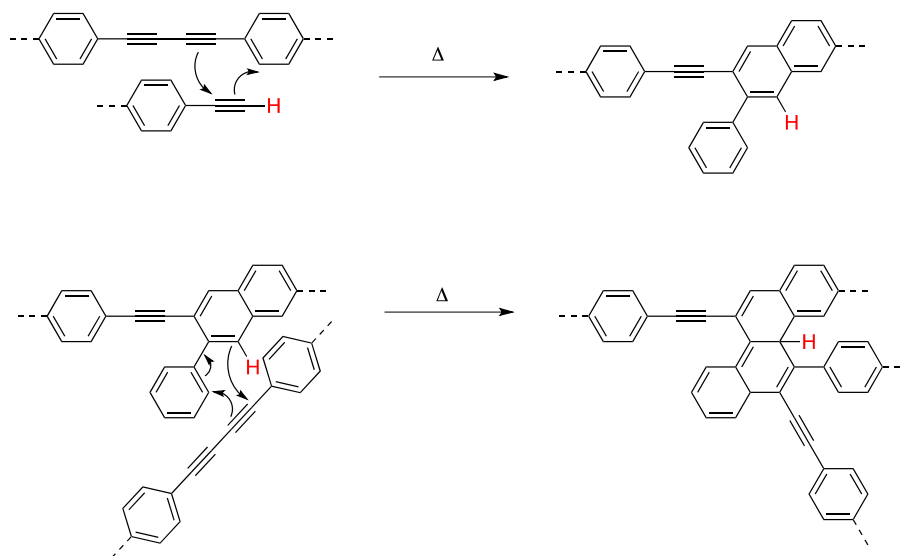


Figure 1.3. Preparation of graphitic materials from diphenylacetylene under elevated temperature and high pressure.¹³

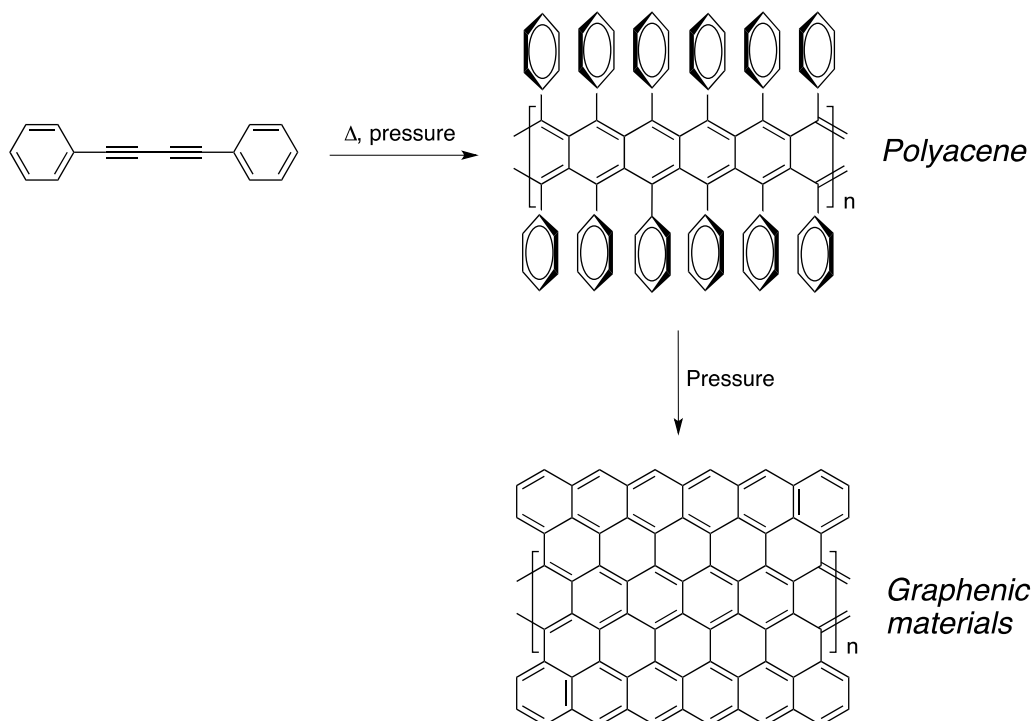


Figure 1.4. Possible pathway proposed by Kojima and coworkers for the formation of amorphous cross-linked carbon from PPBs upon heat treatment.¹⁴

In 2006, Ozaki and coworkers undertook the detailed study on pyrolysis of PPBs by thermoanalysis.¹³ Using a combination of spectroscopic tools, they showed that PPBs do not actually graphitize upon heat treatment, even when temperature as high as 3000°C were used. Instead, amorphous carbon containing sp^3 -hybridized carbon atoms is produced. The plausible mechanism of carbonization involved the cross-linking of polymer chains through a Diels-Alder mechanism involving both butadiyne or terminal alkyne and a phenyl group, as shown in Figure 1.3. These results clearly indicate that PPBs can serve as carbon-rich reactive precursors for the preparation of amorphous graphitic carbon but that high quality, defect-free graphite or graphene would be difficult to prepare using this strategy.

Another way of preparing amorphous graphitic carbon is to use low molecular-weight molecules containing butadiyne unit rather than polymers as PPBs. Kojima and coworkers studied the transformation of 1,4-diphenyl-1,3-butadiyne by thermal annealing under elevated pressure (0.1-500 MPa).¹⁴ Interestingly, the reaction proceeds with a gas evolution, indicating that hydrogen was lost during the annealing process. This result, along with the absence of alkyne signal in the infrared spectrum, suggests that the reaction did not proceed through a 1,4-addition mechanism to form PDA. In fact, the Raman spectrum of the insoluble black material confirms the presence of graphitized carbon materials, mostly CNTs, that are likely to be the product of dehydrogenation of polyacene-like precursors as shown in Figure 1.4. It is important to mention that the final compounds were not characterized precisely so the final results are still not validated.

In the early 2000s, the group of Hlavaty explored the reaction of very simple oligoynes derivatives for the preparation of carbon nanomaterials. In their first report in this area, Hlavaty and coworkers discovered that multi-walled CNTs and graphene-like materials could be prepared through low temperature processes using 1-iodohexa-1,3,5-triyne and hexa-1,3,5-triyne.¹⁵ Because of their instability, both derivatives undergo carbonization in solution at room temperature when stored under argon for one to two days, the iodo derivative being a little less reactive than the free hexa-1,3,5-triyne. Interestingly, two reaction mechanisms can be predominant depending on the concentration of the starting materials during the carbonization: the so-called “two-dimensional” polymerization took place when the solution was diluted to form thermodynamically stable graphene-like

structures while increasing the concentration yield the “one-dimensional” polymerization favourably (see Figure 1.5). Transmission electron microscopy (TEM) analysis revealed that the graphitic materials thus produced are made of multi-walled CNTs with diameter ranging from 10 to 20 nanometers. Similar results were obtained when α,ω -dialkalihexatriynides were used as starting materials. This was among the first examples of low-temperature ($\leq 20^\circ\text{C}$) chemical synthesis of CNTs from carbon-rich, reactive molecules.

Solid-state polymerization of oligoynes can also be used to prepare nanostructured surfaces made of carbon-rich nanomaterials. In 2005, Zhao and coworkers exploited the high reactivity of tetraynes to prepare C_{60} -embedded carbon nanospheres on a mica surface.¹⁶ After spin-coating of a C_{60} -terminated tetrayne derivative, called the “molecular dumbbell” (Figure 1.6), the surface was heated up at 160°C for one hour, allowing intermolecular reactions between the tetrayne moieties to produce monodisperse, carbon-rich nanospheres over a relatively large scale. Because the starting material cannot stack following the proper orientation for the topochemical polymerization owing to the presence of bulky C_{60} , the polymerization mechanism is considered to be rather random, as observed by the large exothermic peak in DSC measurements. The high steric hindrance also leads to a quite low degree of polymerization, which is believed to be beneficial to obtain homogeneous nanospheres across the surface.

All the examples above are strong indication of the relatively high reactivity of alkyne upon heating. However, these high-temperature processes are conceptually not very different to what can be achieved with simpler carbon molecules feedstock to form amorphous graphitic carbon. In this regard, the strategy based on the use of alkyne-containing molecules is not that advantageous, especially if it does not lead to materials with unique properties. Therefore, efforts have been devoted recently to prepare carbon nanomaterials from oligoyne derivatives using milder conditions. These strategies exploit the high reactivity of oligoyne moieties toward topochemical polymerization in the solid state to prepare reactive intermediates, mostly PDAs, which can be transformed into graphitic materials using mild conditions. The most representative example of this strategy was reported by Goroff and coworkers who used co-crystals of 1,4-diiodo-1,3-butadiyne

and a nitrogen-containing host to prepare poly(diiododiacetylene) (PIDA)¹⁷ that further undergo a graphitization reaction upon treatment with Lewis bases at room temperature as shown in Figure 1.7.¹⁸ The Lewis base-driven transformation of PIDA to graphitic material is likely the result of the formation of polyynes intermediate, accompanied by the loss of iodine (I₂), that rapidly decompose to form a network of sp² carbon atoms. This hypothesis has been verified by treating low molecular weight 1,2-diiodoalkene with pyrrolidine that induced the dehalogenation of alkene to give the corresponding alkyne in high yield. The final black material appeared as long fibers that exhibited higher electrical conductivity than the starting PIDA and resembles in many points the nanofibers obtained from pyrolysis of PIDA at 900°C.¹⁹

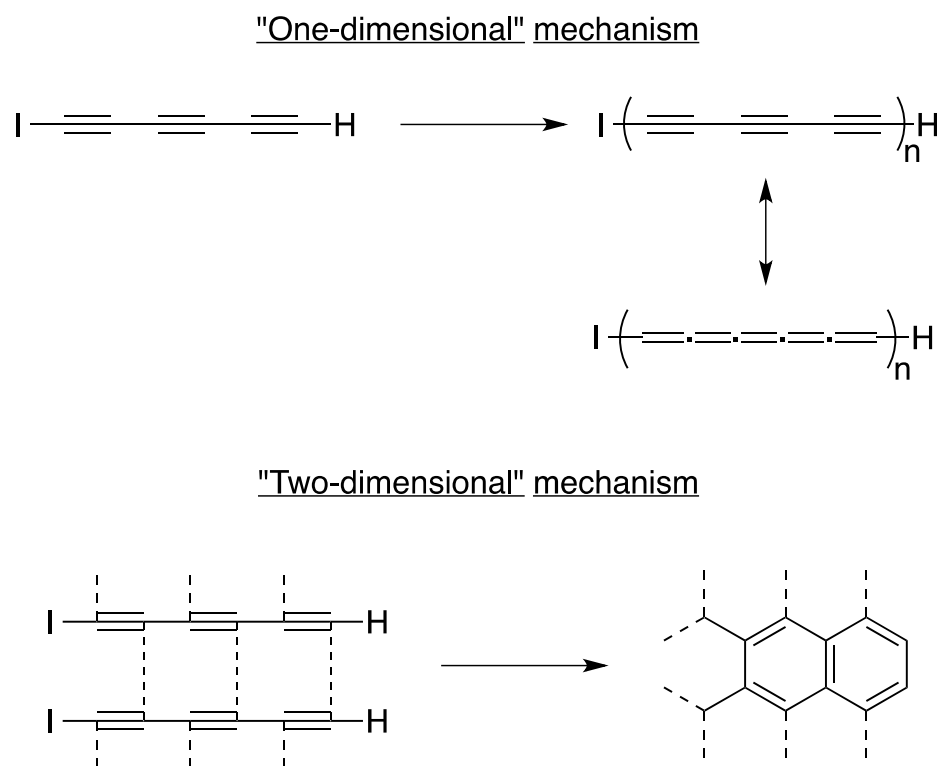


Figure 1.5. Suggested “one-dimensional” and “two-dimensional” mechanisms for the solid-state polymerization of 1-iodohexa-1,3,5-triyne at room temperature.¹⁸

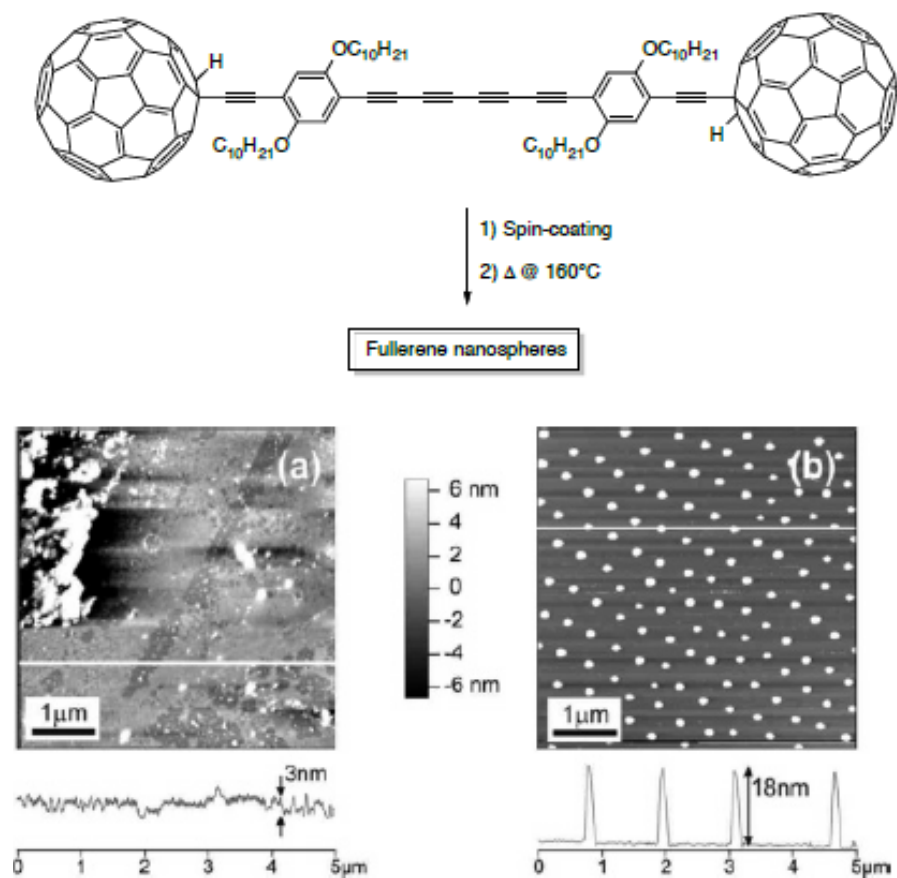


Figure 1.6. The “molecular dumbbell” used as starting materials for the preparation of carbon nanospheres (above) and AFM images of the “molecular dumbbell” before (a) and after (b) thermal annealing at 160°C for 1h.¹⁶ Copyright 2005 American Chemical Society

1.6.2 Carbon-Rich Materials From Self-Assembled Oligoynes

Using the knowledge acquired on the topochemical polymerization of oligoynes, researchers recently make a step further by preparing nanomaterials with precise sizes and shapes. Using supramolecular chemistry, oligoyne-containing building blocks possessing specific functional groups that allow intermolecular interactions can be assembled to form ordered arrays of molecules capable of reacting through topochemical polymerizations to stabilize the assembly.

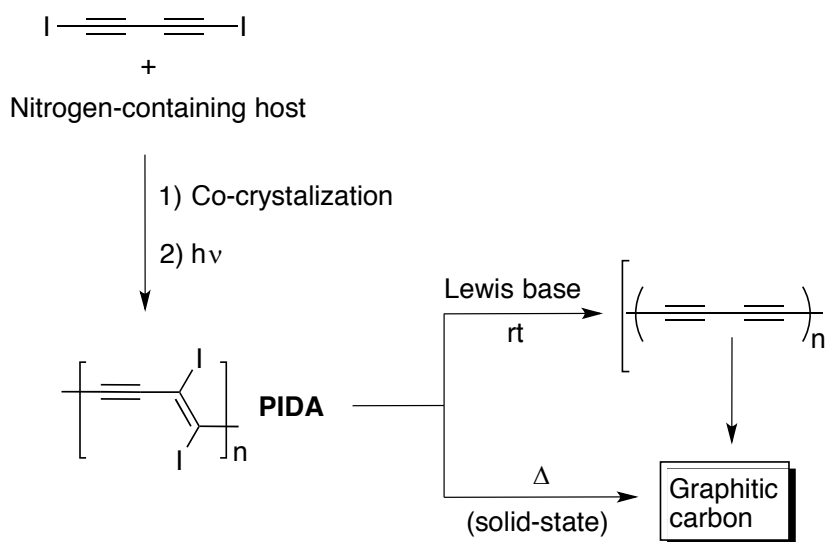


Figure 1.7. Preparation of graphitic carbon from readily accessible poly(diiododiacetylene) (PIDA).^{18,19}

One of the first attempts of the covalent fixation of a supramolecular assembly through topochemical polymerization was achieved on dehydrobenzo[*n*]annulenes (DBAs) that can assemble into tubular structures in the solid state depending on their functional groups substitution pattern. Moreover, DBA offers significant ring strain that can be exploited to make the butadiyne more reactive, thus driving the topochemical polymerization, although it was proved that solid-state packing is even more important than ring strain to drive this reaction.²⁰ The first attempts to cross-link butadiyne-containing macrocycles through topochemical polymerization was accomplished in 1974 by Baughman and coworkers and later on by Bloor on a macrocycle (CMA) with only one butadiyne unit as shown on.²¹

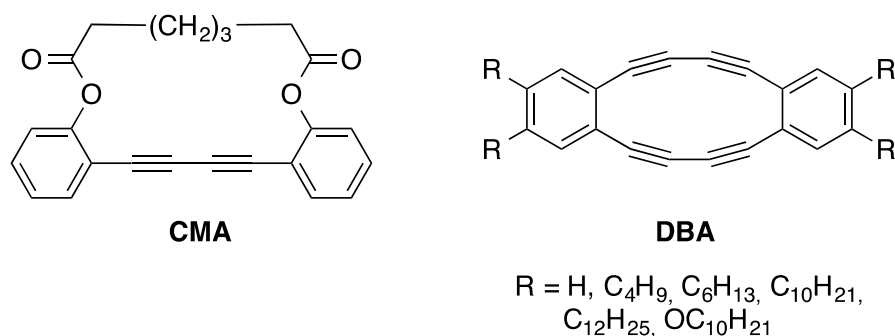


Figure 1.8. CMA and DBAs prepared by Baughman and Swager, respectively.²¹

Upon thermal annealing or exposure to UV or γ -ray irradiation, colorless crystals of CMA became deeply colored and the product formed was insoluble in organic solvents. The infrared and Raman spectroscopy and X-ray diffraction pattern clearly indicated that a PDA was formed from this macrocycle. However, there was no evidence of the formation of a tubular structure.

It was not until twenty years later that another attempt to obtain controlled polymerization of butadiyne-containing macrocycles to make nanotubes was reported. In 1994, Swager and coworkers prepared soluble macrocycles of the DBA family (Figure 1.8) and tested their reactivity upon heating by DSC analyses.^{21, 22} Interestingly, the apparent stability of the different DBAs depends on the substitution pattern on the phenyl groups. While electron-donating groups prevent the macrocycles from decomposing in ambient conditions, their hydrogen analogues decompose very rapidly at room temperature and exploded under gentle heating.²² DSC analysis reveals a very intense, exothermic sharp peak between 100 and 120°C when DBA bearing alkyl chains are heated and the ΔH values of these processes are in agreement with the values reported for the topochemical polymerization of butadiyne units.¹² However, infrared spectroscopy showed no evidence of PDA after the thermal process, suggesting that the starting DBAs did not undergo a typical 1,4-addition reaction. In fact, the polymerization reaction is rather random and intramolecular reaction to form a 6-5-6-5-6 fused ring system seemed to occur as well. This reaction has been tested in solution with molecular iodine as the electrophile to initiate the

reaction and yielded a tetraiodo-fused system that can be oxidized to a fused fluorenone upon exposure to oxygen.

A year after Swager's report, Vollhardt and coworkers showed that three-membered, one butadiyne-containing DBA underwent a clean topochemical polymerization to give a PDA.²³ The final PDA seemed to appear as nanotubes based on the packing mode of the DBAs as observed by X-ray diffraction. However, no experimental evidence proved the presence of such tubular structure. Two years after their initial report, the same group reported the preparation of onion- and tube-like closed-shell carbon particles from the explosive decomposition of four-membered DBAs, as shown in Figure 1.9.²⁴ While this DBA did not undergo a topochemical polymerization under UV irradiation, it literally exploded violently when heated under vacuum at 245°C with a flash of orange light, gas evolution (CH₄ and H₂) and the formation of a black powder. As shown on the TEM image on Figure 1.9, the carbon materials thus produced is made of graphitic onions and capped multi-walled CNTs. Although this method leads to useful carbon materials, it does not allow control over their sizes, shapes and properties. Haley²⁵ and Komatsu²⁶ have prepared other DBAs in order to test their reactivity upon heating. However, the materials obtained after thermal process were not characterized in detail.

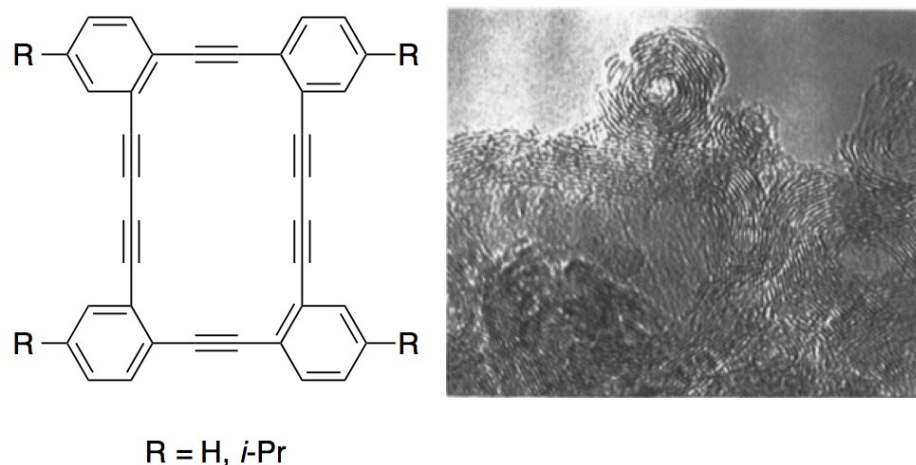


Figure 1.9. Vollhardt's DBAs and TEM image of the carbon materials obtained after their thermal decomposition.²⁴ Copyright 1997 American Chemical Society

In order to prepare more reactive macrocycles, Rubin and coworkers prepared nonbenzoannulated dehydroannulene macrocycles (Figure 1.10).²⁷ Benzoannulation is believed to have a stabilizing effect on the dehydroannulene scaffold in addition to hinder the reaction site. While the non-functionalized (R=H) and methyl acetate-decorated macrocycles did not stack properly to undergo topochemical polymerization, the methyl alcohol derivatives stacked properly in the crystal to create nanochannels of macrocycles in which the butadiyne moieties face each other due to the macrocycle's planar conformation. One could expect that upon polymerization, covalently linked organic nanotubes could be created. Despite the almost ideal conformation for the topochemical polymerization, the crystals of methyl alcohol-decorated macrocycles are stable under ambient conditions and start turning brown at 110°C. It is noteworthy that crystals of the non-functionalized macrocycles exploded very rapidly under ambient conditions due to close C-C contact and lack of solvent inclusion within the crystals. However, the materials produced from this explosion were not further characterized.

The group of Shimizu was the first to report the preparation of nanotubes using topochemical polymerization of butadiyne-embedded macrocycles.²⁸ Starting from a very simple butadiyne-containing macrocycles obtained in two steps, they were able to grow crystals in which the inter-macrocycles distance and tilt angle are close to the ideal values to allow topochemical polymerization, as shown in Figure 1.11. The choice of amide functions to drive the self-assembly into columns through H-bonding was motivated by their ability to provide structural parameters that are close to that required for the topochemical polymerization. As expected, the polymerization can be initiated upon thermal annealing (180°C for 12 h) or UV irradiation to afford dark purple/brown crystals that were insoluble in organic solvent suggesting the formation of PDAs. Beside the ideal structural parameters, the enhanced reactivity of this macrocycle can be attributed to the presence of a more flexible bonding environment nearby the butadiyne moieties, thus enabling conformational change within the crystal lattice. Although it leads to insoluble carbon-rich materials, this strategy proved that it was possible to obtain nanostructured materials from controlled topochemical polymerization.

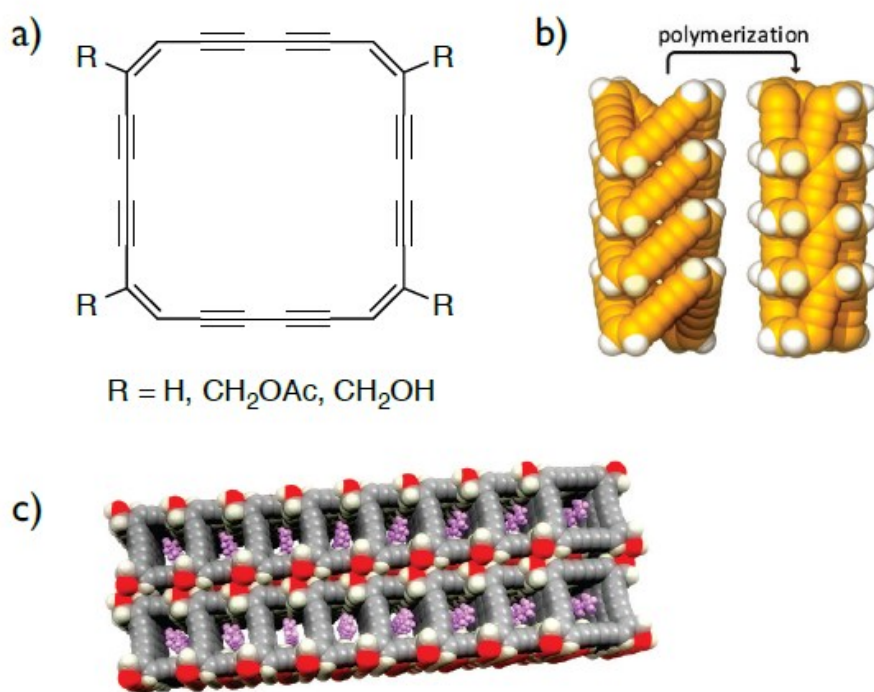


Figure 1.10. Structures of non-benzoannulated dehydroannulenes (a), schematic of a stack of the same macrocycle undergoing a topochemical polymerization (b) and the packing diagram of macrocycles where R = CH₂OH (c).²⁷ Copyright 2010 American Chemical Society

Two years after Shimizu's report, Fowler and coworkers also reported the preparation of nanotubes from similar macrocycles but again the nanotubes formed were not soluble enough to be further characterized.²⁹

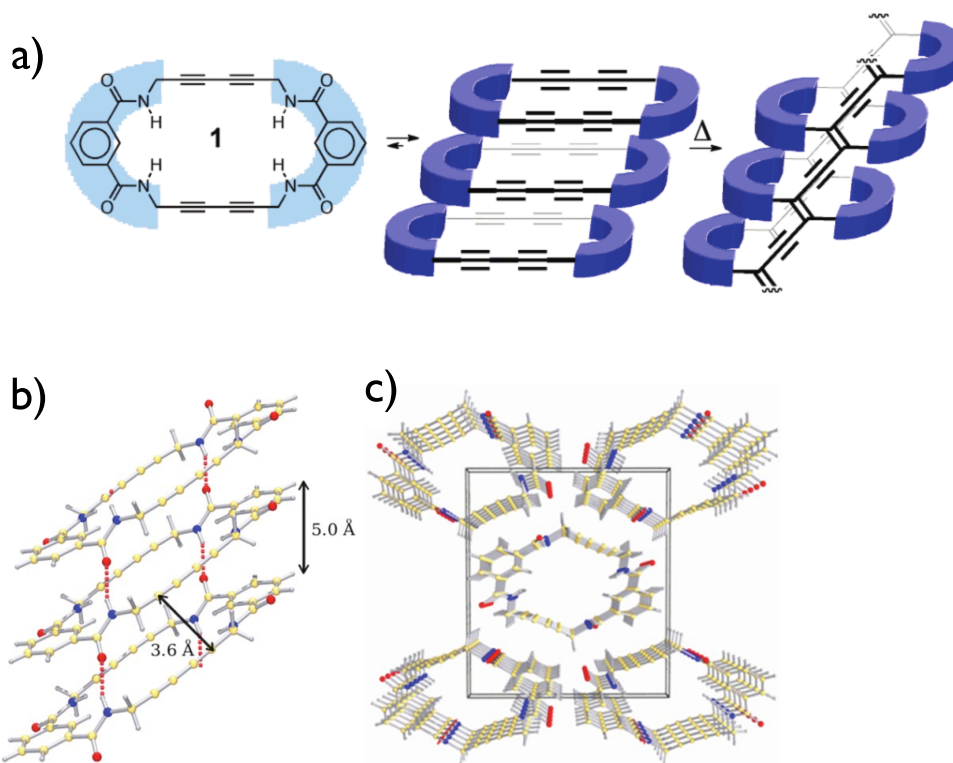


Figure 1.11. Structures (a) and X-ray crystal structure (b and c) of the butadiyne-containing macrocycle prepared by Shimizu and coworkers.²⁸ Copyright 2010 American Chemical Society

The topochemical polymerization of butadiyne can also be used to prepare semi-conducting, one-dimensional nanowires very efficiently. In this regard, Morin and coworkers recently demonstrated that a star-shaped molecule containing three butadiyne moieties could be used to prepare tens of nanometers-long nanowires.³⁰ The covalent interconnection between the PDA chains within a nanowire could be potentially use to extend the conjugation of PDA in the second dimension, thus decreasing its band gap. The absence of chromic properties for these nanowires proved that the PDA adopted a rigid and planar configuration.

In addition to nanotubes and nanowires, butadiyne-containing molecules can be used to prepare various types of nanoarchitectures and one of the most common and useful in nanoscience is nanoparticle. The first to apply the topochemical polymerization of oligoynes to the preparation of nanoparticles was Olesik's group.³¹ In order to obtain

spherical particles in the micrometers regime, they employed an emulsion polymerization using dibutyloctatetrayne as the carbon-rich source dissolved in poly(vinyl alcohol), using water as the continuous phase. After heating the suspension for 48 h at 80°C, the particles were isolated and heated at 800°C in a furnace to yield the final graphitized particles. The resulting particles can still be easily dispersed in various organic solvents, meaning that the pyrolysis step did not lead to aggregation between particles. Also, depending of the polymerization conditions, particles from few micrometers to few hundreds of micrometers were prepared. Interestingly, some of these spherical particles exhibit rather high porosity ($SA_{\text{BET}} = 611 \text{ m}^2/\text{g}$), making these particles potential candidates for gas storage and catalyst applications. Almost at the same time, the same group reported the preparation of much smaller carbon nanospheres by self-assembling an amphiphilic octatetrayne derivative in water that undergo a topochemical polymerization at 65°C.³² Surprisingly, the same suspension yield very thin films of carbon rather than nanospheres when it is kept at room temperature, meaning that various shapes of carbon materials can be obtained by carefully adjusting the kinetic parameters.

More recently, Morin and coworkers reported that an organogel of a tetrayne derivative could be polymerized to yield green fluorescent carbonaceous nanoparticles that are soluble in common organic solvents.³³ After purification by SEC, TEM images showed that polydispersity index of these nanoparticles was rather high with diameters ranging from 130 to 350 nm. In this case, the production of nanoparticles is quite surprising considering that the starting tetrayne organogel was made of long one-dimensional nanofibers. One would have expected a morphological retention upon polymerization as Olesik showed in case of emulsion polymerization. This nanofibers-to-nanoparticles transformation is not understood yet and did not occur when the xerogel rather than the organogel was irradiated. To the best of knowledge, this was first example of the preparation of carbonaceous nanoparticles at room temperature.

Hollow carbon nanospheres can also be obtained using the topochemical polymerization of oligoynes. Frauenrath and coworkers recently reported the preparation of such nanoarchitectures by using an amphiphilic hexayne derivative that spontaneously self-assembled into water to give vesicles whose walls can be stabilized covalently through

polymerization of the hexayne moieties (Figure 1.12).³⁴ The polymerization is conducted under UV irradiation at 1°C in water, proving the high reactivity of the hexayne moieties upon irradiation. In order to narrow the size distribution of these nanospheres, extrusion through a polycarbonate membrane can be performed, giving nanospheres with diameter of ca. 100 or 60 nm on average, depending on the pore sizes of the membranes. The main advantage of the low temperature process is the possibility of introducing biologically active molecules at the surface of the vesicles, opening the way to the use of this material in biochemical or sensing applications.

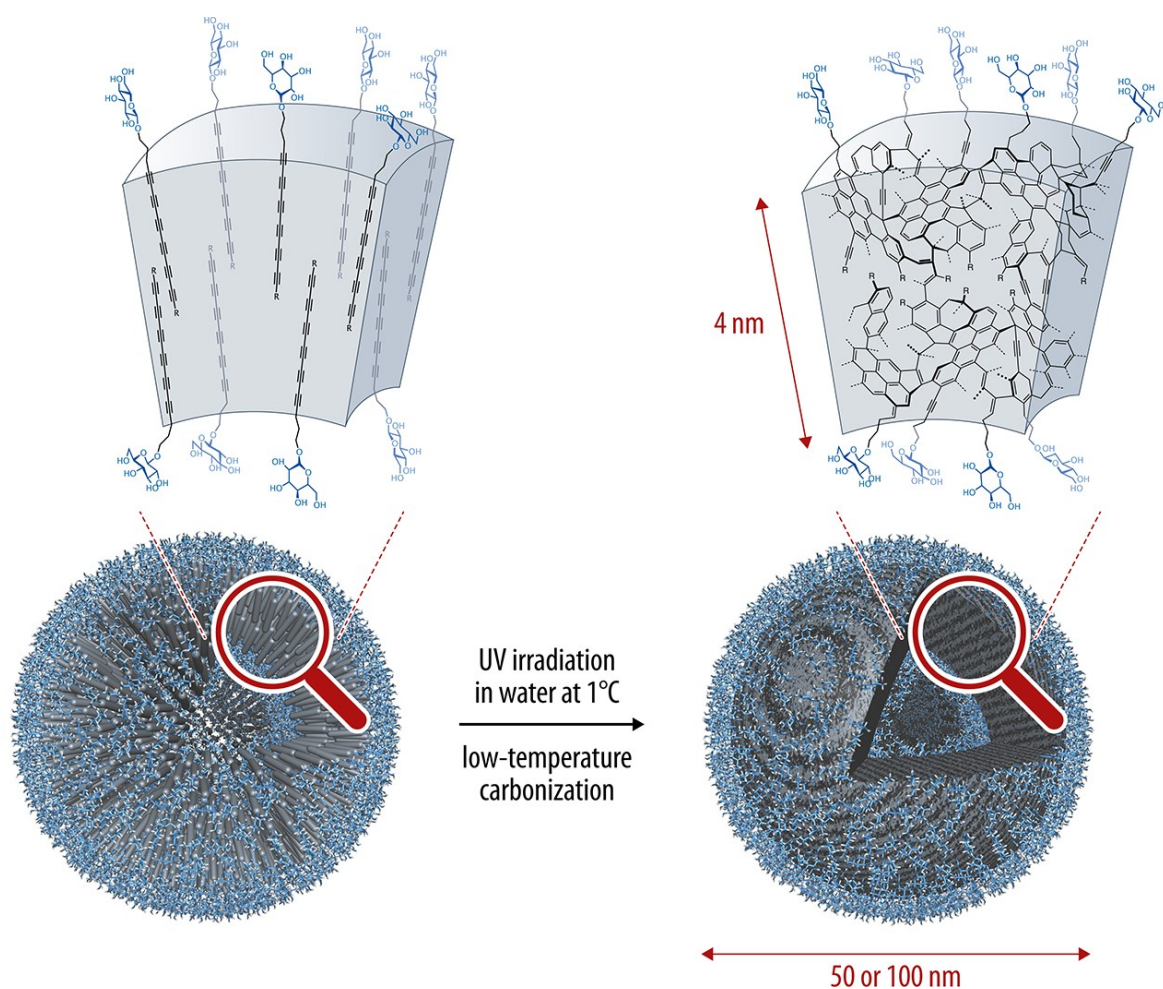


Figure 1.12. Preparation of hollow carbon nanospheres with controlled morphology through topochemical polymerization of an amphiphilic hexayne derivative.³⁴ Copyright 2012 American Chemical Society

1.7 Carbon-Rich Nanomaterials from Organometallic Precursors

Metal complexation with precursors possessing specific functionality has proved to be an interesting avenue toward nanostructured materials with new properties and their large-scale preparation. A particularly interesting method was developed using the affinity between cobalt complexes and alkynes leading to highly reactive organometallic complexes upon heating. In some cases, supramolecular chemistry can be used to guide the assembly of these complexes, leading to more interesting architectures.

1.7.1 Carbon-rich Nanomaterials From Cobalt-Encapsulated Dehydroannulene

In late 90s, Vollhardt and coworkers revisited their work (*vide supra*) on DBAs by increasing their reactivity through complexation of their alkyne moieties with an organocobalt compound. This was simply achieved by mixing a DBA and $\text{Co}_2(\text{CO})_8$.³⁵ Upon heating of the resulting complex, it was observed that the carbonization occurred at much lower temperature (200°C) than that required for the carbonization of cobalt-free DBA. TEM analysis on the powder obtained after the pyrolysis showed that even though carbonization already took place at low temperature, thermal treatment (800°C for 6 h in optimal cases) produced a much better yield of onions and multi-walled CNTs, graphitic and some amorphous carbon (Figure 1.13). In addition, dark spots can be noticed on carbon nanoarchitectures due to cobalt deposition on the sidewalls of the formed materials.

The observation of the high reactivity of Co-containing dehydroannulene when heated to undergo carbonization led to the synthesis of a complete family of new cobalt complexes.³⁶ With the synthesis of new macrocycles, it was possible to vary the sizes and properties of precursors in order to study the influence of these parameters on the materials resulting the thermal decomposition. For example, it was noted that, by introducing a ferrocenyl group in the dehydroannulene, molecular arrangement was modified and more ordered. Interestingly, the properties of explosive decomposition depended on supramolecular order and not from the intrinsic strain contained within the molecular structure.

The results obtained with dehydroannulene also bring research a step further by bringing the use pyrolysis of cobalt-alkyne complexes in the synthesis of CNTs and nano-onions in

grams scale. Vollhardt and coworkers showed that by using small molecules such as ethynylbenzene and diphenylbutadiyne as source of alkyne for the complexation of organocobalt compounds, it was possible to obtain a good amount of carbon-rich materials with a relatively good control over their structures and properties.³⁷ Moreover, addition of another carbon source such as fullerene and anthracene or catalysts such as $[\text{Ni}(\text{cod})_2]$ / tolane (1:1; cod = cycloocta-1, 5-diene) directly influenced the width, the length and the amount of nanotubes formed during the pyrolysis.

1.7.2 Carbon-rich materials from organometallic complexes of hexabenzocoronene and related structures

As previously demonstrated, the chemical nature of the carbon source is a crucial parameter for the control of the structural features of the resulting carbon nanomaterials. Thus, researchers investigated pyrolysis of molecules with different sizes and shapes to study the structure-properties relationship. Among the different families of reactive precursors used, *hexa-*peri**-hexabenzocoronenes (HBCs) are particularly interesting since it contains a high carbon/hydrogen ratio. In 2005, Müllen and coworkers reported the synthesis and pyrolysis of novel HBCs containing alkynes functionalities complexed with cobalt (see Figure 1.14).³⁸ By performing the pyrolysis of these materials (250°C for 3 h and 600 to 1000°C for 8 h), a black powder was recovered. SEM and TEM analysis revealed that the black residue was made of CNTs and bamboo-like structures with different aspect ratios. Moreover, these well-defined structures have been obtained in near-quantitative yield, meaning that this material was obtained without any production of amorphous carbons or other graphitic carbon nanostructures such as onions. The nanotubes and bamboo-like structures have showed diameters of about 33 ± 2 nm and inner diameters of about 16 ± 1 nm. TEM analysis also revealed that higher pyrolysis temperatures lead to more ordered nanotubes walls. It is also important to mention that the cobalt content in the precursors is mainly found at the tips of the nanotubes, as it is the case for CNTs produced through the CVD process.

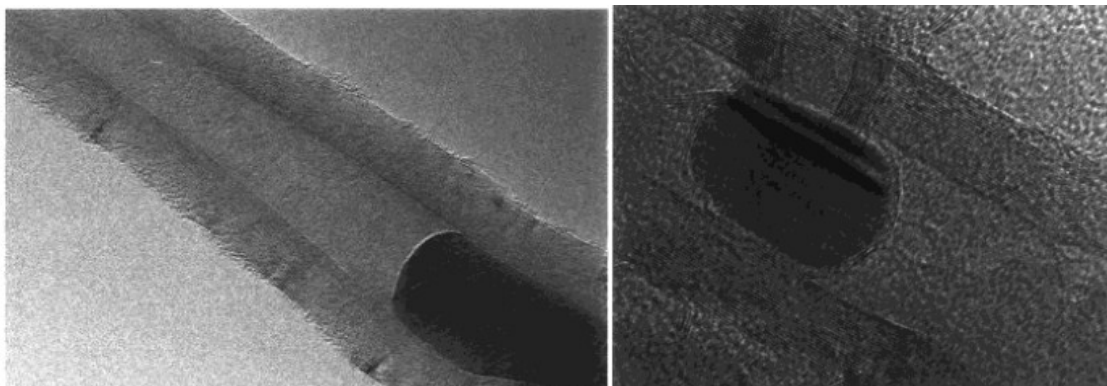


Figure 1.13. TEM images of CNTs containing crystalline cobalt from dehydroannulene cobalt complexes.³⁵ Copyright 1999 American Chemical Society

In order to demonstrate the versatility of the solid-state pyrolysis using disk-like molecules and to demonstrate the importance of the precursor's structure on the final nanoarchitecture, Müllen and coworkers carried out the pyrolysis of several different compounds.³⁹ Generally, CNTs have been obtained by pyrolysis of molecules with graphenic structure in high yields. In addition, by reducing the cobalt/carbon ratio in the precursor, a larger amount of CNTs was obtained. Alternatively, by performing the pyrolysis of materials with a non-graphenic, linear structure, carbon nanorods were obtained. Instead of cobalt, ruthenium complex could also be used. The major difference with these complexes is the attachment point onto the molecules. With ruthenium, the metal is positioned over a π -electrons system (face-on) rather than on a specific functional group. With these complexes, larger nanorods and a significant amount of graphitic materials were obtained, demonstrating the importance of the position and the nature of the metal in the pyrolysis process.

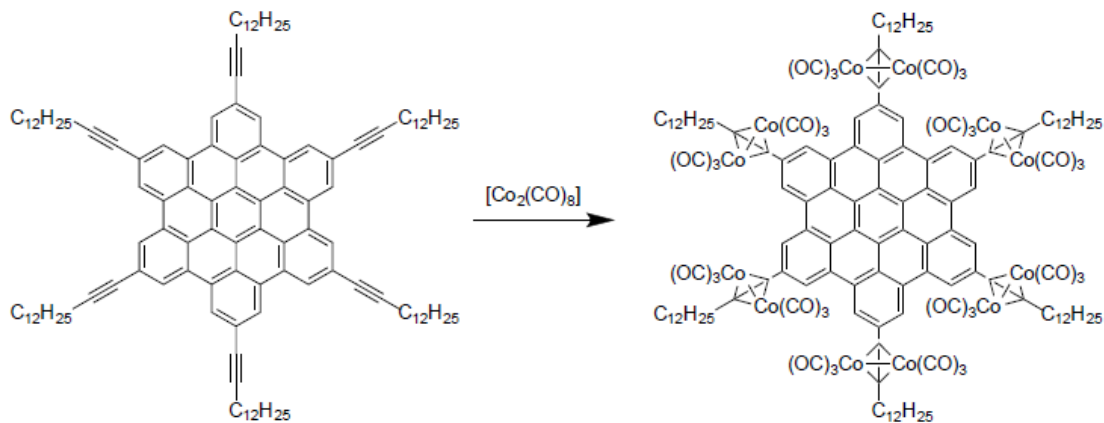


Figure 1.14. HBC-Co complex leading to carbon nanomaterials upon pyrolysis.³⁸

Given that solid-state pyrolysis can lead to well-defined nanoarchitectures, synthesis of CNTs doped with nitrogen was carried out in order to obtain nanoarchitectures with improved electronic properties. To do this, the pyrolysis of metallo phthalocyanine derivatives, easily accessible, was realized.⁴⁰ Pyrolysis of cobalt and iron phthalocyanines at different temperatures led to metal/organic hybrids nanowires and nanotubes with well-defined parameters. TEM analysis showed the presence of multi-walled CNTs with diameters of 20 to 60 nm and a wall thickness of 5 to 10 nm. In addition, the presence of some notable shaded area indicated twists in the structure, suggesting the introduction of five and seven membered cycles in the graphitic structures. Also, the presence of cobalt and iron crystals as well as 2 to 4% pyridine-like molecules within the final carbon-rich materials had also been observed.

1.7.3 Carbon-rich materials from polymeric organometallic precursors

Carbon-rich polymers are also interesting precursors for the preparation of carbon nanomaterials, although they are only few examples reported in the literature. Reported in 2005 by Müllen and coworkers, the pyrolysis of polyphenylene dendrimers, a particularly rigid class of macromolecules, proved to be a very efficient method to obtain CNTs, nanospheres and nanorods.⁴¹ Given the monodispersity of the dendrimer unit and ease of complexation between peripheral functions and organocobalt compound, pyrolysis yields are generally excellent. By heating polyphenylene dendrimer/cobalt complexes at 160°C, large nanorods (size from 200 to 500 nm) can be obtained. Using this same organometallic

complex but by subjecting it to a fast pyrolysis, it is possible to make hybrid carbon/cobalt nanoparticles rather than nanorods. When the heating rate is slow, CNTs can be obtained. This significant difference in the nanostructures obtained from the same carbon-rich precursor illustrates the importance of pyrolysis conditions on the final structure.

In a similar trend, Bunz and coworkers reported the synthesis of carbon/cobalt nanospheres through pyrolysis of a specific cobalt-containing poly (*p*-phenyleneethynylene).⁴² By heating the hybrid polymer, large microspheres, with sizes up to 0.03 mm, were obtained. However, smaller microspheres with size averaging 1.8 microns with a narrow size distribution can be prepared.

Ferrocene derivatives are particularly interesting organometallic compounds to induce carbonization of carbon-rich precursors since it allows the preparation of hybrid carbon/iron nanoarchitectures. Generally used as catalyst and/or as feedstock in the synthesis of CNTs by CVD, π -extended ferrocenyl complexes could directly lead to well-defined carbon nanomaterials upon pyrolysis.⁴³ Major part of the collected material appeared as nanocapsules, sometimes filled with Fe and P from starting precursors, having an average diameter of 100 nm, an average wall thickness of 16 nm and a length varying from 220 to 700 nm with no other amorphous carbon by-products. This result suggested that a near-quantitative yield of nanocapsules was obtained.

Synthesis of multi-walled CNTs containing iron nanoparticles was also achieved by pyrolysis of butadiynyl-ferrocene-containing compounds.⁴⁴ The pyrolysis reaction was followed by TGA and the formation of nanotubes occurs at around 700°C. TEM analysis shows the formation of carbonaceous materials as a complex assortment of randomly oriented multi-walled CNTs with metal nanoparticles and a small amount of amorphous carbon scattered throughout the sample. It has been shown that the mechanism of formation of multi-walled CNTs occurs from the thermal decomposition of the ferrocene units, which initially produces Fe atoms that act as a seed for the multi-walled CNTs formation. In fact, the aromatic units in the precursor interact with the Fe Atoms to form carbon-containing nanoparticles such as Fe₃C, which appear to be a precursor to the multi-walled CNTs. Pyrolysis of such compound therefore leads to production of multi-walled CNTs at much lower temperatures than that used in the CVD method.

The formation of carbon-rich nanostructured materials allows the production of new materials with very interesting properties. In the field of molecular electronics, hybrid materials are particularly interesting for the preparation of new types of electrodes. More precisely, theoretical calculation showed that nanostructured materials containing tin could present interesting properties as electrode materials. Müllen and coworkers reported the encapsulation of tin in a carbon matrix for the first time in 2008.⁴⁵ Their strategy relied on the pyrolysis of carbon/organotin complexes, more precisely allyltriphenyltin (ATP-Sn), a particularly reactive reagent in polymerization reactions. When heated at 700°C, a black powder is produced and XRD and TEM analyses revealed that tin nanoparticles encapsulated in a carbon matrix with sizes ranging from 2 to 10 nm was produced. These new materials have also shown interesting properties for lithium storage battery.

A very recent approach reported by Müllen and coworkers uses the formation of an organometallic complex on the surface of graphene with the aim to further grow CNTs (Figure 1.15).⁴⁶ To perform the *in situ* synthesis of such carbon nanoarchitectures, the authors had the idea of using the post-functionalization of graphene followed by insertion of alkyne-containing molecules capable of forming cobalt complexes. These cobalt complexes can then serve as seed for growing CNTs. To verify the presence of alkyne on graphene sheet prior to pyrolysis, IR spectroscopy was used and revealed the presence of strong absorption bands associated to alkyne functionalities. Complexation of cobalt was made by mixing the functionalized graphene with $\text{Co}_2(\text{CO})_8$. After being extensively rinsed with THF, the resulting powder was used as a precursor in CVD fed by a mixture of $\text{CH}_2/\text{H}_2/\text{Argon}$. TEM analysis of the resulting material clearly demonstrated the presence of CNTs on the graphene sheet, which is due to carbon growing on the complexed cobalt onto the graphene layer. Interestingly, the CNTs are randomly and horizontally stacked between the graphene layers. Such graphene/CNT composite materials are expected to be promising electrode materials in various energy storage devices.

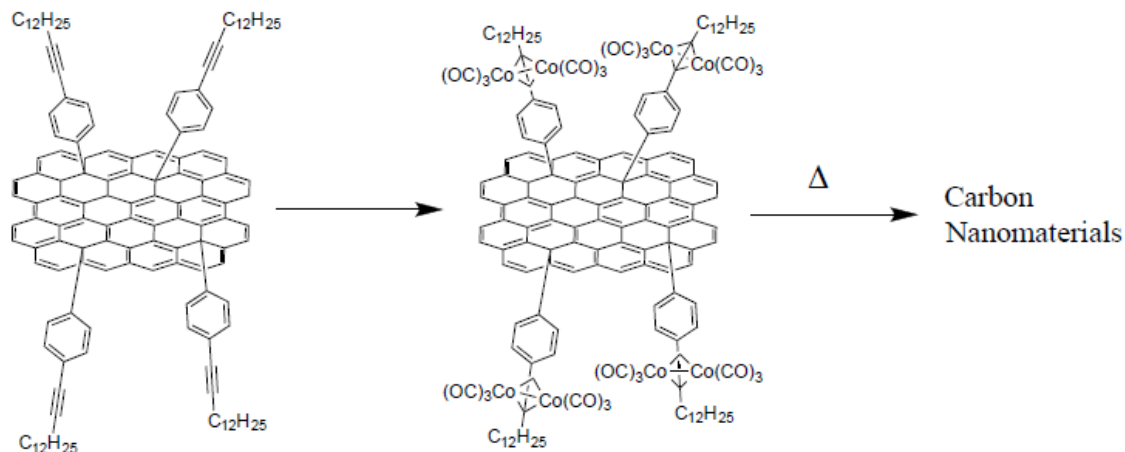


Figure 1.15. Cobalt-containing graphene layer to graphene/CNTs composite film.⁴⁶

1.8 Carbon-Rich Materials from Hexabenzocoronene (HBC) and Polymer Precursors

Polymers organizing in interconnected 3D networks can also be used as reactive precursors, with the potential advantage of leading to porous carbon networks once pyrolyzed. The 3D structure already present before the formation of carbon nanomaterials can also be modified or controlled by the polymerization method used, choice of monomers and chemical modifications. In addition, pyrolysis of these molecules generally gives high rate of carbonization and pyrolysis yields. Despite the need to conduct pyrolysis, unlike some approaches previously discussed with oligoynes, temperatures required to obtain such nanomaterials are relatively low, which makes this method more accessible than what is generally used for the synthesis of such materials.

In 2002, Müllen and coworkers reported the use of hexa-*peri*-hexabenzocoronenes (HBCs) as high molecular weight precursors without metal complexation for the preparation of carbon nanomaterials.⁴⁷ These molecules, because of their disc shape, have very interesting liquid crystalline properties, which provide a very organized 3D structure. This arrangement was used to pre-orient the molecules before performing a pyrolysis at relatively low temperature. After heating to the mesophase transition temperature in order to form a highly ordered and stable columnar mesophase, the material was heated to 400°C. MALDI-TOF mass spectrometric analysis showed partial oligomerization and revealed that

it occurs in two steps, which are 1) preferential cleavage of the alkyl bonds and formation of free radicals followed by 2) an intermolecular cross-linking. It is important to note here that the aromatic nature of the HBCs and most of the alkyl chains remain intact during the oligomerization at 400°C. Following this first stage of pyrolysis, a final pyrolysis at 800°C was achieved. Carbonization occurred at this temperature and led to a mixture of nanostructured carbon nanomaterials, including carbon nanospheres (with diameter ranging from a few hundred nanometers to 2 μm), carbon microfibers (up to 10 μm in cross section, with a peculiar bamboo-like shape) and bundles of carbon nanowires (Figure 1.16). This study also highlighted the importance of the heating steps, choice of substrate on which pyrolysis takes place and on the alkyl substitution pattern on HBC precursors over the resulting structure of resulting carbon nanomaterials.

To increase control over nanoarchitectures obtained after pyrolysis of HBCs, Müllen and coworkers also performed pyrolysis of the same precursors in a porous alumina membrane.⁴⁸ The trapping and confinement of these large molecules inside mesopores promotes π -stacking and allows the formation of a rigid three-dimensional structure, as in the formation of a liquid crystalline mesophase. After pyrolysis (up to 900°C), formation of graphitized nanotubes exactly the same diameter as the original mesopores was observed. After full removal of the template, single CNTs with lengths of several to tens of microns were obtained. The average outer diameter is about 100 nm and the wall thickness is around 20 nm. HRTEM measurements on the resulting CNTs showed structured graphitic walls formed of highly ordered graphene layers with a layer-to-layer distance of about 0.34 nm.

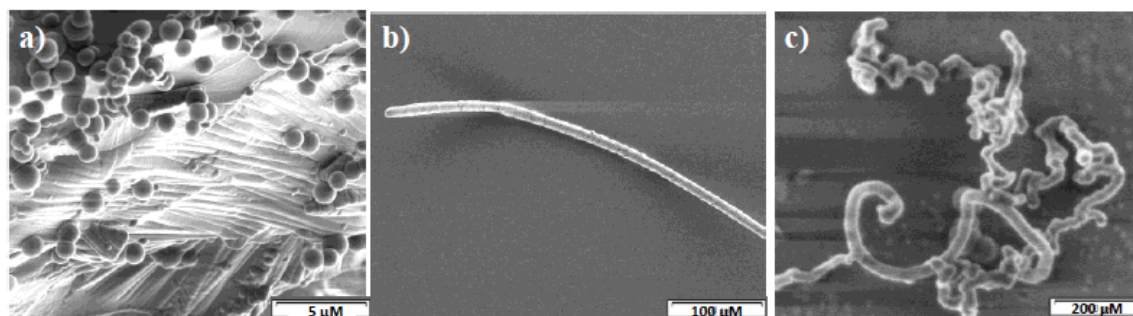


Figure 1.16. SEM images of a) carbon nanospheres (scale bar 5 μm) b) carbon microfibers (scale bar 100 μm) and c) bundles of carbon nanowires (scale bar 200 nm) formed after

pyrolysis at 800°C of HBCs precursors in an ordered mesophase.⁴⁷ Copyright 2002 American Chemical Society

More recently, the same group used a polymer network made of 1,3,5-tris-2'-biphenylbenzene and different cross-linker co-monomers (1,4-diethynylbenzene or 4,4'-diethynylbiphenyl) to obtain highly cross-linked, high molecular weight polymers.⁴⁹ In addition, because of its rigidity and twisted 3D structure, 1,3,5-tris-2'-biphenylbenzene prevents the formation of tightly packed polymer chains and allows the formation of well-defined 3D structures. When these polymers are precipitated from solution, long tubular assemblies with open ends and diameters ranging from 250 to 400 nm and wall thickness between 50 to 100 nm, were formed. Pyrolysis at 600°C was achieved to graphitize the structures with full retention of the structure morphology. The porosities of the materials obtained was measured and very high specific surface areas (up to 900 m²/g) were obtained, opening the way for their use as electrodes materials in electrochemical double layered capacitor (EDLC).

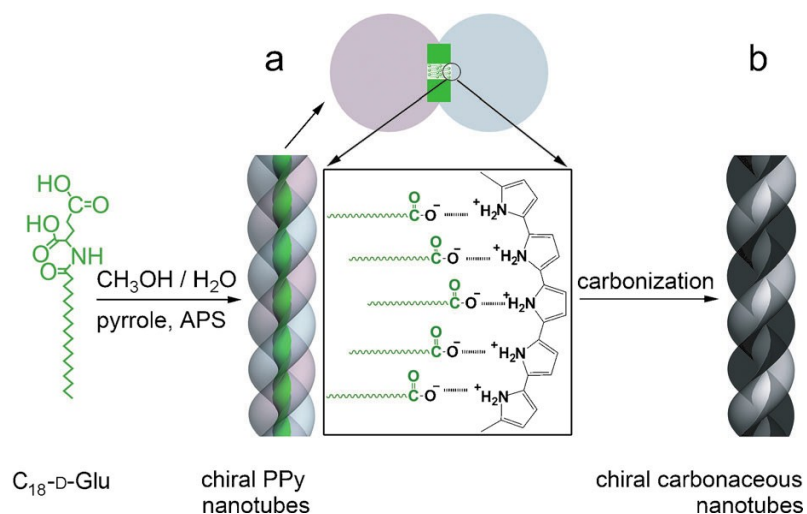


Figure 1.17. Synthesis of chiral polypyrrole nanotubes and CNTs. a) polypyrrole nanotubes prepared by self-assembly of C18-d-Glu (template) with ammonium persulfate (APS) as initiator and b) carbonaceous CNTs prepared by carbonization of polymeric nanotubes under an Ar atmosphere.⁵⁰ Copyright 2013 Wiley

Control of chirality can also be obtained through proper templating of carbon-rich precursors. In this regard, the group of Che and coworkers reported the synthesis of nanotubes with a partially graphitized enantiopure structure (Figure 1.17).⁵⁰ Using a self-assembled polypyrrole derivative forming helical nanotubes, those were heated to form carbonaceous structured architectures. Interestingly, conservation of helical tubular structure was observed, despite the use of high temperature (up to 950°C). The supramolecular self-assembly step was directed by the electrostatic interaction between polypyrrole and an amphiphilic chiral enantiopure *N*-acylamino acid molecules. Then, a subsequent polymerization of the pyrrole units was achieved. The nanotubes present unique optical properties and enantiomeric purity. These properties are also observed after pyrolysis, leading the way for the synthesis of enantiopure nanotubes, which are very difficult to prepare using traditional CVD methods. These materials also present high reversible storage capacity of lithium ions.

Although research on carbon nanomaterials has been a hot topic for a while, research on hybrid methods between all-organic and physical strategies to prepare them is still in its infancy. Alkyne-containing molecules, because of their high reactivity toward physical stimuli, proved to be promising building blocks when self-assembled to prepare carbon nanomaterials of various sizes and shapes. Using oligoynes derivatives, nanotubes, nanoparticles, nanovesicles, nanowires and other nanostructures have been prepared. As demonstrated in this review, the advantage of these precursors (Sections 2 and 3) compare to other non-alkynylated derivatives (Sections 4 and 5) is the possibility to conduct chemical transformations towards carbon nanomaterials at relatively low temperatures, often below 300°C. This is particularly important when carbon nanomaterials have to be grown on temperature-sensitive surfaces used in the electronics industry (silicon for example). Moreover, low temperature processes are expected to provide a better control over the size and shape of the final nanomaterials through morphological retention of the initial assemblies of reactive precursors. Low-temperature processes are also compatible with the introduction of functional groups to provide the newly formed carbon nanomaterials with unique properties.

Nonetheless, significant amount of work still need to be done in order to extend even more the scope of this strategy and to make it a real useful method that materials scientists will use on a regular basis to prepare carbon nanomaterials. For now on, the hybrid strategy showed great promises towards the preparation of well-defined carbon nanomaterials. The fact that the sizes and shapes of carbon nanomaterials can be controlled by the organization mode of the reactive precursors is probably the most important intrinsic advantage of the hybrid methods over the physical ones and many examples of that have been presented in this review. However, the hybrid methods do not offer an alternative to traditional physical methods for the large-scale production of materials yet. Before hybrid methods become the benchmark of carbon nanomaterials production methods, several requirement need to be fulfilled:

- 1) Low-cost, expeditious synthesis of reactive precursors;
- 2) Efficient and reproducible self-assembly of these precursors;
- 3) Morphological retention of the assemblies during the carbonization process to prepare on-demand, specific nanostructures;
- 4) Clean conversion to well-defined carbon materials with minimal side reactions;
- 5) Modulation of the properties of the carbon nanomaterials through variation in the chemical composition of the precursors.

Although these challenges will certainly take time to be overcome, one can expect that the increasing number of research team working to tackle these problems will accelerate the pace of discoveries in this area and that large-scale production of carbon nanomaterials using hybrids methods will arrive sooner than later.

1.9 Objectifs des travaux

Dans le cadre des présents travaux de thèse, plusieurs objectifs sont visés. Premièrement, le développement d'une nouvelle approche pour la synthèse contrôlée de nanoarchitectures

bien définies est visé. Pour ce faire, nous proposons d'utiliser la réaction topochemique de polymérisation des unités diyne pour former des polydiacétylènes. Par cette méthode, il sera possible, dans un premier temps, d'assembler différents monomères de façon supramoléculaire pour, par la suite, utiliser la polymérisation afin de réticuler l'assemblage vers un assemblage entièrement covalent. Un second objectif du projet présenté est la synthèse de nanotubes organiques en utilisant un précurseur réactif macrocyclique. Étant donné l'importance des nanotubes en science des matériaux, la synthèse contrôlée de ces nanomatériaux est souhaitable. Les méthodes physiques et chimiques présentement utilisées possèdent plusieurs lacunes (voir figure 1.1) ce qui ouvre la porte à l'approche hybride pour obtenir des nanotubes de façon contrôlée. Finalement, un dernier objectif principal du projet de recherche est l'élaboration d'une stratégie pouvant permettre l'utilisation des nano-architectures de polydiacétylènes vers la synthèse de nanomatériaux entièrement constitués de carbone. Cet objectif représente le dernier pas à franchir vers l'obtention de nanotubes de carbone et de graphène de façon bien définie.

Au départ, nous proposons d'utiliser la réactivité des alcynes comme force motrice vers la formation de nanomatériaux. Les alcynes, comme il a été démontré en introduction, représentent un groupement réactif et facile à insérer synthétiquement. La chimie des alcynes est bien connue et les couplages carbone-carbone nécessaires à leur installation sont des réactions polyvalentes et efficaces. Les groupements alcyoniques et diyne représentent des précurseurs de choix vers les nano-architectures car ils peuvent également mener aux polydiacétylènes, chaînes polymériques que nous proposons d'utiliser comme liens entre les divers constituants des architectures supramoléculaires.

Il est important de mentionner que l'utilisation des polydiacétylènes comme chaîne pour la réticulation intermoléculaire n'est pas fortuite. Comme il a été présenté dans les pages précédentes, cette unité possède plusieurs avantages comme la facilité de préparation sans catalyseurs et sans réactifs précis. Cette unité possède également une bonne stabilité et est facilement caractérisable par les techniques spectroscopiques usuelles. De plus, le majeur avantage est que les polydiacétylènes représentent d'intéressants précurseurs vers les composés graphitiques, ce qui peut mener à l'obtention de matériaux riches en carbone directement à partir des nano-architectures de PDAs obtenues. Ultimement, l'approche

présentée dans cette thèse permettra d'effectuer un choix précis du monomère de départ, et ainsi augmenter le contrôle possible sur les architectures finales.

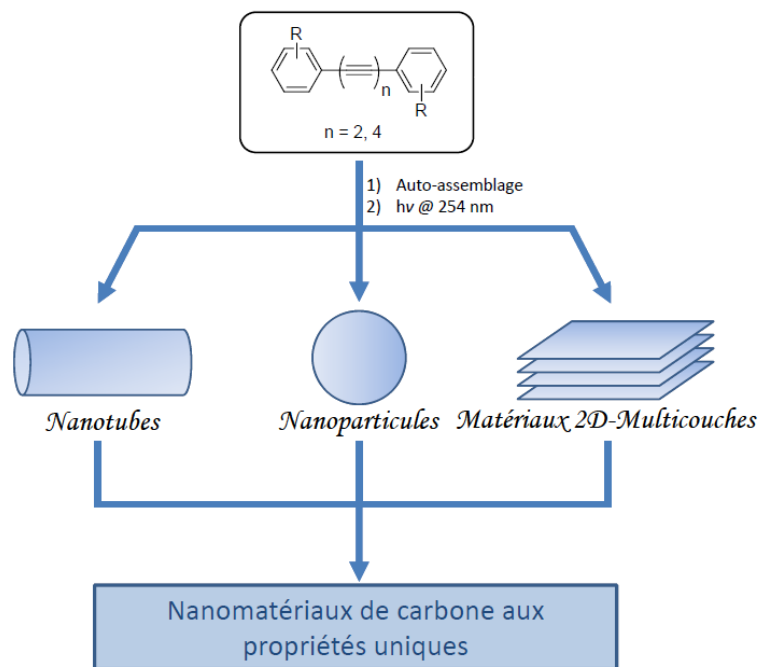


Figure 1.18. Approche générale proposée vers l'obtention de matériaux riches en carbones

Dans la littérature, la formation de polydiacétylènes est généralement obtenue à l'état cristallin. En contrôlant les paramètres et conditions de cristallisation, il est possible d'obtenir un empilement moléculaire possédant les paramètres nécessaires à la polymérisation topochemique des unités diyne. Cette approche est particulièrement intéressante étant donné l'importante efficacité de la réaction de polymérisation, ce qui mène généralement à de bons rendements. Cependant, la cristallisation de quantités importantes de molécules reste très difficile et peut prendre beaucoup de temps. Une approche différente, basée sur les interactions supramoléculaires afin d'obtenir les paramètres requis pour la polymérisation des unités diyne est donc souhaitable et pourrait permettre l'obtention de quantités plus importantes de polydiacétylènes et ce, beaucoup plus rapidement. Afin d'éviter la polymérisation à l'état cristallin, nous proposons donc d'utiliser l'état gel. L'état gel, un état semi-ordonné, représente une avenue intéressante

étant donné sa facilité de préparation. De façon plus précise, un gel représente un état semi-ordonné majoritairement composé d'un solvant emprisonné dans un réseau tridimensionnel complexe. Ainsi, lorsqu'une molécule forme un réseau supramoléculaire ordonné sous l'influence de diverses interactions, les molécules de solvant peuvent s'insérer dans ce réseau créant par le fait même une matrice ordonnée, majoritairement constituée de micro et nanofibres enchevêtrées. Cette organisation semi-solide confère au gel certaines propriétés mécaniques mais la résistance est très dépendante de plusieurs facteurs comme la température, la concentration du gélateur, le réseau supramoléculaire, etc. Un gel se caractérise également par la nature du solvant utilisé. On parlera donc d'organogel lorsqu'un solvant organique sera utilisé avec un gélateur ainsi qu'un hydrogel lorsque ce solvant sera de l'eau. Dans ce projet, nous proposons l'utilisation d'organogel étant donné l'insolubilité des molécules utilisées dans l'eau. Contrairement à l'état cristallin, l'état gel est un état pouvant s'adapter à différents paramètres structuraux. Ainsi, lorsqu'un changement d'organisation se produit, la matrice peut se réorganiser et ce, sans perdre les propriétés mécaniques et structurelles de départ. Cela représente donc un grand avantage des gels par rapport aux cristaux en tant que gabarit pour des réactions topochimiques. De plus, de plus grandes quantités de matériaux peuvent être préparées ce qui constitue un autre avantage majeur. Il est également important de mentionner que dans le cadre de ce projet, nous parlerons d'état gel et de gel partiel. Cette différence résulte seulement d'une caractérisation qualitative des propriétés mécaniques.

Dans la littérature, plusieurs molécules possédant différentes fonctions précises et des unités diynes ont pu être polymérisées directement à l'état gel pour obtenir des PDAs. Pour ce faire, différents substituants favorisant un état gel sont introduits sur les monomères comme des fonctions amide (pont hydrogène), des chaînes aliphatiques (interactions van der Waals) ainsi que des noyaux aromatiques (interactions π - π). Nous proposons donc d'incorporer ces éléments à notre design pour favoriser l'empilement supramoléculaire des macrocycles et monomères à l'état gel, ce qui pourra permettre leur photopolymérisation sur de plus grandes quantités.

Suite à l'élaboration et au contrôle de la réaction topochimique de polymérisation des unités diynes, il sera possible de passer à l'objectif principal de ces travaux qui est

d'utiliser l'approche décrite précédemment pour l'obtention de nanotubes organiques rigides. Pour ce faire, nous proposons d'utiliser un monomère bien défini : les macrocycles de type phénylacétylène (PAMs). Ces macrocycles possèdent premièrement une large cavité interne pouvant permettre la formation de tubes et possèdent une rigidité intrinsèque. De plus, étant donné la présence de fonctions diynes internes, la polymérisation topochimique des diacétylènes pourra être utilisée sans modifications majeures des macrocycles. La synthèse des PAMs est également bien connue, ce qui permettra le contrôle bien précis des substituants afin de favoriser la gélification des macrocycles en nanotubes supramoléculaires pouvant être par la suite réticulé. Afin de favoriser l'empilement supramoléculaire, des fonctions amides seront introduites au squelette des macrocycles. Ces amides permettront la formation de liaisons hydrogène intermoléculaires qui pourront également diriger les macrocycles les uns par rapport aux autres afin d'obtenir un assemblage bien structuré possédant les paramètres requis pour la réaction de réticulation. Afin de favoriser la polymérisation, nous proposons également d'incorporer en tête des macrocycles des unités diynes aliphatiques qui permettront la formation de liaisons intermoléculaires à l'extérieur des macrocycles. Ces substituants augmenteront donc le rendement de polymérisation étant donné leur plus faible rigidité (degrés de liberté augmentés). Une fois la synthèse des nanotubes covalents réalisés, une caractérisation complète des architectures sera effectuée en utilisant différentes techniques comme la spectroscopie UV visible, la spectroscopie Raman et la diffraction des rayons X. Finalement, la présence des structures tubulaires sera confirmée par microscopie électronique à transmission (TEM) et à balayage (SEM). Suite à l'obtention des macrocycles, une optimisation des paramètres sera effectuée afin d'augmenter la polyvalence de notre approche. Premièrement, l'effet de la configuration de la fonction amide pourra être évalué. Cette configuration joue un rôle crucial dans la formation des liaisons hydrogènes et influencera directement la polymérisation des unités diynes. Il sera aussi possible d'incorporer des fonctions supplémentaires aux macrocycles comme des chaînes polaires favorisant l'assemblage supramoléculaire. Finalement, la modulation de la cavité interne finale pourra être effectuée en utilisant des monomères plus larges comme les macrocycles de type phénylènebutadiynylène (PBMs)

Afin d'aller un pas plus loin vers la synthèse contrôlée de nanotubes entièrement constitués de carbone, nous proposons également d'effectuer la pyrolyse des nanotubes organiques obtenus par l'approche proposée. Les polydiacétylènes sont connus pour procéder à une cycloaromatisation par exposition à différents stimuli comme la chaleur, etc. Ainsi, nous croyons qu'en effectuant la pyrolyse des nanotubes, il sera possible de faire réagir les polydiacétylènes des nanotubes pour complètement aromatiser la structure, ce qui devrait mener à l'obtention de nanotubes entièrement faits de carbone. Ces nanotubes auront, comme avantage, de posséder une structure bien définie ce qui peut être difficile d'obtenir par les méthodes traditionnelles de synthèse des nanotubes de carbone.

Le projet de recherche présenté dans le cadre de cette thèse est donc un projet qui pourra mener à l'obtention de nouvelles architectures riches en carbone de manière bien contrôlée. La réalisation de ces objectifs ouvrirait la porte à une nouvelle méthodologie de synthèse de nanotubes et autres architectures aux nouvelles propriétés pouvant trouver des applications diverses en science des matériaux.

1.10. Références

- [1] A. Hirsch, *Nat. Mater.* 2010, **9**, 868; E. H. L. Falcao and F. Wudl, *J. Chem. Technol. Biotechnol.* 2007, **82**, 524.
- [2] M. S. Dresselhaus, G. Dresselhaus and P. C. Eklund, *Science of Fullerenes and Carbon Nanotubes*, Ed.: Academic Press, San Diego, 1996.
- [3] O. Zhou, H. Shimoda, B. Gao, S. Oh, L. Fleming and G. Yue, *Acc. Chem. Res.* 2002, **35**, 1045.
- [4] T. N. Hoheisel, S. Schrettl, R. Szilluweit and H. Frauenrath, *Angew. Chem. Int. Ed.* 2010, **49**, 6496; E. T. Chernick and R. R. Tykwinski, *J. Phys. Org. Chem.* 2013, Early View, DOI: 10.1002/poc.3160.
- [5] M. M. Boorum, Y. V. Vasilev, T. Drewello and L. T. Scott, *Science* 2001, **294**, 828; L. T. Scott, M. M. Boorum, B. J. McMahon, S. Hagen, J. Mack, J. Blank, H. Wegner and A. de Meijere, *Science* 2002, **295**, 1500 ; C. D. Simpson, G. Mattersteig, K. Martin, L. Gherghel, R. E. Bauer, H. J. Räder and K. Müllen, *J. Am. Chem. Soc.* 2004, **126**, 3139 ; E. H. Fort, P. M. Donovan and L. T. Scott, *J. Am. Chem. Soc.* 2009, **131**, 16006; L. Dössel, L. Gherghel, X. Feng and K. Müllen, *Angew. Chem. Int. Ed.* 2011, **50**, 2540; K. Matsui, Y. Segawa, T. Namikawa, K. Kamada and K. Itami, *Chem. Sci.* 2013, **4**, 84.

-
- [6] P. Fritsch, *Liebigs Ann. Chem.* 1894, **279**, 319; W. P. Buttenberg, *Liebigs Ann. Chem.* 1894, **279**, 324; H. Wiechell, *Liebigs Ann. Chem.* 1894, **279**, 337; D. Seyferth, R. S. Marmor and P. Hilbert, *J. Org. Chem.* 1971, **36**, 1379; E. J. Corey and P. L. Fuchs, *Tetrahedron Lett.* 1972, **13**, 3769; J. C. Gilbert and U. Weerasooriya, *J. Org. Chem.* 1982, **47**, 1837; K. Sonogashira, *J. Organomet. Chem.* 2002, **653**, 46.
- [7] P. Cadiot and W. Chodkiewicz, *Chemistry of Acetylenes*, Ed.: H. G. Viehe, Marcel Dekker, New York, 1969, Chap 9; P. Siemsen, R. C. Livingston and F. Diederich, *Angew. Chem. Int. Ed.* 2000, **39**, 2633; E. Méta y, Q. Hu and E. Negishi, *Org. Lett.* 2006, **8**, 5773.
- [8] G. Wegner, *Natureforsch., B: Chem. Sci.* 1969, **24**, 824; G. Wegner, *Makromol. Chem.* 1972, **154**, 35.
- [9] J. Xiao, M. Yang, J. W. Lauher and F. W. Fowler, *Angew. Chem. Int. Ed.* 2000, **39**, 2132; A. Sarkar, S. Okada, H. Matsuzawa, H. Matsuda and H. Nakanishi, *J. Mater. Chem.* 2000, **10**, 819; J. W. Lauher, F. W. Fowler and N. S. Goroff, *Acc. Chem. Res.* 2008, **41**, 1215; R. H. Baughman and K. C. Yee, *J. Polym. Sci. Part D* 1978, **13**, 219; Y. Zhao, T. Lu, G. M. Bernard, T. Taerum, R. McDonald, R. E. Wasylishen and R. R. Tykwinski, *Can. J. Chem.* 2012, **90**, 994.
- [10] J. Economy, H. Jung and T. Gogeva, *Carbon* 1992, **30**, 81.
- [11] M. Kijima, H. Tanimoto, H. Shirakawa, A. Oya and T.-T. Liang, *Carbon* 2001, **39**, 287.
- [12] A. Sarkar and S. S. Talwar, *Bull. Chem. Soc. Jpn.* 1999, **72**, 859.
- [13] J.-i. Ozaki, M. Ito, H. Fukazawa, T. Yamanobe, M. Hanaya and A. Oya, *J. Anal. Appl. Pyrolysis*, 2006, **77**, 56.
- [14] Y. Kojima, M. Tsuji, T. Matsuoka and H. Takahashi, *J. Polym. Sci. Part A: Polym. Chem.* 1994, **32**, 1371.
- [15] J. Hlavaty, L. Kavan, N. Kasahara and A. Oya, *Chem. Comm.* 2000, 737; J. Hlavaty, L. Kavan and J. Kubista, *Carbon* 2002, **40**, 345; J. Hlavaty, L. Kavan, K. Okabe and A. Oya, *Carbon* 2002, **40**, 1147.
- [16] N. Zhou, E. F. Merschrod S. and Y. Zhao, *J. Am. Chem. Soc.* 2005, **127**, 14154.
- [17] A. Sun, J. W. Lauher and N. S. Goroff, *Science* 2006, **312**, 1030.
- [18] L. Luo, D. Resch, C. Wilhelm, C. N. Young, G. P. Halada, R. J. Gambino, C. P. Grey and N. S. Goroff, *J. Am. Chem. Soc.* 2011, **133**, 19274.
- [19] L. Luo, C. Wilhelm, C. N. Young, C. P. Grey, G. P. Halada, K. Xiao, I. N. Ivanov, J. Y. Howe, D. B. Geohegan and N. S. Goroff, *Macromolecules* 2011, **44**, 2626.

-
- [20] V. Enkelmann and H. J. Graf, *Acta Crystallogr.* 1978, **B34**, 3715.
- [21] a) Q. Zhou, P. J. Carroll and T. M. Swager, *J. Org. Chem.* 1994, **59**, 1294. b) R. H. Baughman and K. C. Yee. *J. Polym. Sci. A: Polym. Chem.* 1974, **12**, 2467.
- [22] O. M. Behr, G. Eglinton, A. R. Galbraith and R. A. Raphael, *J. Chem. Soc.* 1960, 3614.
- [23] K. P. Baldwin, A. J. Matzger, D. A. Scheiman, C. A. Tessier, K. P. C. Vollhardt and W. J. Youngs, *Synlett* 1995, 1215.
- [24] R. Boese, A. J. Matzger and K. P. C. Vollhardt, *J. Am. Chem. Soc.* 1997, **119**, 2052.
- [25] M. M. Haley, M. L. Bell, J. J. English, C. A. Johnson and T. J. R. Weakly, *J. Am. Chem. Soc.* 1997, **119**, 2956.
- [26] T. Nishinaga, N. Nodera, Y. Miyata and K. Komatsu, *J. Org. Chem.* 2002, **67**, 6091.
- [27] M. Suzuki, A. Comito, S. I. Khan and Y. Rubin, *Org. Lett.* 2010, **12**, 2346.
- [28] Y. Xu, M. D. Smith, M. F. Geer, P. J. Pellechia, J. C. Brown, A. C. Wibowo and L. S. Shimizu, *J. Am. Chem. Soc.* 2010, **132**, 5334.
- [29] T.-J. Hsu, F. W. Fowler and J. W. Lauher, *J. Am. Chem. Soc.* 2012, **134**, 142.
- [30] J. R. Néabo, S. Rondeau-Gagné, C. Vigier-Carrière and J.-F. Morin, *Langmuir* 2013, **29**, 3446.
- [31] L. Ding and S. V. Olesik, *Chem. Mater.* 2005, **17**, 2353.
- [32] L. Ding and S. V. Olesik, *Nano Lett.* 2004, **4**, 2271.
- [33] J. R. Néabo, C. Vigier-Carrière, S. Rondeau-Gagné and J.-F. Morin, *Chem. Comm.* 2012, **48**, 10144.
- [34] R. Szilluweit, T. N. Hoheisel, M. Fritzsche, B. Ketterer, A. F. Morral, D. Demurtas, V. Laporte, R. Verel, S. Bolisetty, R. Mezzenga and H. Frauenrath, *Nano Lett.* 2012, **12**, 2573.
- [35] P. I. Dosa, C. Erben, V. S. Iyer, K. P. C. Vollhardt and I. M. Wasser. *J. Am. Chem. Soc.* 1999, **121**, 10430.
- [36] M. Laskoski, W. Steffen, J. G. Morton, M. D. Smith and U. H. Bunz. *J. Am. Chem. Soc.* 2002, **124**, 13814.
- [37] V. S. Iyer, K. P. C. Vollhardt and R. Wilhelm. *Angew. Chem.* 2003, **115**, 4515.
- [38] J. Wu, B. El Hamaoui, J. Li, L. Zhi, U. Kolb and K. Müllen. *Small*, 2005, **1**, 210.

-
- [39] B. El Hamaoui, L. Zhi, J. Wu, J. Li, N. T. Lucas, Z. Tomović, U. Kolb and K. Müllen. *Adv. Funct. Mater.* 2007, **17**, 1179; L. Zhi, Y. S. Hu, B. E. Hamaoui, X. Wang, I. Lieberwirth, U. Kolb, J. Maier and K. Müllen. *Adv. Mater.* 2008, **20**, 1727.
- [40] L. Zhi, T. Gorelik, R. Friedlein, J. Wu, U. Kolb, W. R. Salaneck and K. Müllen. *Small*, 2005, **1**, 798; L. Zhi, T. Gorelik, J. Wu, U. Kolb and K. Müllen. *J. Am. Chem. Soc.* 2005, **127**, 12792.
- [41] B. El Hamaoui, L. Zhi, J. Wu, U. Kolb and K. Müllen. *Adv. Mater.* 2005, **17**, 2957.
- [42] S. Scholz, P. J. Leech, B. C. Englert, W. Sommer, M. Weck and U. H. F. Bunz. *Adv. Mater.* 2005, **17**, 1052.
- [43] D. Jain, A. Winkel and R. Wilhelm, *Small* 2006, **2**, 752.
- [44] M. Laskoski, T. M. Keller and S. B. Qadri, *Carbon* 2007, **45**, 443.
- [45] G. L. Cui, Y. S. Hu, L. J. Zhi, D. Q. Wu, I. Lieberwirth, J. Maier and K. Müllen. *Small* 2007, **3**, 2066.
- [46] Q. Su, Y. Liang, X. Feng and K. Müllen. *Chem. Commun.* 2010, **46**, 8279.
- [47] L. Herghel, C. Kübel, G. Lieser, H. J. Räder and K. Müllen, *J. Am. Chem. Soc.* 2002, **124**, 13130.
- [48] L. Zhi, J. Wu, J. Li, U. Kolb and K. Müllen. *Angew. Chem. Int. Ed.* 2005, **44**, 2120.
- [49] F. Xinliang, Y. Liang, L. Zhi, A. Thomas, D. Wu, I. Lieberwirth, U. Kolb and K. Müllen. *Adv. Funct. Mater.* 2009, **19**, 2125.
- [50] S. Liu, Y. Duan, X. Feng, J. Yang and S. Che, *Angew. Chem. Int. Ed.* 2013, **52**, 6858.

Chapitre 2.

L'importance de la configuration de l'amide sur les propriétés de gélification et sur la polymérisation topochemique de macrocycles de type phénylacétylène

The importance of the amide configuration on the gelation process and topochemical polymerization of phenylacetylene macrocycles

Simon Rondeau-Gagné,^a Jules Roméo Néabo,^a Maude Desroches,^a Katy Cantin,^a Armand Soldera^b and Jean-François Morin^{*,a}

a Département de Chimie and Centre de Recherche sur les Matériaux Avancés (CERMA), 1045 Ave de la Médecine, Pavillon A.-Vachon, Université Laval, Québec, Qc, Canada G1V 0A6 Fax: 1 418-656-7916; Tel: 1 418-656-2812; E-mail: jean-francois.morin@chm.ulaval.ca

b Département de Chimie, Université de Sherbrooke, Sherbrooke, Québec, Canada J1K 2R1 Fax: 1 819-821-8017; Tel: 1 819-821-7650; E-mail: armand.soldera@usherbrooke.ca

Publié dans la revue *Journal of Materials Chemistry C*, **2013**, *1*, 2680-2687.

2.1 Préambule

Cet article présente la synthèse de macrocycles de type phénylacétylène portant des fonctions amide permettant l'auto-assemblage sous forme de gel. Les propriétés des macrocycles ainsi que leur réactivité y sont présentées, mettant en lumière l'effet des substituants sur la polymérisation topochemique. Ma contribution à cet article est majeure. Premièrement, j'ai effectué la synthèse de tous les monomères et macrocycles présentés. J'ai effectué la détermination des propriétés de gélification de tous les macrocycles et j'ai effectué la caractérisation des assemblages avant et après photopolymérisation. J'ai également participé à la rédaction de l'article et à la recherche bibliographique.

2.2 Résumé

Deux séries de macrocycles de type phénylacétylène (PAMs) contenant un amide ont été préparées et autoassemblées par gélification dans un solvant organique. Leurs propriétés de gélification ainsi que leurs arrangements moléculaires dans l'état de xérogel, leurs caractéristiques morphologiques et leur réactivité vis-à-vis de la polymérisation topochemique des unités butadiynes incorporées dans la structure ont été étudiées en lien avec la configuration de l'amide. Les PAMs de la série 1, avec l'atome d'azote de la fonction amide lié directement aux groupes phényles (dérivés de type acétanilide) ont montré une organisation moléculaire moins organisée et moins réactive à la polymérisation topochemique que les PAMs de la série 2 ayant la configuration d'amide inversée (dérivés de type benzamide). L'importance de la configuration de l'amide dans le processus de gélification a été confirmée par des calculs théoriques à l'aide de la théorie fonctionnelle de la densité. De plus, l'architecture calculée pour une série de molécules s'est avérée incompatible avec la réaction topochemique, ce qui est en accord avec l'observation expérimentale. La combinaison réelle des expériences et des calculs permet donc la conception de nouveaux nanotubes organiques rigides liés par liaisons covalentes.

2.3 Abstract

Two series of amide-containing phenylacetylene macrocycles (PAMs) were prepared and self-assembled through gelation process in organic solvent. Their gelation properties along with their molecular arrangements in the xerogel state, their morphological features and their reactivity toward the topochemical polymerization of the butadiyne units embedded

within the structure were studied with respect to the amide configuration. The PAMs of series 1 with the nitrogen atom of the amide function directly attached to the phenyl groups of the PAMs (acetanilide derivatives) showed less organized molecular organization and less reactivity toward topochemical polymerization than the PAMs of series 2 with the inverted amide configuration (benzamide derivatives). The importance of the amide configuration in the gelation process was confirmed by theoretical calculations at the density functional theory level. Moreover, the computed architecture for molecules of series 1 was shown to be incompatible with topochemical reaction in agreement with experimental observation. The actual combination of experiments and calculations allows the design of larger covalently-linked, rigid organic nanotubes.

2.4 Introduction

Self-assembly of π -conjugated molecules is a convenient way to create new materials that can be useful in organic electronics.¹ Molecules such as hexabenzocoronene (HBC),² porphyrins,³ oligo-ynes⁴ and π -conjugated oligomers⁵ have been widely used as building blocks in self-assembled architectures to prepare nanotubes, nanowires, nanoparticles, 2D polymers and so on. Among others, phenylacetylene macrocycles (PAMs) are particularly interesting carbon-rich materials that can provide rigid and shape-persistent 1D tubular assemblies because of their inner cavity.⁶ Moreover, PAMs can be easily functionalized through chemical synthesis, allowing the fine-tuning of their structural and electronic properties. Nevertheless, controlling their self-assembly remains the ultimate goal to make them available for electronic application.

Although the self-assembly of PAMs can be achieved on surface⁷ and in solid⁸ and solution states,⁹ their organization in well-ordered array of molecules is difficult to control and the physical and electronic properties of the resulting supramolecular architectures are difficult to predict prior to their synthesis. However, among methods for the self-assembly of such macrocycles, gelation appeared to be particularly effective, especially to achieve long-range aggregation.¹⁰ It actually yields stacking of PAMs as previously observed in gelation of carbazole-based arylene-ethynylene macrocycles^{10a,b} The major driving force for PAMs stacking are π - π interactions, although other weak interactions such as van der Waals interactions between peripheral alkyl chains can also explain their particular structure.

Recently, we reported an amide-containing PAM, which can be gelified in a large number of organic solvents owing to intermolecular hydrogen bonding.^{10c,11} These structural features are interesting assets to conceive desired self-assembled systems. In particular, we were interested in organized macrocycles that undergo topochemical photopolymerization via the diyne units embedded within the PAM skeleton. Moreover, amide moieties are interesting groups to achieve this goal since their structural parameters, i.e. intermolecular distance and tilt angle, are ideal features for topochemical polymerization of butadiyne moieties in the solid state.^{4f,12} PAMs with amide and butadiyne moieties should be of particular interest with their controlled organization.

To better grasp the self-assembly mechanism, we report the synthesis, characterization and molecular simulation of two types of amide-containing PAMs. The macrocycles differ from the configuration of the amide function (Figure 2.1). The **PAM 1** series possesses the nitrogen atom directly attached to the head and tail phenyl groups of the PAMs (acetanilide derivatives) while the amide configuration in the **PAM 2** series (benzamide derivatives) is inverted (carbonyl directly attached to the phenyl ring). Moreover, two PAMs (**1b** and **2b**) are bearing butadiyne units within the alkyl side chains. They make the formation of covalently linked nanotubes available through topochemical polymerization to form polydiacetylene (PDA). To specifically address the orientation of PAMs in gel state, calculations at the density functional theory (DFT) approximation level have been performed. Experimental and calculation data were thus combined to better address structural parameters that govern the self-assembly of PAMs in the gel state. Accordingly, this study is aimed at further improving the reactivity of butadiyne-containing PAMs for the formation of covalently-linked nanotubes through topochemical polymerization.

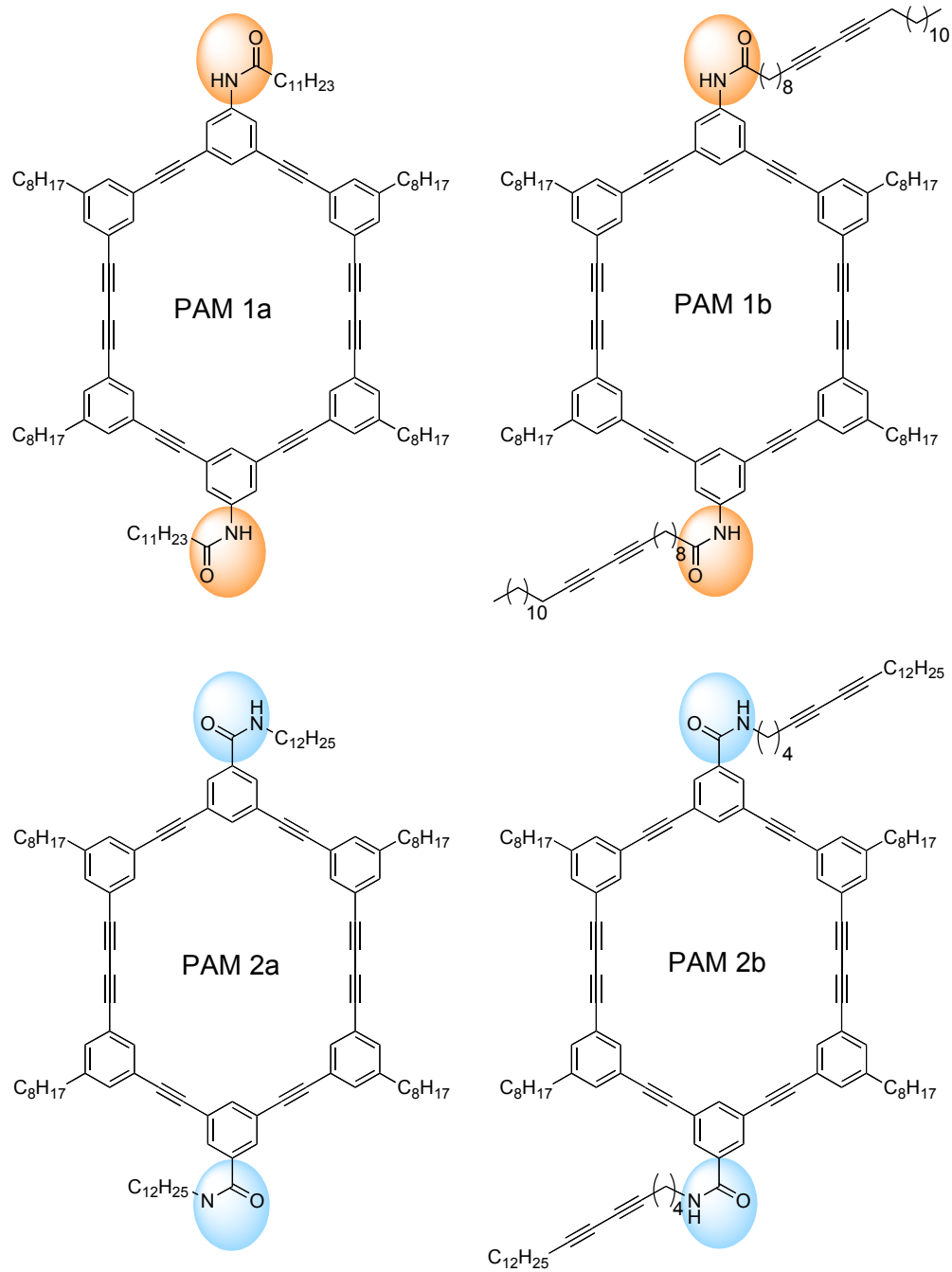
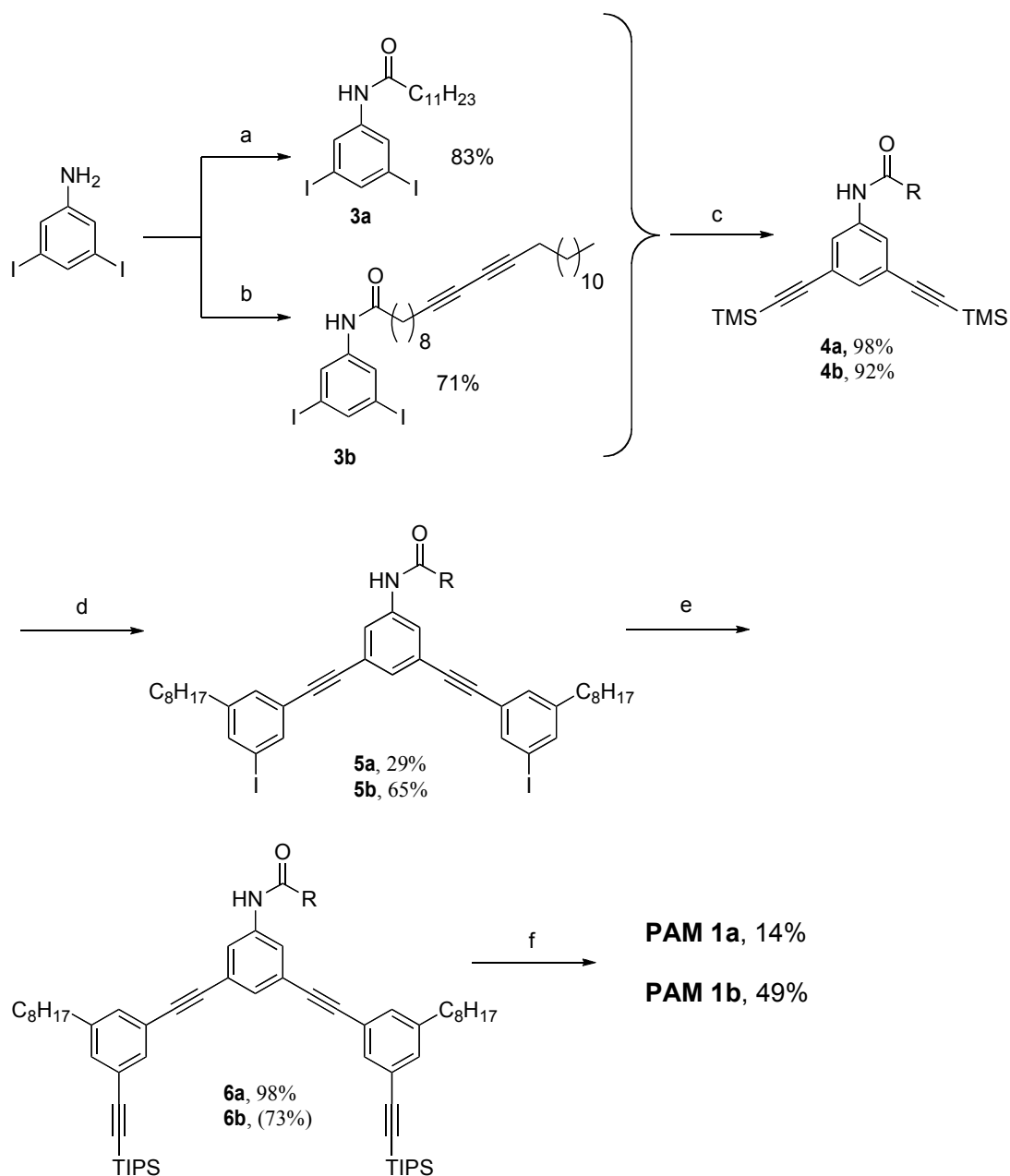


Figure 2.1 Structure of PAMs **1a**, **1b**, **2a** and **2b**.

2.5 Results and Discussion

2.5.1 Synthesis

The synthetic pathway to PAM **1a** is depicted in Scheme 2.1. Starting from 3,5-diiodoaniline,¹³ an amide was formed by acylation with lauroyl chloride (83% yield). Then, standard Castro-Stephen-Sonogashira cross-coupling was used to introduce trimethylsilylacetylene (TMSA) to provide compound **4a** in excellent yield. The two trimethylsilyl (TMS) protecting groups were removed using potassium hydroxide and a standard Castro-Stephen-Sonogashira coupling with 3,5-diiodooctylbenzene^{10c} was performed to obtain the half-macrocycle **5a** in 29% yield. It is noteworthy that even with a large excess of 3,5-diiodooctylbenzene, we have not been able to avoid the formation of linear oligomers formation and that explain the relatively low yield obtained. After, Castro-Stephen-Sonogashira coupling was used to install two triisopropylsilylacetylene (TIPSA) groups to provide compound **6a** in excellent yield. Finally, after removal of triisopropylsilyl (TIPS) protecting groups with tetrabutylammonium fluoride (TBAF), the ring closing reaction was performed using modified Eglinton¹⁴ conditions to provide PAM **1a** in a relatively low yield (14%). This low yield is comparable to other non-templated macrocyclization reported and it can be explained by the formation of linear oligomers even if the reaction was performed under high dilution conditions (10^{-3} M).¹⁵



Scheme 2.1. Synthetic pathway to PAMs **1a** and **1b**.

a) $C_{11}H_{23}COCl$, Et_3N , CH_2Cl_2 ; b) 10,12-pentacosadiynoic acid, EDC, DMAP, CH_2Cl_2 ; c) TMSA, $PdCl_2(PPh_3)_2$, CuI, Et_3N , THF; d) i. KOH, THF, MeOH, ii. 3,5-diiodooctylbenzene, $PdCl_2(PPh_3)_2$, CuI, DIPEA, THF; e) TIPS, $PdCl_2(PPh_3)_2$, CuI, Et_3N , THF; f) i. TBAF, THF, ii. CuCl, $CuCl_2$, Pyridine.

The same synthetic approach was used for the synthesis of macrocycle **1b** (scheme 2.1). Starting with 3,5-diiodoaniline, external diyne group was introduced by using a standard amidation procedure with commercially available 10,12-pentacosadiynoic acid in 71%. Afterwards, TMSA groups were installed by Castro-Stephen-Sonogashira coupling to provide compound **4b** in excellent yield. TMS group were removed using potassium hydroxide without purification and Castro-Stephen-Sonogashira coupling was performed in order to obtain half-macrocycle **5b**. The reaction yield (65%) is rather high when compared to the previous half-macrocycle formation and the reason for this quite surprising result is unknown. TIPS protecting groups were then introduced on the half-macrocycle by Castro-Stephen-Sonogashira coupling to provide compound **6b**. In the final step, the TIPS protecting groups were removed using TBAF and the crude product was used for the Eglinton ring-closing reaction to provide PAM **1b** in moderate yield (49%). This relatively high yield can be attributed to the remarkably high solubility of PAM **1b** allowing for easier purification process. It is noteworthy that the synthesis of PAMs **2a** and **2b** has been previously reported elsewhere.^{10c,11}

2.5.2 Characterization

In order to get better understanding on the influence of the amide groups configuration on gelation properties of PAMs, gelation tests in common organic solvents were performed. Standard gelification tests were achieved by dissolving the corresponding PAM in different solvents (1.0 wt/vol %). The resulting suspension was heated near the boiling point of the solvent and was allowed to cool down at room temperature resulting in a gel (G), partial gel (PG), solution (S), precipitate (P) or an insoluble mixture (I). The resulting gels were opaque or translucent. The gelation properties of amide-containing PAMs are summarized in Table 2.1. Surprisingly, the acetanilide derivatives, PAMs **1a** and **1b**, exhibited very poor gelation capability in most of the solvents tested. Thus, only partial gelification was obtained in non-polar aromatic solvents (toluene and benzene). For the benzamide derivatives, PAMs **2a** and **2b**, gel states were obtained in most of the solvents tested at relatively low concentrations. This result indicates that the configuration of the amide group has a clear impact on the self-assembly process. One explanation most likely lies in the presence of the nitrogen atom linked to the macrocycle that leads to an increase in the electron density on PAMs **1** core due to its lone pair. It thereby decreases the strength of

the π - π interaction between the PAMs molecules. Another reason for the very poor gelification of the acetanilide derivatives should stem from the directionality of the whole assembly geometry it leads to. Specifically, stacking of the PAMs **1a** and **1b** imposed by the directionality of the hydrogen bonding, should be unfavourable to generate long-range aggregation in the gel state. This later hypothesis will be discussed in more details in the theoretical calculations section. Further characterizations of PAMs of both series were needed to complement calculations. They were carried out on organogels prepared from the solvent exhibiting the best gelation properties.

Table 2.1 Gelation properties of amide-containing PAMs at 1.0 w/v %

Solvents	Observations			
	PAM 1a	PAM 1b	PAM 2a	PAM 2b
Toluene	PG	PG	G	S
Benzene	PG	PG	G	G
Pyridine	S	S	S	S
THF	S	S	S	P
MeOH	I	I	P	I
Ethyl acetate	P	S	G	G
Cyclohexane	P	S	G	G
Hexanes	P	P	G	G
CHCl ₃	S	S	S	S
CH ₂ Cl ₂	S	S	P	S

To reveal morphology of gels constituted of PAMs molecules, scanning-electron microscopy (SEM) is particularly well adapted. A small amount of gel was dried and deposited on a metal substrate. SEM images are shown in Figure 2.2. Both gels exhibit fibrils but mainly differ from each other by their density and their diameter. SEM images show a network of very small fibrils for PAMs **1a** and **1b**, while they display a very dense

network of fibrils assembled into bigger bundles for PAMs **2a** and **2b**. This morphological difference between the **1** and **2** series should lead to variations in macroscopic properties, and in particular in gel formation: gels from PAMs **2a** and **2b** are stronger and free-standing compared to those made from PAMs **1a** and **1b**. Those distinctions in morphology between the two series strengthen the importance of the amide configuration in the gel formation, and thus in the self-association of PAMs.

Additional evidence of self-aggregation of the macrocycles in the solid state is given by MALDI-ToF analysis. Mass spectrometry analysis reveals that, in addition to the peak corresponding to the mass of the molecular ion, peaks at higher molecular weight are also detected. They are attributed to supramolecular oligomers made of precise number of macrocycles. These high molecular weight species have been found for all macrocycles, regardless of the configuration of the amide. Species up to the hexamer [M₆] were observed, confirming the self-assembly of PAMs. Such aggregation behaviour has been already observed by mass spectrometry in the case of PAMs,^{9h} metallocycles¹⁶ and others macrocyclic compounds.¹⁷

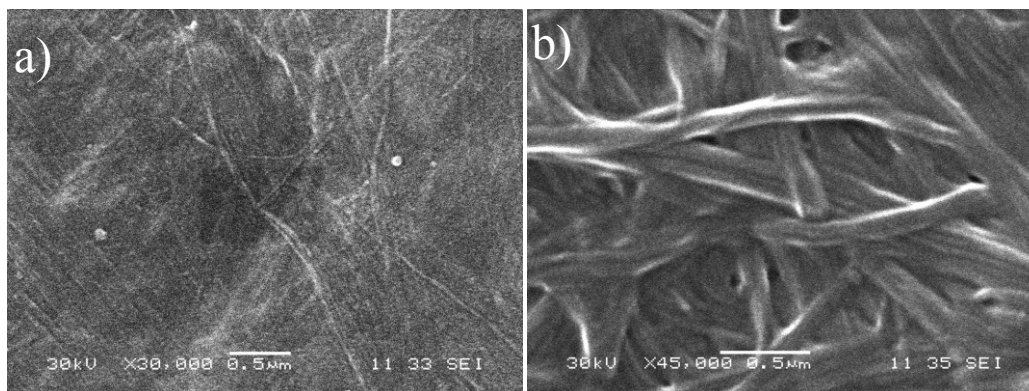


Figure 2.2. SEM images of a) dried gel of PAM **1a** in toluene (10 mg/mL), and b) dried gel of PAM **2a** in toluene (10 mg/mL). Scale bars of 0.5 µm for a) and b).

X-ray diffraction (XRD) analysis was also performed on dried gels of PAMs **1a**, **1b**, **2a** and **2b** to assess the self-assembly mode for the PAMs presented in this study. PAM **2b** in cyclohexane showed broad peaks at $2\theta = 3.1^\circ$ (28.1 Å) and the harmonic at 6.3° (13.9 Å). The broad peak denotes that no long distance correlation exists.¹⁸ Conversely, the XRD

pattern of the dried gel of PAM **2a** in the same solvent shows a sharp peak (100) at $2\theta = 2.5^\circ$ (35.3 Å), revealing a high correlation between molecules. Interestingly, the situation is completely different when ethyl acetate (EtOAc) is used as the solvent in the gelation process. In fact, XRD of a xerogels of PAM **2b** prepared from EtOAc showed several peaks at low diffraction angle, and large peaks at large angles. Such a pattern suggests a columnar arrangement with molecules randomly distributed along the column. Investigation of this molecular arrangement is out of the scope of this article, and will be specifically carried out through a complete SAXS analysis. In the same solvent (EtOAc), PAM **2a** showed much less organization. This difference in the level of organization between **2a** and **2b** suggests that the nature of the long alkyl chain attached to the head and the tail of the macrocycle has a significant impact on the intermolecular interactions during the gelation process. Also, the dissimilarities observed between organizations for different solvents is indicative of the importance in the choice of the solvent for the gelation process.

The diffractograms of the PAMs **1** series showed similar pattern than PAM **2b** (EtOAc) in the small angle region ($2\theta = 4.1$ and 7.2°), suggesting a similar organization mode. Unfortunately, the dissimilarities between the diffractograms obtained for the series **1** and **2** and the use of different solvents to make the gels do not allow drawing conclusion about the difference in the level of organization for the two series.

After the characterization of the supramolecular assembly of PAMs in the gel state, photopolymerization of the butadiyne units was attempted in both gel and xerogel states obtained from different solvents. The purpose of this reaction is to form covalently linked architectures from supramolecular assemblies by the formation of polydiacetylene (PDA).¹⁹ Moreover, because of their internal cavity, PAMs are excellent candidates to form organic nanotubes following this process.¹¹ However, in order for the topochemical polymerization to occur, strict structural parameters between butadiyne units are required, namely a distance of 4.9Å between the two reactive carbon atoms and an angle of 45° relative to the butadiyne axis.^{19,20} Our group and others have recently reported that by using proper elements of design, topochemical polymerization of macrocycles can take place both in the gel^{11,21} and crystalline state.²² To organize PAMs prior to topochemical reaction, we decided to proceed to self-assembly through gelation process. Compare to crystals

formation, self-assembly via gelation process is easier and less time consuming. Moreover, organogels proved to be as efficient as the crystalline state for the topochemical polymerization of butadiyne-containing molecules.²³ It was also established that the amide groups facilitate the gelation process in organic solvents.^{3d,4f,4g,10c,11} Thus, to investigate the influence of the amide configuration on the efficiency of the photopolymerization, several irradiation tests at 254 nm were performed. Usually, the appearance of a bluish colour associated with the formation of polydiacetylene primarily confirms the success of the reaction. For organogel of PAM **1a** (benzene), a strong orange colour appeared after irradiation for 24h. This colour change is accompanied by a significant loss of the gel viscosity, which confirms that partial reaction of the butadiyne units or degradation occurred. The same phenomenon happened for PAM **1b** that contains more reactive external aliphatic diynes moieties. The loss of the gel state could be attributed to a significant conformational change within the gel, thus disturbing the rather weak hydrogen bond network.^{4f,24} In the case of PAM **2a**, the gel state remains intact during the irradiation, but only a small colour change from off-white to greenish was observed, indicating that topochemical polymerization occurred at low rate to give low molecular-weight PDAs. In the case of the PAM **2b** however, a strong blue colour appeared rapidly during the irradiation of the gel in ethyl acetate, without the loss of viscosity during the process. It is worth mentioning that only ethyl acetate yielded a reactive gel. The preservation of the gel state during the topochemical polymerization served as another empirical proof that the amide configuration in PAMs **2** series yields a much stronger supramolecular assembly. A similar colour change was observed for PAMs **2** series when thin films of xerogels (ethyl acetate) were irradiated. At this point, there is no experimental evidence to explain the success of topochemical polymerization in ethyl acetate only. Further analyses using SAXS techniques must be carried out in order to reveal the effect of solvent in conformational changes. However, comparison with PAMs **1** series suggests that there is a clear effect of the amide configuration on the gelation properties, and thereby, on the efficiency of topochemical polymerization.

To further characterize the covalent architecture formed upon irradiation of PAMs **2** series, xerogels of PAMs **2a** and **2b** was irradiated and the blue materials, **poly-2a** and **poly-2b**, respectively, were purified using semi-preparative size-exclusion chromatography. Only soluble, high molecular weight blue materials (ca. 10-20% yield) were recovered. It is worth mentioning that the photopolymerization of PAM **2b** was much faster than that of PAM **2a**. For the former, few hours were sufficient to obtain a deep blue material while several days were necessary for the later to polymerize properly. Moreover, **poly-2a** presents itself as greenish-blue in solution, suggesting that very short PDA oligomers were formed upon irradiation. The different reactivity observed between PAMs **2a** and **2b** can probably be ascribed to the increase reactivity of butadiyne units embedded within the long peripheral alkyl chains.¹¹ Our hypothesis is that once the outer PDA formed in PAM **2b**, the butadiyne units within the macrocycle skeleton adopt a more favourable conformation to undergo a topochemical polymerization. The higher level of organization found by XRD analysis can also account for better reactivity of **2b** compare to **2a**.

To assess the conversion of all the butadiyne units into PDA within PAMs **2** series upon irradiation with UV light, Raman spectroscopy was performed before and after irradiation of the dried organogels. Raman spectra of **poly-2a** and **poly-2b** showed a band around 2095 cm^{-1} and a complete disappearance of the band around 2220 cm^{-1} , meaning that all the butadiyne were converted to ene-yne moiety.

2.5.3. Theoretical Calculations

All calculations were realized with the Gaussian 09 package.²⁵ The equilibrium geometries were computed using the density functional theory (DFT). The 6-31G(d,p) basis set was employed with the hybrid M05-2X exchange-correlation functional.²⁶ This functional was recommended for systems with weak dispersion interactions, such as hydrogen bonding.²⁷

Theoretical calculations were performed on series **1** and **2** to gain better understanding on the role of the amide configuration on the intermolecular interactions and packing behaviour of PAMs. From a computational viewpoint, the huge number of degrees of freedom related to the studied molecules makes the exploration of the configurational space inappropriate. Variations in the dihedral angles of the functional group, differences in the shape of the core²⁸ and the influence of the number of stacking molecules, should be

studied extensively to find conformations of minimum energy. Moreover, thermal energy increases the number of available configurations, and the effect of solvent will yield different geometries, as it has been uncovered in the experimental part. A different approach is thus proposed. It benefits from merging experimental and computational results.

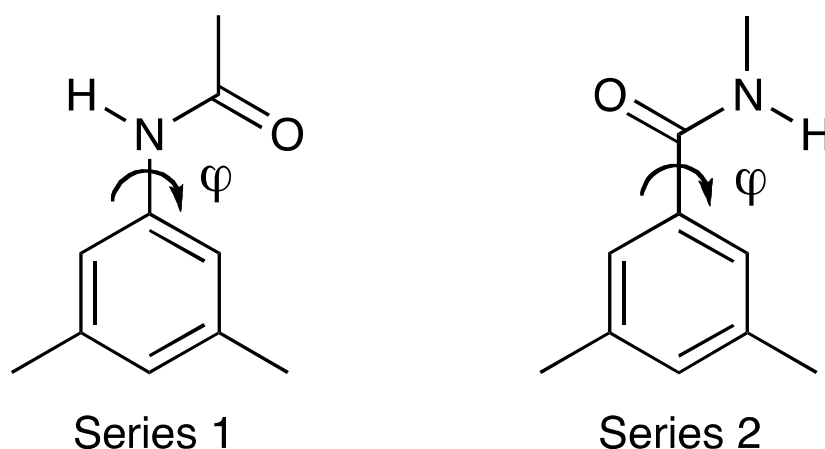


Figure 2.3 Two different amide configurations studied

In primary calculations, the core of the molecules is simplified in order to reduce the number of degrees of freedom, and thus allowing a better exploration of the configurational space. The core is replaced by a dimethyl phenyl group (Figure 2.3). The first investigation consists in finding conformations exhibiting the lowest potential energy. These conformations define the rotamers. These rotamers are then used to locate dimer conformations with minimum energy without exploring the entire surface of potential energy. To locate the rotamers, the scanning of the dihedral angle associated with the bond linking the amide group to the phenyl is carried out. The potential energy is thus reported with respect to this torsion angle (Figure 4). The height of the crossing barrier is found the same for both molecules, in order of 4.8 kcal/mol. For the series 1, it separates two rotamers whose amide group lies in the phenyl plane. For the series 2, the main crossing barrier distinguishes two rotamers that exhibit their amide group at an angle of 27 deg. from the phenyl plane. By symmetry, there is another crossing barrier that separates two rotamers. Its magnitude is low, in order of 0.5 kcal/mol. This value corresponds to a thermal energy of 250 K. It thus reveals that the amide group is able to flip easily between

the two states. To reveal conformations of dimers, the distinction between these two rotamers has no incidence in the results, since it is governed by the hydrogen bonding. Accordingly, only two rotamers are considered for each molecule.

The search for the conformations of minimum energy for dimers can be a very complex task, due to the important surface of potential energy that needs to be explored. However, from XRD measurements, it has been demonstrated that the two cores are assembled according to a “p-p-stacking”-like structure. Since there are two rotamers for each molecule, two possible arrangements of molecules in a dimer are examined: the two amide groups point in the same direction, the so-called parallel conformation, and conversely the anti-parallel orientation shows the two amide groups in opposite direction. Conformations with the lowest energy are displayed in Table 2.2. For each system, the stabilized energy is also shown. This energy corresponds to the difference between two times the energy of one molecule less the computed energy of the dimer. It is thus associated with the gain in energy stemming from the formation of hydrogen bonding, and π stacking, by associating the two molecules.²⁹ It is thus associated with the gain in energy stemming from the formation of hydrogen bonding by associating the two molecules.

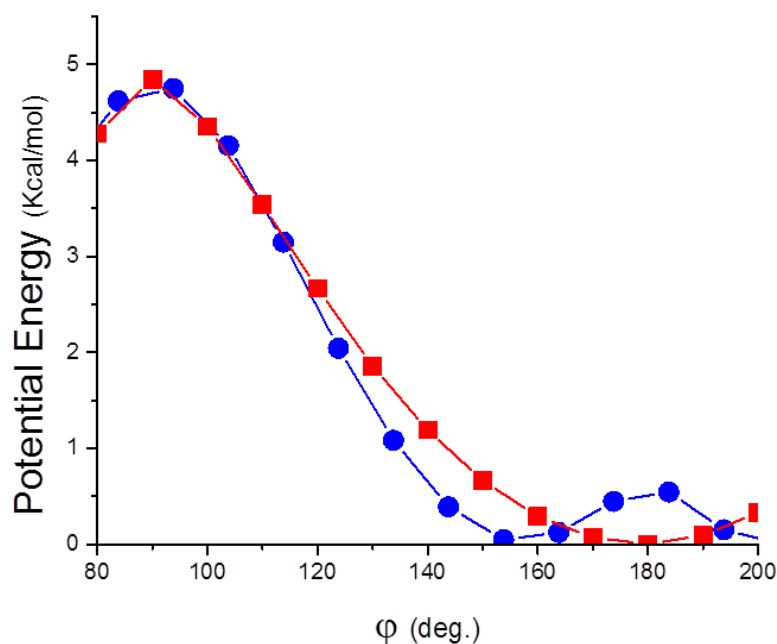
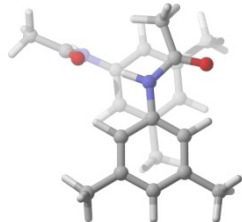
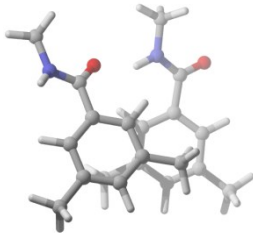
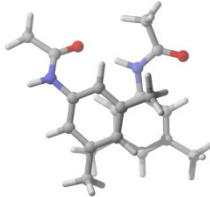
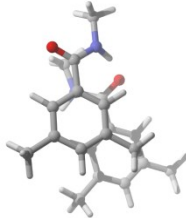


Figure 2.4. Potential energy, red (■) and blue (●) for molecules of series **1** and **2** respectively, with respect of the dihedral angle, ϕ , associated to the bond linking the amide function to the phenyl group (Figure 2.3).

The stabilizing energy exposed in Table 2.2, is clearly low, revealing that hydrogen bonds are important in stabilizing the dimer. Molecules from series **1** exhibit the lowest energy for both arrangements. However, to create hydrogen bonding, the phenyl groups must rotate leading to amide group pointing in different directions, as revealed by the angle between the two bonds linking the amide to the phenyl group (Table 2.2). Such an assembly can explain the fact that no topochemical reaction has been observed in the molecules of series **1**: geometrical features cannot be attained following such architecture. Conversely, rather small angles are found for molecules from the series **2** (Table 2.2), indicating that phenyl groups do not have to rotate greatly to make hydrogen bonding. Moreover, it can be observed that phenyl of dimers from series **2** are not superposed (Table 2.2). Can such assemblies compatible with arrangement of the cores without any functional groups? To address this question, calculations were carried out in systems constituted of these two cores. One core is then rotated and translated while the other remained fixed.

The two cores are placed at a distance of 3.6 Å, which is a good approximation for the macrocycles intermolecular distance.³⁰ The rotation operation consists in rotating one core while maintaining the other fixed. The axis of symmetry is the line joining the mass centres of the two molecules. At each 2 deg. angle, energy is computed. The value of the computed energy with respect to the rotation angle is shown in the Figure 2.5. It shows that the energy decreases until it reaches a minimum in energy at an angle of 6 deg., where it stays relatively constant until 18 deg., and then it increases. Difference in energy in the plateau is in order of 0.1 kcal/mol. An arrow in Figure 5 indicates the value of the angle for the series **2** parallel dimer. It thus falls into the domain when the arrangement of the cores is optimal.

Table 2.2. Conformation of minimum energy for molecules of series **1** and **2**,³¹ see text for details.

Orientation	Series 1	Series 2
Parallel		
Energy (kcal/mol)	-14.8	-13.8
Angle (deg.)	44	14
Anti-parallel		
Energy (kcal/mol)	-14.8	-14.1
Angle (deg.)	65	8

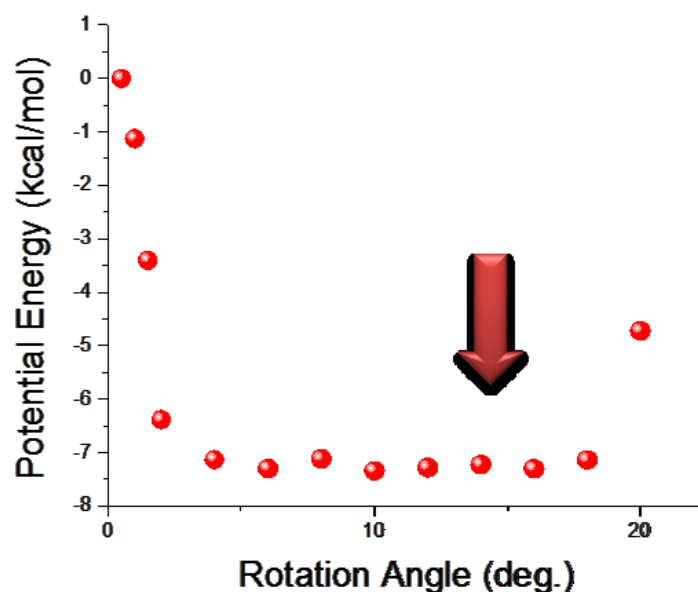


Figure 2.5. Potential energy with respect to the rotation angle between the cores.

The translation operation consists in mapping the plane of displacement of one core while keeping the other one, which is kept fixed, as displayed in Figure 2.6. Each 0.5 Å step, the potential energy is computed. The stemming isoenergetical contour map with difference between contour of 0.4 kcal/mol is shown in Figure 2.7. A cross reveals the position of the series 2 antiparallel dimer. It is located in a domain where the interaction energy between the two cores is low.

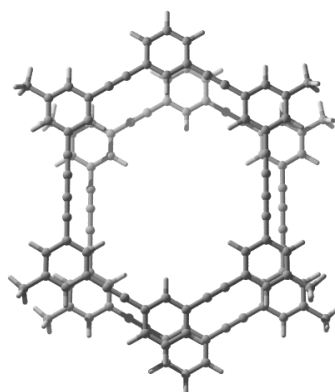
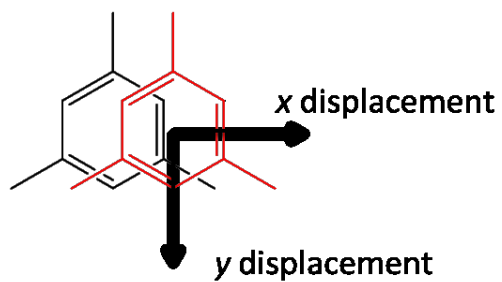


Figure 2.6. Schematic representation of the translation of one core in relation to the other core.

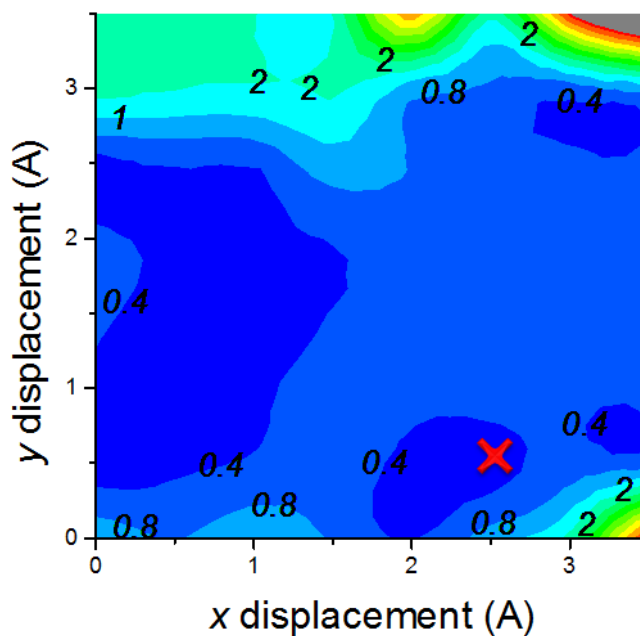


Figure 2.7. Isoenergetic plot with x and y displacement corresponding to translation shown in figure 2.6.

Rotation and translation operations revealed that there is compatibility between the favourable “p-p-stacking” of cores and minimum energy of PAMs **2** series dimers.

2.6 Conclusions

In summary, we have prepared and characterized two new phenylacetylene macrocycles (PAM, series **1**) that are acetanilide derivatives, i.e. they bear amide functionalities with the nitrogen atom attached to the phenyl units of the PAM. We have compared them to two isomers (series **2**) that are benzamide derivatives, i.e. the amide functions are attached to the phenyl group through the carbon atom of the carbonyl group. We have shown the major role of the amide configuration in the self-assembly behaviour upon gelation and in the reactivity of the embedded butadiyne units upon irradiation. We have found that the amide configuration is of primary importance for the success of topochemical polymerization of PAMs. While series **2** are reactive upon UV irradiation to give the PDA, series **1** failed to react under the same conditions. Calculations have shown that lower energy for molecules of series **1** involves rotation of the entire molecules leading to an architecture that is incompatible with the topochemical reaction. These calculations are in agreement with experimental data stemming from XRD and SEM and the poor gelation ability of PAMs. Amide functions with the proper configuration will thus be installed on wider PAMs in order to prepare larger covalently-linked, rigid organic nanotubes.

2.7 Supporting Information

2.7.1 General

Chemical reagents were purchased from Sigma-Aldrich Co. Canada, Alfa Aesar Co., TCI America Co. or Oakwood Products Inc. and were used as received. Solvents used for organic synthesis were obtained from Fisher Scientific (except THF from Sigma- Aldrich Co. Canada) and purified with a Solvent Purifier System (SPS) (Vacuum Atmosphere Co., Hawthorne, USA). Other solvents were obtained from Fisher Scientific and were used as received. Tetrahydrofuran (THF) and triethylamine (Et₃N) used for Sonogashira reactions were degassed 30 minutes prior to use. All anhydrous and air sensitive reactions were performed in oven-dried glassware under positive argon pressure. Analytical thinlayer chromatographies were performed with silica gel 60 F254, 0.25 mm pre-coated TLC plates

(Silicycle, Québec, Canada). Compounds were visualized using 254 nm and/or 365 nm UV wavelength and/or aqueous sulfuric acid solution of ammonium heptamolybdate tetrahydrate (10 g/100 mL H₂SO₄ + 900 mL H₂O). Flash column chromatographies were performed on 230-400 mesh silica gel R10030B (Silicycle, Québec, Canada).

Apparatus

Nuclear magnetic resonance (NMR) spectra were recorded on a Varian Inova AS400 spectrometer (Varian, Palo Alto, USA) operating at 400 MHz (¹H) and 100 MHz (¹³C). High resolution mass spectra (HRMS) were recorded with an Agilent 6210 Time-of-Flight (TOF) LC-MS apparatus equipped with an ESI or APPI ion source (Agilent Technologies, Toronto, Canada). MALDI-TOF measurements were performed on a Bruker Biflex IV equipped with nitrogen laser. FT-IR was recorded in ATR mode on Infrared spectrometer (Thermo-Nicolet Magne 850) equipped with Golden Gate. UVvisible absorption spectra were recorded on a Varian diode-array spectrophotometer (model Cary 500) using 3-mm path length quartz cells. Scanning electron microscopy (SEM) images were taken using a JEOL JSM-6360 LV. X-ray diffraction was recorded on Siemens X-rays diffractometer (Model S3 D5000).

Gelation test

To test the gelation properties of PAMs in a given solvent, we proceeded as follow: in a vial, a PAMs was dissolved in a solvent. After dissolution by sonication, the vial was sealed and heated until a clear solution was obtained. The clear solution was allowed to slowly cool down at room temperature. The stability of the gel was confirmed by tube inversion. SEM imaging Organogel obtained in ethyl acetate was deposited on a stainless steel substrate and allowed to dry for 3--4 days. Then, gold particles were sputtered on dried gel prior to imaging.

Computation

All calculations were realized with the Gaussian 09 package.¹ The equilibrium geometries were computed using the density functional theory (DFT). The 6-31G(d,p) basis set was employed with the hybrid M05-2X exchange-correlation functional.² This functional was recommended for systems with weak dispersion interactions, such as hydrogen bonding.

2.7.2 Synthetic procedure

Compound 3a. A 100 mL round bottom flask equipped with a magnetic stir bar was charged with 3,5-diiodoaniline (2.50 g, 7.25 mmol) and Et₃N (3.03 mL, 21.7 mmol) in CH₂Cl₂ (18 mL) under N₂ atmosphere. In another round bottom flask equipped with a magnetic stir bar, a solution of lauroyl chloride (2.51 mL, 10.8 mmol) in CH₂Cl₂ (18 mL) under N₂ atmosphere was prepared. The first solution was added dropwise to the other and the resulting solution was stirred overnight. The reaction mixture was diluted with CH₂Cl₂, washed with water (3x), dried with sodium sulfate and the solvent was removed under reduced pressure. The crude product was purified by flash chromatography on silica gel using hexanes to 20% EtOAc/hexanes as eluents to afford compound **3a** (3.16 g, 83% yield) as a white amorphous powder. m.p: 105-109°C; ¹H NMR (CDCl₃, 400 MHz): 7.89 (s, 2H), 7.76 (s, 1H), 7.22 (s, 1H), 2.33 (t, J = 7.4 Hz, 2H), 1.69 (m, 2H), 1.26 (m, 16H), 0.88 (t, J = 6.7 Hz, 3H); ¹³C NMR (CDCl₃, 100 MHz): 171.8, 140.9, 140.0, 135.1, 127.8, 123.2, 94.7, 37.9, 32.1, 29.8, 29.7, 29.6, 29.4, 25.7, 22.9, 14.4. HRMS (APPI-TOF) m/z calcd for C₁₈H₂₇I₂NO[M+H]⁺: 528.0255, found 528.0259; FTIR (ATR): 3275m, 2916m, 2850m, 1656m, 1558m.

Compound 4a. A 100 mL round bottom flask equipped with a magnetic stir bar was charged with **3a** (3.00 g, 3.02 mmol), degassed THF (56 mL), degassed TEA (3.13 mL, 22.8 mmol), PdCl₂(PPh₃)₂ (160 mg, 0.23 mmol), CuI (43 mg, 0.23 mmol) and trimethylsilylacetylene (3.21 mL, 22.8 mmol) under argon atmosphere. The reaction mixture was stirred overnight at room temperature, diluted with CH₂Cl₂, washed with NH₄Cl (3x) and dried with sodium sulfate. The solvent was removed under reduced pressure and the crude product was purified by flash chromatography on silica gel using 5% EtOAc/hexanes to 7% EtOAc/hexanes as eluents to afford compound **4a** (2.62 g, 98% yield) as a dark orange oil. ¹H NMR (CDCl₃, 400 MHz): 7.59 (s, 2H), 7.56 (s, 1H), 7.29 (s, 1H), 2.31 (t, J = 7.4 Hz, 2H), 1.67 (m, 2H), 1.24 (m, 16H), 0.87 (t, J = 6.7 Hz, 3H), 0.21 (s, 18H); ¹³C NMR (CDCl₃, 100 MHz): 172.1, 138.2, 131.3, 124.4, 123.2, 103.9, 95.3, 37.9, 32.1, 29.8, 29.7, 29.6, 29.5, 29.4, 25.8, 22.9, 14.4, 0.1. HRMS (APPI-TOF) m/z calcd for C₂₈H₄₅NOSi₂[M+H]⁺: 468.3112, found 468.3125; FTIR (ATR): 3295w, 2923m, 1663m, 1431m, 1248m, 830m.

Compound 5a. A 100 mL round bottom flask equipped with a magnetic stir bar was charged with **4a** (2.60 g, 5.56 mmol), KOH (936 mg, 16.7 mmol), THF (14 mL), MeOH (13 mL) and water (1.0 mL). The reaction mixture was stirred for 15 minutes, diluted with CH₂Cl₂, washed with 10% aqueous HCl (3x) and dried with sodium sulfate. The solvent was removed under reduced pressure and the resulting product was directly charged without further purification in a 100 mL round bottom flask equipped with a magnetic stir bar charged with 3,5-diiodo-1-octylbenzene (4.10 g, 9.27 mmol), degassed THF (30 mL), degassed diisopropylethylamine (4.31 mL, 24.7 mmol), PdCl₂(PPh₃)₂ (87 mg, 0.12 mmol) and CuI (24 mg, 0.12 mmol) under nitrogen atmosphere. The mixture was stirred overnight at room temperature, diluted with CH₂Cl₂, washed with NH₄Cl (3x) and dried with sodium sulfate. The solvent was removed under reduced pressure and the crude product was purified by flash chromatography on silica gel using hexanes to 5% EtOAc/hexanes as eluents to afford compound **5a** (840 mg, 29% yield) as a white amorphous powder: m.p: 86-95°C; ¹H NMR (CDCl₃, 400 MHz): 7.66 (br s, 4H), 7.49 (s, 2H), 7.38 (s, 1H), 7.31 (s, 1H), 7.27 (s, 2H), 2.53 (t, J = 7.7 Hz, 4H), 2.37 (t, J = 7.7 Hz, 2H), 1.72 (m, 2H), 1.59 (m, 4H), 1.25 (m, 36H), 0.88 (m, 9H); ¹³C NMR (CDCl₃, 100 MHz): 145.4, 138.4, 137.9, 137.7, 137.6, 131.2, 130.5, 124.8, 124.2, 122.8, 93.9, 89.9, 88.0, 81.9, 38.1, 35.6, 32.2, 32.1, 31.3, 29.8 (2C), 29.7, 29.6 (2C), 29.5, 29.4 (2C), 25.8, 22.9 (2C), 21.6, 14.4. HRMS (APPI-TOF) m/z calcd for C₅₀H₆₇I₂NO[M+H]⁺: 952.3385, found 952.3412; FTIR (ATR): 3279w, 2915m, 2848m, 1657m, 1536m, 866m.

Compound 6a. A 25 mL round bottom flask equipped with a magnetic stir bar was charged with **5a** (1.00 g, 1.05 mmol), degassed THF (10 mL), degassed Et₃N (0.58 mL, 4.20 mmol), PdCl₂(PPh₃)₂ (37 mg, 0.05 mmol), CuI (10 mg, 0.05 mmol) and triisopropylsilyl acetylene (0.94 mL, 4.20 mmol). The reaction mixture was stirred overnight, diluted with CH₂Cl₂, washed with NH₄Cl and dried with sodium sulfate. The solvent was removed under reduced pressure and the crude product was purified by flash chromatography on silica gel using hexanes to 5 % EtOAc/hexanes as eluents to afford compound **6a** (1.09 g, 98% yield) as an orange oil. ¹H NMR (CDCl₃, 400 MHz): 7.70 (s, 2H), 7.50 (s, 1H), 7.45 (s, 2H), 7.42 (s, 1H), 7.27 (s, 2H), 7.25 (s, 2H), 2.56 (t, J = 7.7 Hz, 4H), 2.35 (t, J = 7.5 Hz, 2H), 1.71 (m, 2H), 1.60 (m, 4H), 1.25 (m, 36H), 1.14 (s, 42H), 0.88 (m, 9H); ¹³C NMR (CDCl₃, 100 MHz): 172.0, 143.5, 138.5, 132.8, 132.3, 131.8,

124.4, 123.9, 123.1, 122.7, 106.7, 91.0, 89.9, 88.6, 81.8, 37.9, 35.8, 32.2 (2C), 31.5, 29.9 (2C), 29.8, 29.7 (2C), 29.6 (2C), 29.5 (2C), 25.8, 22.9 (2C), 18.9, 18.8, 14.4, 11.5; HRMS (APPI-TOF) m/z calcd for $C_{72}H_{109}NOSi_2[M+H]^+$: 1060.8120, found 1060.8158; FTIR (ATR): 3294w, 2923m, 2863m, 1663m, 881m.

PAM 1a. A 50 mL round bottom flask equipped with a magnetic stir bar was charged with **6a** (1.00 g, 0.94 mmol), THF (19 mL) and TBAF 1.0M solution in THF (2.83 mL, 2.83 mmol). The reaction mixture was stirred until complete disappearance of the starting product by TLC, diluted with CH_2Cl_2 , washed with water (3x) and dried with sodium sulfate. The solvent was removed under reduced pressure and the crude product was charged without further purification in a 100 mL round bottom flask charged with degassed pyridine (28 mL). Another 500 mL round bottom flask equipped with a magnetic stir bar was charged with CuCl (6.58 g, 66.4 mmol), $CuCl_2$ (1.38 g, 10.3 mmol) and degassed pyridine (133.7 mL) under N_2 atmosphere. The substrate solution was added dropwise to the catalyst solution over 4 days and the reaction mixture was stirred for an additional 7 days. The reaction mixture was diluted with $CHCl_3$ and poured in water. The organic phase was extracted successively with water, 25% aqueous NH_4OH , water, 10% aqueous CH_3COOH , water, 10% aqueous NaOH and brine. The organic layer was dried with sodium sulfate and the solvent was removed under reduced pressure. The crude product was purified by flash chromatography on silica gel using 30% hexanes/ $CHCl_3$ to $CHCl_3$ as eluent to afford **PAM 1a** (140 mg, 20%) as a white amorphous powder. m.p: $>150^\circ C$; 1H NMR ($CDCl_3$, 400 MHz): 7.58 (s, 4H), 7.49 (s, 4H), 7.39 (s, 2H), 7.24 (s, 4H), 7.20 (s, 4H), 7.10 (s, 2H), 2.50 (t, $J = 7.6$ Hz, 8H), 2.31 (t, $J = 7.2$ Hz, 4H), 1.67 (m, 4H), 1.54 (m, 8H), 1.19 (m, 72H), 0.80 (m, 18H); ^{13}C NMR ($CDCl_3$, 100 MHz): 171.7, 143.8, 138.3, 133.8, 133.7, 132.5, 132.4, 124.3, 123.4, 122.4, 121.2, 89.7, 88.9, 81.2, 74.3, 38.0, 35.7, 32.2, 32.1, 31.2, 29.9 (2C), 29.8 (2C), 29.7, 29.6 (2C), 29.5 (2C), 29.4 (2C), 25.7, 22.9, 14.4; MS (MALDI-TOF): m/z calcd for $C_{108}H_{134}N_2O_2[M+H]^+$: 1492.1, found 1492.1; FTIR (ATR): 3271w, 2920m, 2849m, 1657m, 1536m, 1435m.

Compound 3b. A 100 mL round bottom flask equipped with a magnetic stir bar was charged with 3,5-diiodoaniline (2.50 g, 7.25 mmol), pentacosadiynoic acid (4.07 g, 10.9 mmol), *N*-(3-dimethylaminopropyl)-*N'*-ethylcarbodiimide (2.084 g, 10.9 mmol), 4-

(dimethylamino)pyridine (443 mg, 3.62 mmol) and CH₂Cl₂ (36 mL). The reaction mixture was stirred overnight and diluted with CH₂Cl₂. The organic layer was washed with water (3x), dried with sodium sulfate and the solvent was removed under reduced pressure. The crude product was purified by flash chromatography on silica gel using 10% acetone/hexanes to 20% acetone/hexanes as eluents to afford compound **3b** (3.59 g, 71% yield) as a white viscous solid. ¹H NMR (CDCl₃, 400 MHz): 7.89 (s, 2H), 7.77 (s, 1H), 7.01 (s, 1H), 2.33 (t, J = 7.4 Hz, 2H), 2.24 (t, J = 6.3 Hz, 4H), 1.69 (m, 2H), 1.51 (m, 6H), 1.37 (m, 22H), 0.88 (t, J = 6.4 Hz, 3H); ¹³C NMR (CDCl₃, 100 MHz): 171.4, 140.7, 139.8, 127.6, 94.5, 77.7, 77.5, 65.3, 65.2, 37.6, 31.9, 29.6 (3C), 29.5, 29.4, 29.1 (3C), 28.9, 28.8, 28.7, 28.4, 28.3, 25.3, 22.7, 19.2, 19.1, 14.4; HRMS (APPI-TOF) m/z calcd for C₃₁H₄₅I₂NO[M+H]⁺: 702.1663, found 702.1662; FTIR (ATR): 3298w, 2922m, 2848m, 1670m, 1572m.

Compound 4b. A 250 mL round bottom flask equipped with a magnetic stir bar was charged with **3b** (3.60 g, 5.13 mmol), degassed THF (51 mL), degassed TEA (2.82 mL, 20.5 mmol), PdCl₂(PPh₃)₂ (144 mg, 0.21 mmol), CuI (39 mg, 0.21 mmol) and trimethylsilylacetylene (2.89 mL, 20.5 mmol) under argon atmosphere. The reaction mixture was stirred overnight at room temperature, diluted with CH₂Cl₂, washed with NH₄Cl (3x) and dried with sodium sulfate. The solvent was removed under reduced pressure and the crude product was purified by flash chromatography on silica gel using 5% acetone/hexanes as eluent to afford compound **4b** (3.03 g, 92% yield) as a dark orange oil. ¹H NMR (CDCl₃, 400 MHz): 7.60 (s, 2H), 7.43 (s, 1H), 7.29 (s, 1H), 2.31 (t, J = 7.3 Hz, 2H), 2.22 (t, J = 7.0 Hz, 4H), 1.67 (m, 2H), 1.49 (m, 4H), 1.33 (m, 26H), 0.86 (t, J = 7.0 Hz, 3H), 0.21 (s, 18H); ¹³C NMR (CDCl₃, 100 MHz): 171.9, 138.2, 131.3, 124.2, 123.1, 103.9, 95.4, 77.9, 77.7, 65.6, 65.5, 37.8, 32.2, 31.8, 29.9 (3C), 29.7, 29.6 (2C), 29.4, 29.3, 29.1 (2C), 28.9, 28.6, 28.5, 25.7, 22.9, 19.4, 14.4, 0.09; HRMS (APPI-TOF) m/z calcd for C₄₁H₆₃NOSi₂[M+H]⁺: 642.4521, found 642.4525; FTIR (ATR): 3295w, 2924m, 2854m, 1663m, 1429m, 1249m, 842m.

Compound 5b. A 25 mL round bottom flask equipped with a magnetic stir bar was charged with **4b** (750 mg, 1.17 mmol), potassium hydroxide (197 mg, 3.50 mmol), THF (2.9 mL) and MeOH (2.9 mL). The reaction mixture was stirred until complete

disappearance of the starting product by TLC. After completion, the reaction mixture was diluted with CH₂Cl₂, washed with 10% aqueous HCl (2x), dried with sodium sulfate and the solvent was removed under reduced pressure. The resulting product was charged without further purification in a 25 mL round bottom flask equipped with a magnetic stir bar with 3,5-diiodooctylbenzene (1.33 g, 3.01 mmol), degassed THF (10 mL), degassed DIPEA (1.4 mL, 8.04 mmol), PdCl₂(PPh₃)₂ (28 mg, 0.04 mmol) and CuI (8 mg, 0.04 mmol). The reaction mixture was stirred overnight and diluted with CH₂Cl₂. The organic layer was washed with saturated aqueous NH₄Cl (3x), dried with sodium sulfate and the solvent was removed under reduced pressure. The crude product was purified by flash chromatography on silica gel using hexanes to 10% acetone/hexanes as eluents to afford compound **5b** (732 mg, 65% yield) as a dark orange oil. ¹H NMR (CDCl₃, 400 MHz): 7.68 (s, 2H), 7.66 (s, 2H), 7.49 (s, 2H), 7.38 (m, 2H), 7.27 (s, 2H), 2.52 (t, J = 7.6 Hz, 4H), 2.37 (t, J = 7.6 Hz, 2H), 2.23 (t, J = 6.7 Hz, 6H), 1.72 (m, 2H), 1.58 (m, 4H), 1.49 (m, 6H), 1.26 (m, 42H), 0.87 (m, 9H); ¹³C NMR (CDCl₃, 100 MHz): 171.9, 145.4, 138.4, 137.9, 137.7, 131.2 (2C), 124.8, 124.2, 122.8, 93.9, 89.2, 89.0, 77.9, 77.7, 65.6, 65.5, 37.9, 35.6, 32.2, 32.1, 31.3, 29.9 (3C), 29.7 (2C), 29.6 (2C), 29.5 (3C), 29.4 (2C), 29.1, 29.0, 28.6, 28.5, 25.7 (2C), 22.9 (2C), 19.4 (2C), 14.4: HRMS (APPI-TOF) m/z calcd for C₆₃H₈₅I₂NO[M+H]⁺: 1126.4793, found 1126.4817; FTIR (ATR): 3294w, 2923m, 2852m, 1664m, 1599m, 1553m.

Compound 6b. A 50 mL round bottom flask equipped with a magnetic stir bar was charged with **5b** (2.10 g, 1.87 mmol), degassed THF (18 mL), degassed Et₃N (1.03 mL, 7.46 mmol), PdCl₂(PPh₃)₂ (65 mg, 0.09 mmol), CuI (18 mg, 0.09 mmol) and triisopropylsilyl acetylene (1.67 mL, 7.46 mmol). The reaction mixture was stirred overnight, diluted with CH₂Cl₂, washed with NH₄Cl and dried with sodium sulfate. The solvent was removed under reduced pressure and the crude product was purified by flash chromatography on silica gel using hexanes to 4 % acetone/hexanes as eluents to afford compound **6b** (1.67 g, 73% yield) as an orange oil. ¹H NMR (CDCl₃, 400 MHz): 7.69 (s, 2H), 7.45 (s, 2H), 7.42 (s, 1H), 7.39 (s, 1H), 7.27 (s, 2H), 7.25 (s, 2H), 2.56 (t, J = 7.4 Hz, 4H), 2.35 (t, J = 7.4 Hz, 2H), 2.22 (t, J = 6.8 Hz, 4H), 1.70 (m, 2H), 1.60 (m, 4H), 1.48 (m, 4H), 1.27 (m, 46H), 1.13 (s, 42H), 0.88 (m, 9H); ¹³C NMR (CDCl₃, 100 MHz): 171.9, 143.5, 138.5, 132.8, 132.3, 131.8, 130.6, 124.4, 123.9, 123.1, 122.7, 106.6, 91.1, 89.9,

88.6, 77.8, 77.7, 65.6 (2C), 37.9, 35.8, 32.2, 32.1, 31.4, 29.9 (3C), 29.8, 29.7, 29.6, 29.5 (3C), 29.4 (2C), 29.3, 29.1 (2C), 29.0, 28.6, 28.5, 25.7, 22.9 (2C), 19.4 (2C), 18.9, 14.4, 11.6; HRMS (APPI-TOF) m/z calcd for $C_{85}H_{127}NOSi_2[M+H]^+$: 1234.9529, found 1234.9556; FTIR (ATR): 3294w, 2923m, 2854m, 1663m, 1586m, 880m.

PAM 1b. A 50 mL round bottom flask equipped with a magnetic stir bar was charged with **6b** (1.00 g, 0.81 mmol), THF (16 mL) and TBAF 1.0M solution in THF (2.40 mL, 2.43 mmol). The reaction mixture was stirred until complete disappearance of the starting product by TLC, diluted with CH_2Cl_2 , washed with water (3x) and dried with sodium sulfate. The solvent was removed under reduced pressure. The resulting product was charged without further purification in a 100 mL round bottom flask equipped with a magnetic stir bar with degassed pyridine (25 mL). Another round bottom flask equipped with a magnetic stir bar was charged with CuCl (6.09 g, 61.6 mmol), $CuCl_2$ (1.28 g, 9.54 mmol) and degassed pyridine (123 mL) under N_2 atmosphere. The first solution was added dropwise to the catalyst solution over 4 days and the reaction mixture was stirred for an additional 7 days. The reaction mixture was diluted with $CHCl_3$ and poured in water. The organic phase was extracted successively with water, 25% aqueous NH_4OH , water, 10% aqueous CH_3COOH , water, 10% aqueous NaOH and brine. The organic layer was dried with sodium sulfate and the solvent was removed under reduced pressure. The crude product was purified by flash chromatography on silica gel using 20% hexanes/ $CHCl_3$ to $CHCl_3$ as eluents to afford **PAM 1b** (390 mg, 49% yield) as a white viscous solid. m.p: $>150^\circ C$; 1H NMR ($CDCl_3$, 400 MHz): 7.67 (s, 4H), 7.58 (s, 4H), 7.48 (s, 2H), 7.33 (s, 4H), 7.29 (s, 4H), 7.16 (s, 2H), 2.59 (t, $J = 7.6$ Hz, 8H), 2.39 (t, $J = 7.3$ Hz, 4H), 2.25 (q, $J = 6.9$ Hz, 8H), 1.75 (m, 4H), 1.63 (m, 8H), 1.51 (m, 8H), 1.29 (m, 92H), 0.89 (m, 18H); ^{13}C NMR ($CDCl_3$, 100 MHz): 172.3, 143.3, 137.9, 133.6, 132.2, 132.1, 124.3, 123.5, 123.1 (2C), 122.2, 89.6, 88.9, 81.2, 77.9, 77.7, 74.5, 65.6, 65.5, 37.8 (2C), 35.7, 32.2, 31.2, 29.9 (4C), 29.8, 29.7, 29.6 (2C), 29.4, 29.2, 29.1, 29.0, 28.6 (2C), 28.5, 25.8, 22.9 (2C), 19.5, 17.9, 14.4 (2C), 12.5; MS (MALDI-TOF): calcd for $C_{134}H_{170}N_2O_2[M+H]^+$: 1840.3, found 1842.4; FTIR (ATR): 3300w, 2921m, 2852m, 1668m, 1584m, 1436m.

2.7.3 MALDI-ToF analysis

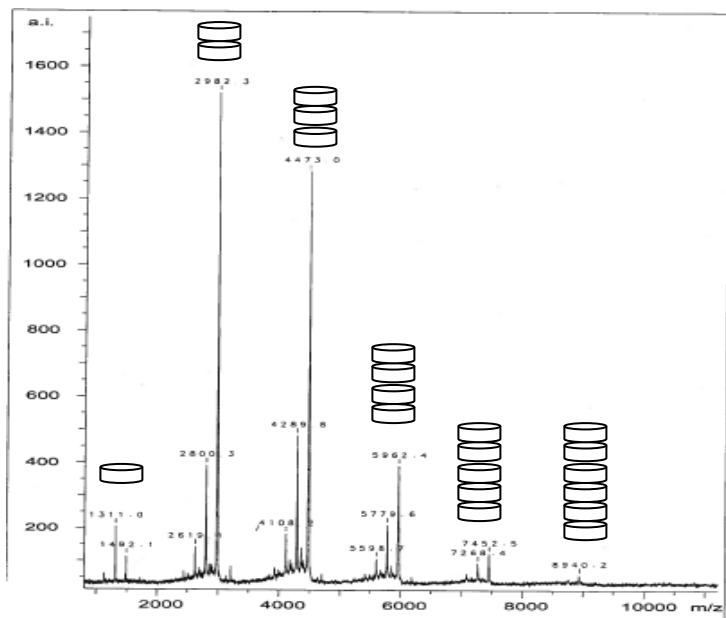


Figure 2.8. MALDI-ToF spectrum of PAM 1a.

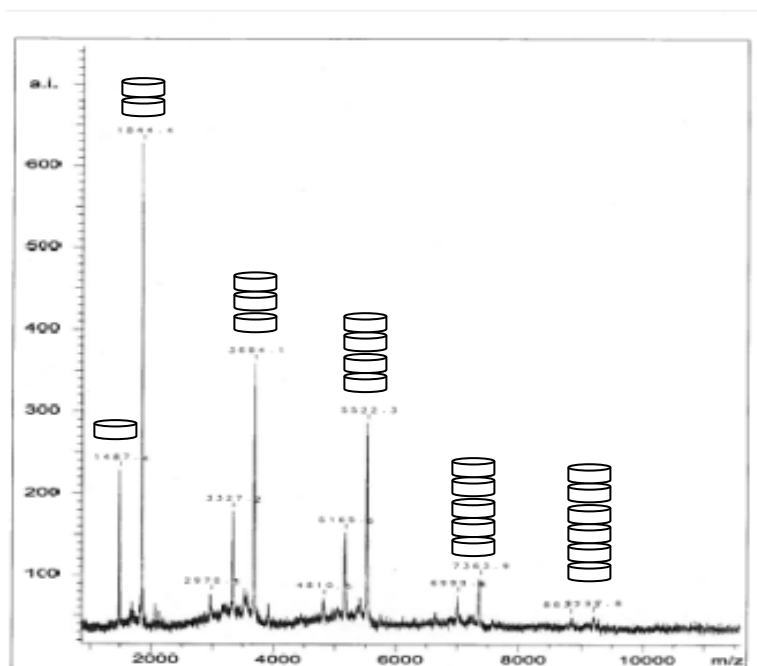


Figure 2.9. MALDI-ToF spectrum of PAM 1b.

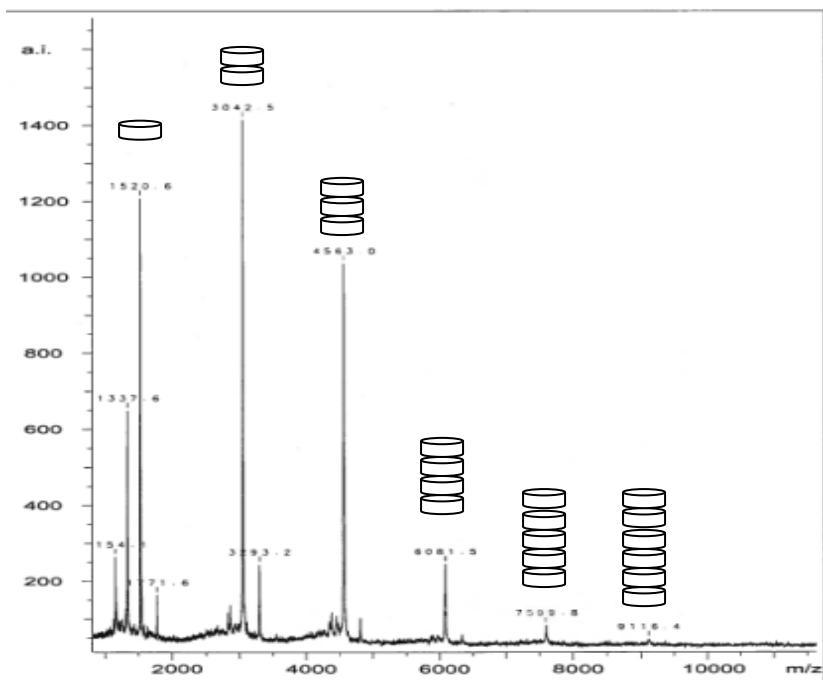


Figure 2.10. MALDI-ToF spectrum of PAM 2a.

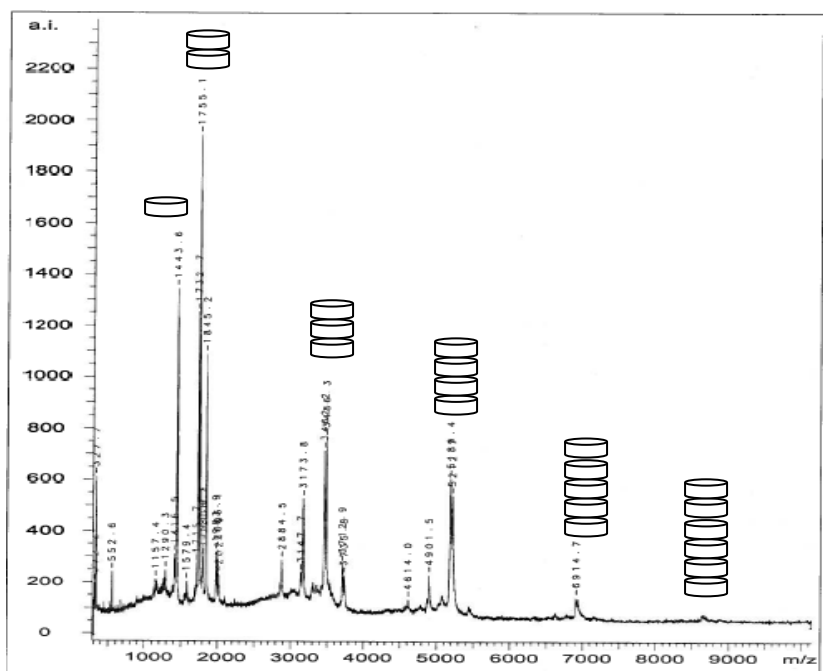


Figure 2.11. MALDI-ToF spectrum of PAM 2b.

2.7.4 XRD analysis

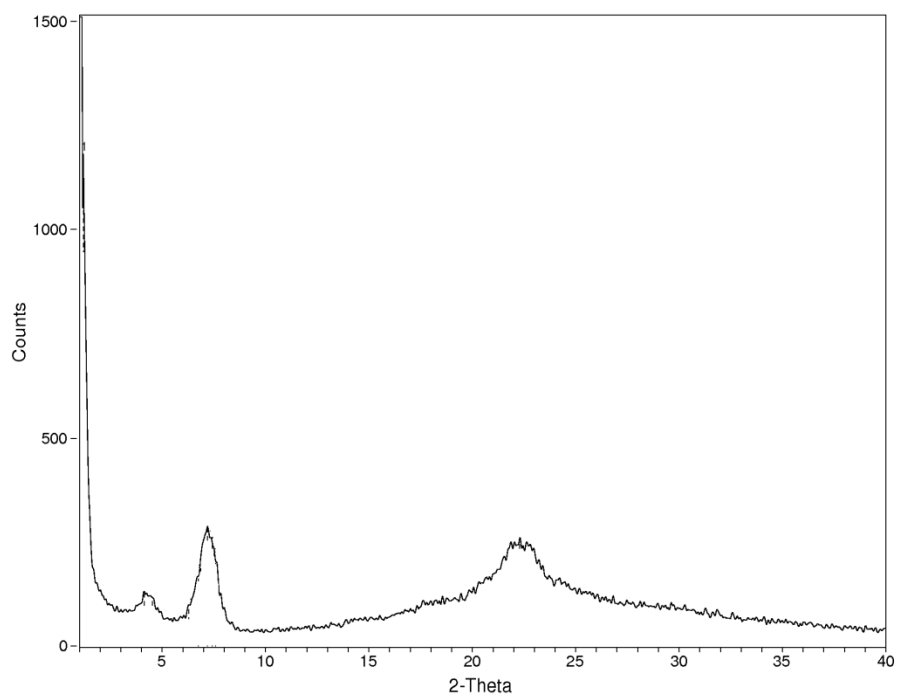


Figure 2.12. X-ray diffraction spectrum of gel of PAM **1a** in toluene (10 mg/mL)

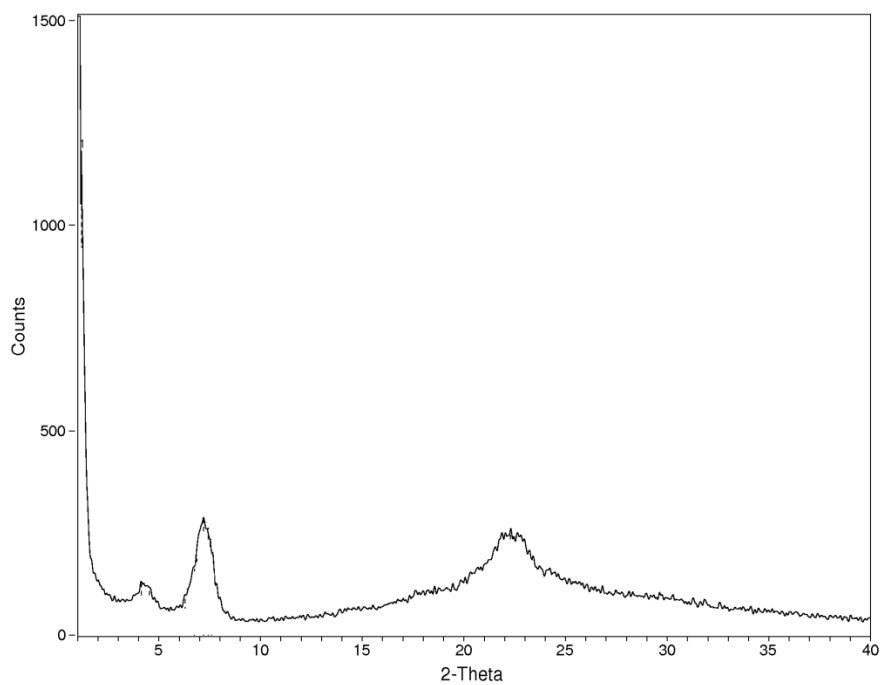


Figure 2.13. X-ray diffraction spectrum of PAM **1b** in toluene (10 mg/mL)

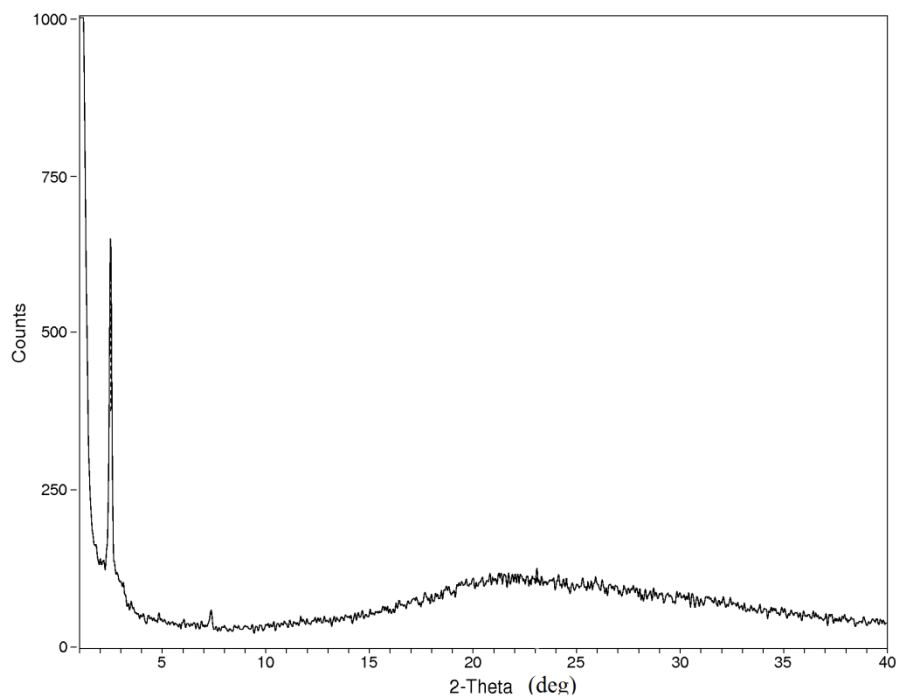


Figure 2.14. X-ray diffraction spectrum of PAM **2a** in cyclohexane (10 mg/mL)

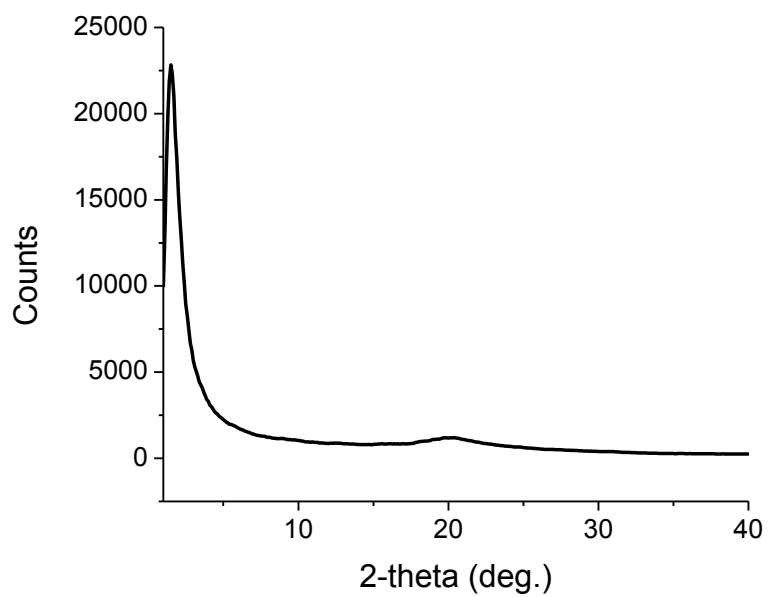


Figure 2.15. X-ray diffraction spectrum of PAM **2a** in ethyl acetate (10 mg/mL)

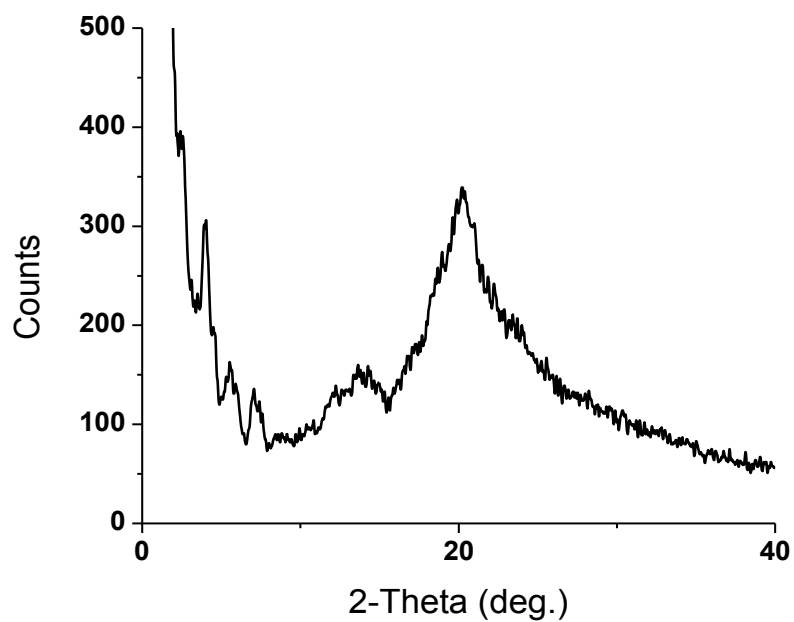


Figure 2.16. X-ray diffraction spectrum of PAM **2b** in ethyl acetate (10 mg/mL)

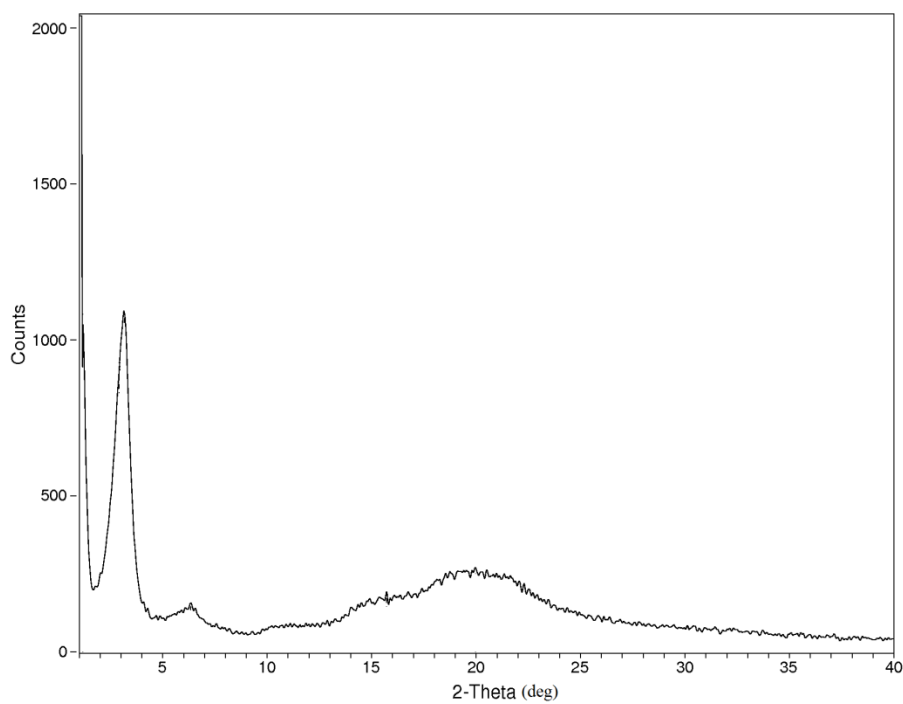


Figure 2.17. X-ray diffraction spectrum of PAM **2b** in cyclohexane (10 mg/mL)

2.7.5 Raman spectroscopy

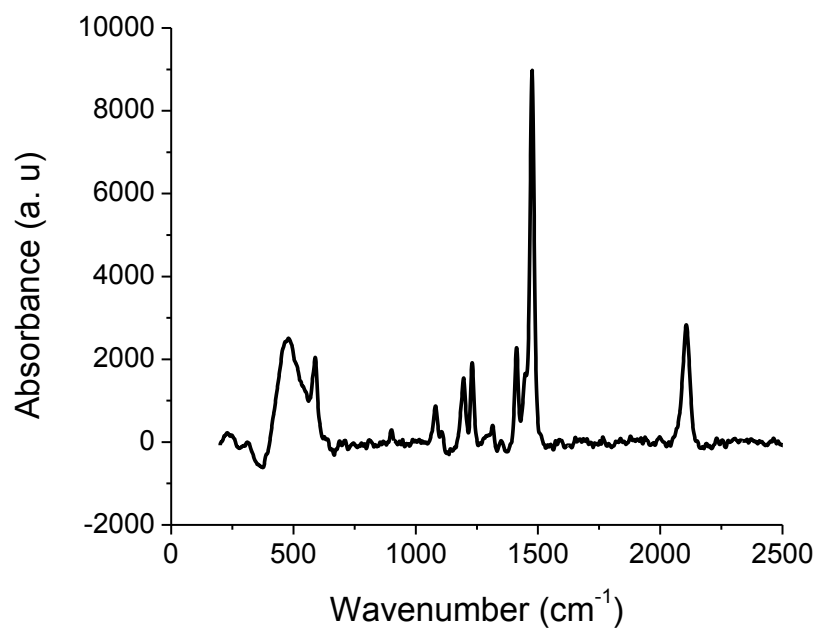


Figure 2.18. Raman spectra of **Poly-2a**.

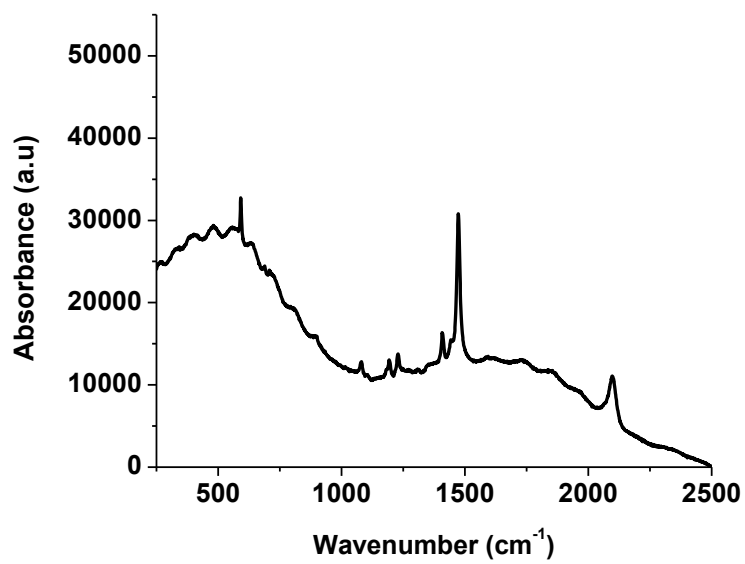


Figure 2.19. Raman spectra of **Poly-2b**.

2.8 Références

- [1] (a) K. Sugiyasu, N. Fujita and S. Shinkai, *Angew. Chem. Int. Ed.* 2004, **43**, 1229; (b) A. Wicklein, S. Ghosh, M. Sommer, F. Würthner and M. Thelakkat, *ACS Nano* 2009, **3**, 1107; (c) S. Banerjee, R. K. Das and U. Maitra, *J. Mater. Chem.* 2009, **19**, 6649; (d) J. Lambrecht, T. P. I. Saragi and J. Salbeck, *J. Mater. Chem.* 2011, **21**, 18266; (e) Y. Sun, L. Jiang, K. C. Schuermann, W. Adriaens, L. Zhang, F. Y. C. Boey, L. De Cola, L. Brunsveld and X. Chen, *Chem. Eur. J.* 2011, **17**, 4746.
- [2] (a) J. Wu, W. Pisula and K. Müllen, *Chem. Rev.* 2007, **107**, 718 and references therein;
- [3] (a) S.-I. Tamaru, M. Nakamura, M. Takeuchi and S. Shinkai, *Org. Lett.* 2001, **3**, 3631; (b) M. Shirakawa, S.-i. Kawano, N. Fujita, K. Sada and S. Shinkai, *J. Org. Chem.* 2003, **68**, 5037; (c) M. Shirakawa, N. Fujita and S. Shinkai, *J. Am. Chem. Soc.* 2003, **125**, 9902; (d) M. Shirakawa, N. Fujita and S. Shinkai, *J. Am. Chem. Soc.* 2005, **127**, 4164; (e) T. Kishida, N. Fujita, K. Sada and S. Shinkai, *J. Am. Chem. Soc.* 2005, **127**, 7298.
- [4] (a) S. Okada, H. Matsuda and A. Masaki, *Chem. Lett.* 1990, 2213; (b) M. Kijima, H. Tanimoto, H. Shirakawa, A. Oya, T.-T. Liang and Y. Yamada, *Carbon* 2001, **39**, 287; (c) L. Ding and S. V. Olesik, *Nano Lett.* 2004, **4**, 2271 (d) M. Kijima, H. Tanimoto, K. Takakura, D. Fujiya, Y. Ayuta and K. Matsuishi, *Carbon* 2007, **45**, 594; (e) T. N. Hoheisel, S. Schrettl, R. Szilluweit and H. Frauenrath, *Angew. Chem., Int. Ed.*, 2010, **49**, 6496; (f) J. R. Néabo, K. I. S. Tohondjona and J.-F. Morin, J.-F. *Org. Lett.* 2011, **13**, 1358; (g) J. R. Néabo, C. Vigier-Carrière, S. Rondeau-Gagné and J.-F. Morin, *Chem. Commun.* 2012, **48**, 10144; (h) R. Szilluweit, T. N. Hoheisel, M. Fritzsche, B. Ketterer, A. F. Morral, D. Demurtas, V. Laporte, R. Verel, S. Bolisetty, R. Mezzenga and H. Frauenrath, *Nano Lett.* 2012, **12**, 2573.
- [5] (a) F. J. M. Hoeben, P. Jonkheijm, E. W. Meijer and A. P. H. J. Schenning, *Chem. Rev.* 2005, **105**, 1491; (b) C. R. L. P. N. Jeukens, P. Jonkheijm, F. J. P. Wijnen, J. C. Gielen, P. C. M. Christianen, A. P. H. J. Schenning, E. W. Meijer and J. C. Maan, *J. Am. Chem. Soc.* 2005, **127**, 8280; (c) A. Ajayaghosh, R. Varghese, V. K. Praveen and S. Mahesh, *Angew. Chem. Int. Ed.* 2006, **45**, 3261.
- [6] For reviews on PAMs, see: (a) J. S. Moore, *Acc. Chem. Res.* 1997, **30**, 402; (b) S. Höger, *J. Polym. Sci. Part A* 1999, **37**, 2685; (c) C. Grave and A. D. Schlüter, *Eur. J. Org. Chem.* 2002, 3075; (d) D. Zhao and J. S. Moore, *Chem. Commun.* 2003, 807; (e) S. Höger, *Chem. Eur. J.* 2004, **10**, 1320; (f) Hoyer, S. *Chem. Eur. J.* 2004, **10**, 1320; (g) W. Zhang and J. S. Moore, *Angew. Chem. Int. Ed.* 2006, **45**, 4416; (h) D. Pasini and M. Ricci, *Curr. Org. Synth.* 2007, **4**, 59; (i) L. Zhang, Y. Che and J. S. Moore, *Acc. Chem. Res.* 2008, **41**, 1596; (j) S. Höger, *Pure Appl. Chem.* 2010, **82**, 821.
- [7] (a) A. S. Shetty, P. R. Fischer, K. F. Stork, P. W. Bohn and J. S. Moore, *J. Am. Chem. Soc.*, 1996, **118**, 9409; (b) A. Datar, D. E. Gross, K. Balakrishnan, X. Yang, J. S. Moore and L. Zang, *Chem. Commun.* 2012, **48**, 8904.

-
- [8] (a) H. Shimura, M. Yoshio and T. Kato, *Org. Biomol. Chem.* 2009, **7**, 3205.; (b) I. Hisaki, H. Senga, H. Shigemitsu, N. Tohnai and M. Miyata, *Chem. Eur. J.* 2011, **51**, 14348.
- [9] (a) J. Zhang and J. S. Moore, *J. Am. Chem. Soc.* 1992, **114**, 9701; (b) A. S. Shetty, J. Zhang and J. S. Moore, *J. Am. Chem. Soc.* 1996, **118**, 1019; (c) Y. Tobe, N. Utsumi, A. Nagano and K. Naemura, *Angew. Chem. Int. Ed.* 1998, **37**, 1285; (d) Y. Tobe, A. Nagano, K. Kawabata, M. Sonoda and K. Naemura, *Org. Lett.* 2000, **2**, 3265; (e) C.-H. Lin and J. M. Tour, *J. Org. Chem.* 2002, **67**, 7761; (f) Y. Tobe, N. Utsumi, K. Kawabata, A. Nagano, K. Adachi, S. Araki, M. Sonoda, K. Hirose and K. Naemura, *J. Am. Chem. Soc.* 2002, **124**, 5350; (g) S. Klyatskaya, N. Dingenouts, C. Rosenauer, B. Müller and S. Höger *J. Am. Chem. Soc.* 2006, **128**, 3150 ; (h) L. Shu and M. Mayor, *Chem. Commun.* 2006, 4134; (i) L. Shu, M. Müri, R. Krupke and M. Mayor, *Org. Biomol. Chem.* 2009, **7**, 1081; (j) H. Wettach, S. Höger, D. Chaudhuri, J. M. Lupton, F. Liu, E. M. Lupton, S. Tretiak, G. Wang, M. Li, S. De Feyter, S. Fischerf and S. Förster, *J. Mater. Chem.* 2011, **21**, 1404 ; (k) L. Li, Y. Che, D. E. Gross, H. Huang, J. S. Moore and L. Zang, *ACS Macro. Lett.* 2012, **1**, 1335;
- [10] (a) K. Balakrishnan, A. Datar, W. Zhang, X. Yang, T. Naddo, J. Huang, J. Zuo, M. Yen, J. S. Moore and L. Zang, *J. Am. Chem. Soc.* 2006, **128**, 6576; (b) N. Naddo, Y. Che, W. Zhang, K. Balakrishnan, X. Yang, J. Zhao, J. S. Moore and L. Zang, *J. Am. Chem. Soc.* 2007, **129**, 6978; (c) K. Cantin, S. Rondeau-Gagné, J. R. Néabo, M. Daigle and J.-F. Morin, *Org. Biomol. Chem.* 2011, **9**, 4440; (d) J. Vollmeyer, S.-S. Jester, F. Eberhagen, T. Prangenberg, W. Mader and S. Höger, *Chem. Commun.* 2012, **48**, 6547;
- [11] S. Rondeau-Gagné, J. R. Néabo, M. Desroches, J. Larouche, J. Brisson and J.-F. Morin, *J. Am. Chem. Soc.* **2013**, *135*, 110.
- [12] (a) M. Shirakawa, N. Fujita, S. Shinkai, *J. Am. Chem. Soc.* 2005, **127**, 4164; (b) Z. Li, F. W. Fowler, J. W. Lauher, *J. Am. Chem. Soc.* 2009, **131**, 634.
- [13] M. Berubé and D. Poirier, *Org. Lett.* 2004, **6**, 3127.
- [14] S. Höger, A.-D. Meckenstock and S. Müller, *Chem. Eur. J.* 1998, **4**, 2423.
- [15] D. O’Krongly, S. R. Denmeade, M. Y. Chiang and R. Breslow, *J. Am. Chem. Soc.* 1985, **107**, 5544.
- [16] P. D. Frischmann, S. Guieu, R. Tabeshi and M. J. MacLachlan, *J. Am. Chem. Soc.* 2010, **132**, 7668.
- [17] (a) A. J. Gallant and M. J. MacLachlan, *Angew. Chem. Int. Ed.* 2003, **42**, 5307; (b) S. Guieu, A. K. Crane and M. J. MacLachlan, *Chem. Commun.* **47**, 2011, 1169.
- [18] (a) A. de Vries, *J. Chem. Phys.* 1979, **70**, 2705; (b) A. Soldera, M.-A. Beaudoin, G. O’Brien and J. Lessard, *Liq. Cryst.* 2005, **32**, 1223.
- [19] (a) G. Wegner, *Natureforsch. B: Chem. Sci.* 1969, **24**, 824 ; (b) G. Wegner, *Makromol. Chem.* 1972, **154**, 35.
- [20] F. W. Fowler, J. W. Lauher, In *Carbon-Rich Compounds*; M. M. Haley, R. R. Tykwinski, Eds.; Wiley-Vch Verlag GmbH & Co: Weinheim, 2006.
- [21] J. Nagasawa, M. Yoshida and N. Tamaoki, *Eur. J. Org. Chem.* 2011, 2247.

-
- [22] (a) Y. Xu, M. D. Smith, M. F. Geer, P. J. Pellechia, J. C Brown, A. C. Wibowo and L. S. Shimizu, *J. Am. Chem. Soc.* 2010, **132**, 5334 ; (b) T.-J. Hsu, F. W. Fowler and J. W. Lauher, *J. Am. Chem. Soc.* 2012, **134**, 142.
- [23] For representative examples, see: (a) N.Tamaoki, S. Shimada, Y. Okada, A. Belaïssaoui, G. Kruk, K. Yase and H. Matsuda, *Langmuir* 2000, **16**, 7545. (b) J. Nagasawa, M. Kudo, S. Hayashi and N. Tamaoki, *Langmuir* 2004, **20**, 7907 ; (c) K. Aoki, M. Kudo and N. Tamaoki, *Org. Lett.* 2004, **6**, 4009 ; (d) X. Nie and G. Wang, *J. Org. Chem.* 2006, **71**, 4734; (e) (f) N. Fujita, Y. Sakamoto, M. Shirakawa, M. Ojima, A. Fujii, M. Ozaki and S. Shinkai, *J. Am. Chem. Soc.* 2007, **129**, 4134 ; (f) E. Jahnke, J. Weiss, S. Neuhaus, T. N. Hoheisel and H. Frauenrath, *Chem. Eur. J.* 2009, **15**, 338; (g) S. R. Diegelmann, N. Hartman, N. Markovic and J. D. Tovar, *J. Am. Chem. Soc.* 2012, **134**, 2028.
- [24] O. J. Dautel, M. Robitzer, J.-P. Lère-Porte, F. Serein-Spirau and J. J. E. Moreau, *J. Am. Chem. Soc.* 2006, **128**, 16213.
- [25] M. J. Frisch, G. W. Trucks, H. B. Schlegel, G. E. Scuseria, M. A. Robb, J. R. Cheeseman, G. Scalmani, V. Barone, B. Mennucci, G. A. Petersson, H. Nakatsuji, M. Caricato, X. Li, H. P. Hratchian, A. F. Izmaylov, J. Bloino, G. Zheng, J. L. Sonnenberg, M. Hada, M. Ehara, K. Toyota, R. Fukuda, J. Hasegawa, M. Ishida, T. Nakajima, Y. Honda, O. Kitao, H. Nakai, T. Vreven, J. Montgomery, J. A. ; , J. E. Peralta, F. Ogliaro, M. Bearpark, J. J. Heyd, E. Brothers, K. N. Kudin, V. N. Staroverov, R. Kobayashi, J. Normand, K. Raghavachari, A. Rendell, J. C. Burant, S. S. Iyengar, J. Tomasi, M. Cossi, N. Rega, N. J. Millam, M. Klene, J. E. Knox, J. B. Cross, V. Bakken, C. Adamo, J. Jaramillo, R. Gomperts, R. E. Stratmann, O. Yazyev, A. J. Austin, R. Cammi, C. Pomelli, J. W. Ochterski, R. L. Martin, K. Morokuma, V. G. Zakrzewski, G. A. Voth, P. Salvador, J. J. Dannenberg, S. Dapprich, A. D. Daniels, Ö. Farkas, J. B. Foresman, J. V. Ortiz, J. Cioslowski and D. J. Fox, *Gaussian 09*, (2009) Gaussian, Inc., Wallingford CT.
- [26] Y. Zhao, N. E. Schultz and D. G. Truhlar, *J. Chem. Theory Comput.* 2006, **2**, 364.
- [27] S. K. Kolev, P. St Petkov, M. A. Rangelov and G. N. Vayssilov, *J. Phys. Chem. A* 2011, **115**, 14054.
- [28] Y. Tobe, N. Utsumi, A. Nagano, M. Sonoda and K. Naemura, *Tetrahedron* 2001, **57**, 8075.
- [29] (a) Y. Yang, B. Samas, V. O. Kennedy, D. Macikenas, B. L. Chaloux, J. A. Miller, R. L. Speer, J. Protasiewicz, A. A. Pinkerton and M. E. Kenney, *J. Chem. Phys. A* **2011**, *115*, 12474; (b) Y. Yang, V. O. Kennedy, J. B. Updegraph, B. Samas, D. Macikenas, B. Chaloux, J. A. Miller, E. M. Van Goethem and M. E. Kenney, *J. Chem. Phys. A* **2012**, *116*, 8718;
- [30] O. Y. Mindyuk, M. R. Stetzer, P. A. Heiney, J. C. Nelson and J. S. Moore, *Adv. Mater.* **1998**, *10*, 1363.
- [31] Images from CYLview code [CYLview, 1.0b; Legault, C. Y., Université de Sherbrooke, 2009 (<http://www.cylview.org>)]

Chapitre 3.

Polymérisation topochimique de macrocycles de phénylacétylène : une nouvelle stratégie pour la préparation de nanobâtonnets organiques

Topochemical polymerization of phenylacetylene macrocycles: a new strategy for the preparation of organic nanorods

Simon Rondeau-Gagné, Jules Roméo Néabo, Maude Desroches, Jérémie Larouche, Josée Brisson and Jean-François Morin*

Département de Chimie and Centre de Recherche sur les Matériaux Avancés (CERMA), 1045 Ave de la Médecine, Pavillon Alexandre-Vachon, Université Laval, Québec, QC, Canada G1V 0A6.

Publié dans la revue *Journal of the American Chemical Society*, **2013**, 135, 110-113.

3.1 Préambule

Cet article présente la synthèse d'un macrocycle de type phénylacétylène portant, dans sa périphérie, des unités diyne réactives vis-à-vis d'une polymérisation topochemique. Grâce aux fonctions amides, permettant l'auto-assemblage sous forme de gel, il a été possible d'effectuer la polymérisation sur ce monomère rigide, réaction jusque-là impossible sur les PAMs. Les nano-architectures formées ont été caractérisées et ont présenté une structure de bâtonnet. Ma contribution à ce travail est majeure. J'ai participé à la synthèse de tous les produits et à la caractérisation des nano-architectures finales. J'ai également participé à la recherche bibliographique et à la rédaction de l'article.

3.2 Résumé

Des nanobâtonnets organiques solubles ont été préparés à partir de macrocycles de phénylacétylène en utilisant la polymérisation topochemique d'unités butadiynes placées à l'intérieur et à l'extérieur du squelette des macrocycles. Les macrocycles contenant des groupes amide ont été autoassemblés dans un mode colonnaire à l'état gel dans l'acétate d'éthyle. Lors d'une irradiation avec de la lumière UV, les signaux Raman associés aux butadiynes ont complètement disparu, ce qui signifie que les nouveaux nanobâtonnets sont bel et bien liés de manière covalente.

3.3 Abstract

Soluble organic nanorods were prepared from phenylacetylene macrocycles using the topochemical polymerization of butadiyne moieties placed both inside and outside the macrocycles' skeleton. Macrocycles containing amide groups were self-assembled in a columnar fashion through the formation of an organogel in ethyl acetate. Upon irradiation with UV light, the Raman signals associated to butadiyne units completely vanished, meaning that covalently linked nanorods have been created.

3.4 Introduction

The supramolecular self-assembly of macrocycles is one of the most popular strategies to prepare organic nanotubes with new properties for different applications including host-guest chemistry,¹ scaffolding² and gas storage.³ One major drawback of these supramolecular assemblies is their relative kinetic instability. Because they rely on weak interactions such as hydrogen bonding, π - π and van der Waals interactions, the conditions

in which they are employed and characterized are very restricted, limiting their use in devices. Thus, strategies to improve their stability have been developed and one of the most promising ones is the covalent attachment between the macrocycles once the supramolecular assembly is formed. This strategy has proven to be successful with many types of macrocycles such as cyclodextrin,⁴ cyclic oligopeptides⁵ and calixarene.⁶ Many attempts to prepare nanotubes from phenylacetylene macrocycles (PAMs) in the crystalline state using 1,3-butadiyne topochemical polymerization⁷ have been reported, but most of them failed⁸ or have led to rapid decomposition to produce undefined, insoluble carbon residues.^{9,10}

Recently, we attempted to use this strategy to make stable organic nanotubes from phenylacetylene macrocycle (PAM) **1** (Figure 3.1)¹¹ by cross-linking the butadiyne moieties through photo-induced topochemical reactions to yield polydiacetylene (PDA)-walled nanotubes. However, we found that only very short PDA oligomers were formed under UV irradiation and that the yield of polymerization was very low, although PDA formation from non-macrocyclic 1,4-diarylbutadiyne derivatives in the gel state proved to be efficient.¹² We hypothesized that the butadiyne moieties were not reactive because of the high rigidity of the macrocycle.¹³ One way to drive the topochemical polymerization is to heat the butadiyne-containing materials in the solid state. Shimizu¹⁴ and Lauher¹⁵ independently used this strategy very recently to prepare insoluble, non-processable nanotubes from macrocycles with flexible backbones. However, heating the PAM **1** in the solid state, which was not crystalline but in a dried gel state, destroyed the hydrogen bonds network that holds the macrocycles in a face-to-face configuration. Therefore, we have designed a new macrocycle (PAM **2**, Figure 3.1) possessing cross-linkable butadiyne units with two alkyl fragments at both ends, providing a more flexible environment that should enable the topochemical polymerization. The cross-linking of those units at the exterior of the macrocycle should lead to a covalently linked, stable organic nanotube that could be further heated to allow topochemical polymerization of the butadiyne moieties present within the PAM backbone.

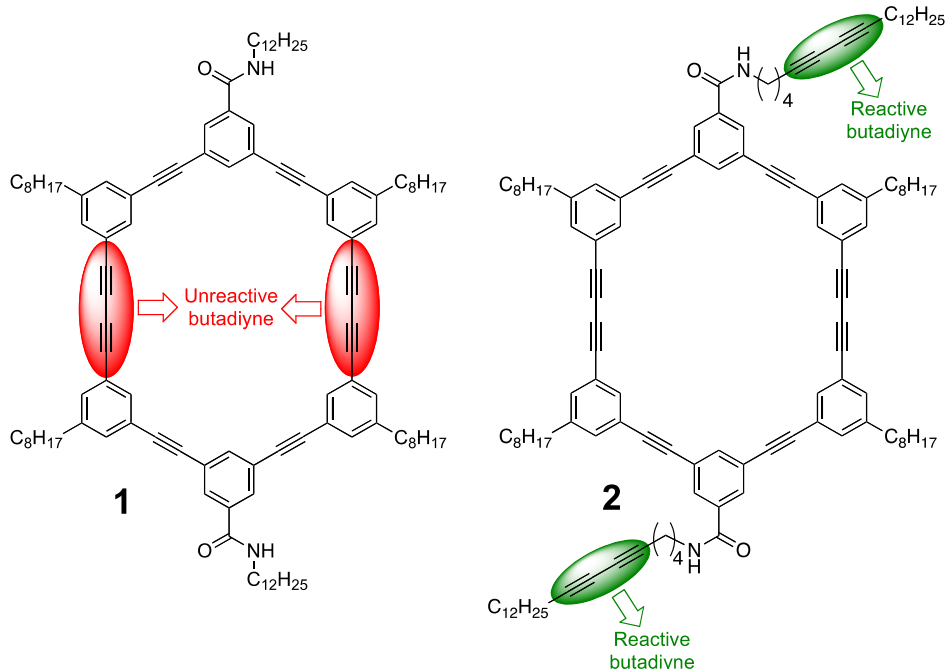


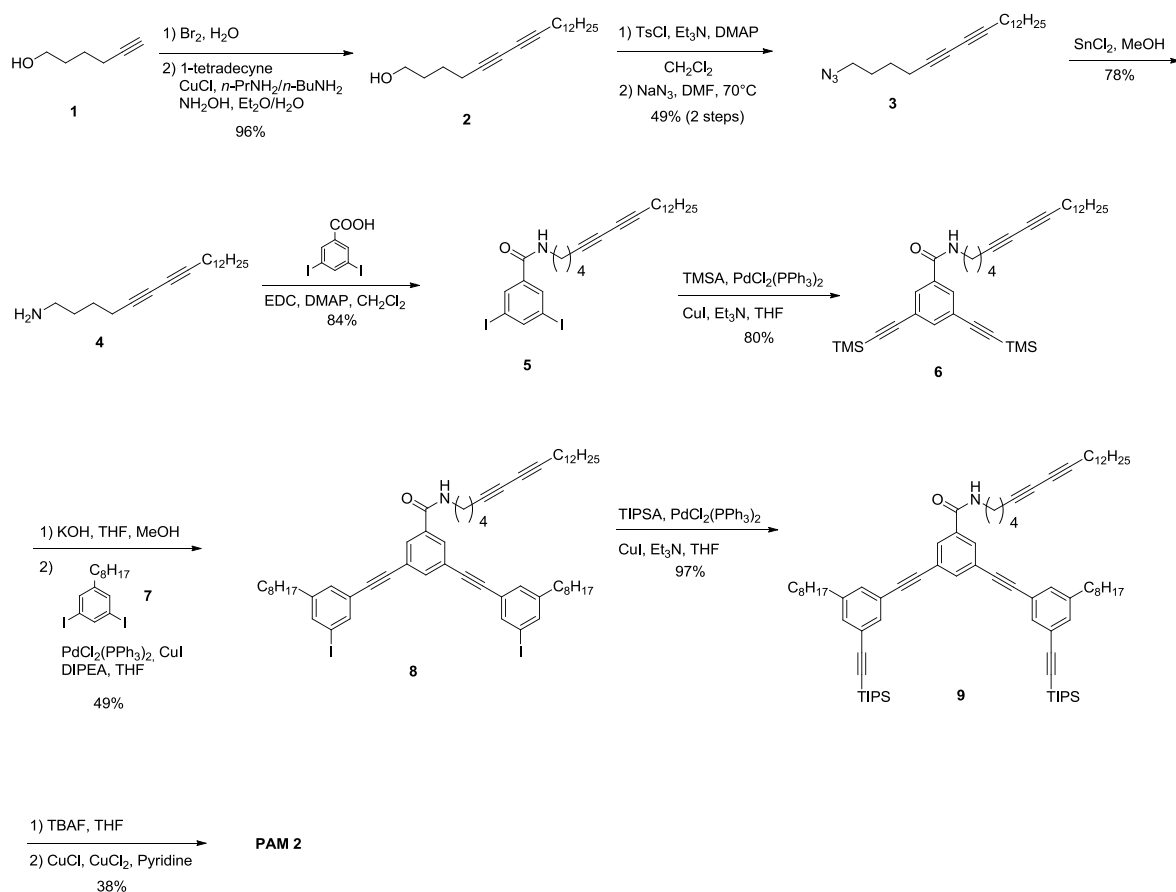
Figure 3.1. Phenylacetylene macrocycles **1** and **2**.

Herein, we report the synthesis, self-assembly and topochemical polymerization in the gel state of a phenylacetylene macrocycle (PAM **2**) bearing multiple cross-linkable butadiyne moieties, leading to soluble, one-dimensional nanorods. At this time, it is not possible to confirm whether or not the resulting architectures possess an inner cavity. To the best of our knowledge, this is the first report of a controlled topochemical polymerization involving a six-membered PAM, although many over the years have pursued this goal. The use of rigid, conjugated and carbon-rich macrocycles represents a necessary step toward the preparation of shape-persistent, non-graphitic nanotubes and nanorods with unique semi-conducting properties.

3.5 Results and Discussion

We have reported the synthesis of PAM **1** previously¹¹ and the synthesis of PAM **2** is shown on Scheme 3.1. Starting from 5-hexyn-1-ol, a bromination reaction on the terminal alkyne was conducted with bromine to yield the corresponding bromoalkyne that was immediately subjected to a Cadiot-Chodkiewicz¹⁶ coupling reaction with 1-tetradecyne to yield compound **2** in 96% yield over 2 steps. Then, the hydroxyl group was replaced by an azido group using a tosylate intermediate to give compound **3**. The azido group was then

reduced into amino using tin chloride and the resulting compound **4** was coupled to 3,5-diiodobenzoic acid¹¹ using standard Steglich conditions to give compound **5** in 84% yield. Sonogashira coupling was used to install trimethylsilylacetylene (TMSA) and both 3 and 5 position and the alkyne groups were then deprotected. The resulting compound was coupled again through Sonogashira coupling to 3,5-diiodo-octylbenzene¹¹ in moderate yield. Another Sonogashira coupling was performed on the iodo-bearing positions with triisopropylsilylacetylene (TIPSA) and the resulting molecule (compound **9**) was deprotected using tetrabutylammonium fluoride (TBAF) to provide the half-macrocycle. Finally, a ring closure reaction using Eglinton conditions was performed in dilute solution to give the PAM **2** in moderate 38% yield. PAM **2** was purified by standard column chromatography and shows moderate to good solubility in common organic solvents.



Scheme 3.1. Synthesis of PAM2

The gelation properties of PAM **2** were studied in common organic solvents and the detailed results are presented in the Table 3.1 in the Supporting Information (SI) section. PAM **2** gelified in several solvents including benzene, acetone, cyclohexane and hexanes. In those solvents, translucent gels were obtained at a concentration as low as 1.0 wt%. In ethyl acetate however, very stable but opaque gels were obtained at the same concentration, leading to larger crystallites within the organogel (see Figure 3.6 in SI). It is worth noticing that further characterization of the ethyl acetate organogel had to be performed quickly since it turns blue very rapidly under ambient conditions, indicating the formation PDA within the supramolecular assembly.

To gain better insight on the nanoscale morphology of the ethyl acetate organogel, scanning electron microscopy (SEM) analysis has been performed and the results are shown in Figure 3.2. As expected, the organogel of PAM **2** is made of microns-long fibers with diameter of about 200 nm. As we observed previously for PAM **1**, the fibers stacked to form few microns-thick bundles, suggesting strong interfiber interactions.^{8,17}

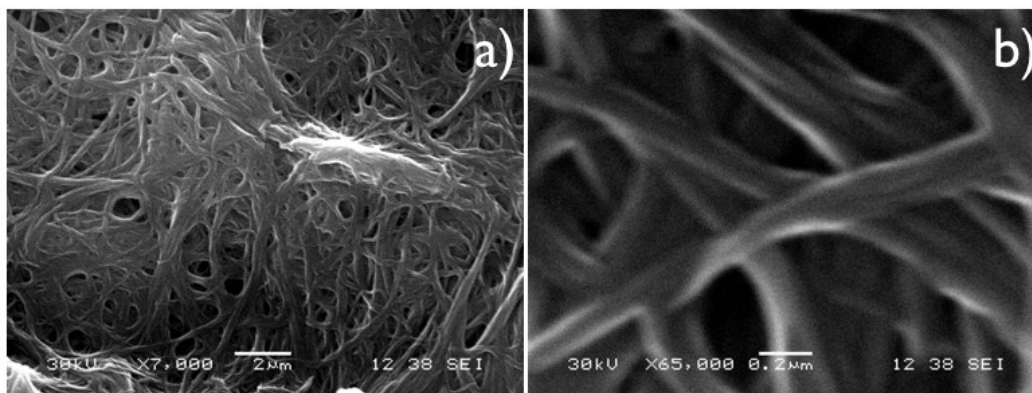


Figure 3.2. SEM images of dried ethyl acetate organogel from PAM2 (10 mg/mL). Scale bars are (a) 2 μm and (b) 0.2 μm .

XRD analysis on the same dried gel was also performed in order to obtain information about the intermolecular interactions and the distances within the supramolecular assembly. The XRD pattern is rather complex and shows peaks in the small angle region at $2\theta = 7.0$

and 4.0, corresponding to a ratio of $1:1/\sqrt{3}$, which can be indexed as the (100) and (110) reflections of a hexagonal lattice (Col_h) (see Figure 3.7 in SI).^{11,18} The other peaks in the small angle region cannot be attributed with certainty yet but are likely to be attributed to a columnar phase with different symmetry. The broad peak centered at $2\theta = 20.2$ (4.39 \AA) can be ascribed to the intracolumnar liquid-like order between the alkyl chains. These results suggest that the macrocycles within the organogel phase are in proper orientation to react with each other through topochemical reactions to give a nanotubular structure.

In order to connect the macrocycles to fix the supramolecular assembly, topochemical polymerization of the external butadiyne units was attempted using UV light (254 nm) on the organogel. Organogels obtained from different solvents, all at a concentration of 10 mg/mL, were tested. Interestingly, only the organogel obtained from ethyl acetate turned blue under UV light irradiation for 24 hours (see Figure 3.6 SI). After the reaction, the ethyl acetate was removed and chloroform was added, providing an intense blue solution with slight turbidity (see Figure 3.6 in SI). This solution was analyzed by size-exclusion chromatography (SEC) after it was filtered on a 0.45 micron filter. It is worth mentioning that appreciable amount of insoluble blue material was left on the filter (ca. 30-50wt% of the irradiated material) As shown in Figure 3.10 the SI section, high-molecular weight materials have been formed upon irradiation, although PAM **2** is still present in rather high concentration. Hence, semi-preparative SEC experiment was performed to isolate the higher molecular weight fraction between 6 and 7.5 minutes. About 3 milligrams of intense blue materials was thus obtained from 20 milligrams of PAM **2**, resulting in a yield of ca. 15% of soluble, cross-linked material. It is worth mentioning that the nanorods stay soluble as long as they were not dried in which case they can be dispersed but not resolubilized. The other fractions (retention time higher than 8 minutes) were also collected but no further analysis was performed on them since they appear as bluish green materials, suggesting incomplete topochemical polymerization.

The optical properties of the SEC-purified blue material were studied by UV-visible spectroscopy in chloroform solution. A broad absorption band with a λ_{max} of 654 nm appeared upon irradiation, which is characteristic of the PDA backbone (see Figure 3.9 in SI). As an empirical proof of the formation of organic nanorods, the thermochromic

properties of this material were studied both in solution and in the solid state. As expected, no sign of thermochromism both in solution and in the solid state was detected in the numerous conditions tested, which indicates that the PDAs formed are in a very rigid environment without possibility of chain torsion. This result eliminates at some point the possibility of having a covalent polymer chain in which the macrocycles are attached at only one end to each other. In this particular case, one can assume that the resulting PDA would exhibit chromism properties due to the steric hindrance between the macrocycles that would force the polymer chain to twist, especially when polar solvents like DMSO and DMF are used to break the intramolecular hydrogen bonds network.

To assess whether or not all the external diyne moieties have been consumed upon irradiation to form PDA, the purified blue material was analyzed by Raman spectroscopy and the results are shown in Figure 3.3. The powder spectrum of PAM **2** exhibits a strong band at 2222 cm^{-1} associated to the stretching mode of the diyne moieties. Unexpectedly, this band disappears completely upon irradiation for 24 hours, suggesting that all the diyne moieties, even those within the macrocycle skeleton, reacted to give PDA derivatives as shown in Figure 3.11 in SI. This was confirmed by the appearance of new bands at 1473 and 2096 cm^{-1} attributed to the stretching vibration modes of newly formed alkene and alkyne groups, respectively. Although the driving force for the topochemical polymerization of the diyne units inside the macrocycle is not yet understood, we hypothesize that topochemical polymerization reactions occur on the outer part of the macrocycle first and, consequently, positioned properly the diyne moieties inside the macrocycle to undergo the second topochemical polymerization. The lack of diyne signals in the final material discard the possibility of having a single-point attachment between two macrocycles. This result is in perfect agreement with the absence of thermochromic properties of the blue material obtained after UV irradiation.

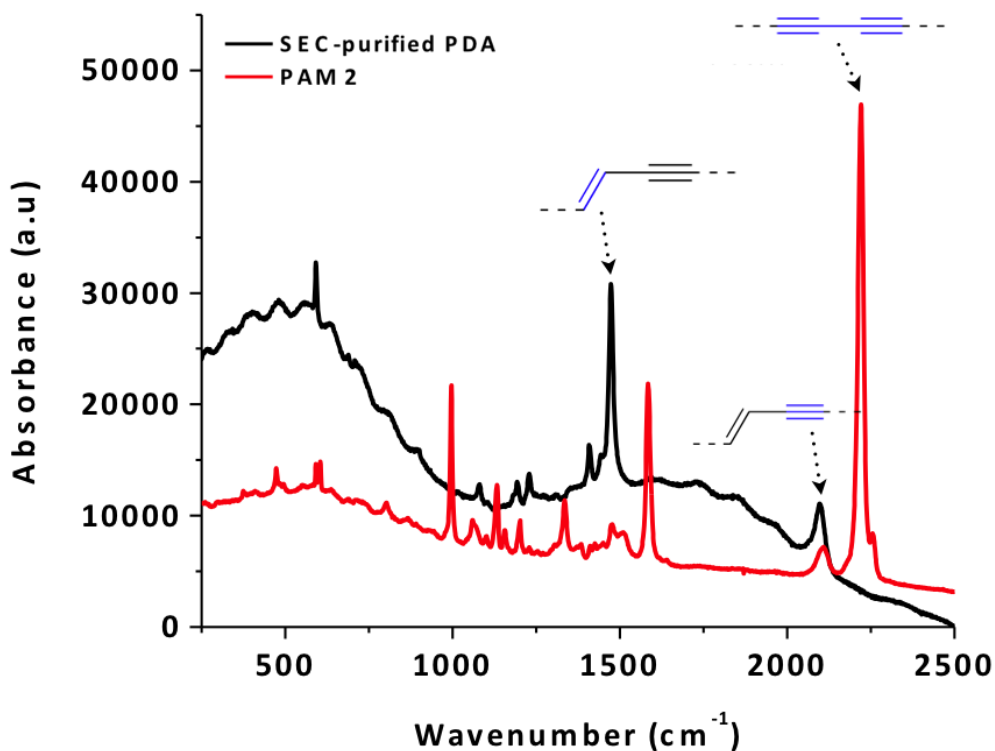


Figure 3.3. Raman spectra of PAM 2 (red) and SEC-purified blue material (black).

Powder XRD analysis was performed on nanorods obtained after SEC purification and the diffractogram is presented on Figure 3.8 in SI. Interestingly, a broad peak at $2\theta = 20.2$ (4.39 \AA) is still present, indicating that intramolecular alkyl chain interactions have been preserved. Also, a less intense and broad peak appears at $2\theta = 3.6$ (24.5 \AA), which corresponds to the nanorods diameter.

High-resolution transmission electron microscopy (HRTEM) measurements were recorded on the purified nanorods and the results are shown on Figure 3.4. The nanorods formed are several tens of nanometers-long and 2 to 3 nanometers wide, which is in perfect agreement with the structural parameters calculated by molecular modeling and the distance measured by XRD analysis. The length of the nanorods also suggests that topochemical polymerization can be accomplished over a long range (several tens of macrocycles). Although it was not possible to visualize in internal void of the nanorods by HRTEM, the presence of columnar phases and the π - π stacking between the macrocycles within the organogel phase of PAM 2, as proven by XRD analysis, serve as strong indication that the

resulting material is made of covalently-linked one-dimensional stacks of macrocycle, probably forming tubular architectures with a calculated internal diameter of ca. 8 Å (see Figure 3.11 in SI). In fact, intercolumnar topochemical reactions are unlikely since the formation of PDA is very dependent on the distance between monomer (~ 4.9 Å) and the angle (45°) between the reacting butadiyne units.⁷ For the same reason, cross-linking reactions occurring in amorphous phases (if present) are highly improbable, leaving the formation of 1D nanorods, as shown in Figure 3.5, as the only plausible product.

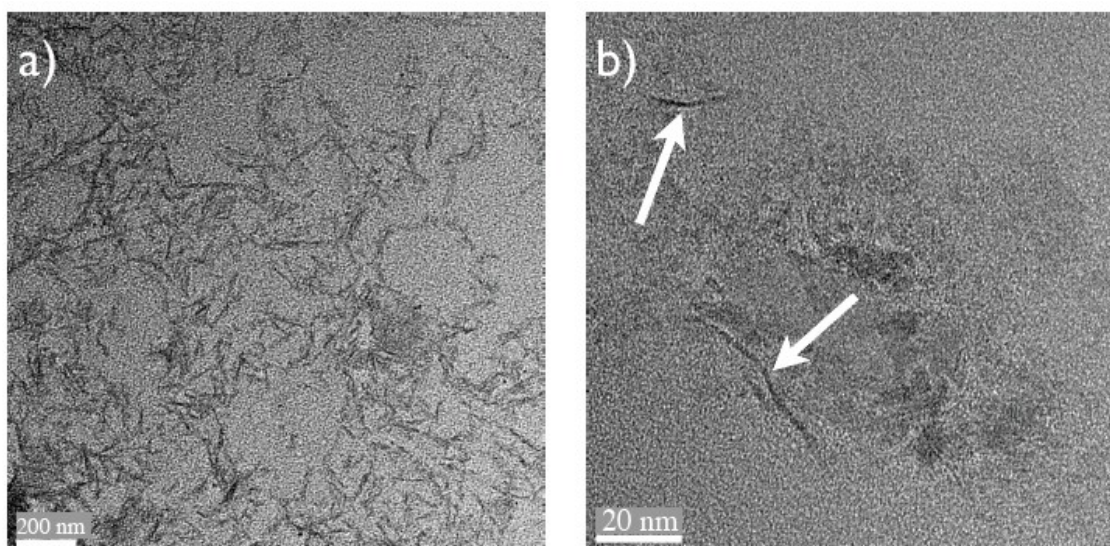


Figure 3.4. HRTEM images of the nanorods. Scale bars are 200 nm (a) and 20 nm (b).

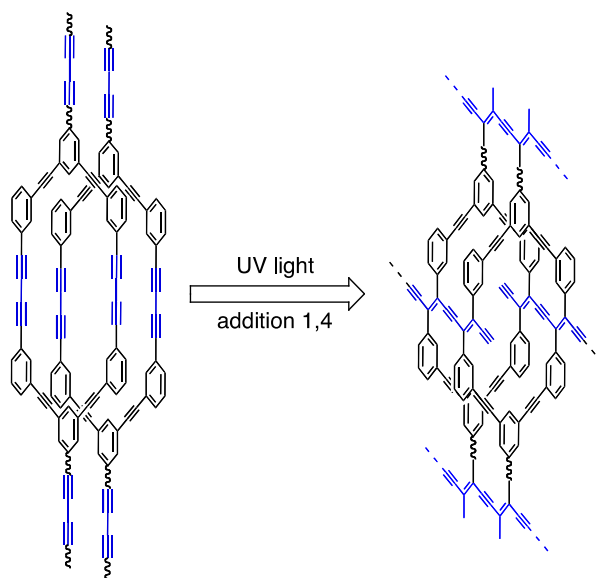


Figure 3.5. Proposed mechanism for the topochemical polymerization between macrocycles in the dried gel state.

3.6 Conclusion

In conclusion, new soluble organic nanorods were prepared from phenylacetylene macrocycles through the topochemical reactions of butadiyne units properly located within the macrocycle structure. This finding opens the way the formation of non-graphitic, semi-conducting nanorods and nanotubes for electronic applications. Our efforts are now directed towards the preparation of new macrocycles as building blocks that will lead to nanorods with different diameters. We also plan to investigate the porous properties of these new architectures for gas storage and separation. This study will allow us to assess whether or not the nanorods have a formal internal cavity.

3.7 Supporting Information

3.7.1 General

Chemical reagents were purchased from Sigma-Aldrich Co. Canada, Alfa Aesar Co., TCI America Co. or Oakwood Products Inc. and were used as received. Solvents used for organic synthesis were obtained from Fisher Scientific (except THF from Sigma-Aldrich Co. Canada) and purified with a Solvent Purifier System (SPS) (Vacuum Atmosphere Co., Hawthorne, USA). Other solvents were obtained from Fisher Scientific and were used as received. Tetrahydrofuran (THF) and triethylamine (Et_3N) used for Sonogashira reactions

were degassed 30 minutes prior to use. All anhydrous and air sensitive reactions were performed in oven-dried glassware under positive argon pressure. Analytical thin-layer chromatographies were performed with silica gel 60 F254, 0.25 mm pre-coated TLC plates (Silicycle, Québec, Canada). Compounds were visualized using 254 nm and/or 365 nm UV wavelength and/or aqueous sulfuric acid solution of ammonium heptamolybdate tetrahydrate (10 g/100 mL H₂SO₄ + 900 mL H₂O). Flash column chromatographies were performed on 230-400 mesh silica gel R10030B (Silicycle, Québec, Canada). TEM copper grids pre-coated with amorphous carbon were purchased from Ted Pella, Inc. (Redding, USA).

Apparatus

Nuclear magnetic resonance (NMR) spectra were recorded on a Varian Inova AS400 spectrometer (Varian, Palo Alto, USA) at 400 MHz (¹H) and 100 MHz (¹³C). High resolution mass spectra (HRMS) were recorded with an Agilent 6210 Time-of-Flight (TOF) LC-MS apparatus equipped with an ESI or APPI ion source (Agilent Technologies, Toronto, Canada). MALDI-TOF measurements were performed on a Bruker Biflex IV equipped with nitrogen laser. FT-IR was recorded in ATR mode on Infrared spectrometer (Thermo-Nicolet Magne 850) equipped with Golden Gate. UV-visible absorption spectra were recorded on a Varian diode-array spectrophotometer (model Cary 500) using 3-mm path length quartz cells. Scanning electron microscopy (SEM) images were taken using a JEOL JSM-6360 LV. Transmission electron microscopy (TEM) images were taken using a JEOL-1230. High resolution transmission microscopy (HRTEM) images were taken using a JEOL 2100 equipped with a field emission gun. X-ray diffraction was recorded on Siemens X-rays Diffractometer (Model S3 D5000).

Gelation test

To test the gelation properties of PAM **2** in a given solvent, we proceeded as follow: in a vial, PAM **2** was dissolved in a solvent. After dissolution by sonication, the vial was sealed and heated until a clear solution was obtained. The clear solution was allowed to slowly cool down at room temperature. The stability of the gel was confirmed by tube inversion.

SEM imaging

Organogel obtained in ethyl acetate was deposited on a stainless steel substrate and allowed to dry for 3-4 days. Then, gold particles were sputtered on dried gel prior to imaging.

TEM imaging

The SEC-purified PDA was dissolved in CHCl_3 and was sonicated for two hours. The resulting solution was directly deposited on a copper grid pre-coated with amorphous carbon and slowly evaporated prior to imaging.

3.7.2 Synthetic procedure

Compound 2. A 250 mL round bottom flask equipped with a magnetic stir bar was charged with KOH (4.60 g, 81.5 mmol) in H_2O (80 mL) at 0°C . Bromine (1.26 mL, 24.5 mmol) was added dropwise followed by 5-hexyn-1-ol (2.25 mL, 20.4 mmol). The mixture was stirred for 2 hours at 0°C in the dark and was then diluted with AcOEt, washed with brine (3x), dried with sodium sulfate and the solvent was removed under reduced pressure. The crude product was then charged without further purification in a 250 mL round bottom flask equipped with a magnetic stir bar with 30% aqueous *n*-BuNH₂ (92.6 mL) and CuCl (92 mg, 0.92 mmol). Small amount of hydroxylamine was added to the solution after appearance of a blue colour. Another 100 mL round bottom flask equipped with a magnetic stir bar was charged with 1-tetradecyne (5.70 mL, 23.2 mmol) and Et₂O (46 mL). The solution was added dropwise to the catalyst/bromoalkyne solution. At this step, hydroxylamine was continually added until a blue color appeared. A small amount of *n*-PrNH₂ was added until the reaction mixture become translucent and the mixture was stirred for 2 hours. The reaction mixture was then diluted with AcOEt, washed with 10% aqueous HCl (3x), dried with sodium sulfate and the solvent was removed under reduced pressure to afford compound **2** (6.62 g, 96% yield) as a colorless oil. ¹H NMR (CDCl_3 , 400 MHz): 3.66 (t, *J* = 6.1 Hz, 2H), 2.31 (t, *J* = 6.3 Hz, 2H), 2.24 (t, *J* = 7.0 Hz, 2H), 2.18 (t, *J* = 7.0 Hz, 1H), 1.65 (m, 4H), 1.51 (m, 4H), 1.37 (m, 4H), 1.26 (m, 12H), 0.87 (t, *J* = 7.1 Hz, 3H); ¹³C NMR (CDCl_3 , 100 MHz): 78.1, 77.7, 68.3, 65.9, 32.2, 31.9, 29.9 (3C), 29.7, 29.6, 29.3, 29.1, 28.7, 28.6, 24.8, 22.9, 19.4, 18.6, 14.4; HRMS (APPI-TOF) *m/z* calcd for $\text{C}_{20}\text{H}_{34}\text{O}[\text{M}+\text{H}]^+$: 291.2682, found 291.2695; FTIR (ATR): 3314w, 2920m, 2852m, 1466w, 1059w.

Icosa-5,7-diynyltosylate. A 250 mL round bottom flask equipped with a magnetic stir bar was charged with compound **2** (6.50 g, 23.4 mmol), CH₂Cl₂ (74 mL), tosyl chloride (6.39 g, 33.6 mmol), DMAP (273 mg, 2.24 mmol) and Et₃N (9.23 mL, 67.1 mmol). The reaction mixture was stirred for 2 hours, diluted with CH₂Cl₂, washed with water (3x), dried with sodium sulfate and the solvent was removed under reduced pressure. The crude product was purified by flash chromatography on silica gel using hexanes to 4% acetone/hexanes as eluents to afford compound **3** (5.5 g, 56% yield) as a colorless oil. ¹H NMR (CDCl₃, 400 MHz): 7.73 (d, *J* = 8.2 Hz, 2H), 7.31 (t, *J* = 8.0 Hz, 2H), 3.99 (t, *J* = 6.4 Hz, 2H), 2.40 (s, 3H), 2.18 (q, *J* = 6.4 Hz, 4H), 1.70 (m, 2H), 1.47 (m, 4H), 1.32 (m, 2H), 1.21 (m, 20H), 0.83 (t, *J* = 7.0 Hz, 3H); ¹³C NMR (CDCl₃, 100 MHz): 145.0, 133.2, 130.1, 128.0, 127.2, 78.1, 76.2, 70.1, 66.3, 65.3, 32.1, 29.9 (3C), 29.7, 29.6, 29.3, 29.1, 28.5, 28.0, 24.4, 22.9, 21.8, 19.4, 18.7, 14.4; HRMS (APPI-TOF) *m/z* calcd for C₂₇H₄₀O₃S[M+H]⁺: 446.2804, found 446.2816; FTIR (ATR): 3449b, 2924m, 2854m, 1176m.

Compound 3. A 25 mL round bottom flask equipped with a magnetic stir bar was charged with icosa-5,7-diynyltosylate (2.50 g, 5.60 mmol), DMF (5.6 mL) and sodium azide (914 mg, 14.1 mmol) under nitrogen. The reaction was heated to 70°C and was stirred for 3 hours. The reaction mixture was diluted with Et₂O, washed with water (3x), dried with sodium sulfate. The solvent was removed under reduced pressure to afford compound **3** (1.56 g, 88% yield) without further purification as a colorless oil. ¹H NMR (CDCl₃, 400 MHz): 3.31 (t, *J* = 6.6 Hz, 2H), 2.31 (t, *J* = 6.7 Hz, 2H), 2.25 (t, *J* = 6.7 Hz, 2H), 1.72 (m, 2H), 1.61 (m, 2H), 1.52 (m, 4H), 1.37 (m, 2H), 1.26 (m, 14H), 0.88 (t, *J* = 6.9 Hz, 3H); ¹³C NMR (CDCl₃, 100 MHz): 77.2, 76.7, 50.9, 31.9, 29.7 (3C), 29.5, 29.4, 29.1, 28.9, 28.3, 27.9, 22.4, 22.7, 19.2, 18.8, 14.1; HRMS (APPI-TOF) *m/z* calcd for C₂₀H₃₃N₃[M+H]⁺: 316.2747, found 316.2759; FTIR (ATR): 3026w, 2924m, 2852w, 2096w, 1493m, 1452m.

Compound 4. A 25 mL round bottom flask equipped with a magnetic bar was charged with compound **3** (2.00 g, 6.33 mmol), MeOH (8 mL) and tin chloride (3.50 g, 15.8 mmol) at 0°C. The reaction mixture was stirred for 4 hours at room temperature and was diluted with Et₂O. The organic layer was washed with 1M NaOH (3x), dried with sodium sulfate and the solvent was removed under pressure to afford compound **4** (1.43 g, 78% yield) without further purification as a white solid. ¹H NMR (CDCl₃, 400 MHz): 3.69 (s, 2H),

2.78 (t, $J = 6.7$ Hz, 2H), 2.29 (t, $J = 6.7$ Hz, 2H), 2.23 (t, $J = 6.9$ Hz, 2H), 1.60 (m, 4H), 1.50 (m, 2H), 1.36 (m, 2H), 1.25 (m, 14H), 0.87 (t, $J = 7.1$ Hz, 3H); ^{13}C NMR (CDCl_3 , 100 MHz): 78.1, 76.9, 65.9, 65.3, 41.2, 32.1, 31.5, 29.9 (3C), 29.7, 29.6, 29.3, 29.1, 28.6, 25.8, 22.9, 19.4, 19.2, 14.4; HRMS (APPI-TOF) m/z calcd for $\text{C}_{20}\text{H}_{35}\text{N}[\text{M}+\text{H}]^+$: 290.2482, found 290.9854; FTIR (ATR): 3750w, 2921m, 2851m, 2337w.

Compound 5. A 50 mL round bottom flask equipped with a magnetic stir bar was charged with 3,5-diiodobenzoic acid (1.20 g, 3.21 mmol), CH_2Cl_2 (16 mL), EDC (923 mg, 4.81 mmol), DMAP (196 mg, 1.61 mmol) and compound **4** (1.39 g, 4.81 mmol). The reaction mixture was stirred overnight and diluted with CH_2Cl_2 . The organic layer was washed with water (3x), dried with sodium sulfate and the solvent was removed under reduced pressure. The crude product was purified by flash chromatography on silica gel using hexanes to 7% acetone/hexanes as eluents to afford compound **5** (1.73 g, 84% yield) as a white powder. m.p: 76-79°C; ^1H NMR (CDCl_3 , 400 MHz): 8.11 (s, 1H), 7.99 (s, 2H), 6.5 (m, 1H), 3.43 (q, $J = 6.0$ Hz, 2H), 2.30 (t, $J = 6.7$ Hz, 2H), 2.23 (t, $J = 6.8$ Hz, 2H), 1.72 (m, 2H), 1.59 (m, 2H), 1.49 (m, 2H), 1.35 (m, 2H), 1.24 (m, 16H), 0.87 (t, $J = 6.8$ Hz, 3H); ^{13}C NMR (CDCl_3 , 100 MHz): 164.9, 147.9, 138.2, 135.5, 117.7, 95.1, 78.4, 76.8, 66.3, 65.3, 39.9, 32.2, 29.9 (3C), 29.7, 29.6, 29.4, 28.8, 28.6, 25.8, 22.9, 19.5, 19.2, 14.4; HRMS (APPI-TOF) m/z calcd for $\text{C}_{27}\text{H}_{37}\text{I}_2\text{NO}[\text{M}+\text{H}]^+$: 646.1037, found 646.1064; FTIR (ATR): 3281w, 2919m, 2850m, 1638m, 1536m.

Compound 6. A 100 mL round bottom flask equipped with a magnetic stir bar was charged with **5** (1.73 g, 2.68 mmol), degassed THF (26 mL), degassed Et_3N (1.47 mL, 10.7 mmol), $\text{PdCl}_2(\text{PPh}_3)_2$ (75 mg, 0.11 mmol), CuI (20 mg, 0.11 mmol) and trimethylsilylacetylene (1.51 mL, 10.7 mmol) under argon atmosphere. The reaction mixture was stirred overnight at room temperature, diluted with CH_2Cl_2 , washed with NH_4Cl (3x) and dried with sodium sulfate. The solvent was removed under reduced pressure and the crude product was purified by flash chromatography on silica gel using 10% acetone/hexanes as eluent to afford compound **6** (1.26 g, 80% yield) as a dark orange oil. ^1H NMR (CDCl_3 , 400 MHz): 7.78 (s, 2H), 7.65 (s, 1H), 6.35 (m, 1H), 3.44 (q, $J = 6.4$ Hz, 2H), 2.31 (t, $J = 6.6$ Hz, 2H), 2.23 (t, $J = 6.6$ Hz, 2H), 1.72 (m, 2H), 1.59 (m, 2H), 1.51 (m, 2H), 1.36 (m, 2H), 1.25 (m, 16H), 0.88 (t, $J = 7.0$ Hz, 3H), 0.24 (s, 18H); ^{13}C NMR

(CDCl₃, 100 MHz): 166.2, 137.8, 135.2, 130.3, 124.2, 103.3, 96.4, 78.2, 76.7, 66.2, 65.3, 39.4, 32.1, 29.9 (3C), 29.7, 29.6, 29.3, 29.1, 28.9, 28.6, 25.8, 22.9, 19.4, 19.1, 14.4, 0.04; HRMS (APPI-TOF) *m/z* calcd for C₃₇H₅₅NOSi₂[M+H]⁺: 586.3895, found 586.3915; FTIR (ATR): 3317b, 2925m, 2854m, 1640m, 1250m.

Compound 8. A 25 mL round bottom flask equipped with a magnetic stir bar was charged with compound **6** (1.20 g, 2.15 mmol), KOH (362 mg, 6.45 mmol), THF (5.3 mL) and MeOH (5.3 mL). The reaction mixture was stirred until complete disappearance of the starting product by TLC. After completion, the reaction mixture was diluted with CH₂Cl₂, washed with 10% aqueous HCl (2x), dried with sodium sulfate and the solvent was removed under reduced pressure. The resulting product was charged without further purification in a 50 mL round bottom flask equipped with a magnetic stir bar with compound **7** (3.75 g, 8.49 mmol), degassed THF (17 mL), degassed DIPEA (2.37 mL, 13.6 mmol), PdCl₂(PPh₃)₂ (48 mg, 0.07 mmol) and CuI (13 mg, 0.07 mmol). The reaction mixture was stirred overnight and diluted with CH₂Cl₂. The organic layer was washed with saturated aqueous NH₄Cl (3x), dried with sodium sulfate and the solvent was removed under reduced pressure. The crude product was purified by flash chromatography on silica gel using hexanes to 10% acetone/hexanes as eluents to afford compound **8** (900 mg, 49% yield) as a dark orange oil. ¹H NMR (CDCl₃, 400 MHz): 7.84 (s, 2H), 7.73 (s, 1H), 7.69 (s, 2H), 7.52 (s, 2H), 7.29 (s, 2H), 6.28 (m, 1H), 3.48 (q, *J* = 6.4 Hz, 2H), 2.53 (t, *J* = 7.8 Hz, 4H), 2.33 (t, *J* = 6.8 Hz, 2H), 2.22 (t, *J* = 6.8 Hz, 2H), 1.75 (m, 2H), 1.60 (m, 6H), 1.49 (m, 2H), 1.26 (m, 38H), 0.88 (m, 9H); ¹³C NMR (CDCl₃, 100 MHz): 166.2, 145.5, 138.2, 137.7, 137.1, 135.6, 131.2, 130.0, 124.5, 124.2, 94.0, 89.8, 88.7, 78.4, 76.8, 66.3, 65.3, 39.9, 35.6, 32.2, 32.1, 31.4, 31.2, 28.9 (3C), 29.7, 29.6 (2C), 29.5, 29.4, 29.3, 29.1, 28.9, 28.6, 25.8, 22.9 (2C), 19.4, 19.2, 14.4; HRMS (APPI-TOF) *m/z* calcd for C₅₉H₇₇I₂NO[M+H]⁺: 1070.4167, found 1070.4186; FTIR (ATR): 3312b, 2924m, 2853m, 1637w, 1593w, 1553w.

Compound 9. A 25 mL round bottom flask equipped with a magnetic stir bar was charged with compound **8** (1.10 g, 1.03 mmol), degassed THF (10 mL), degassed Et₃N (0.57 mL, 4.11 mmol), PdCl₂(PPh₃)₂ (36 mg, 0.05 mmol), CuI (10 mg, 0.05 mmol) and triisopropylsilylacetylene (0.92 mL, 4.11 mmol). The reaction mixture was stirred

overnight, diluted with CH₂Cl₂, washed with NH₄Cl and dried with sodium sulfate. The solvent was removed under reduced pressure and the crude product was purified by flash chromatography on silica gel using 5% acetone/hexanes as eluent to afford compound **9** (1.18 g, 97% yield) as an orange oil. ¹H NMR (CDCl₃, 400 MHz): 7.86 (s, 2H), 7.77 (s, 1H), 7.48 (s, 2H), 7.29 (s, 2H), 7.27 (s, 2H), 6.33 (m, 1H), 3.48 (q, *J* = 6.4 Hz, 2H), 2.57 (t, *J* = 7.6 Hz, 4H), 2.33 (t, *J* = 6.7 Hz, 2H), 2.22 (t, *J* = 6.7 Hz, 2H), 1.74 (m, 2H), 1.62 (m, 6H), 1.49 (m, 2H), 1.27 (m, 38H), 1.14 (s, 42H), 0.88 (m, 9H); ¹³C NMR (CDCl₃, 100 MHz): 166.3, 143.6, 137.1, 135.6, 132.9, 132.5, 131.9, 129.8, 127.2, 124.4, 124.0, 122.8, 106.5, 91.2, 90.7, 88.0, 78.3, 76.8, 66.3, 65.3, 39.8, 35.8, 32.2, 32.1, 31.5, 29.9 (3C), 29.7 (2C), 29.6, 29.5 (2C), 29.4, 29.1, 28.9, 28.6, 25.9, 22.9 (2C), 19.4, 19.2, 18.9, 14.4, 11.6; HRMS (APPI-TOF) *m/z* calcd for C₈₁H₁₁₉NOSi₂[M+H]⁺: 1178.8903, found 1178.8947; FTIR (ATR): 3317b, 2923m, 2855m, 1639m, 1590m, 1462m.

PAM 2. A 50 mL round bottom flask equipped with a magnetic stir bar was charged with compound **9** (700 mg, 0.59 mmol), THF (12 mL) and TBAF 1.0M solution in THF (1.78 mL, 1.78 mmol). The reaction mixture was stirred until complete disappearance of the starting product by TLC, diluted with CH₂Cl₂, washed with water (3x) and dried with sodium sulfate. The solvent was removed under reduced pressure. The resulting product was charged without further purification in a 50 mL round bottom flask equipped with a magnetic stir bar with degassed pyridine (15 mL). Another round bottom flask equipped with a magnetic stir bar was charged with CuCl (3.65 g, 36.9 mmol), CuCl₂ (768 mg, 5.71 mmol) and degassed pyridine (74 mL) under N₂ atmosphere. The first solution was added dropwise to the catalyst solution over 4 days using a syringe pump and the reaction mixture was stirred for an additional 7 days. The reaction mixture was diluted with CHCl₃ and poured in water. The organic phase was extracted successively with water, 25% aqueous NH₄OH, water, 10% aqueous CH₃COOH, water, 10% aqueous NaOH and brine. The organic layer was dried with sodium sulfate and the solvent was removed under reduced pressure. The crude product was purified by flash chromatography on silica gel using 20% hexanes/CHCl₃ to CHCl₃ as eluents to afford **PAM 2** (390 mg, 49% yield) as a white amorphous powder. m.p.: >150°C; ¹H NMR (CDCl₃, 400 MHz): 7.71 (s, 2H), 7.64 (s, 4H), 7.49 (s, 4H), 7.20 (s, 4H), 7.18 (s, 4H), 6.70 (s, 2H), 3.53 (q, *J* = 7.0 Hz, 4H), 2.53 (t, *J* = 7.5 Hz, 8H), 2.39 (t, *J* = 6.9 Hz, 4H), 2.24 (t, *J* = 6.9 Hz, 4H), 1.83 (m, 4H), 1.69 (m, 4H),

1.62 (m, 8H), 1.52 (m, 4H), 1.29 (m, 76H), 0.90 (m, 18H): ^{13}C NMR (CDCl_3 , 100 MHz): 166.7, 143.2, 135.1, 133.4, 132.1, 129.6, 129.3, 127.0, 123.9, 122.9, 122.1, 90.1, 88.1, 80.9, 78.1, 76.6, 74.3, 66.1, 65.1, 41.9, 39.7, 35.5, 31.9, 31.1, 29.7 (3C), 29.5, 29.4, 29.3 (2C), 29.1, 28.9, 28.7, 28.4, 25.7, 22.7 (2C), 21.5, 19.2, 19.0, 17.7, 14.1, 12.3; MS (MALDI-TOF): m/z calcd for $\text{C}_{126}\text{H}_{154}\text{N}_2\text{O}_2[\text{M}+\text{H}]^+$: 1727.1, found 1732.7; FTIR (ATR): 3271w, 2919m, 2851m, 1638m, 1592m, 1015b, 802m.

3.7.3 Gelation Properties

Table 3.1. Gelation properties of PAM 2 at 1.0 w/v %

Solvent	Observation
toluene	S
1,2-dichlorobenzene	G
benzene	G
pyridine	S
tetrahydrofuran	P
methanol	I
acetone	G
ethyl acetate	G
acetonitrile	P
cyclohexane	G
1,4-dioxane	P
hexanes	G
1,2-dichloroethane	PG
chloroform	S
ethanol	I
dichloromethane	S

S = Soluble

G = Gelation

P = Precipitate

I = Insoluble

PG = Partial gelation

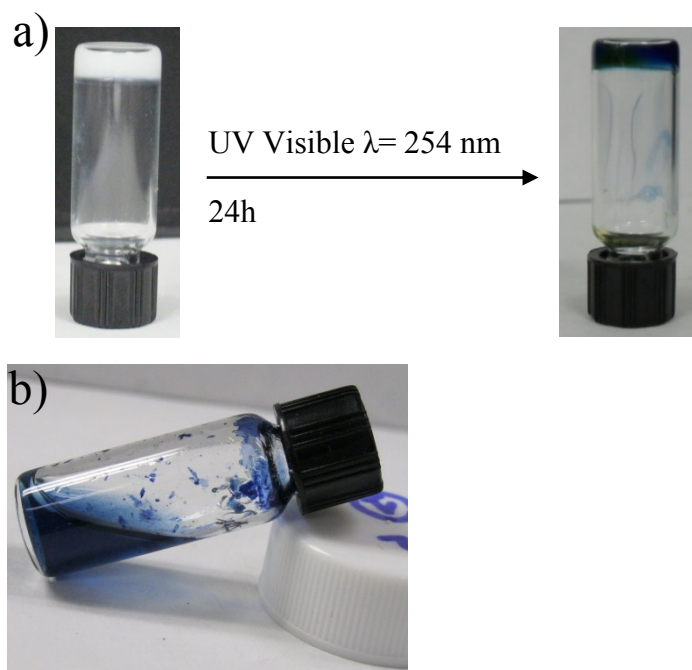


Figure 3.6. a) Organogel of PAM **2** in ethyl acetate (10 mg/mL) before and after the topochemical polymerization, b) Solution of PAM **2** organogel in CHCl_3 after the topochemical polymerization.

3.7.4 XRD analysis

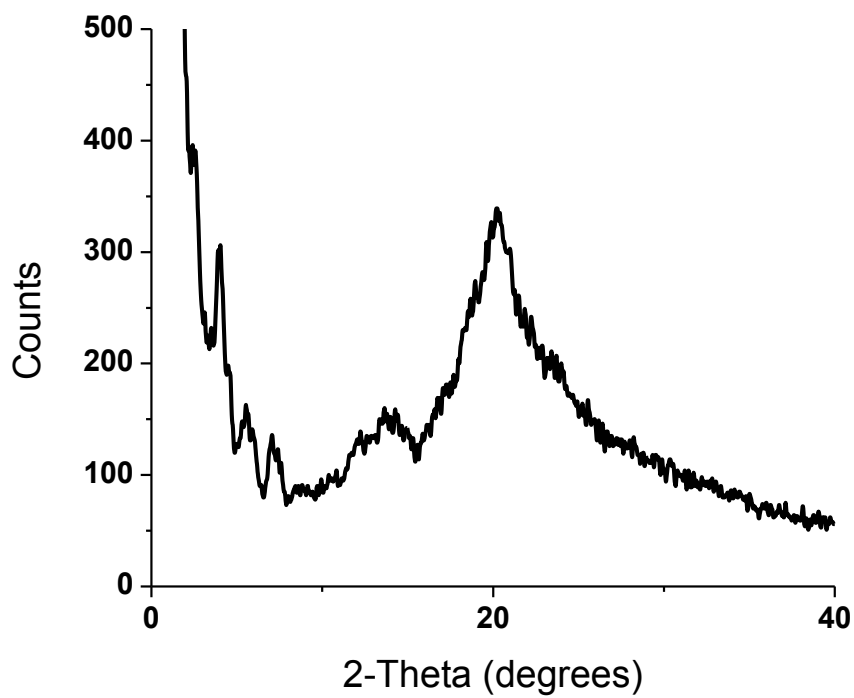


Figure 3.7. X-ray diffraction spectrum of PAM 2 gel in ethyl acetate (10 mg/mL)

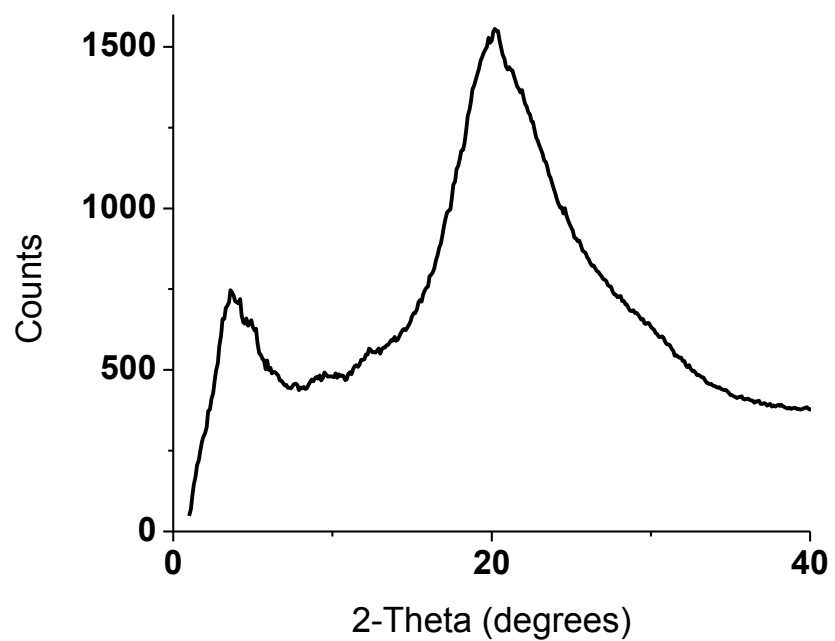


Figure 3.8. X-Ray diffraction spectrum of SEC-purified PDA

3.7.5. UV Visible spectroscopy

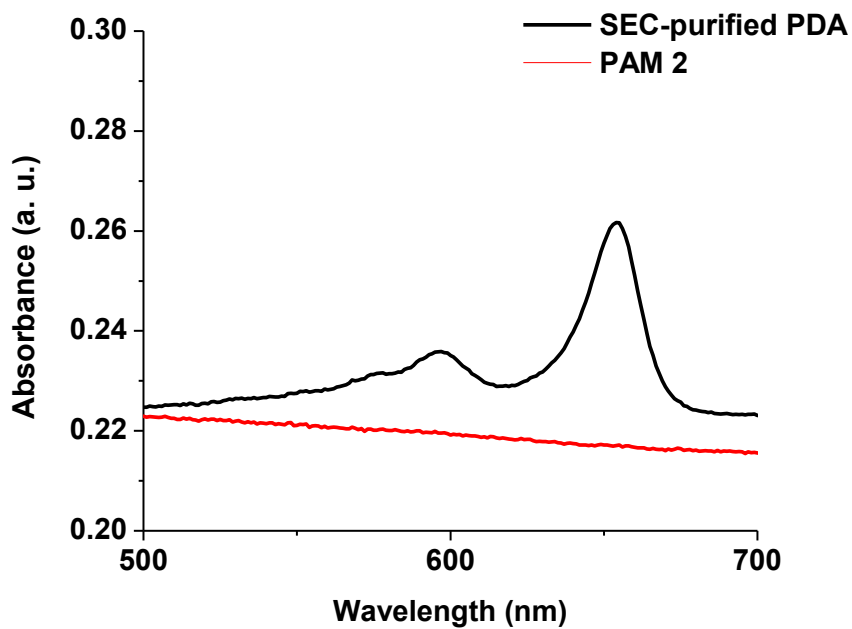


Figure 3.9. UV Visible spectrum of PAM 2 and SEC-purified PDA in CHCl_3

3.7.6. SEC chromatography

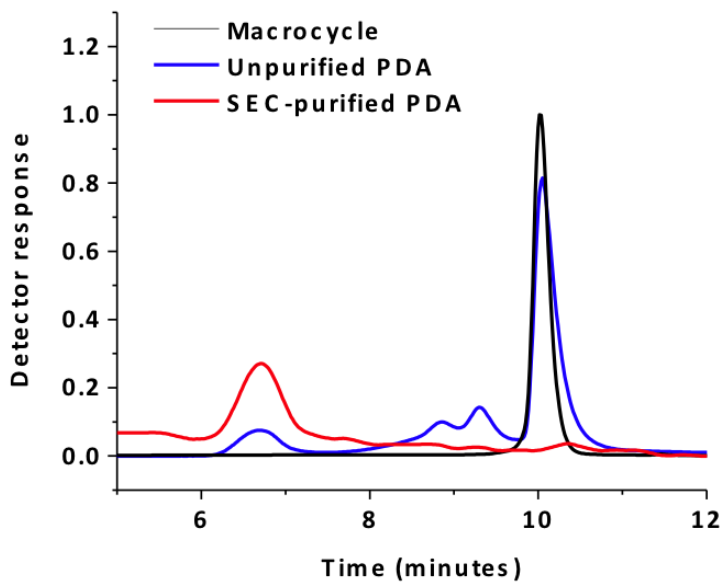


Figure 3.10. SEC chromatograms of PAM 2 before (black) and after (blue) UV irradiation. The red trace corresponds to the SEC-purified blue material.

3.7.7. Theoretical representation

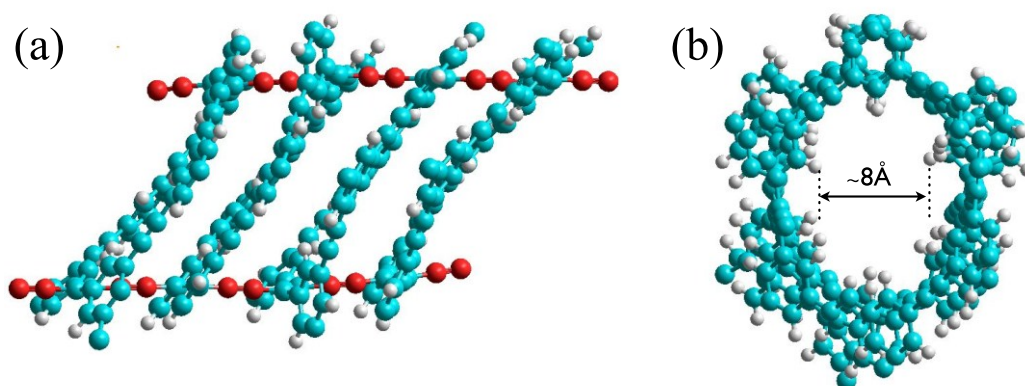


Figure 3.11. Models of side view (a) and front view (b) of the nanotube after the topochemical polymerizations. Red spheres on (a) are the alkyne carbon atoms of the PDA chains. Peripheral groups have been omitted for clarity.

3.8. Références

- [1] (a) Prince, R. B.; Okada, T.; Moore, J. S. *Angew. Chem. Int. Ed.* **1999**, *38*, 233-236. (b) Prince, R. B.; Barnes, S. A.; Moore, J. S. *J. Am. Chem. Soc.* **2000**, *122*, 2758-2762. (c) Organo, V. G.; Rudkevich, D. M. *Chem. Comm.* **2007**, 3891-3899. (d) Tan, C.; Pinto, M. R. Kose, M. E.; Ghiviriga, I.; Schanze, K. S. *Adv. Mater.* **2004**, *16*, 1208-1212. (e) Tanatani, A.; Mio, M. J.; Moore, J. S. *J. Am. Chem. Soc.* **2001**, *123*, 1792-1793.
- [2] Block, M. A. B.; Kaiser, C.; Khan, A.; Hecht, S. *Topp. Curr. Chem.* **2005**, *245*, 89-150.
- [3] Dawn, S.; Dewal, M. B.; Sobransingh, D.; Paderes, M. C.; Wibowo, A. C.; Smith, M. D.; Krause, J. A.; Pellechia, P. J.; Shimizu, L. S. *J. Am. Chem. Soc.* **2011**, *133*, 7025-7032.
- [4] Harada, A.; Li, J.; Kamachi, M. *Nature* **1993**, *364*, 516-518.
- [5] Ghadiri, M. R.; Granja, J. R.; Milligan, R. A.; McRee, D. E.; Khazanovich, N. *Nature* **1993**, *366*, 324-327.
- [6] Ikeda, A.; Shinkai, S. *J. Chem. Soc. Chem. Comm.* **1994**, 2375-2376.
- [7] (a) G. Wegner, *Natureforsch., B: Chem. Sci.* **1969**, *24*, 824-832; b) G. Wegner, *Makromol. Chem.* **1972**, *154*, 35-48.
- [8] (a) Hisaki, I.; Sakamoto, Y.; Shigemitsu, H.; Tohnai, N.; Miyata, M. *Cryst. Growth. Des.* **2009**, *9*, 414-420. (b) Zhou, Q.; Carroll, P. J.; Swager, T. M. *J. Org. Chem.* **1994**, *59*, 1294-1301. (c) Suzuki, M.; Comito, A.; Khan, S. I.; Rubin, Y. *Org. Lett.*

- 2010**, *12*, 2346-2349. (d) Nishinaga, T.; Nodera, N.; Miyata, Y.; Komatsu, K. *J. Org. Chem.* **2002**, *67*, 6091-6096.
- [9] (a) Boese, R.; Matzger, A. J.; Vollhardt, K. P. C. *J. Am. Chem. Soc.* **1997**, *119*, 2052-2053. (b) Haley, M. M.; Bell, M. L.; English, J. J.; Johnson, C. A.; Weakley, T. J. R. *J. Am. Chem. Soc.* **1997**, *119*, 2956-2957. (c) Nomoto, A.; Sonoda, M.; Yamaguchi, Y.; Ichikawa, T.; Hirose, K.; Tobe, Y. *J. Org. Chem.* **2006**, *71*, 401-404.
- [10] Baldwin, K. P.; Matzger, A. J.; Scheiman, D. A.; Tessier, C. A.; Vollhardt, K. P. C.; Youngs, W. J. *Synlett* **1995**, 1215-1218.
- [11] Cantin, K.; Rondeau-Gagné, S.; Néabo, J. R.; Daigle, M.; Morin, J.-F. *Org. Biomol. Chem.* **2011**, *9*, 4440-4443.
- [12] Néabo, J. R.; Tohondjona, K. I. S.; Morin, J.-F. *Org. Lett.* **2011**, *13*, 1358-1361.
- [13] During the course of this study, Tamaoki et al. have reported the formation of nanotubes from flexible, non-PAM macrocycles using UV irradiation. See: Nagasawa, J.; Yoshida, M.; Tamaoki, N. *Eur. J. Org. Chem.* **2011**, *2011*, 2247-2255.
- [14] Xu, Y.; Smith, M. D.; Geer, M. F.; Pellechia, P. J.; Brown, J. C.; Wibowo, A. C.; Shimizu, L. S. *J. Am. Chem. Soc.* **2010**, *132*, 5334-5335.
- [15] Hsu, T.-J.; Fowler, F. W.; Lauher, J. W. *J. Am. Chem. Soc.* **2012**, *134*, 142-145.
- [16] Xie, H.; Zhang, S.; Li, H.; Zhang, X.; Zhao, S.; Xu, Z.; Song, X.; Yu, X.; Wang, W. *Chem. Eur. J.* **2012**, *18*, 2230-2234.
- [17] Zhang, P.; Wang, H.; Liu, H.; Li, M. *Langmuir* **2010**, *26*, 10183-10190.
- [18] (a) Balakrishnan, K.; Datar, A.; Zhang, W.; Yang, X.; Naddo, T.; Huang, J.; Zuo, J.; Yen, M.; Moore, J. S.; Zang, L. *J. Am. Chem. Soc.* **2006**, *128*, 6576-6577. (b) Shimura, H.; Yoshio, M.; Kato, T. *Org. Biomol. Chem.* **2009**, *7*, 3205-3207.

Chapitre 4.

Nanotubes organiques rigides à partir de macrocycles de phénylène-butadiynylène

Rigid organic nanotubes from phenylene-butadiynylene macrocycles

Simon Rondeau-Gagné, Jules Roméo Néabo, Maude Desroches, Isabelle Levesque, Maxime Daigle, Katy Cantin and Jean-François Morin*

Département de Chimie and Centre de Recherche sur les Matériaux Avancés (CERMA), 1045 Ave de la Médecine, Pavillon Alexandre-Vachon, Université Laval, Québec, QC, Canada G1V 0A6.

Publié dans la revue *Chemical Communications*, **2013**, 49, 9546-9848.

4.1 Préambule

Cet article présente la synthèse de macrocycles rigides plus larges et réactifs à la polymérisation des unités diyne pour former des nanotubes organiques. Les nanoarchitectures obtenues présentent des cavités internes plus larges ce qui démontre la possibilité de contrôle de la structure finale par l'approche hybride. Ma contribution à cet article est majeure. J'ai participé à la synthèse de tous les composés et à leur caractérisation. J'ai également effectué tous les assemblages, les réactions de photopolymérisation et la caractérisation des nanotubes finaux.

4.2 Résumé

Des nanotubes organiques rigides ont été préparés à partir de macrocycles de type phénylbutadiynylene par polymérisation topochemique dans l'état de xérogel. Toutes les six unités butadiyne incorporées au squelette macrocyclique ont subi la polymérisation, créant ainsi des nanotubes rigides contenant six chaînes de polydiacétylènes situées parallèles l'une par rapport à l'autre.

4.3 Abstract

Rigid organic nanotubes were prepared from six-membered phenyl-butadiynylene macrocycles through topochemical polymerization in the xerogel state. All six butadiyne units underwent polymerization, thus creating rigid nanotubes with six polydiacetylene chains laying parallel one relative to each other.

4.4 Introduction

Alike carbon nanotubes, organic nanotubes show numerous interesting features for different applications, including host-guest chemistry and organic electronics.¹ However, reliable and straightforward synthetic strategy must be developed before they can be considered as serious alternative to other materials. A promising strategy to prepare them is to assemble macrocyclic building blocks to obtain supramolecular nanotubes and to link them covalently to fix the tubular organization.² Among strategies used to link supramolecular organization, topochemical polymerization of 1,3-butadiynes, yielding to polydiacetylene (PDA), is particularly interesting since no metal catalyst or additive are needed to drive this polymerization.³ However, specific and strict intermolecular structural parameters are needed for this reaction to occur.⁴ Recently, we and others demonstrated

that a gel state can be used to obtain such critical parameters, allowing the preparation of high molecular weight PDAs from building blocks of different sizes and shapes.⁵ We have also shown that the incorporation of specific elements of design allow the control over molecular organization in phenylacetylene macrocycles (PAMs) assembly, allowing topochemical polymerization between macrocycles in the xerogel state.⁶ The material obtained after topochemical polymerization was made of soluble, PDA-walled conjugated nanorods.

In order to prepare larger, rigid and more robust PDA-walled organic nanotubes, we have chosen to prepare six-membered phenylene-butadiynylene macrocycles (**PBM1** and **PBM2**, Figure 4.1) that possess six 1,4-diaryl-1,3-butadiyne units (rather than only two for PAMs) that could potentially undergo topochemical polymerization to form PDA. Compared to PAMs, PBMs are known to provide stronger π - π interactions owing to the electron-withdrawing effect of the butadiyne moiety, thus enabling the self-association of macrocycles in different solvents through gel formation.⁷ Moreover, PBMs are much larger than PAMs, which could allow the introduction of internal binding functionalities in addition to provide nanotubes with better host ability.⁸ Nonetheless, the controlled polymerization of PBM frameworks remains a challenging but worthy task considering that it would open the way to the preparation of non-graphitic, semi-conducting nanotubes with unique properties. In this regard, very few attempts to cross-link PBMs and related butadiyne-containing cyclic molecules through controlled topochemical polymerization have been reported but none of them lead to nanotubes that can be solubilized, handled easily and characterized as a unimolecular entity.⁹

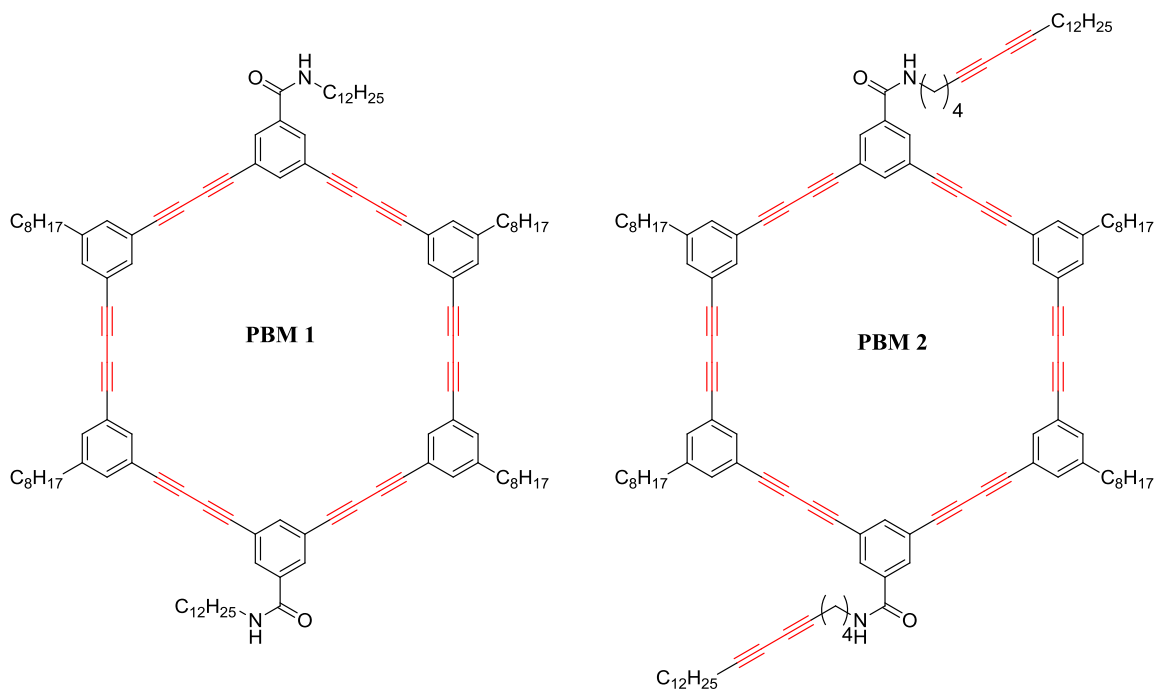


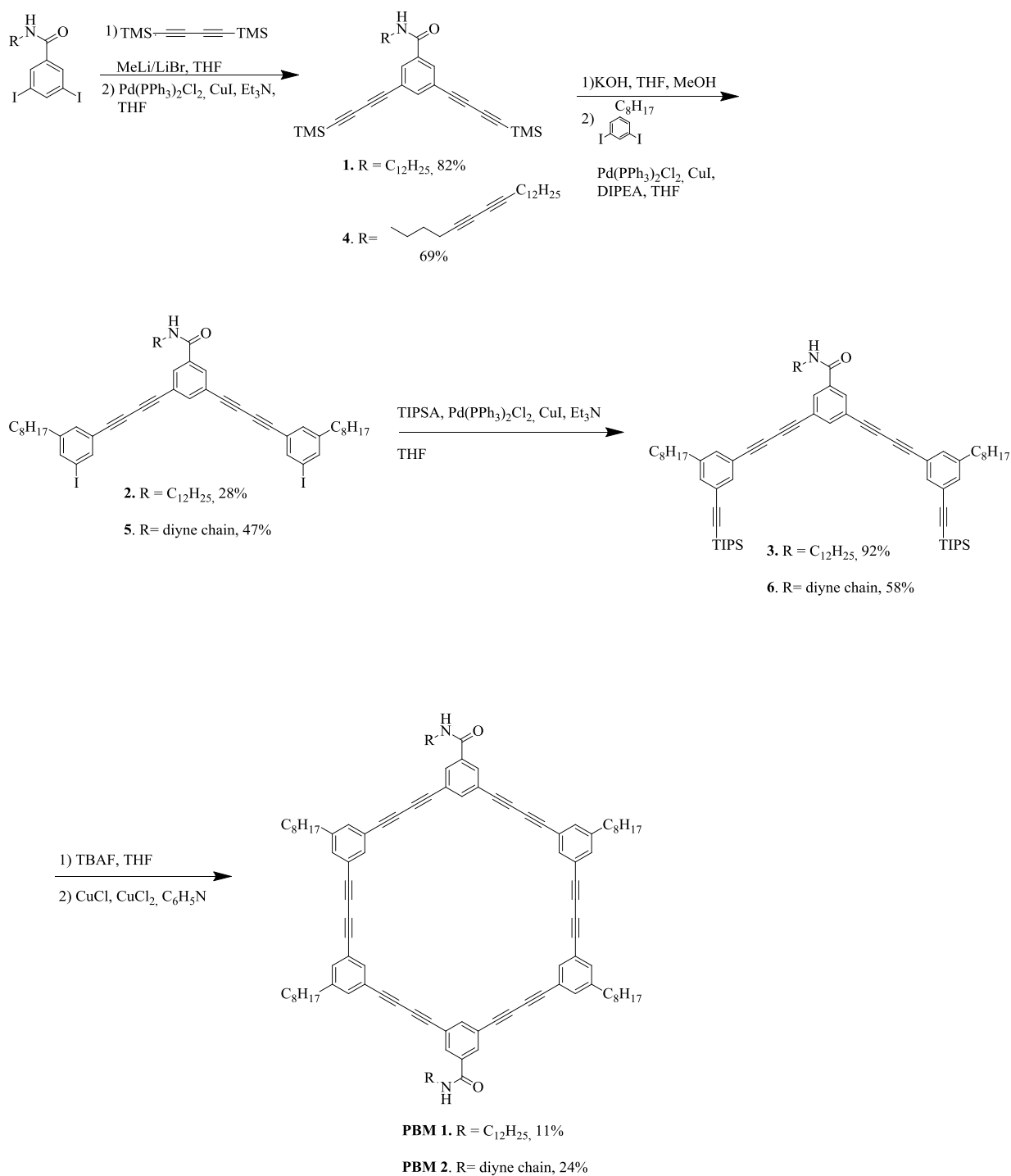
Figure 4.1. Structure of **PBM1** and **PBM2**

Herein, we report the synthesis, gelation properties and topochemical polymerization in the xerogel state of two phenylene-butadiynylene macrocycles (**PBM1** and **PBM2**). The resulting materials were characterized with Raman and UV-visible spectroscopy and transmission electron microscopy (TEM) to determine the efficiency of the topochemical polymerization and to assess the formation of nanotubes. Beside the preparation of new materials with unique properties, this study permits to evaluate the versatility of our general strategy to prepare organic nanotubes with different sizes, shapes and functions.

4.5 Results and discussion

The synthetic pathway for **PBM1** is depicted in Scheme 4.1. Starting from *N*-dodecyl-3,5-diiido-benzamide,^{6a} TMS-protected diacetylenes were introduced by Castro-Stephen-Sonogashira coupling reaction using monodeprotected 1,4-*bis*(trimethylsilyl)butadiyne¹⁰ to afford compound **1** with good yield. Deprotection of diyne units with potassium hydroxide was then conducted before introduction of 1-octyl-3,5-diiodobenzene^{6a} using standard Castro-Stephen-Sonogashira coupling to obtain half-macrocycle **2** in rather low yield (28%). It is noteworthy that the low yield is due to the formation of linear oligomers, which are common side-products for this kind of statistic coupling. TIPS-protected acetylenes

were then installed on the half-macrocycle by standard Castro-Stephen-Sonogashira coupling to obtain **3** in excellent yield (92%). After removal of TIPS using tetrabutylammonium fluoride (TBAF), the deprotected half-macrocycle was directly used without purification in the ring closing reaction using modified Eglinton conditions to provide **PBM1** in relatively low yield (11%).¹¹ This low yield of cyclization can be attributed to the relative instability of diyne units and the moderate solubility of **PBM1**.^{12,9b} Identical synthetic approach was used for **PBM2** and it is also depicted in Scheme 1. The yields for each step are similar to those obtained for **PBM1**.



Scheme 4.1. Synthesis of **PBM1** and **PBM2**.

In order to obtain proper intermolecular orientation and distance between macrocycles prior to the topochemical polymerization, **PBM1** and **PBM2** were gelified in different

organic solvents. Gelation process was chosen over crystal formation to organize molecules since it is much less time-consuming. Moreover, we have shown previously that the topochemical polymerization of 1,4-diarylbutadiyne moieties can be very efficient in the gel state compared to the crystalline state since the former accommodate conformational changes better.^{5c} Standard gelation tests were achieved by dissolving the corresponding PBM in different solvents (1 to 10 wt/vol %). The resulting suspension was heated near the boiling point of the solvent and was allowed to cool down at room temperature. Unexpectedly, gelation was not observed in any solvents tested except for cyclohexane, which gave a translucent organogel for **PBM1** and **PBM2**. This result is surprising given that PAMs bearing the same outer decorations presented good gelation properties in a large number of solvents.⁶ We hypothesize that this significant difference in the self-assembly between PAMs and PBMs process of can be attributed to the better solubility of PBMs.¹³

The distance and orientation between the macrocycles within the xerogel state were studied by powder X-ray diffraction (PXRD) analysis. PXRD spectrum of **PBM1** is presented in SI (Figure 4.5). A rather broad peak at $2\theta = 4.1$ (30.4\AA) is observed and can be attributed to a (100) reflection of a columnar lattice, most likely with a hexagonal symmetry. Moreover, a broad and intense peak at $2\theta = 21.5$ (4.3\AA) is observed and can be attributed to liquid-like order between the alkyl chains. The PXRD spectrum thus suggests that macrocycles are stacking on top of each other to form tubular assemblies as observed for similar macrocycles and discotic liquid crystals.^{8,14} Moreover, the columnar organization of PBMs suggests the presence of an inner empty cavity within the column although it was not possible to assess with certainty the presence of such a cavity based on the sole PXRD analysis.

Knowing that the macrocycles of **PBM1** in the xerogel state are stacking in a face-to-face configuration, which is an essential prerequisite for the topochemical polymerization to occur, a thin film of the xerogel obtained from a cyclohexane gel was deposited on a glass substrate and submitted to irradiation using UV light ($\lambda = 254$ nm) for a 48h period. Appearance of a dark blue color, associated with the formation of PDA, was observed for **PBM1** after irradiation. For **PBM2**, a slight change in color was observed after irradiation turning the white xerogel to yellow. This slight color change account for an incomplete

polymerization and/or degradation of the supramolecular network. Surprisingly, the incorporation of external diynes did not drive the topochemical polymerization, as it was the case for the PAM family.^{6a}

The purification of cross-linked **PBM1**, **PDA1**, was conducted using size-exclusion chromatography (SEC) (Bio-Beads SX-1) and a UV-visible spectrum of **PDA1** was recorded in CHCl₃ (see Figure 4.6 in SI). As expected, apparition of a broad absorption band with a λ_{max} at 640 nm was observed, which is characteristic of a PDA backbone. For every 10 mg of **PBM1** deposited as a gel, about 1 mg of soluble blue material can be obtained after purification by SEC, which represents a yield of about 10%.

In order to evaluate the extent of reaction of the butadiyne units, Raman spectroscopy has been performed on a xerogel of **PBM1** and on purified **PDA1** and the spectra are shown in Figure 4.7. The Raman spectrum of **PBM1**, performed on the xerogel, exhibited a strong band at 2224 cm⁻¹ and a smaller one at 1593 cm⁻¹, which can be attributed to the diyne units. Unexpectedly, those bands disappeared almost completely (conversion >95%) after UV irradiation. This is confirmed by the appearance of new bands at 2112 cm⁻¹ and 1477 cm⁻¹, which can be attributed respectively to the stretching modes of alkyne and alkene moieties of the newly formed ene-yne functions. It is important to mention that those bands are present, at a lesser extent, in the powder spectrum of **PBM1**. This phenomenon is due to partial crosslinking of the very reactive **PBM1** induced by the Raman laser.¹⁵ However, the complete disappearance of diyne vibrational bands in the **PDA1** spectrum clearly showed that all the butadiyne units contained in the macrocycles reacted to form a rigid nanoarchitecture in which six PDA chains lay parallel one relative to each other, as represented on Figure 4.2. The reaction of all the butadiyne units eliminates the possibility of incomplete polymerization or open-like structures.

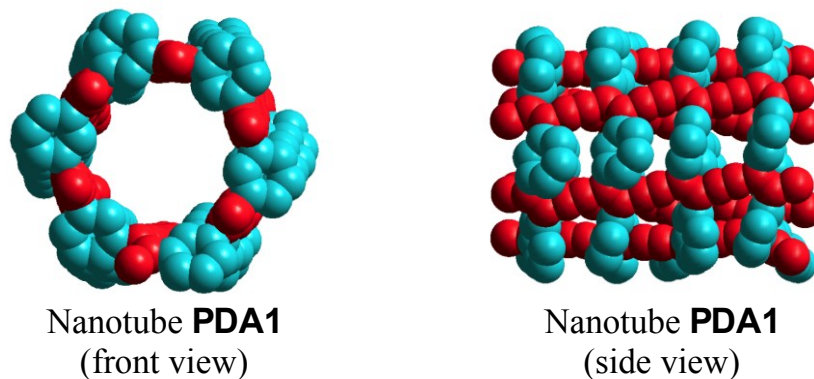


Figure 4.2. Structure and PDA1 in front and side views. Side groups and hydrogen atoms have been omitted for clarity. The red and blue carbon atoms represent the PDA chains and the phenyl groups, respectively.

TEM imaging was performed on **PDA1** to visualize the resulting architecture. As shown in Figures 4.3 and 4.8, the nanotubes appeared mostly as individualized entities, although some bundles can be found. Unlike PAMs, the PBMs-based nanotubes seem much more rigid and their internal empty cavity can be clearly visualized. Such a high rigidity is possible only if all the butadiyne units have reacted to form PDA chain, confirming the result obtained in Raman spectroscopy. Moreover, long nanotubes (few tens of nanometers-long) with very narrow polydispersity index (Figure 4.3a) can be prepared, thus proving the efficiency of the butadiyne topochemical polymerization embedded within the PBM scaffold. The exact diameter of the nanotubes (theoretical value = 2.5 nm) is very difficult to assess because of the relatively poor contrast obtained in TEM imaging for non-graphitic carbon materials on carbon substrate. Experiments are still underway to address this issue. This result is also a clear indication that topochemical polymerization happened exclusively in an intracolumnar fashion to create a 1D nanoarchitecture.

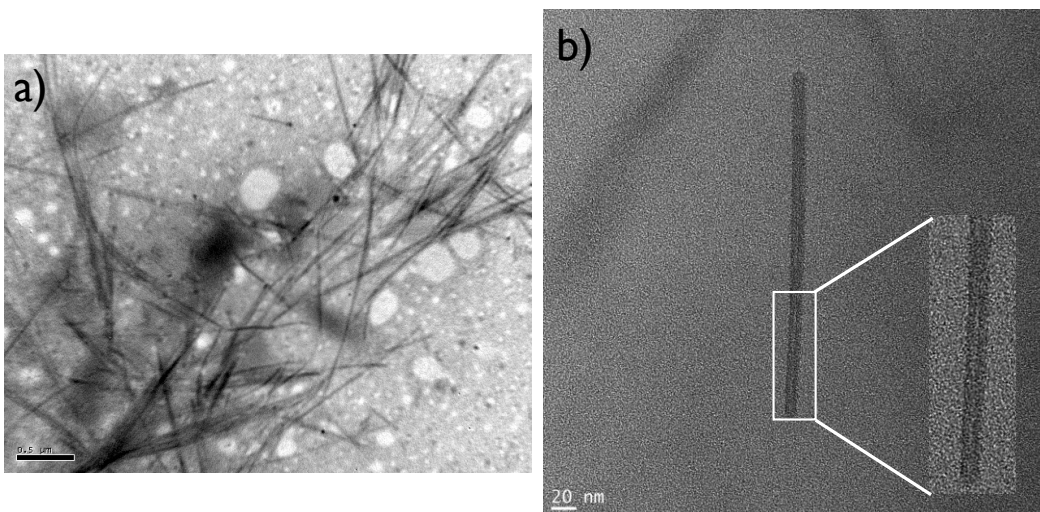


Figure 4.3. TEM (a) and HRTEM (b) images of the nanotubes. Scale bars are 500 nm (a) and 20 nm (b).

4.6. Conclusion

In summary, synthesis and gelation of new phenylene-butadiynylene macrocycles bearing amide functionalities was accomplished. PXRD of the resulting xerogels analysis showed a columnar organization in which the PBM stacked on top of each other, allowing the use of topochemical polymerization of the PBMs' inner butadiyne units to stabilize the supramolecular architecture. Raman spectroscopy performed on the resulting 1D nanoarchitectures confirmed that all the butadiyne units disappeared upon irradiation. HRTEM proved that the covalent nanoarchitectures thus created is rigid and possess an internal void. Thermal graphitization of this structure to create well-defined carbon nanotubes is underway.

4.7 Supporting information

4.7.1 General

Chemical reagents were purchased from Sigma-Aldrich Co. Canada, Alfa Aesar Co., TCI America Co. or Oakwood Products Inc. and were used as received. Solvents used for organic synthesis were obtained from Fisher Scientific (except THF from Sigma- Aldrich Co. Canada) and purified with a Solvent Purifier System (SPS) (Vacuum Atmosphere Co., Hawthorne, USA). Other solvents were obtained from Fisher Scientific and were used as

received. Tetrahydrofuran (THF) and triethylamine (Et₃N) used for Castro-Stephen-Sonogashira reactions were degassed 30 minutes prior to use. All anhydrous and air sensitive reactions were performed in oven-dried glassware under positive argon pressure. Analytical thin-layer chromatographies were performed with silica gel 60 F254, 0.25 mm pre-coated TLC plates (Silicycle, Québec, Canada). Compounds were visualized using 254 nm and/or 365 nm UV wavelength and/or aqueous sulfuric acid solution of ammonium heptamolybdate tetrahydrate (10 g/100 mL H₂SO₄ + 900 mL H₂O). Flash column chromatographies were performed on 230-400 mesh silica gel R10030B (Silicycle, Québec, Canada).

Apparatus

Nuclear magnetic resonance (NMR) spectra were recorded on a Varian Inova AS400 spectrometer (Varian, Palo Alto, USA) at 400 MHz (¹H) and 100 MHz (¹³C). High-resolution mass spectra (HRMS) were recorded with an Agilent 6210 Time-of-Flight (TOF) LC-MS apparatus equipped with an ESI or APPI ion source (Agilent Technologies, Toronto, Canada). MALDI-TOF measurements were performed on a Bruker Biflex IV equipped with nitrogen laser. UV-visible absorption spectra were recorded on a Varian diode-array spectrophotometer (model Cary 500) using 3-mm path length quartz cells. Scanning electron microscopy (SEM) images were taken using a JEOL JSM-6360 LV. Transmission electron microscopy (TEM) images were taken using a JEOL-1230. High resolution transmission microscopy (HRTEM) images were taken using a JEOL 2100 equipped with a field emission gun. X-ray diffraction was recorded on Siemens X-rays Diffractometer (Model S3 D5000). Raman spectra were recorded at 22.0 ± 0.5°C using a LABRAM 800HR Raman spectrometer (Horiba Jobin Yvon, Villeneuve d'Ascq, France) coupled to an Olympus BX 30 fixed stage microscope. The excitation light source was the 632.8 nm line of an He-Ne laser (Melles Griot, Carlsbad, CA). The laser beam was focused 100× long working distance objectives, generating an intensity at the sample of approximately 5-10mW. The confocal hole and the entrance slit of the monochromator were generally fixed at 200 and 100 μm, respectively. Data were collected by a one-inch open electrode Peltier-cooled CCD detector (1024 × 256 pixels).

Gelation test

To test the gelation properties of PAMs in a given solvent, we proceeded as follows: in a vial, a PAM was dissolved in a solvent. After dissolution by sonication, the vial was sealed and heated until a clear solution was obtained. The clear solution was allowed to slowly cool down at room temperature. The stability of the gel was confirmed by tube inversion.

SEM imaging

Organogel obtained in cyclohexane was deposited on a stainless steel substrate and allowed to dry for 3-4 days. Then, gold particles were sputtered on dried gel prior to imaging.

TEM imaging

The SEC-purified cross-linked material (PDA-walled nanotubes) was dissolved in CHCl_3 and was sonicated for two hours. The resulting solution was directly deposited on a copper grid pre-coated with amorphous carbon prior to imaging.

4.7.2 Synthetic procedure

Compound 1. An oven dried 500 mL round bottom flask equipped with a magnetic stir bar was charged with (trimethylsilyl)buta-1,3-diyne (3.0 g, 15.4 mmol), THF (170 mL) and methylolithium lithium bromide complex in THF (10.3 mL, 15.4 mmol, 1.5 M solution). The reaction mixture was stirred under nitrogen atmosphere for 3 hours and diluted with *n*-pentane. The organic layer was extracted with NH_4Cl (3x), dried with Na_2SO_4 and concentrated under vacuo to 10% of the initial volume. The organic layer was then added

to a 250 mL round bottom flask equipped with a magnetic stir bar charged 3,5-diiodododecylamide (2.76 g, 5.09 mmol), PdCl₂(PPh₃)₂ (143 mg, 0.20 mmol), CuI (39 mg, 0.20 mmol) and triethylamine (51 mL). The reaction mixture was stirred overnight and diluted with CH₂Cl₂. The organic layer was extracted with NH₄Cl (3x), dried with Na₂SO₄ and the solvents were removed under reduce pressure. The crude product was purified by flash chromatography on silica gel using hexanes to 5% EtOAc/hexanes as eluents to afford compound **1** (2.22 g, 82% yield) as an orange oil. ¹H NMR (CDCl₃, 400 MHz): 7.81 (s, 2H), 7.63 (s, 1H), 6.20 (m, 1H), 3.41 (q, *J* = 6.4 Hz, 2H), 1.59 (m, 2H), 1.32 (m, 18H), 0.88 (m, 3H), 0.24 (s, 18H); ¹³C NMR (CDCl₃, 100 MHz): 165.7, 138.7, 136.1, 131.9, 123.1, 92.6, 87.6, 76.3, 74.7, 40.7, 32.3, 30.0 (3C), 29.9 (2C), 29.8, 29.7, 27.4, 23.1, 14.5, 0.08. HRMS (APPI-TOF) *m/z* calcd for C₃₃H₄₇NOSi₂[M+H]⁺: 530.3269, found 530.3293.

Compound 2. A 25 mL round bottom flask equipped with a magnetic stir bar was charged with compound **1** (1.50 g, 2.56 mmol), K₂CO₃ (1.06 g, 7.68 mmol), THF (6 mL) and MeOH (6 mL). The reaction mixture was stirred until complete disappearance of the starting product by TLC. The reaction mixture was then diluted with benzene, washed with 10% aqueous HCl (2x), dried with sodium sulfate and the solvent was concentrated under vacuo to 10% of the initial volume. The organic layer was added without further purification to a 50 mL round bottom flask equipped with a magnetic stir bar charged with 3,5-diiodooctylbenzene (3.78 g, 8.56 mmol), degassed Et₃N (14 mL), PdCl₂(PPh₃)₂ (80 mg, 0.11 mmol) and CuI (22 mg, 0.11 mmol). The reaction mixture was stirred overnight and diluted with CH₂Cl₂. The organic layer was washed with saturated aqueous NH₄Cl (3x), dried with sodium sulfate and the solvent was removed under reduced pressure. The crude product was purified by flash chromatography on silica gel using hexanes to 10% acetone/hexanes as eluents to afford compound **2** (1.04 g, 28% yield) as a dark orange oil. ¹H NMR (CDCl₃, 400 MHz): 7.86 (s, 2H), 7.71 (s, 1H), 7.68 (s, 2H), 7.55 (s, 2H), 7.30 (s, 2H), 6.28 (s, 1H), 3.44 (q, *J* = 6.8 Hz, 2H), 2.53 (t, *J* = 7.2 Hz, 4H), 1.58 (m, 8H), 1.29 (m, 36H), 0.88 (m, 9H); ¹³C NMR (CDCl₃, 100 MHz): 165.7, 145.3, 138.8, 138.2 (2C), 135.8, 131.8, 131.3, 122.9 (2C), 93.7, 81.1, 79.7, 75.5, 74.2, 40.3, 35.3, 31.9, 31.8, 31.0, 29.6

(4C), 29.5, 29.4, 29.3 (2C), 29.2, 29.1, 26.9, 22.7, 22.6, 14.1 (2C); HRMS (APPI-TOF) m/z calcd for $C_{55}H_{69}I_2NO[M+H]^+$: 1014.3541, found 1014.3583.

Compound 3. A 25 mL round bottom flask equipped with a magnetic stir bar was charged with compound **2** (500 mg, 0.49 mmol), degassed THF (5 mL), degassed Et_3N (0.54 mL, 3.95 mmol), $PdCl_2(PPh_3)_2$ (14 mg, 0.02 mmol), CuI (4 mg, 0.02 mmol) and triisopropylsilylacetylene (0.44 mL, 1.98 mmol). The reaction mixture was stirred overnight, diluted with CH_2Cl_2 , washed with NH_4Cl and dried with sodium sulfate. The solvent was removed under reduced pressure and the crude product was purified by flash chromatography on silica gel using hexanes to 5% acetone/hexanes as eluents to afford compound **3** (510 mg, 92% yield) as an orange oil. 1H NMR ($CDCl_3$, 400 MHz): 7.85 (s, 2H), 7.72 (s, 1H), 7.47 (s, 2H), 7.29 (s, 4H), 6.17 (m, 1H), 3.44 (q, $J = 6.2$ Hz, 2H), 2.55 (t, $J = 7.8$ Hz, 4H), 1.61 (m, 8H), 1.29 (m, 36H), 1.12 (s, 42H), 0.88 (m, 9H); ^{13}C NMR ($CDCl_3$, 100 MHz): 165.7, 143.7, 138.4, 136.0, 133.7, 133.3, 132.6, 131.4, 124.1, 123.1, 121.6, 106.2, 91.7, 82.4, 79.5, 75.9, 73.7, 40.6, 35.7 (2C), 32.2, 32.1, 31.4, 29.8 (4C), 29.6 (3C), 29.5, 27.2, 22.9 (2C), 18.9, 18.8, 14.4 (2C), 11.5 (2C). HRMS (APPI-TOF) m/z calcd for $C_{77}H_{111}NOSi_2[M+H]^+$: 1122.8277, found 1122.8324.

PBM 1. A 25 mL round bottom flask equipped with a magnetic stir bar was charged with compound **3** (500 mg, 0.45 mmol), THF (9 mL) and TBAF (1.34 mL, 1.34 mmol, 1.0M solution in THF). The reaction mixture was stirred until complete disappearance of the starting product by TLC, diluted with CH_2Cl_2 , washed with water (3x), dried with sodium sulfate and the solvent was removed under reduced pressure. The resulting product was charged without further purification in a 50 mL round bottom flask equipped with a magnetic stir bar with degassed pyridine (16 mL). Another round bottom flask equipped with a magnetic stir bar was charged with $CuCl$ (3.47 g, 35.1 mmol), $CuCl_2$ (730 mg, 5.43 mmol) and degassed pyridine (70 mL) under N_2 atmosphere. The first solution was added dropwise to the catalyst solution over 4 days using a syringe pump and the reaction mixture was stirred for an additional 7 days. The reaction mixture was diluted with $CHCl_3$ and

poured in water. The organic layer was extracted successively with water, 25% aqueous NH_4OH , water, 10% aqueous acetic acid, water, 10% aqueous NaOH and brine. The organic layer was dried with sodium sulfate and the solvent was removed under reduced pressure. The crude product was purified by flash chromatography on silica gel using 20% hexanes/ CHCl_3 to CHCl_3 as eluents to afford **PBM 1** (37 mg, 9 % yield) as a light yellow amorphous powder. ^1H NMR (C_6D_6 , 400 MHz): 7.73 (s, 2H), 7.71 (s, 4H), 7.58 (s, 4H), 7.28 (s, 4H), 6.96 (s, 4H), 5.03 (m, 2H), 3.17 (q, $J = 6.7$ Hz, 4H), 2.18 (t, $J = 7.2$ Hz, 8H), 1.57 (s, 10H), 1.33 (s, 58H), 1.20 (m, 20H), 0.88 (m, 18H); ^{13}C NMR (CDCl_3 , 100 MHz): 165.5; 143.8; 143.5; 135.8; 133.8; 133.6; 133.2; 131.1; 121.9; 121.8; 121.7; 81.7; 80.8; 79.5; 75.6; 74.3; 73.9; 40.4; 35.9; 31.9; 31.8; 30.9; 29.7 (2C); 29.6 (2C); 29.5; 29.4 (2C); 29.2; 29.1; 27.0; 22.7; 22.6; 17.7; 14.1 (2C). HRMS (APPI-TOF) m/z calcd for $\text{C}_{118}\text{H}_{138}\text{N}_2\text{O}_2[\text{M}+\text{H}]^+$: 1616.0758, found 1616.0751.

Compound 4. An oven dried 500 mL round bottom flask equipped with a magnetic stir bar was charged with (trimethylsilyl)buta-1,3-diyne (2.5 g, 12.9 mmol), THF (143 mL) and methyllithium lithium bromide complex (8.6 mL, 12.9 mmol, 1.5 M solution in THF). The reaction mixture was stirred under nitrogen atmosphere for 3 hours and was diluted with *n*-pentane. The organic layer was extracted with NH_4Cl (3x), dried with Na_2SO_4 and concentrated under vacuo to 10% of the initial volume. The organic layer was then added to a 250 mL round bottom flask equipped with a magnetic stir bar charged with *N*-icosa-5,7-diyne-3,5-diiodo-benzamide (2.74 g, 4.24 mmol), $\text{PdCl}_2(\text{PPh}_3)_2$ (119 mg, 0.17 mmol), CuI (32 mg, 0.17 mmol) and triethylamine (53 mL). The reaction mixture was stirred overnight and diluted with CH_2Cl_2 . The organic layer was extracted with NH_4Cl (3x), dried with Na_2SO_4 and the solvent was removed under reduced pressure. The crude product was purified by flash chromatography on silica gel using hexanes to 7% acetone/hexanes as eluents to afford compound **4** (1.87 g, 69% yield) as an orange oil. ^1H NMR (400 MHz, CDCl_3): 7.82 (s, 2H), 7.64 (s, 1H), 6.24 (m, 1H), 3.6 (q, $J = 6.6$ Hz, 2H), 2.33 (t, $J = 6.6$ Hz, 2H), 2.25 (t, $J = 6.6$ Hz, 2H), 1.73 (m, 2H), 1.61 (m, 2H), 1.51 (m, 2H), 1.36 (m, 2H), 1.26 (m, 16H), 0.88 (m, 3H), 0.24 (s, 18H). ^{13}C NMR (100 MHz, CDCl_3): 165.8; 138.9; 135.9; 131.9; 123.1; 92.7; 87.6; 78.6; 76.9; 76.3; 74.6; 66.5; 65.4; 40.0; 32.3; 32.0; 30.0

(3C); 29.9; 29.8; 29.5; 29.3; 28.9; 28.7; 25.9; 23.1; 19.6; 19.3; 14.6; 0.59. HRMS (APPI-TOF) m/z calcd for $C_{41}H_{55}NOSi_2[M+H]^+$: 634.3895, found 634.3903.

Compound 5. A 25 mL round bottom flask equipped with a magnetic stir bar was charged with compound **4** (1.80 g, 2.84 mmol), KOH (478 mg, 8.51 mmol), THF (7 mL) and MeOH (7 mL). The reaction mixture was stirred until complete disappearance of the starting product by TLC. The reaction mixture was then diluted with benzene, washed with 10% aqueous HCl (2x), dried with sodium sulfate and the solvent was concentrated under vacuo to 10% of the initial volume. The organic layer was added without further purification to a 50 mL round bottom flask equipped with a magnetic stir bar charged with 3,5-diiodooctylbenzene (5.87 g, 13.3 mmol), degassed THF (13 mL), degassed DIPEA (3.70 mL, 21.2 mmol), $PdCl_2(PPh_3)_2$ (75 mg, 0.11 mmol) and CuI (20 mg, 0.11 mmol). The reaction mixture was stirred overnight and diluted with CH_2Cl_2 . The organic layer was washed with saturated aqueous NH_4Cl (3x), dried with sodium sulfate and the solvent was removed under reduced pressure. The crude product was purified by flash chromatography on silica gel using hexanes to 10% acetone/hexanes as eluents to afford compound **5** (1.4 g, 47% yield) as a dark orange oil. 1H NMR (400 MHz, $CDCl_3$): 7.86 (s, 2H), 7.75 (s, 1H), 7.57 (s, 2H), 7.49 (s, 2H), 7.32 (s, 2H), 6.19 (m, 1H), 3.50 (q, $J = 6.6$ Hz, 2H), 2.54 (t, $J = 7.6$ Hz, 4H), 2.36 (t, $J = 6.6$ Hz, 2H), 2.26 (t, $J = 6.6$ Hz, 2H), 1.77 (m, 2H), 1.61 (m, 10H), 1.53 (m, 2H), 1.27 (m, 34 H), 0.89 (m, 9H). ^{13}C NMR (100 MHz, $CDCl_3$): 165.4; 145.2; 138.7; 138.3; 135.6; 131.7; 131.3; 129.5; 127.0; 123.2; 122.9; 93.3 (2C); 80.9; 79.6; 77.8; 76.3; 75.5; 74.3; 65.1; 41.9; 39.6; 36.1; 35.3; 34.5; 31.9; 31.1; 29.7; 29.5; 29.4; 29.3; 29.2; 29.1; 29.0; 28.9; 28.6; 28.4; 26.9; 25.6; 25.2; 19.2; 18.8; 11.3. HRMS (APPI-TOF) m/z calcd for $C_{63}H_{77}I_2NO[M+H]^+$: 1118.4167, found 1118.4188.

Compound 6. A 25 mL round bottom flask equipped with a magnetic stir bar was charged with compound **5** (1.35 g, 1.21 mmol), degassed THF (12 mL), degassed Et_3N (1.32 mL, 9.66 mmol), $PdCl_2(PPh_3)_2$ (34 mg, 0.05 mmol), CuI (10 mg, 0.05 mmol) and triisopropylsilylacetylene (1.08 mL, 4.83 mmol). The reaction mixture was stirred

overnight, diluted with CH₂Cl₂, washed with NH₄Cl and dried with sodium sulfate. The solvent was removed under reduced pressure and the crude product was purified by flash chromatography on silica gel using hexanes to 5% acetone/hexanes as eluents to afford compound **6** (860 mg, 58% yield) as an orange oil. ¹H NMR (400 MHz, CDCl₃): 7.87 (s, 2H), 7.75 (s, 1H), 7.49 (s, 2H), 7.31 (s, 2H), 6.15 (m, 1H), 3.50 (q, *J* = 6.6 Hz, 2H), 2.57 (t, *J* = 7.6 Hz, 4H), 2.36 (t, *J* = 6.6 Hz, 2H), 2.26 (t, *J* = 6.6 Hz, 2H), 1.78 (m, 2H), 1.61 (m, 10H), 1.53 (m, 2H), 1.27 (m, 34 H), 1.14 (m, 42H), 0.88 (m, 9H). ¹³C NMR (100 MHz, CDCl₃): 165.5; 143.5; 135.6; 133.4; 132.3; 129.6; 127.0; 123.9; 122.9; 121.4; 105.9; 91.4; 90.2; 82.1; 81.5; 79.3; 78.0; 76.5; 75.7; 73.6; 66.1; 65.1; 41.9; 39.7; 35.5; 31.9 (2C); 31.1; 29.7 (2C); 29.6; 29.5; 29.4; 29.3; 29.2; 29.1; 28.9; 28.6; 28.4; 25.6; 22.7 (2C); 19.2; 18.9; 18.6; 18.5; 14.1; 11.3. HRMS (APPI-TOF) *m/z* calcd for C₈₅H₁₁₉NOSi₂[M+H]⁺: 1226.8903, found 1226.8918.4

PBM 2. A 50 mL round bottom flask equipped with a magnetic stir bar was charged with compound **6** (850 mg, 0.69 mmol), THF (14 mL) and TBAF (2.08 mL, 2.08 mmol, 1.0M solution in THF). The reaction mixture was stirred until complete disappearance of the starting product by TLC, diluted with CH₂Cl₂, washed with water (3x), dried with sodium sulfate and the solvent was removed under reduced pressure. The resulting product was charged without further purification in a 50 mL round bottom flask equipped with a magnetic stir bar with degassed pyridine (19 mL). Another round bottom flask equipped with a magnetic stir bar was charged with CuCl (4.61 g, 46.6 mmol), CuCl₂ (970 mg, 7.22 mmol) and degassed pyridine (94 mL) under N₂ atmosphere. The first solution was added dropwise to the catalyst solution over 4 days using a syringe pump and the reaction mixture was stirred for an additional 7 days. The reaction mixture was diluted with CHCl₃ and poured in water. The organic phase was extracted successively with water, 25% aqueous NH₄OH, water, 10% aqueous acetic acid, water, 10% aqueous NaOH and brine. The organic layer was dried with sodium sulfate and the solvent was removed under reduced pressure. The crude product was purified by flash chromatography on silica gel using 20% hexanes/CHCl₃ to CHCl₃ as eluents to afford **PBM 2** (146 mg, 24 % yield) as a white amorphous powder. ¹H NMR (400 MHz, CDCl₃): 7.74 (s, 2H), 7.65 (s, 4H), 7.44 (s, 4H),

7.19 (s, 4H), 7.17 (s, 4H), 6.77 (m, 2H), 3.51 (q, $J = 6.4$ Hz, 4H), 2.49 (t, $J = 7.3$ Hz, 8H), 2.38 (t, $J = 6.4$ Hz, 4H), 2.26 (t, $J = 6.4$ Hz, 4H), 1.81 (m, 4H), 1.65 (m, 8H), 1.54 (m, 8H), 1.31 (m, 76H), 0.91 (m, 18H). ^{13}C NMR (100 MHz, CDCl_3): 165.8, 143.3, 137.3, 135.4, 134.1, 132.8, 130.7, 129.4, 126.9, 122.8, 121.9, 81.4, 80.6, 79.3, 78.0, 76.4, 75.5, 74.2, 73.8, 65.9, 64.9, 41.8, 35.3, 31.8, 31.7, 30.8, 29.5 (2C), 29.4, 29.3, 29.2, 29.1, 28.9, 28.7, 28.4, 28.2, 25.5, 22.5, 21.3, 19.1, 18.8, 17.9, 17.6, 13.9, 12.1. HRMS (APPI-TOF) m/z calcd for $\text{C}_{134}\text{H}_{154}\text{N}_2\text{O}_2[\text{M}+\text{H}]^+$: 1824.2083, found 1824.2019.

4.7.3. Scanning-electron microscopy (SEM) imaging

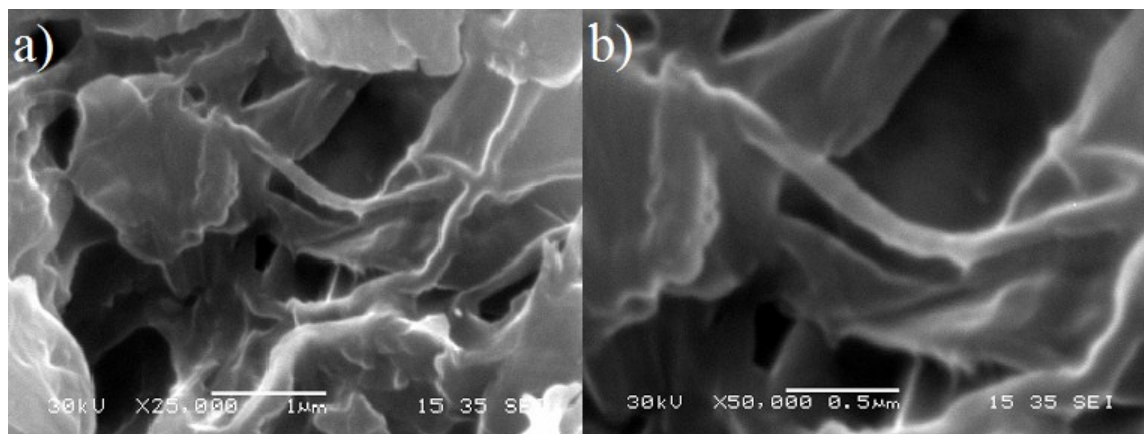


Figure 4.4. SEM images of dried gel of **PBM1** in cyclohexane (10 mg/mL)

4.7.4. Powder X-rays diffraction analysis

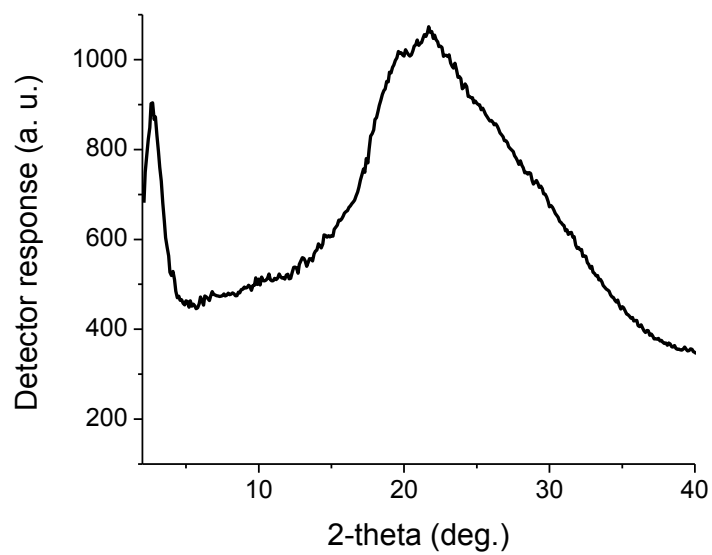
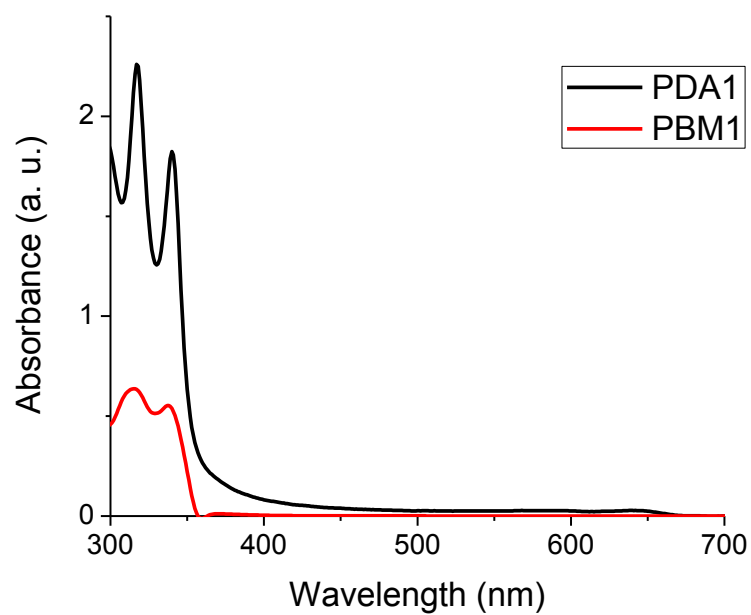


Figure 4.5. X-rays diffractogram for **PBM1** gel in cyclohexane (10 mg/mL).

4.7.5. UV-visible spectroscopy



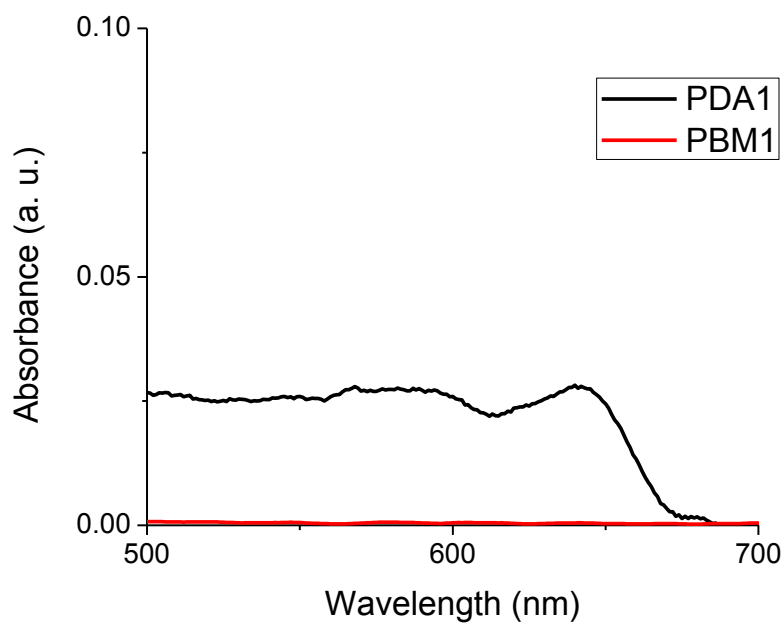


Figure 4.6. UV visible spectra of **PBM1** and **PDA1** in CHCl_3

4.7.6 Raman spectroscopy

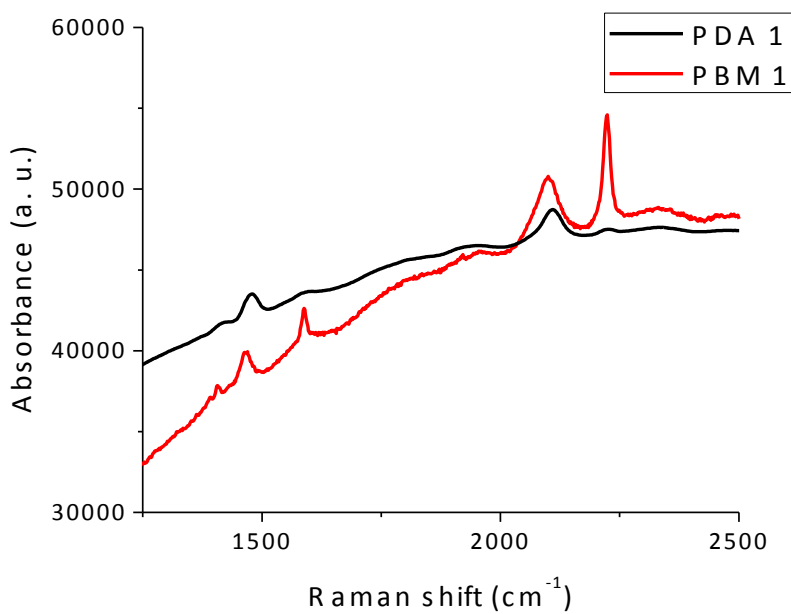


Figure 4.7. Raman spectra of **PBM1** (red) and **PDA1** (black).

4.7.7. TEM images of the nanotubes

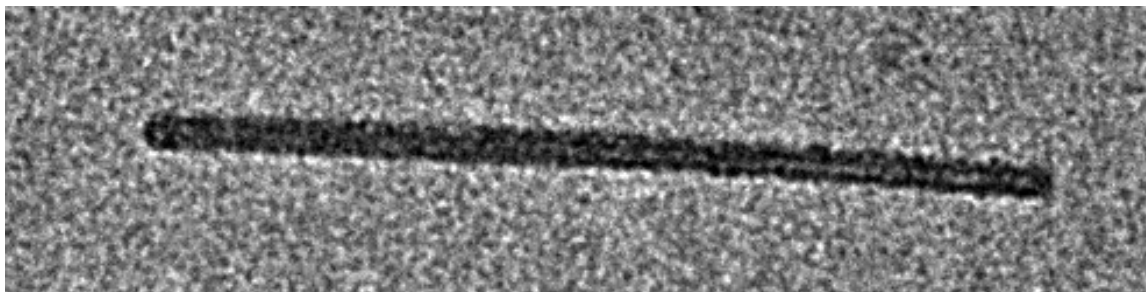


Figure 4.8. TEM image of a single nanotube. The channel inside the nanotube can be clearly differentiate, especially on the right side of the nanotube.

4.8 Références

- [1] (a) D. T. Bong, T. D. Clark, J. R. Granja, M. R. Ghadiri, *Angew. Chem. Int. Ed.* 2001, **40**, 988-1011; (b) R. García-Fandiño, M. Amorín, J. R. Granja, in *Supramolecular Chemistry: From Molecules to Nanomaterials*; J. W. Steed, P. A. Gale, John Wiley & Sons, Ltd. 2012; (c) M. A. Balbo Block, C. Kaiser, A. Khan, S. Hecht, *Top. Curr. Chem.* 2005, **245**, 89-150.
- [2] (a) Y. Xu, M. D. Smith, M. F. Geer, P. J. Pellechia, J. C. Brown, A. C. Wibowo, L. S. Shimizu, *J. Am. Chem. Soc.* 2010, **132**, 5334-5335; (b) J. Nagasawa, M. Yoshida, N. Tamaoki, *Eur. J. Org. Chem.* 2011, 2247-2255; (c) T.-J. Hsu, F. W. Fowler, J. W. Lauher, *J. Am. Chem. Soc.* 2012, **134**, 142-145.
- [3] (a) G. Wegner, *Natureforsch., B: Chem. Sci.* 1969, **24**, 824-83; (b) G. Wegner, *Makromol. Chem.* 1972, **154**, 35-48.
- [4] M. M. Haley, R. R. Tykwinski, *Carbon-Rich Compounds: From Molecules to Materials*, John Wiley & Sons, 2006.
- [5] (a) K. Aoki, M. Kudo, N. Tamaoki, *Org. Lett.* 2004, **6**, 4009-4012; (b) O. J. Dautel, M. Robitzer, J.-P. Lère-Porte, F. Serein-Spirau, J. J. E. Moreau, *J. Am. Chem. Soc.* 2006, **128**, 16213-16223; (c) J. R. Néabo, K. I. S. Tohondjona, J.-F. Morin, *Org. Lett.* 2011, **13**, 1358-1361; (d) J. R. Néabo, S. Rondeau-Gagné, C. Vigier-Carrière, J.-F. Morin, *Langmuir* 2013, **29**, 3446-3452.
- [6] (a) K. Cantin, S. Rondeau-Gagné, J. R. Néabo, M. Daigle, J.-F. Morin, *Org. Biomol. Chem.* 2011, **9**, 4440-4443; (b) S. Rondeau-Gagne, J. R. Néabo, M. Desroche, K. Cantin, A. Soldera, J.-F. Morin, *J. Mat. Chem. C* 2013, **1**, 2680-2687; (c) S. Rondeau-Gagné, J.R. Néabo, M. Desroches, J. Larouche, J. Brisson, J.-F. Morin, *J. Am. Chem. Soc.* 2013, **135**, 110-113.

- [7] (a) Y. Tobe, N. Utsumi, K. Kawabata, A. Nagano, K. Adachi, S. Araki, M. Sonoda, K. Hirose, K. Naemura, *J. Am. Chem. Soc.* 2002, **124**, 5350-5364; (b) Ng, M.-F.; Yang, S.-W. *J. Phys. Chem. B* 2007, **111**, 13886-13893.
- [8] Y. Tobe, N. Utsumi, A. Nagano, K. Naemura, *Angew. Chem. Int. Ed.* 1998, **37**, 1285-1287.
- [9] (a) K. C. Yee, *J. Polym. Sci : Polym. Chem.* 1979, **17**, 3637-3646; (b) A. Nomoto, M. Sonoda, Y. Yamaguchi, T. Ichikawa, K. Hirose, Y. Tobe, *J. Org. Chem.* 2006, **71**, 401-404.
- [10] A. B. Holmes, G. E. Jones, *Tetrahedron Lett.* 1980, **21**, 3111-3112.
- [11] S. Höger, A. D. Meckenstock, S. Müller, *Chem. Eur. J.*, 1998, **4**, 2423-2434.
- [12] D. O’Krongly, S. R. Denmeade, M. Y. Chiang, R. Breslow, *J. Am. Chem. Soc.* 1985, **107**, 5544-5545.
- [13] Y. Tobe, N. Utsumi, A. Nagano, M. Sonoda, K. Naemura, *Tetrahedron*, 2001, **57**, 8075-8083.
- [14] S. Laschat, A. Baro, N. Steinke, F. Giesselmann, C. Hägele, G. Scalia, R. Judele, E. Kapatsina, S. Sauer, A. Schreivogel, M. Tosoni, *Angew. Chem. Int. Ed.* 2007, **46**, 4832-4887.
- [15] The partial laser-induced cross-linking of **PBM1** during Raman experiments was impossible to avoid since sufficient laser power must be used to overcome the fluorescence background emission from **PBM1**. Over three different laser sources were used and none of them allowed to solve the problem. Somehow, this prove the high reactivity of **PBM1** under illumination.

Chapitre 5.

Nanomatériaux de carbone à partir de la pyrolyse de nanobâtonnets de polydiacétylènes

Carbon nanomaterials from pyrolysis of polydiacetylene-walled nanorods

Simon Rondeau-Gagné, Jules Roméo Néabo, Maxime Daigle, Isabelle Levesque, Maude Desroches and Jean-François Morin *

Département de Chimie and Centre de Recherche sur les Matériaux Avancés (CERMA), Université Laval, 1045 ave. de la Médecine, Québec, QC, Canada, G1V 0A6

Publié dans le journal *Materials Research Express*, **2014**, *1*, 015602.

5.1. Préambule

Cet article présente la synthèse de nouveaux matériaux riches en carbone à partir de la pyrolyse de nanobâtonnets décrits précédemment. Cette transformation a pour but d'aller vers la synthèse contrôlée de matériaux tout carbone, pouvant trouver d'intéressantes applications en électronique et autres domaines. Ma contribution à cet article est majeure. J'ai effectué toutes les réactions de pyrolyses, les caractérisations des nouveaux matériaux ainsi que toute l'imagerie électronique présentée. J'ai également participé à la recherche bibliographique et à la rédaction du manuscrit.

5.2. Résumé

La pyrolyse de nanobâtonnets de polydiacétylène, obtenus à partir d'un précurseur macrocyclique rigide a été réalisée. L'analyse thermogravimétrique a montré que la pyrolyse a causé une perte des chaînes aliphatiques et des changements structuraux au PDA, pour produire de nouvelles nano-architectures riches en carbone. Cette réaction de pyrolyse a été confirmée par spectroscopie Raman et UV-visible. L'imagerie TEM réalisée sur le matériau obtenu a montré la formation d'un réseau de nanofibrilles enchevêtrées contenant différents types de nanostructures riches en carbone.

5.3. Abstract

Pyrolysis of polydiacetylene-walled nanorods obtained from a rigid and shape-persistent macrocyclic precursor was performed. The thermogravimetric analysis showed that pyrolysis caused a loss of aliphatic chains and structural changes of PDAs to produce carbon-rich nanoarchitectures, as confirmed by Raman and UV-visible spectroscopy. The TEM imaging performed on the resulting material showed formation of an entangled nanofibrils network containing various types of nanostructures.

5.4 Introduction

Among the new classes of molecules used in modern electronics and energy conversion and storage devices, carbon nanomaterials, such as carbon nanotubes and graphene, are particularly interesting because of their excellent electronic properties and relative ease of preparation. The possibility to control their properties, especially electronic and optical ones, through careful modulation of their size, shape and chemical nature allowed materials scientists to prepare custom-made materials that meet the strictest requirements of electronics industry [1-4]. It is therefore not surprising to see more research focusing on the chemical modification of these materials and on the formation of hybrid materials with unique electronic properties [5-8]. Recently, carbon nanomaterials showed their utility in electronic devices such as field-effect transistors (OFETs) [9-11], organic solar cells (OPVs) [12-14] and lithium ions battery [15].

Traditionally, physical methods that use simple, non-organized carbon sources as feedstock such as chemical vapor deposition (CVD), laser ablation, combustion of hydrocarbons and other high-temperature processes are used to prepare carbon nanomaterials [16-19]. Despite their widespread utilization, physical methods suffer from drawbacks regarding production setup, energy consumption, purity and structural uniformity of the final materials. Besides, these methods usually offer poor control over the properties of the resulting materials, although significant improvement have been made in this regard recently [20]. To overcome this problem, many efforts have been spent to develop new synthetic methodologies toward well-defined carbon-rich nanomaterials using milder conditions. Among the advances made in the synthesis of carbon nanomaterials, the use of well-defined, reactive organic precursors became a particularly attractive approach. For example, transformation of cyclophane led to graphitic materials in a relatively quick and simple way, at much lower temperatures than CVD [21-23]. Similarly, Müllen and coworkers recently reported the pyrolysis of hexa-*peri*-hexabenzocoronene (HBCs) toward different well-defined carbon-rich nanomaterials [24-26]. These examples showed the importance of the chemical and morphological nature of the carbon source in the preparation of a large library of nanostructured materials, going from 1D nanotubes to 2D graphenes that can be used in different applications [27-29].

Recently, we and others reported the formation of high-molecular weight polydiacetylene (PDA) through the topochemical polymerization of self-assembled diynes-containing precursors in the xerogel state [30-32]. We have shown that it was possible to modulate the structural parameters of the resulting polydiacetylene by carefully varying the chemical nature of the precursors [33,34]. Thus, we have been able to obtain different types of carbon nanomaterials such as nanoparticles [35], nanorods [36] and nanotubes [37]. Among these, organic nanorods formed from shape-persistent diyne-containing phenylacetylene macrocycles (PAMs) are particularly interesting since they are rigid, which should prevent the nanorods from collapsing (Figure 1) [38]. In addition, the PDA materials are soluble and easily purified after the topochemical polymerization, enabling their characterization. Although PDAs possess limitation regarding organic electronics applications due to poor charge transport properties, phenyl-appended PDAs and other ene-yne containing molecules proved to be very interesting precursors toward carbon-rich nanomaterials since they can undergo cycloaromatization reaction upon exposure to light, heat or catalysts [39]. Using self-assembled alkyne-containing and PDA precursors, graphitic materials of different sizes and shapes with very interesting properties have been prepared [40,41]. However, no attempt to pyrolyze alkyne-containing nanotubes in the aim to retain the nanotubes configuration while graphitizing the walls has been reported yet. Pyrolysis and explosive decompositions of other alkynes-containing precursors that yield to graphite-like structures have been reported, but none of them gave ordered materials with specific size and shape [42-47]. The use pre-organized reactive precursors (nanorods in this study) could open the way to a new strategy for the preparation of carbon nanotubes whose structural parameters could be controlled by proper design of the precursors and their building blocks.

Herein, we report the pyrolysis of organic PDA-walled nanorods formed from rigid PAMs [48]. The initial hypothesis was that the covalently-linked nanorods architecture would keep its size and shape during the pyrolysis process, thus leading to graphitized nanorods, or nanotubes, with narrow diameter distribution. Morphology-retaining carbonization has been reported previously during the pyrolysis of a helical polyacetylene film and amorphous carbon nanoparticles [49,50]. The carbon nanomaterials obtained after pyrolysis of PDA nanorods in different conditions have been characterized using

thermogravimetric analysis, vibrational spectroscopy and electron microscopy. The strategy we sought to study is shown in Figure 5.1.

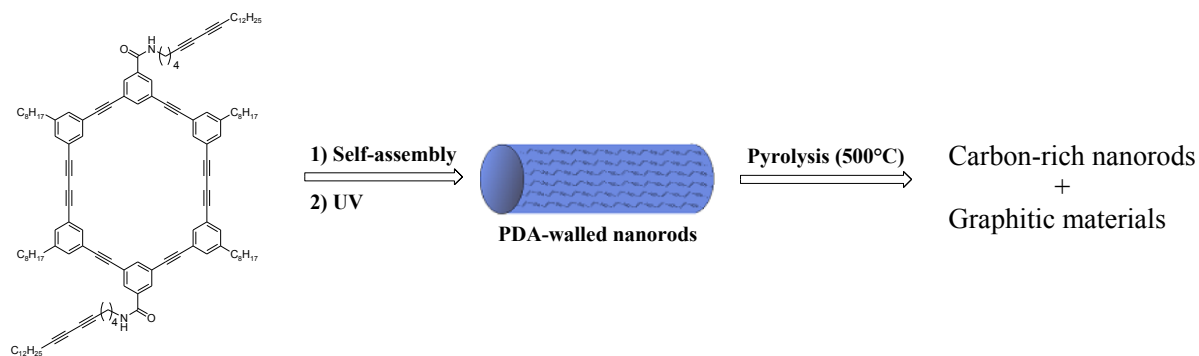


Figure 5.1. Pathway toward carbon-rich material from organic PDA nanorods [38]

5.5 Experimental

5.5.1 Sample preparation

For the preparation of carbon nanomaterials from PAMs, the following procedure was used. PAM was dissolved in EtOAc at a concentration of 10 mg/mL [38]. The vial was then heated until a translucent solution was obtained and was cooled to room temperature. The organogel formed was deposited on a glass slide and irradiated with UV ($\lambda = 254$ nm) for 24 h. The resulting blue fibers (PDA) were dissolved in $CHCl_3$ and loaded on a size-exclusion chromatography column (Bio-Beads) eluting with $CHCl_3$ to remove unreacted PAM. The purified PDA-walled nanorods were then charged in a glass tube sealed under vacuum and heated at 500°C (10 °C/min) for 4 h. The resulting black powder was characterized without further purification. The pyrolysis of cobalt-containing PAMs has been performed as followed: The purified PDA-walled nanorods were mixed with a solution of $Co_2(CO)_8$ (20 eq./macrocycle) in $CHCl_3$. After stirred for 1 hour, the solution was evaporated and the residue was washed several times with a 2N NaOH solution. The residual powder was then placed in a glass tube and sealed under vacuum. Pyrolysis of materials was carried out by heating at 500°C (10 °C/min) for 4 h. The resulting black powder was characterized without further purification.

5.5.2 Characterization

UV-visible absorption spectra were recorded on a Varian diode-array spectrophotometer (model Cary 500) using 3-mm path length quartz cells. TGA measurements were done on a Mettler Toledo (TGA/SDTA851e). Transmission electron microscopy (TEM) images were taken using a JEOL-1230. High resolution transmission microscopy (HRTEM) images were taken using a JEOL 2100 equipped with a field emission gun. Raman spectra were recorded at $22.0 \pm 0.5^\circ\text{C}$ using a LABRAM 800HR Raman spectrometer (Horiba Jobin Yvon, Villeneuve d'Ascq, France) coupled to an Olympus BX 30 fixed stage microscope. The excitation light source was the 514 nm line of an He-Ne laser (Melles Griot, Carlsbad, CA). The laser beam was focused 100 \times long working distance objectives, generating an intensity at the sample of approximately 5-10mW. The confocal hole and the entrance slit of the monochromator were generally fixed at 200 and 100 μm , respectively. Data were collected by a one-inch open electrode Peltier-cooled CCD detector (1024 \times 256 pixels). Pyrolysis was performed using a Thermo Scientific oven, Lindberg/Blue model.

5.6. Results and discussion

To gain some insights on the pyrolysis reaction performed on PDA-walled nanorods, thermogravimetric analysis under a nitrogen atmosphere (TGA) was performed. A predetermined amount of pure PDA-walled nanorods was heated to 900 $^\circ\text{C}$ at a heating rate of 10 $^\circ\text{C}/\text{minute}$. As shown in Figure 5.2, the first weight lost process began at around 400 $^\circ\text{C}$ and extend to 500 $^\circ\text{C}$. At this temperature, a weight loss of about 40% of initial mass was observed, which can be associated with the loss of peripheral aliphatic chains, representing a theoretical 38% of the total mass of the nanorods. This observation is therefore in agreement with the considerable loss of solubility after pyrolysis. By continuing the heating process, a second significant mass loss was observed between 500 and 700 $^\circ\text{C}$. At this temperature, almost complete degradation of the nanorods was observed leaving a net weight of 1.8% of the original mass. In the light of this analysis, we hypothesized that new carbon-rich nanoarchitectures appeared at temperatures as low as 400 $^\circ\text{C}$. Moreover, the almost complete mass loss at 700 $^\circ\text{C}$ suggests that thermodynamically stable, defect-free graphitic structures have never been formed during the process. Instead, defects-containing graphite-like structures, which could be decomposed into volatile molecules upon further heating, seemed to be formed upon

heating. This extensive decomposition could also be the results of oxidation by traces amount of oxygen [51]. Thus, the temperature of the pyrolysis experiments to form carbon-rich nanotubes had to be carefully chosen in order to avoid extensive degradation. In this regard, we decided to set the pyrolysis temperature to 500°C.

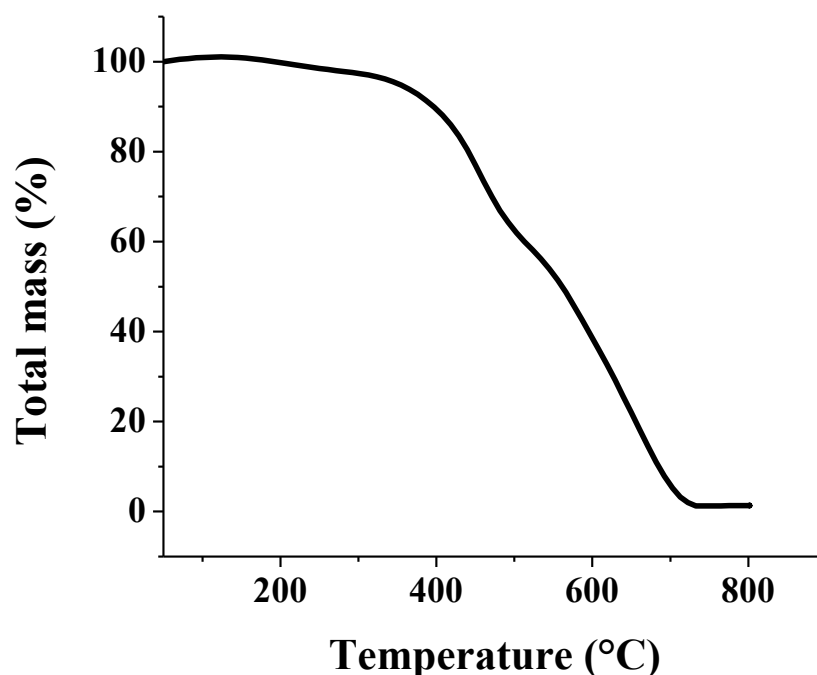


Figure 5.2. Thermogravimetric analysis (TGA) of pyrolysed PDA-walled nanorods

To confirm the disappearance of the PDA backbone after pyrolysis at 500°C, UV-visible spectroscopy was performed. Despite the low solubility of the pyrolyzed material, it was possible to solubilize enough material to make a diluted solution for this analysis. Therefore, the UV-visible spectrum is not representative of the whole sample, but only of its soluble fractions. As shown in Figure 5.3, the peak associated with the PDA backbone at $\lambda_{\text{max}} = 650$ nm completely disappeared after pyrolysis, meaning that the nature of the material changed during the thermal process. The peak at around 340 nm is likely associated to the $\pi \rightarrow \pi^*$ transition of aromatic rings that remained intact after the pyrolysis since no change in its position or shape was observed after pyrolysis [52]. This result

suggests that heating PDA-walled nanorods at 500°C is enough to alter the PDA backbone but not enough to graphitize the entire carbonaceous scaffold.

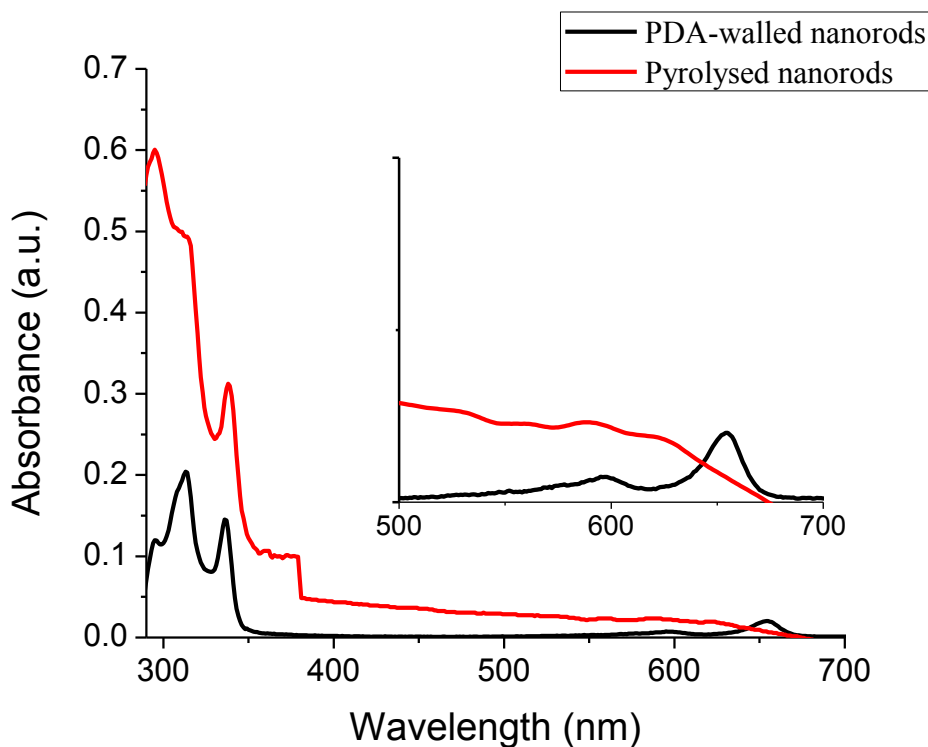


Figure 5.3. UV-visible spectra of PDA-walled nanorods (black line) and pyrolyzed nanorods (red line) in CHCl_3 .

In order to gain insight on the nature of the material obtained after pyrolysis, Raman spectroscopy was used. The main advantage of this tool is its high sensitivity to the ene-yne functionality and to the D and G bands of graphitic structures. Raman spectra of the PDA-walled nanorods precursor and its pyrolyzed analog are shown in Figure 5.4. Interestingly, pyrolyzed nanorods exhibited two main bands at 1372 cm^{-1} and 1603 cm^{-1} that can be associated with D and G bands of a graphitic material, respectively. In addition, the complete disappearance of the bands associated to the ene-yne moiety of the PDA at 1473 and 2096 cm^{-1} can be observed. This result indicated a complete transformation of the PDA to form carbon-rich material upon heating. The presence of a relatively intense band D shows the formation of a graphitic structure with defects [53], probably caused by

incomplete graphitization reaction. In addition, the width of the D and G bands also indicates the presence of undefined graphite-like materials rather than crystalline, well-organized ones [54]. Nonetheless, the presence of defects in graphitic materials can be beneficial for some applications since it leads to the creation of a band gap, an essential parameter for organic electronic devices [55].

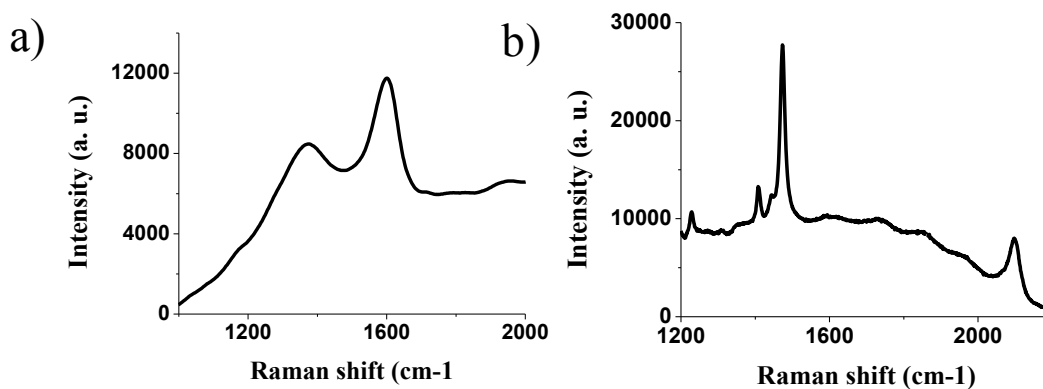


Figure 5.4. Raman spectrum of a) pyrolysed nanorods and b) PDA-walled nanorods, ($\lambda = 514$ nm)

Given that the primary objective of the pyrolysis was to obtain carbon nanorods from organic nanorods, transmission electron microscopy (TEM) analysis was performed to gain access to the nanostructures obtained after pyrolysis and to verify the initial hypothesis regarding the morphology retention. Thus, a sample of pyrolyzed nanorods was dispersed in CHCl_3 by sonication and deposited on a copper grid coated with a carbon film. The images obtained from the PDA-walled nanorods precursor and its pyrolyzed analogs are shown in Figure 5.5.

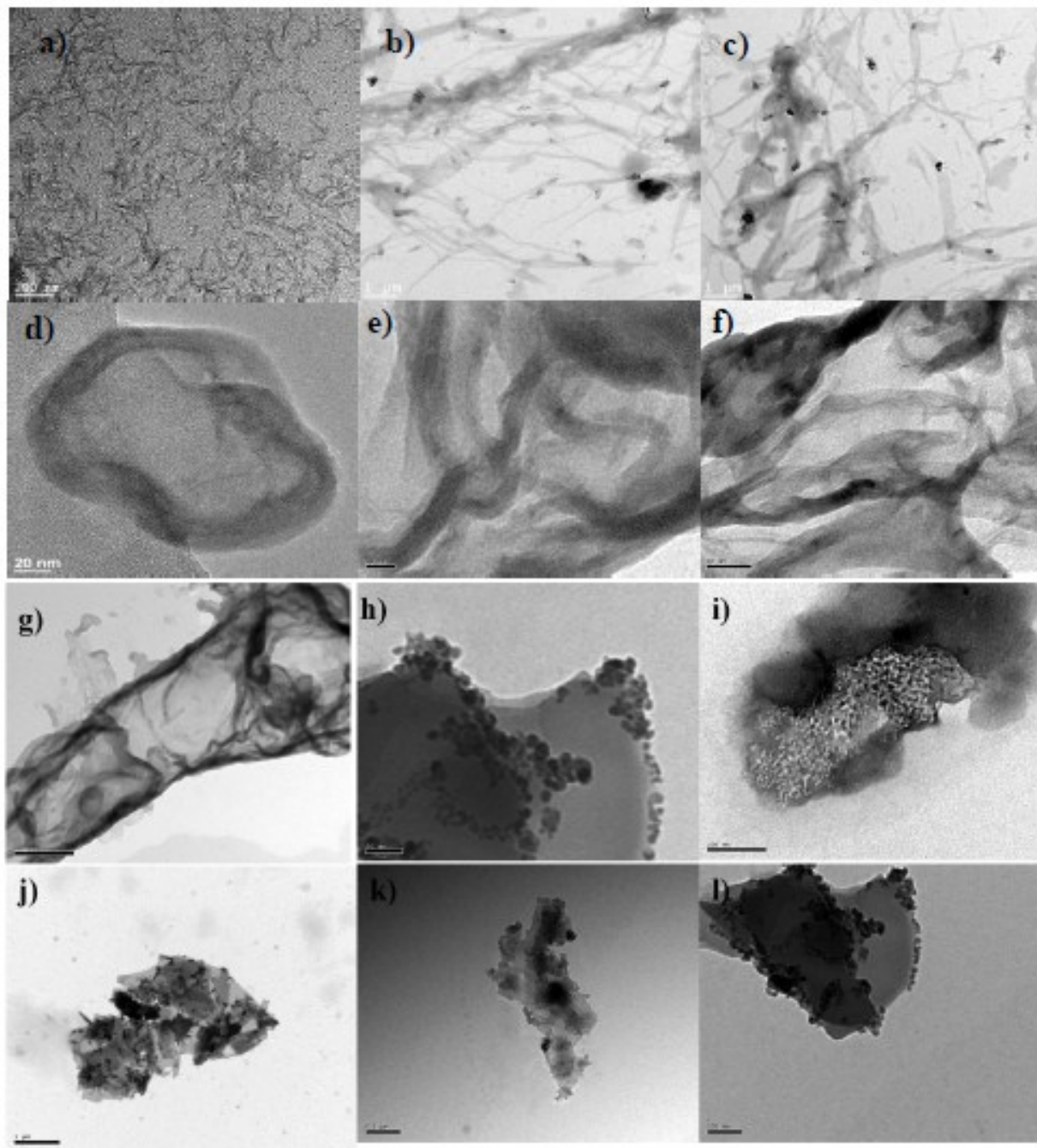


Figure 5.5. HRTEM image of PDA-walled nanorods a) before [38] (Copyright 2013 American Chemical Society) and b) to d) after pyrolysis and TEM images of PDA walled-nanorods e) and f) after pyrolysis. Scale bars are a) 200 nm, b) and c) 1 μm , d) and e) 20 nm, f) 50 nm, g) 200 nm, h) 50 nm, i) 100 nm, j) 1 μm , k) 0.2 μm and l) 100 nm

As previously reported [38], the PDA-walled nanorods obtained after topochemical polymerization of PAMs have a narrow distribution of lengths and diameters. The poor contrast in TEM, mainly due to the nature of the sample, makes it difficult to visualize but small nanorods with length of few tens of nanometers with width of few nanometers can be observed. It is important to mention that because of strong intermolecular interactions between nanorods, these tend to form tight bundles. After pyrolysis of these nanorods, a mixture of different nanoarchitectures can be observed by HRTEM. As shown in Figure 5.5, the different architectures obtained have length and width that goes from few nanometers to microns. Observed nanostructures in HRTEM are summarized in Table 5.1. In the micron scale, nanoarchitectures that look like aggregates of long thin and narrow sheets resembling nanoribbons can be observed. By going a little deeper into the sample (figure 5.5 e-f), we observed that these nanoribbons seem to be made of stacks of sheets. Although we have not been able to quantify the number of sheets present in these features, one can argue that they are made of only few layers based on their relatively high transparency to electrons. In most cases, large nanoribbons with lengths of several tens of nanometers with widths of varying from 20 nm to more than 100 nm can be observed.

Table 5.1. Carbon-rich features observed by HRTEM after pyrolysis of PDA-walled nanorods

Features	Lengths	Width	Description
Nanofibers	> 100 nm	20-50 nm	Entangled carbon-rich nanofibers, Figures 5b and 5c
Nanoribbons	> 100 nm	20-100 nm	Multilayer graphite-like material, Figures 5e to 5l
Onions	100 nm	20-80 nm	Multilayer carbon onions, Figures 5d, 5j, 5h and 5l

Although the material after pyrolysis is very interesting, the strategy we used did not allow keeping the initial morphology of the starting materials. However, we cannot rule out the possibility of formation of graphitized nanorods throughout this process since large portion of the material formed after pyrolysis appeared as aggregates similar to those observed in

PDA-walled nanorods. Attempts to better disperse the sample after pyrolysis did not yield to better result, which is an indication of the strong intermolecular interactions between the nanorods. Thus, other methods of dispersion and different temperature plateaux will have to be used in order to increase the structural retention during pyrolysis and to facilitate the observation of these new carbon-rich nanoarchitectures by HRTEM.

In order to increase the reactivity of the PDA nanorods precursors at 500°C and to ensure better graphitization yield, alkynes were complexed with cobalt atoms prior to pyrolysis [56]. This approach has been reported previously and showed that it can be used for the formation of interesting well-defined, carbon-rich materials. This approach also provides an opportunity to prepare hybrid carbonaceous materials [42,57,58].

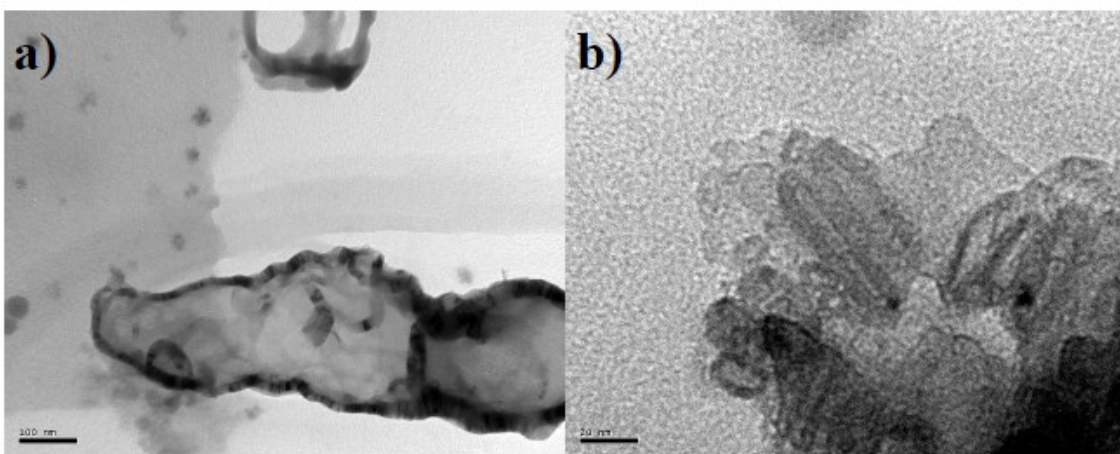


Figure 5.6. TEM imaging of pyrolyzed cobalt-containing PDA-walled nanorods. Scale are a) 100 nm and b) 20 nm.

Thus, cobalt-containing PDA-walled nanorods were subjected to pyrolysis at 500°C for 4 hours and the resulting material was imaged using TEM. The results are shown in Figure 5.6. The first observation made is the significant increase of contrast compared with cobalt-free pyrolyzed materials. It was also possible to observe several aggregates, mostly nanoparticles of cobalt-rich compounds. At a scale of 100 nm (Figure 5.6a), nanomaterials presenting a similar structure than to those obtained during cobalt-free pyrolysis were observed, indicating the rather limited influence of the activation of alkyne on the final nanostructures. Nonetheless, the formation of bundles of nanofibers and nanosheets similar

to few-layers graphene can be observed. By going deeper into the sample, the presence of elongated oval nanoarchitectures with a diameter of about 10 nm was observed. These features are probably resulting from the starting nanorods bundles that were complexed by cobalt atom on their periphery prior to pyrolysis, leading to carbon-rich nanorods with larger diameters. Further characterizations are underway to verify this hypothesis. However, pyrolysis of nanorods containing cobalt seems an interesting avenue toward the formation of new hybrid organometallic nanoarchitectures.

5.7 Conclusion

In conclusion, the pyrolysis of PDA-walled nanorods obtained by topochemical polymerization of rigid phenylacetylene macrocycles has been made. The pyrolysis has been carried out at relatively low temperature (500 °C), causing a loss of peripheral aliphatic chains and resulting in formation of new carbon-rich materials. After pyrolysis, TEM imaging showed tight networks of graphite-like nanoarchitectures with diameters of few tens of nanometers. Despite the high probability of formation of nanorods, it was impossible to make their observation, mainly because of the difficulty to suspend the pyrolyzed materials in common organic solvents. Nonetheless, formation of these new carbon-rich nanostructures is an important step toward the use of nanostructured PDAs as precursors for new materials for various applications.

5.8. Références

- [1] Avouris P. 2002 *Acc. Chem. Res.* 35 1026.
- [2] Avouris P. 2010 *Nano lett.* **10** 4285.
- [3] Wu J, Pisula W, Müllen K. 2007 *Chem. Rev.* **107** 718.
- [4] Baughman R H, Zakhidov A A, de Heer W A. 2002 *Science* **297** 787.
- [5] Tung V C, Chen L M, Allen M J, Wassei J K, Nelson K, Kaner R B, Yang Y. 2009 *Nano lett.* **9** 1949.
- [6] Lee D H, Kim J E, Han T H, Hwang J W, Jeon S, Choi S Y, Hong S H, Lee W J, Ruoff R S, Kim S O. 2010 *Adv. Mater.* **22** 1247.

- [7] Dong X, Bing L, We A, Cao X, Chan-Park M B, Zhang H, Li L-J, Huang W, Chen P. 2011 *Carbon* **49** 2944.
- [8] Zhuangjun F, Yan J, Zhi L, Zhang Q, Wei T, Feng J, Zhang M, Qian W, Wei F. 2010 *Adv. Mater.* **22** 3723.
- [9] Pang S, Hernandez Y, Feng X, Müllen K. 2011 *Adv. Mater.* **23** 2779.
- [10] Martel R A, Schmidt T, Shea H R, Hertel T, Avouris P. 1998 *App. Phys. Lett.* 1998 **73** 2447.
- [11] Schwierz F. 2010 *Nature Nanotech.* **5** 487.
- [12] Gomez De Arco L, Zhang Y, Schlenker C W, Ryu K, Thompson M E, Zhou C. 2010 *ACS Nano*, **4** 2865.
- [13] Wan X, Long G, Huang L, Chen Y. 2011 *Adv. Mater.* **23** 5342.
- [14] Zhu H, Wei J, Wang K, Wu D. 2009 *Sol. Energ. Mat. Sol. Cells*, **93** 1461.
- [15] Pumera, M. 2011 *Energy Environ. Sci.* **4** 668.
- [16] Dai H. 2002 *Acc. Chem. Res.* **35** 1035.
- [17] Jia X, Campos-Delgado J, Terrones M, Meunier V, Dresselhaus M S. 2011 *Nanoscale*, **3** 86.
- [18] Bhaviripudi S, Mile E, Steiner S A, Zare A T, Dresselhaus M S, Belcher A M, Kong, J. 2007 *J. Am. Chem. Soc.* **129** 1516.
- [19] Cheung C L, Kurtz A, Park H, Lieber C M. 2002 *J. Phys. Chem. B*, **106** 2429.
- [20] Delhaes P. 2002 *Carbon*, **40** 641.
- [21] Dosa P I, Erben C, Iyer V S, Vollhardt K P C, Wasser I M. 1999 *J. Am. Chem. Soc.* **121** 10430.
- [22] Baldwin K P, Matzger A J, Scheiman D, Tessier C A, Vollhardt K P C, Youngs W J. 1995 *Synlett* **1995** 1215.
- [23] Boese R, Matzger A J, Vollhardt K P C. 1997 *J. Am. Chem. Soc.* **119** 2052.
- [24] Wu J, El Hamaoui B, Li J, Zhi L, Kolb U, Müllen K. 2005 *Small*, **1** 210.
- [25] El Hamaoui B, Zhi L, Wu J, Li J, Lucas N T, Tomović Z, Kolb U, Müllen K. 2007 *Adv. Funct. Mater.* **17** 1179.
- [26] Zhi L, Hu Y S, Hamaoui B E, Wang X, Lieberwirth I, Kolb U, Maier J, Müllen K. 2008 *Adv. Mater.* **20** 1727.
- [27] Cui G L, Hu Y S, Zhi L J, Wu D Q, Lieberwirth I, Maier J, Müllen K. 2007 *Small*, **3** 2066.

- [28] Cui G L, Zhi L J, Thomas A, Lieberwirth I, Kolb U, Müllen K. 2007 *ChemPhysChem*, **8** 1013.
- [29] Su Q, Liang Y, Feng X, Müllen K. 2010 *Chem. Commun.* **46** 8279.
- [30] Aoki K, Kudo M, Tamaoki N. 2004 *Org. Lett.* **6** 4009.
- [31] Dautel O J, Robitzer M, Lère-Porte J-P, Serein-Spirau F, Moreau J J E. 2006 *J. Am. Chem. Soc.* **128** 16213.
- [32] Néabo J R, Tohoundjona K I S, Morin J-F. 2011 *Org. Lett.* **13** 1358.
- [33] Cantin K, Rondeau-Gagné S, Néabo J R, Daigle M, Morin J-F. 2011 *Org. Biomol. Chem.* **9** 4440.
- [34] Rondeau-Gagné S, Néabo J R, Desroches M, Cantin K, Soldera A, Morin J-F *J. Mater. Chem. C*, **1** 2680.
- [35] Néabo J R, Vigier-Carrière C, Rondeau-Gagné S, Morin J-F. 2012 *Chem. Commun.* 48 10144.
- [36] Néabo J R, Rondeau-Gagné S, Vigier-Carrière C, Morin J-F. 2013 *Langmuir*, **29** 3446.
- [37] Rondeau-Gagné S, Neabo J R, Desroches M, Levesque I, Daigle M, Cantin K, Morin J-F. 2013 *Chem. Commun.* **49** 9546.
- [38] Rondeau-Gagné S, Néabo J R, Desroches M, Larouche J, Brisson J, Morin J-F. 2013 *J. Am. Chem. Soc.* **135** 110.
- [39] Hitt D M, O'Connor J M. 2011 *Chem. Rev.* **111** 7904.
- [40] Hoheisel T N, Schrettl S, Szilluweit R, Frauenrath, H. 2010 *Angew. Chem. Int. Ed.* **49** 6496.
- [41] Rondeau-Gagné S, Morin J-F. 2013 *Chem. Soc. Rev.* DOI:10.1039/C3CS60210A
- [42] Laskoski M, Steffen W, Morton J G, Smith M D, Bunz U H. 2002 *J. Am. Chem. Soc.* **124** 13814.
- [43] Ozaki J I, Ito M, Fukazawa H, Yamanobe T, Hanaya M, Oya A. 2006 *J. Anal. App. Pyrolysis*, **77** 56.
- [44] Baughman R H, Yee K C. 1978 *J. Polym. Sci. Macromol. Rev.* **13** 219.
- [45] Zhou Q, Carroll P J, Swager T M. 1994 *J. Org. Chem.* **59** 1294.
- [46] Haley M M, Bell M L, English J J, Johnson C A, Weakley T J. 1997 *J. Am. Chem. Soc.* **119** 2956.
- [47] Nishinaga T, Nodera N, Miyata Y, Komatsu K. 2002 *J. Org. Chem.* **67** 6091.

- [48] Although the presence of a cavity inside PAMs suggests that the resulting nanoarchitectures would be nanotubes, we have not been able to observe their cavity, even by HRTEM due to poor contrasts. Thus, we employed the term “nanorods” rather than “nanotubes” throughout this manuscript to designate the PDA-walled precursor.
- [49] Kyotani M, Matsushita S, Nagai T, Matsui Y, Shimomura M, Kaito A, Akagi K. 2008 *J. Am. Chem. Soc.* **130** 10880.
- [50] Ding L, Olesik S V. 2005 *Chem. Mater.* **17** 2353.
- [51] Gherghel L, Kübel C, Lieser G, Räder H J, Müllen K. 2002 *J. Am. Chem. Soc.* **124** 13130.
- [52] Apicella B, Alfe M, Barbella R, Tregrossi A, Cijolo A. 2004 *Carbon*, **42** 1583.
- [53] Cançado L G, Jorio A, Martins Ferreira E H, Stavale F, Achete C A, Capaz R B, Moutinho M V O, Lombardo A, Kulmala T S, Ferrari A. C. 2011 *Nano lett.* **11** 3190.
- [54] Knight D S, White W B. 1989 *J. Mater. Res.* **4** 385.
- [55] Cao L, Meziani M J, Sahu S, Sun Y P. 2012 *Acc. Chem. Res.* **46** 171.
- [56] Nicholas K M, Pettit R. 1971 *Tetrahedron Lett.* **12** 3475.
- [57] Scholz S, Leech P J, Englert B C, Sommer W, Weck M, Bunz U H. 2005 *Adv. Mat.* **17** 1052.
- [58] Burghard M. 2003 *Angew. Chem. Int. Ed.* **42** 5929.

Chapitre 6.

Augmentation de la réactivité des macrocycles de type phénylacétylène vis-à-vis la polymérisation topochemique par la modification des chaînes périphériques

Improving the Reactivity of Phenylacetylene Macrocycles Toward Topochemical Polymerization by Side-Chains Modification

Simon Rondeau-Gagné,[‡] Jules Roméo Néabo,[‡] Maxime Daigle, Katy Cantin and Jean-François Morin*

Département de Chimie and Centre de recherche sur les Matériaux Avancés (CERMA), Université Laval, 1045 avenue de la Médecine, Québec, Québec, Canada, G1V 0A6

‡ Ces auteurs ont participé à ce travail de façon égale

Article accepté dans la revue *Beilstein J. Org. Chem.* **2014**, *10*, 1613-1619.

6.1 Préambule

Cet article présente nos récents efforts pour augmenter la réactivité des macrocycles vis-à-vis de la polymérisation topochemique des unités diynes. Nous avons également visé l'augmentation des rendements de polymérisation, afin d'obtenir de plus grandes quantités de nanoarchitectures. Ma participation à cet article est majeure. J'ai effectué toutes les synthèses ainsi que toute la caractérisation des nouveaux produits. J'ai également participé à la recherche bibliographique et à la rédaction de l'article.

6.2. Résumé

La synthèse et l'auto-assemblage de deux nouveaux organogélateurs à base de macrocycles de type phénylacétylène (PAMs) ont été réalisés. Des chaînes latérales polaires, de type éthoxyéthanol, ont été incorporées pour modifier le mode d'assemblage à l'état de gel. Avec ces modifications, il a été possible d'augmenter la réactivité des macrocycles à une polymérisation topochemique ainsi que les rendements de polymérisation obtenus.

6.3. Abstract

The synthesis and self-assembly of two new phenylacetylene macrocycles (PAMs) organogelators were performed. Polar side chains, namely ethoxyethanol, were incorporated to modify the assembly mode in the gel state. With these modifications, it was possible to increase the reactivity of the macrocycles toward topochemical polymerization.

6.4 Introduction

The self-assembly of molecular building blocks is an increasingly popular method for the preparation of new semiconducting materials. Rational design of building blocks and their assembly using non-covalent interactions can provide control over the size, shape and electronic properties of the resulting nanoarchitectures.¹ It is therefore not surprising that supramolecular interactions are regularly used to afford long-range molecular organization for organic and molecular electronics applications in which high-level of organization is required to reach good charge transport properties.² However, supramolecular assemblies often suffer from poor stability, meaning that variation of the storage and device operation conditions can perturb the molecular organization, leading to a decline of the materials efficiency overtime.³ In this regard, the covalent immobilization of supramolecular assemblies using physical stimuli (heat or light) is an interesting way to obtain stable,

organized materials.⁴ For example, self-assembled butadiyne-containing molecules can be polymerized in a gel or crystalline state to yield polydiacetylenes (PDAs) following a 1,4-addition mechanism, thus fixing the initial molecular organization through covalent bonds formation.⁵ In order for this polymerization to proceed, the molecules within the assembly must be oriented relative to each other following critical parameters, namely a distance of ≤ 4.9 Å and a tilt angle of 45° between the monomers.^{5a} Thus, careful selection of functional groups onto the molecule is needed to reach these requirements.⁶

Recently, many research groups used this strategy to design several types of π -conjugated monomers capable of hydrogen bonding to create nanowires,⁷ nanoparticles,⁸ nanotubes⁹ and two-dimensional layered materials¹⁰ from organogels. The key to success was to obtain a good balance between solubility and gelation properties. Moreover, subtle changes in the chemical nature of the building blocks can have a dramatic impact on the self-assembly process. This was exemplified in the case of nanotubes obtained from self-assembled butadiyne-containing macrocycles, which stack on top of each other in columnar fashion to give supramolecular nanotubular structures.¹¹ Among other things, we have shown that inversion of the amide group configuration (acetanilide vs. benzamide) at two different positions on phenylacetylene macrocycles (PAMs) leads to significant changes of the gelation properties and, consequently, on the critical parameters needed for polymerization through 1,4-addition reaction.^{11f} In fact, the acetanilide configuration provides macrocycles to can barely self-assembled in organic solvents while the benzamide configuration yields to macrocycles with much greater gelation properties that allow the formation of PDA-based nanorods. Nonetheless, the polymerization of diyne units within PAMs to give covalent nanotubes is very slow and gives low yields of polymerization, generally too low to be determined accurately.^{11f,12} In order to increase the efficiency of polymerization, the incorporation of external diyne chains on the PAMs core have been realized.^{9d} This design allowed us to increase the yield of polymerization to 15%. However, addition of external diynes units is synthetically tedious and a more efficient strategy to significantly increase the yield of the topochemical polymerization is necessary.

In order to take a step further toward a better comprehension of the self-assembly of PAMs and to increase the polymerization yield, we decided to introduce substituents on the inside

of the macrocycles, more precisely polar ethoxyethanol. Such a polar group proved to be useful to increase the intermolecular interactions between PAMs through hydrogen bonding in the solid state.¹³ We hypothesized that this structural change could provide better control over the molecular organization of PAMs and, consequently, could lead to higher yield of PDA-walled nanotubes through PAMs polymerization. Herein, we report the synthesis, gelation properties and topochemical polymerization of a new series of PAMs (**PAM2** and **PAM3**, Figure 6.1) with polar side chains pointing inside the macrocyclic scaffold.

PAM2 and **PAM3** possess some structural dissimilarity. First, **PAM2** possesses two ethoxyethanol chains and two amide groups in the benzamide configuration while **PAM3** contains four of each. It is important to mention that the alcohol chains positioned for synthetic ease. The synthesis and gelation properties of **PAM1** are reported in the literature.¹² **PAM1** was used in this study as a control molecule because of the absence of ethoxyethanol chains in its structure, providing a reliable comparison.

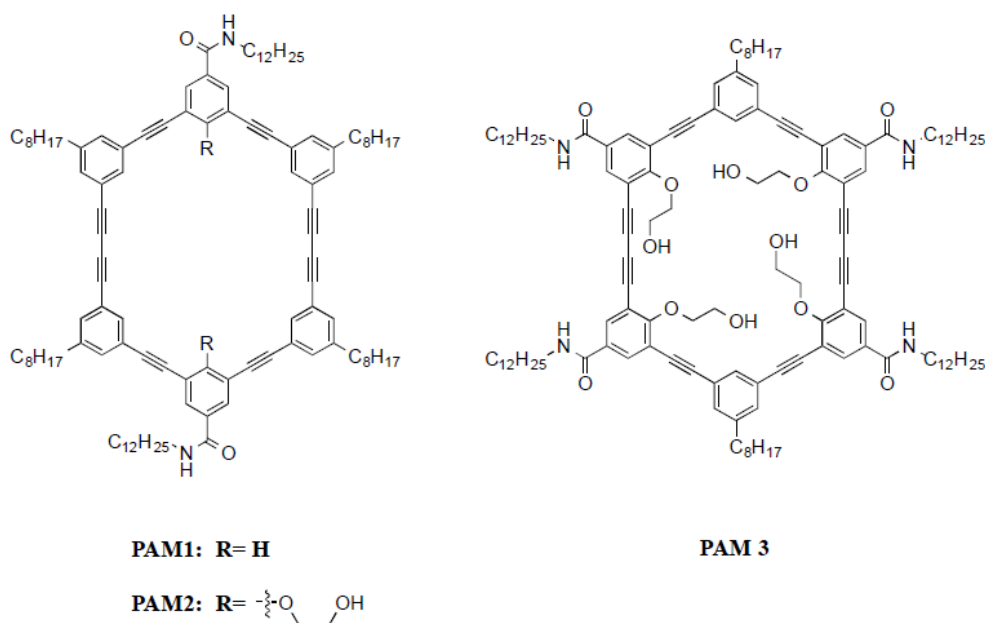


Figure 6.1. Structures of **PAM1-PAM3**

6.5. Results

The synthetic pathway toward **PAM2** and **PAM3** is shown in Scheme 6.1. Starting from commercially available 4-hydroxybenzoic acid, iodination was performed to obtain compound **1** in excellent yield (93 %). Then, ethoxyethanol chains were installed using K_2CO_3 to obtain compound **2** in good yield (61% yield). Amidation using diisopropyl carbodiimide (DIC) and 6-chlorohydroxybenzotriazole (6-ClHOBt) as coupling agents was then performed, followed by protection of the hydroxy moiety with TBS in order to facilitate the further synthetic steps by increasing the solubility of the compound (57 % yield over 2 steps). Then, by using a standard Castro-Stephens-Sonogashira coupling, TMS protecting group were installed (73% yield). After basic removal of the alkyne protective group, the half-macrocycle **5** was obtained by Castro-Stephens-Sonogashira coupling with previously reported 3,5-diiodooctylbenzene¹² in good yields despite of the possible polymerization side reaction (54 % yield). TMS-protected alkynes were, then, installed on the half-macrocycle to afford compound **6** which can be deprotected using potassium hydroxide and directly used in modified Eglinton ring closing reaction in pseudo-high dilution to afford hydroxy-protected PAM. Deprotection was directly performed without purification using TBAF to afford **PAM2** in good yields (88 % yield). Same approach was used for **PAM3**. Starting from previously synthesized compound **3**, the half-macrocycle **9** was obtained by standard Castro-Stephens-Sonogashira coupling with dialkyne **8** in good yield (59 %). It is noteworthy that compound **8** was obtained from oxidative deprotection of compound **7**. After installing TMS-protected alkyne with good yields (compound **10**, 80 % yield), selective removal of TMS using potassium hydroxide and ring closing reaction under modified Eglinton conditions were performed to afford a TBS protected PAM. Deprotection of TBS using TBAF was then realized without purification to afford **PAM3** in rather low yield. We hypothesized that this low yield can be due to the increased steric hindrance for compound **10** (2 OTBS groups) compare to compound **6** (1 OTBS group), impairing the macrocyclization reaction and leading to significant amount oligomerized product. It is noteworthy that purification of **PAM3** was realized by precipitation in methanol. Standard column chromatography has not been effective due to the low solubility of the macrocycle after deprotection of the hydroxy-containing side chains.

The gelation properties of **PAM2** and **PAM3** have been studied and compared to those of **PAM1**. For each PAM, a precise quantity was mixed with the solvent in a capped glass tube. After sonication to breakdown the aggregates, the mixture was heated until a clear solution was obtained. Then, the solution was allowed to slowly cool at room temperature and the formation of the gel was confirmed in each case by the tube inversion method.¹² The gelation properties of **PAM1**, **PAM2** and **PAM3** in different solvents are summarized in Table 6.1. **PAM2**, containing two amides and two ethoxyethanol side chains, has exactly the same gelation properties as **PAM1**, demonstrating the absence of influence of the addition of side chains on the gelation properties. In the case of **PAM3**, however, most of the solvents tested did not lead to gel formation. Thus, only cyclohexane and toluene resulted in a partial gel state. The presence of four amide functions and four ethoxyethanol groups lead to a significant decrease of solubility, even in hot solvents, limiting the formation of organogels.

In order to investigate the crystallization temperature of solvents within the gel and to compare the influence of the ethoxyethanol side chains on the thermal stability of the gel, two gel samples were prepared with **PAM1** and **PAM2** in cyclohexane at a 10 mg/mL concentration and subjected to differential scanning calorimetry (DSC). The DSC analysis was carried at temperatures ranging from 298 to 223 K. In both cases, a very sharp exotherm attributable to the crystallization of supercooled solvent was observed (see Figure 6.6 and 6.7 in the Supporting Information). For **PAM2**, the exotherm at 279 K is closer to the freezing point of cyclohexane (280K) than for **PAM1**, which has an exotherm at 267 K. This result suggests that the gel of **PAM2** might be less organized than that of **PAM1**.¹² By heating the gel from 223 to 298 K, an endotherm was observed in both cases, which is closely related to the melting point of free cyclohexane.

To explore the morphology of the structures created during the gel formation, scanning electron microscopy (SEM) was performed on **PAM2** only since **PAM3** did not present any gelation properties. For SEM analysis, a gel sample was allowed to dry at room temperature on a metallic substrate to form xerogel. Then, gold was sputtered on the sample prior to imaging. SEM images of **PAM2** are shown in Figure 6.2. As previously observed with **PAM1** and other phenylacetylene macrocycles, a dense network of

nanofibrils was formed during the gelation process.¹⁴ These nanofibrils, commonly observed in the gel state, resulted from the strong intermolecular interactions that create long-range one-dimensional arrays of molecules.¹⁵

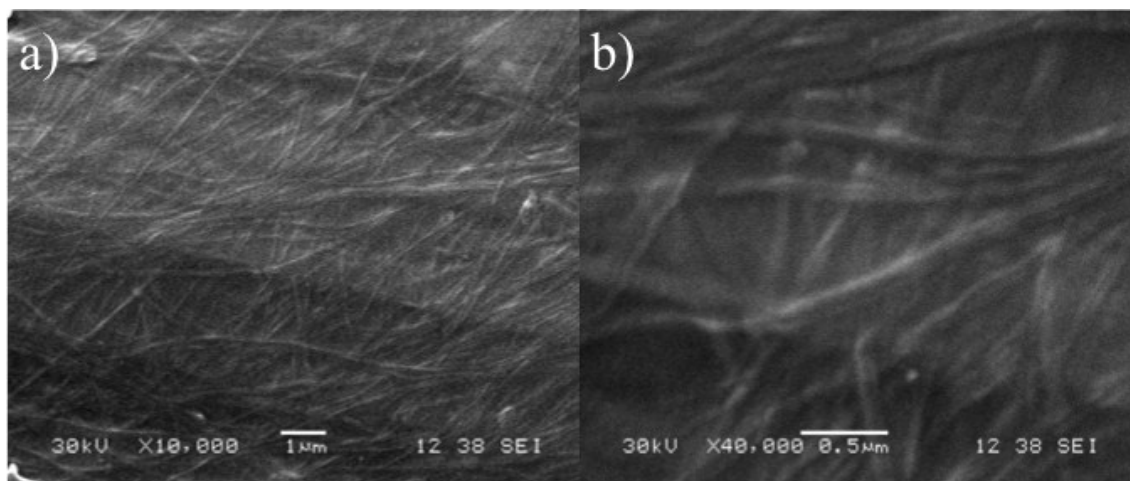


Figure 6.2. Scanning electron microscopy (SEM) images of **PAM2** xerogel in cyclohexane (10 mg/mL). Scales are a) 1 μm and b) 0.5 μm .

In order to gain some insights on the molecular packing within the assembly, X-ray diffraction (XRD) was performed on **PAM2** (see Figure 6.5 in the Supporting Information). Unlike **PAM1**, the presence of a columnar arrangement cannot be established from the diffractogram.^{9d,12} Instead, only a broad peak at $2\theta = 20^\circ$ was observed, indicating the presence of intramolecular liquid-like order between the alkyl chains.^{1b} The absence of well-defined pattern suggests that **PAM2** does not organize as well as **PAM1** in the gel state and that the ethoxyethanol chains are unfavourable for the long-range supramolecular organization.

Despite this unexpected finding, irradiation of a xerogel sample of **PAM2** in cyclohexane (10 mg/mL) was performed for 24 h under UV light (254 nm). The resulting blue material was purified using size-exclusion chromatography (SEC) (Bio-Beads SX-1) to remove all traces of the starting macrocycle. To our surprise, a polymerization yield of 30% (soluble material) was obtained after purification, representing a two-fold increase compared to the best result obtained for the same PAM scaffold. This result suggests that the diyne units in

PAM2 are in a more suitable orientation than **PAM1** to undergo a topochemical polymerization, although gelation properties and XRD result seem to suggest otherwise. It is also possible that the apparent increased for the yield comes from a better solubility of the PDA obtained from **PAM2** compare to that obtained from **PAM1**, although quantitative measurements of the solubility have not been conduct because of the small quantity of materials prepared.

Given the observed polymerization of diyne units, UV-visible spectroscopy was performed to confirm the appearance of polydiacetylene. As shown in Figure 6.3, the UV-visible spectra show absorption bands at 600 and 650 nm, associated with the red and blue bands of the PDA chain, respectively.¹⁶ To determine whether all the diyne units of **PAM2** reacted during irradiation, Raman spectroscopy was performed on the resulting PDA (Figure 6.4). As expected, no band associated with the diyne unit (generally around 2200 cm^{-1}) is present. The final PDA presented bands at 1470 and 2100 cm^{-1} , which could be respectively associated to alkene and alkyne moieties of PDA. It should be noted that these two bands are also present in the Raman spectrum of **PAM2** due to partial photo-induced polymerization during spectrum acquisition. This demonstrates the high reactivity of **PAM2** under UV irradiation. Further research on the resulting nanoarchitectures is currently underway to establish if covalent nanotubes have been formed and to study their properties.

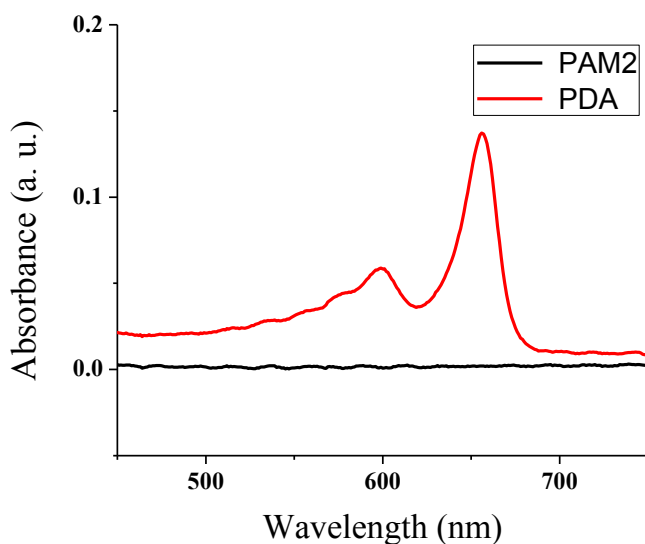


Figure 6.3. UV Visible spectrum of **PAM2** before (black) and after (red) polymerization (PDA).

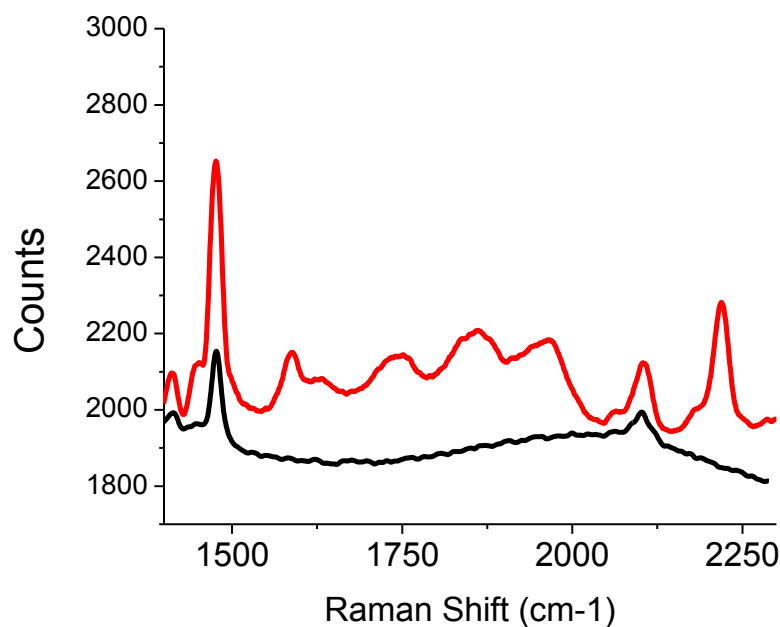


Figure 6.4. Background-corrected Raman spectra of PAM2 (red) and the blue material obtained after UV irradiation (black).

To assess the presence of nanotubes or nanorods, HRTEM analysis has been performed on the purified blue materials. Although one-dimensional features can be observed at different locations on the grid (see Figure 6.8 in the Supporting Information), the images were not clear enough to confirm whether or not **PAM2** has been transformed exclusively into nanotubes or nanorods and attempts to disperse individual molecules in organic solvents failed. Considering the strict structural parameters needed to undergo a topochemical polymerization and the one-dimensional nature of the starting xerogel of **PAM2**, it is unlikely – but not impossible – that the final blue materials can be made of other nanoarchitectures than the nanotubular or nanorods one. Nonetheless, no conclusive remarks can be made and more analysis will have to be performed in order to gain better insight about the final structure of the PDA obtain from **PAM2**.

6.6. Conclusion

In summary, the synthesis and self-assembly of two new phenylacetylene macrocycles were performed. To improve the self-assembly properties in the gel state and further yield to better topochemical polymerization yield, the incorporation of ethoxyethanol side chains was accomplished. The gelation properties demonstrated that the incorporation of two of these chains (**PAM2**) did not affect the gelation properties while the incorporation of four side chains and four amide groups significantly alter the solubility of the resulting PAM (**PAM3**). Topochemical polymerization on self-assembled **PAM2** to yield PDA-based materials proved to be much more efficient than for the ethoxyethanol-free analogues (**PAM1**). Characterization is currently underway to investigate the precise nature of the nanoarchitectures formed.

6.7. Supporting Information

6.7.1. General

Chemical reagents were purchased from Sigma-Aldrich Co. Canada, Alfa Aesar Co., TCI America Co. or Oakwood Products Inc. and were used as received. Solvents used for organic synthesis were obtained from Fisher Scientific (except THF from Sigma-Aldrich Co. Canada) and purified with a Solvent Purifier System (SPS) (Vacuum Atmosphere Co., Hawthorne, USA). Other solvents were obtained from Fisher Scientific and were used as received. Tetrahydrofuran (THF) and triethylamine (Et₃N) used for Castro-Stephen-Sonogashira reactions were degassed 30 minutes prior to use. All anhydrous and air sensitive reactions were performed in oven-dried glassware under positive argon pressure. Analytical thin-layer chromatographies were performed with silica gel 60 F254, 0.25 mm pre-coated TLC plates (Silicycle, Québec, Canada). Compounds were visualized using 254 nm and/or 365 nm UV wavelength and/or aqueous sulfuric acid solution of ammonium heptamolybdate tetrahydrate (10 g/100 mL H₂SO₄ + 900 mL H₂O). Flash column chromatographies were performed on 230-400 mesh silica gel R10030B (Silicycle, Québec, Canada). Nuclear magnetic resonance (NMR) spectra were recorded on a Varian Inova AS400 spectrometer (Varian, Palo Alto, USA) at 400 MHz (¹H) and 100 MHz (¹³C). High-resolution mass spectra (HRMS) were recorded with an Agilent 6210 Time-of-Flight (TOF) LC-MS apparatus equipped with an ESI or APPI ion source (Agilent Technologies,

Toronto, Canada). UV-visible absorption spectra were recorded on a Varian diode-array spectrophotometer (model Cary 500) using 3-mm path length quartz cells. Scanning electron microscopy (SEM) images were taken using a JEOL JSM-6360 LV. X-ray diffraction was recorded on Siemens X-rays Diffractometer (Model S3 D5000). DSC measurements were done on a Mettler Toledo (DSC 823e).

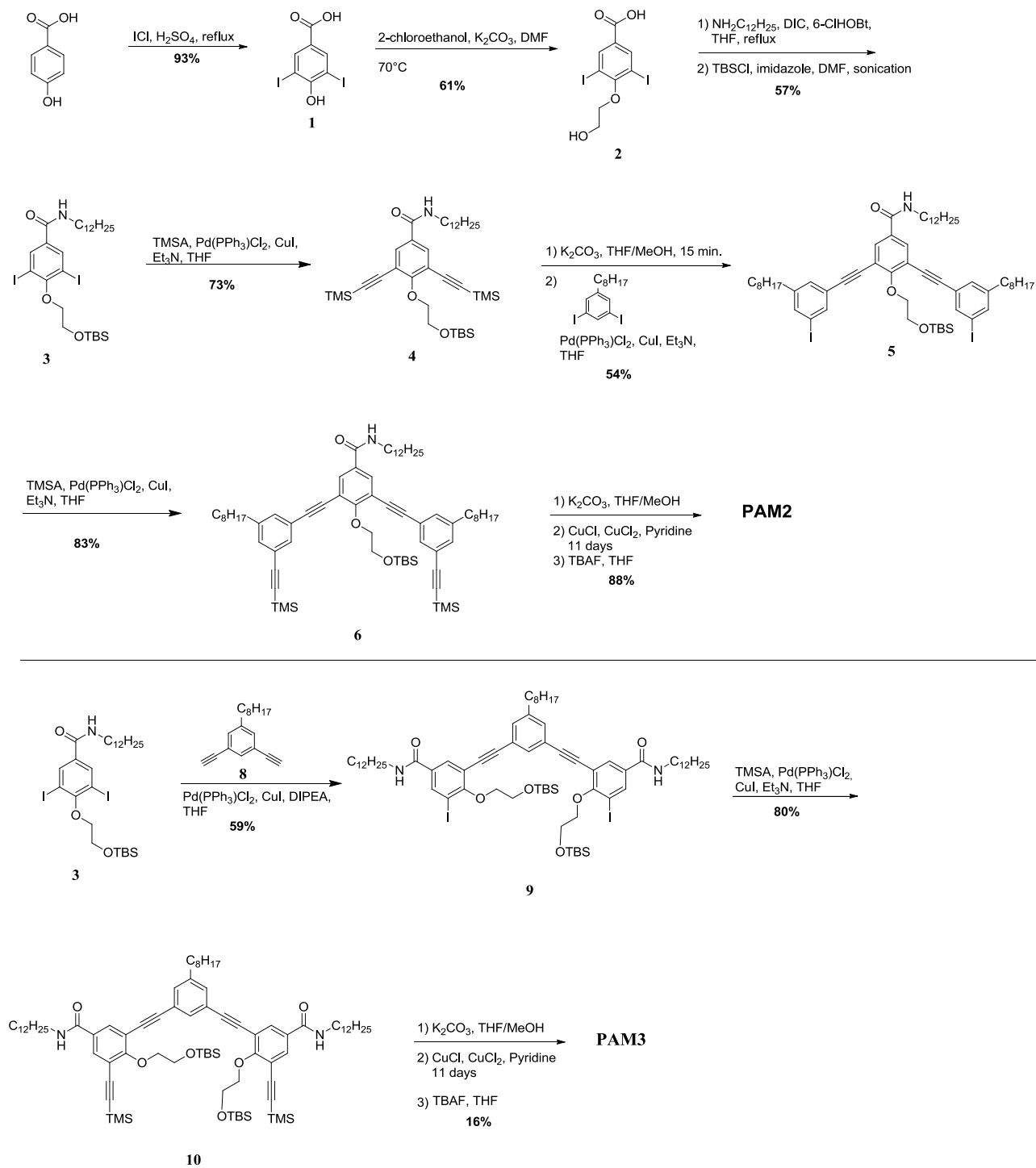
Gelation test

To test the gelation properties of PAMs in a given solvent, we proceeded as follow: in a vial, a PAMs was dissolved in a solvent. After dissolution by sonication, the vial was sealed and heated until a clear solution was obtained. The clear solution was allowed to slowly cool down at room temperature. The stability of the gel was confirmed by tube inversion.

SEM imaging

Organogel obtained in cyclohexane was deposited on a stainless steel substrate and allowed to dry for 3-4 days. Then, gold particles were sputtered on dried gel prior to imaging.

6.7.2 Synthetic pathway



Scheme 6.1. Synthetic pathway to **PAM2** and **PAM3**.

6.7.3. Experimental procedure

Compound 1. A round-bottom flask equipped with a magnetic stir bar is charged with 4-hydroxybenzoic acid (5.00 g, 36.2 mmol), 10 % H₂SO₄ aqueous solution (180 mL) and Iodine monochloride (17.6 g, 108 mmol) at 0°C. Then, the reaction mixture is heated to 80°C and stirred overnight. The precipitated mixture is filtered and washed with sodium bisulfite and water to afford compound **1** (13.1 g, 93% yield) as a white amorphous powder. NMR ¹H (400 MHz, DMSO-d₆): 8.30 (s, 1H); 8.14 (s, 2H). NMR ¹³C (100 MHz, DMSO-d₆): 165.1; 146.6; 140.8; 137.5; 86.6; HRMS was not possible due to low ionization of compound **1** by APPI-TOF and ESI-TOF mass spectroscopy.

Compound 2. A round bottom flask equipped with a magnetic stir bar is charged with compound **2** (14.0 g, 35.9 mmol), water (72 mL), NaOH (5.02 g, 125 mmol) and 2-chloroethanol (8.67 g, 108 mmol). The reaction mixture is heated to 82°C and KI (596 mg, 3.59 mmol) is added. The reaction is then stirred overnight and allowed to cool to rt. The mixture is acidified with HCl to pH=5 and the solid is filtered under vacuo. The filtrate is washed with MeOH, EtOAc and with an hexanes in EtOAc 1:1 mixture to afford compound **2** (9.54 g, 61% yield) as a white amorphous powder. ¹H NMR (400 MHz, DMSO-d₆): 8.28 (s, 2H), 3.96 (t, *J* = 5.1 Hz, 2H), 3.83 (t, *J* = 5.1 Hz, 2H); ¹³C NMR (100 MHz, DMSO-d₆): 164.8; 161.8; 140.9; 130.5; 92.4; 74.9; 60.5; HRMS (ESI-TOF) *m/z* calcd for C₉H₈I₂O₄[M+H]⁺: 434.8585, found 434.8566.

Compound 3. A round bottom flask equipped with a magnetic stir bar is charged with compound **2** (4.50 g, 11.6 mmol), 6-ClHOBt (1.78 g, 10.5 mmol), DIC (1.47 g, 11.6 mmol), dodecylamine (2.24 g, 12.8 mmol) and THF (58 mL). The reaction mixture is

stirred overnight and allowed to cool down. The mixture is then diluted with EtOAc and the organic layer is washed with water (3x), brine and dried with Na₂SO₄. The solvents are removed under reduced pressure and the crude product is directly charged without further purification in a round bottom flask equipped with a magnetic stir. Imidazole (1.84 g, 27.2 mmol), TBSCl (1.96 g, 12.9 mmol) and DMF (10 mL) are then added and the mixture is stirred for 1h in an ultrasonic bath. The mixture is then diluted with EtOAc and the organic layer is washed with water (3x), brine and dried with Na₂SO₄. The crude product is then purified by flash chromatography on silica gel using 10% hexanes in acetone as eluant to afford compound **3** (3.41 g, 57% yield, 2 steps) as a white amorphous powder. ¹H NMR (400 MHz, CDCl₃): 8.13 (s, 2H), 6.13 (m, 1H), 4.05 (m, 4H), 3.39 (q, *J* = 6.7 Hz, 2H), 1.58 (m, 2H), 1.24 (s, 18H), 0.92 (s, 9H), 0.87 (t, *J* = 6.6 Hz, 3H), 0.13 (s, 6H); ¹³C NMR (100 MHz, CDCl₃): 164.0; 160.1; 138.6; 134.0; 90.8; 73.9; 62.2; 40.4; 31.9; 29.6 (3C); 29.5 (2C); 29.3 (2C); 26.9; 25.9; 22.7; 18.4; 14.1; -5.1; HRMS (APPI-TOF) *m/z* calcd for C₂₇H₄₇I₂NO₃Si[M+H]⁺ : 717.1515, found 717.153.

Compound 4. A round bottom flask equipped with a magnetic stir bar is charged under nitrogen with compound **3** (2.00 g, 2.79 mmol), Et₃N (1.5 mL), THF (14 mL), PdCl₂(PPh₃)₂ (78 mg, 0.11 mmol) and CuI (21 mg, 0.11 mmol). TMSA (1.09 g, 11.2 mmol) is then added and the mixture is stirred overnight. The reaction is then diluted with CH₂Cl₂ and the organic layer is washed with NH₄Cl, water and brine. The organic layer is then dried with Na₂SO₄ and the solvent are removed under reduced pressure. The crude product is purified by flash chromatography on silica gel using hexanes to 4% hexanes in acetone as eluents to afford compound **4** (1.34 g, 73% yield) as light orange oil. ¹H NMR (400 MHz, CDCl₃): 7.77 (s, 2H), 6.21 (m, 1H), 4.36 (t, *J* = 5.9 Hz, 2H), 3.98 (t, *J* = 5.9 Hz, 2H), 3.39 (q, *J* = 6.5 Hz, 2H), 1.57 (m, 2H), 1.26 (m, 18H), 0.90 (m, 12H), 0.24 (s, 18H), 0.07 (s, 6H); ¹³C NMR (100 MHz, CDCl₃): 165.5; 163.9; 132.6; 129.6; 117.3; 100.2; 99.9; 74.5; 62.5; 40.2; 34.6; 31.9; 31.6; 29.6 ; 29.5; 29.3; 26.9; 25.8; 25.7; 25.3; 22.6; 20.7; 18.3; 17.9; 14.1; HRMS (APPI-TOF) *m/z* calcd for C₃₇H₆₅NO₃Si₃[M+H]⁺ : 656.4345, found 656.4362.

Compound 5. A round bottom flask equipped with a magnetic stir bar is charged with compound **4** (3.00 g, 2.78 mmol), K₂CO₃ (767 mg, 5.55 mmol), THF (14 mL) and MeOH (14 mL). The reaction is stirred until complete disappearance of the starting product by TLC. The mixture is then diluted with CH₂Cl₂ and washed with water. The organic layer is then dried with Na₂SO₄ and the solvent are removed under reduced pressure. The crude product is used directly with further purification and is charged in a round bottom flask equipped with a magnetic stir bar under nitrogen with 3,5-diiodooctylbenzene (3.33 g, 7.53 mmol) and Et₃N (25 mL). PdCl₂(PPh₃)₂ (71 mg, 0.10 mmol) and CuI (19 mg, 0.10 mmol) are then added and the mixture is stirred overnight. The mixture is diluted with CH₂Cl₂ and the organic layer is washed with NH₄Cl, water, brine and dried with Na₂SO₄. The solvent is removed under reduced pressure and the crude product is purified by flash chromatography on silica gel using hexanes to 6% hexanes in acetone as eluents to afford compound **5** (1.55 g, 54% yield) as light orange oil. ¹H NMR (400 MHz, CDCl₃): 7.84 (s, 2H), 7.69 (s, 2H), 7.53 (s, 2H), 7.30 (s, 2H), 6.02 (m, 1H), 4.45 (t, *J* = 4.8 Hz, 2H), 4.05 (t, *J* = 4.8 Hz, 2H), 3.44 (q, *J* = 6.6 Hz, 2H), 2.54 (t, *J* = 7.4 Hz, 4H), 1.59 (m, 12H), 1.28 (m, 32H), 0.88 (m, 9H), 0.85 (m, 15H); ¹³C NMR (100 MHz, CDCl₃): 165.4; 163.2; 145.3; 137.9; 137.3; 132.2; 130.9; 130.0; 124.6; 117.3; 93.4; 93.2; 85.5; 75.1; 62.7; 40.3; 35.4; 31.9; 31.8; 31.2; 29.6 (4C); 29.5; 29.4; 29.3 (2C); 29.2 (2C); 27.0; 25.9 (2C); 22.7; 22.6; 18.3; 14.1 (2C); HRMS (APPI-TOF) *m/z* calcd for C₅₉H₈₇I₂NO₃Si[M+H]⁺ : 1142.4668, found 1142.4708.

Compound 6. A round bottom flask equipped with a magnetic stir bar is charged under nitrogen with compound **5** (380 mg, 0.33 mmol), Et₃N (3 mL), THF (3 mL), PdCl₂(PPh₃)₂ (9 mg, 0.01 mmol) and CuI (3 mg, 0.01 mmol). TMSA (98 mg, 1.00 mmol) is then added and the mixture is stirred overnight. The reaction is then diluted with CH₂Cl₂ and the organic layer is washed with NH₄Cl, water and brine. The organic layer is dried with Na₂SO₄ and the solvent are removed under reduced pressure. The crude product is purified

by flash chromatography on silica gel using hexanes to 4% hexanes in acetone as eluents to afford compound **6** (243 mg, 83% yield) as light orange oil. ^1H NMR (400 MHz, CDCl_3): 7.84 (s, 2H), 7.47 (s, 2H), 7.30 (s, 2H), 7.29 (s, 2H), 6.04 (m, 1H), 4.46 (t, $J = 5.8$ Hz, 2H), 4.07 (t, $J = 5.8$ Hz, 2H), 3.45 (q, $J = 6$ Hz, 2H), 2.57 (t, $J = 7.4$ Hz, 4H), 1.61 (m, 12H), 1.28 (m, 32H), 0.88 (m, 9H), 0.85 (s, 15H), 0.26 (s, 18H); ^{13}C NMR (100 MHz, CDCl_3): 163.1; 143.4; 132.3 (2C), 132.2; 131.7; 129.9; 123.3; 122.9; 117.6; 104.3; 94.6; 94.1; 84.8; 75.0; 62.7; 40.2; 35.5; 31.9 (2C); 31.2; 29.7 (2C); 29.6 (2C); 29.5; 29.4; 29.3 (3C); 29.2 (2C); 29.1; 26.9; 25.9 (2C); 22.7; 22.6; 18.4; 14.1; 0.08; HRMS (APPI-TOF) m/z calcd for $\text{C}_{69}\text{H}_{105}\text{NO}_3\text{Si}_3[\text{M}+\text{H}]^+$: 1080.7475, found 1080.7531.

PAM2. . A round bottom flask equipped with a magnetic stir bar was charged with compound **6** (270 mg, 0.25 mmol), THF (1.2 mL), MeOH (1.2 mL) and K_2CO_3 (69 mg, 0.50 mmol). The reaction mixture was stirred until complete disappearance of the starting product by TLC, diluted with CH_2Cl_2 , washed with water (3x), dried with sodium sulfate and the solvent was removed under reduced pressure. The resulting product was charged without further purification in a round bottom flask equipped with a magnetic stir bar with degassed pyridine (13 mL). Another round bottom flask equipped with a magnetic stir bar was charged with CuCl (1.88 g, 18.9 mmol), CuCl_2 (395 mg, 2.93 mmol) and degassed pyridine (38 mL) under N_2 atmosphere. The first solution was added dropwise to the catalyst solution over 4 days using a syringe pump and the reaction mixture was stirred for an additional 7 days. The reaction mixture was diluted with CHCl_3 and poured in water. The organic layer was extracted successively with water, 25% aqueous NH_4OH , water, 10% aqueous acetic acid, water, 10% aqueous NaOH and brine. The organic layer was dried with sodium sulfate and the solvent was removed under reduced pressure. A round bottom flask equipped with a magnetic stir bar was then charged with the crude product (without purification), TBAF 1.0 M solution in THF (0.51 mL, 0.51 mmol) and THF (1.7 mL). The reaction was stirred until complete disappearance of the starting product by TLC. The reaction mixture was then concentrated under reduced pressure and poured in MeOH. The precipitate was filtered under vacuo and the solid was dissolved. The crude product

purified by flash chromatography on silica gel using 20% hexanes in acetone as eluent to afford **PAM2** (123 mg, 88% yield) as a white amorphous powder. ^1H (400 MHz, CDCl_3): 7.78 (s, 2H), 7.55 (s, 4H), 7.46 (s, 4H), 7.28 (s, 2H), 7.06 (br s, 8H), 6.96 (m, 2H), 4.55 (t, $J = 4.8$ Hz, 4H), 4.16 (br s, 2H), 3.96 (m, 4H), 3.49 (m, 4H), 2.52 (t, $J = 7.6$ Hz, 8H), 1.73 (m, 4H), 1.60 (m, 8H), 1.29 (m, 78H), 0.88 (m, 16H); ^{13}C NMR: Due to the poor solubility of **PAM2** in common organic solvent, acquisition of clean spectrum was not afforded; HRMS (APPI-TOF) m/z calcd for $\text{C}_{114}\text{H}_{146}\text{N}_2\text{O}_6[\text{M}+\text{H}]^+$: 1640.1254, found 1640.1180.

Compound 7. A round bottom flask equipped with a magnetic stir bar is charged under nitrogen with 3,5-diiodooctylbenzene (1.00 g, 2.26 mmol), Et_3N (1.2 mL, 9.05 mmol), THF (22 mL), $\text{PdCl}_2(\text{PPh}_3)_2$ (64 mg, 0.09 mmol) and CuI (17 mg, 0.09 mmol). Propargylic alcohol (507 mg, 9.05 mmol) is then added and the mixture is stirred overnight. The reaction is then diluted with CH_2Cl_2 and the organic layer is washed with NH_4Cl , water and brine. The organic layer is then dried with Na_2SO_4 and the solvent are removed under reduced pressure. The crude product is purified by flash chromatography on silica gel using 5% CH_2Cl_2 in acetone as eluant to afford compound **7** (598 mg, 89% yield) as light orange oil. ^1H NMR (400 MHz, CDCl_3): 7.29 (s, 1H), 7.19 (s, 2H), 4.47 (s, 4H), 2.74 (s, 2H), 2.49 (t, $J = 7.6$ Hz, 2H), 1.53 (t, $J = 6.2$ Hz, 2H), 1.25 (br s, 9H), 0.87 (t, $J = 6.7$ Hz, 3H); ^{13}C NMR (100 MHz, CDCl_3): 132.0; 131.9; 122.6; 85.09; 51.7; 35.4; 31.9; 31.1; 29.4; 29.2; 29.1; 22.6; 14.1; HRMS was not possible due to low ionization of compound **9** by APPI-TOF and ESI-TOF mass spectroscopy.

Compound 9. A round bottom flask equipped with a magnetic stir bar is charged with compound **8** (600 mg, 2.01 mmol), KOH (1.81 g, 32.2 mmol), MnO_2 (2.79 g, 32.2 mmol) and CH_2Cl_2 (10 mL). The reaction is stirred until complete disappearance of the starting product by TLC. The mixture is then diluted with CH_2Cl_2 and washed with water. The

organic layer is then filtered on celite, dried with Na₂SO₄ and the solvent are removed under reduced pressure. The crude product is used directly with further purification and is charged in a round bottom flask equipped with a magnetic stir bar under nitrogen with compound **3** (901 mg, 1.26 mmol), DIPEA (0.59 mL, 3.36 mmol) and THF (4 mL). PdCl₂(PPh₃)₂ (12 mg, 0.02 mmol) and CuI (3 mg, 0.02 mmol) are then added and the mixture is stirred overnight. The mixture is diluted with CH₂Cl₂ and the organic layer is washed with NH₄Cl, water, brine and dried with Na₂SO₄. The solvent is removed under reduced pressure and the crude product is purified by flash chromatography on silica gel using hexanes to 8% hexanes in acetone as eluents to afford compound **9** (351 mg, 59% yield) as light orange oil. ¹H NMR (400 MHz, CDCl₃): 8.17 (s, 1H), 8.15 (s, 1H), 7.88 (s, 1H), 7.86 (s, 1H), 7.53 (m, 1H), 7.37 (s, 1H), 7.35 (s, 1H), 6.01 (m, 2H), 4.36 (t, *J* = 4.5 Hz, 4H), 4.09 (t, *J* = 4.5 Hz, 4H), 3.44 (q, *J* = 6 Hz, 4H), 2.62 (m, 2H), 1.61 (m, 8H), 1.26 (m, 61H), 0.88 (m, 30H): ¹³C NMR (100 MHz, CDCl₃): 164.8; 161.8; 138.6; 138.3; 134.0; 132.5; 132.0; 131.8 131.7; 122.9; 117.4; 94.6; 92.4; 90.8; 74.9; 62.6; 62.3; 40.3; 31.9 (2C); 31.2; 29.7; 29.6 (3C); 29.5; 29.4 (2C); 29.3 (2C); 29.2; 26.9; 25.9 (2C); 25.8; 22.7 (2C); 18.4; 14.1: HRMS (APPI-TOF) *m/z* calcd for C₇₂H₁₁₄I₂N₂O₆Si₂[M+H]⁺ : 1413.6378, found 1413.6473.

Compound 10. A round bottom flask equipped with a magnetic stir bar is charged under nitrogen with compound **9** (1.60 g, 1.13 mmol), Et₃N (0.62 mL, 4.53 mmol), THF (11 mL), PdCl₂(PPh₃)₂ (40 mg, 0.06 mmol) and CuI (11 mg, 0.06 mmol). TMSA (445 mg, 4.53 mmol) is then added and the mixture is stirred overnight. The reaction is then diluted with CH₂Cl₂ and the organic layer is washed with NH₄Cl, water and brine. The organic layer is dried with Na₂SO₄ and the solvent are removed under reduced pressure. The crude product is purified by flash chromatography on silica gel using hexanes to 5% hexanes in acetone as eluents to afford compound **10** (1.22 g, 80% yield) as light orange oil. ¹H NMR (400 MHz, CDCl₃): 7.84 (s, 1H), 7.81 (s, 2H), 7.75 (s, 2H), 7.31 (s, 2H), 6.02 (m, 2H), 4.40 (t, *J* = 5.7 Hz, 2H), 3.99 (t, *J* = 5.7 Hz, 2H), 3.39 (q, *J* = 6.9 Hz, 4H), 2.57 (m, 2H), 1.58 (m, 8H), 1.22 (br s, 62H), 0.83 (m, 30H), 0.24 (s, 18H): ¹³C NMR (100 MHz, CDCl₃): 163.5; 143.6; 132.5; 132.3; 131.8; 129.8; 123.1; 117.4; 117.3; 100.4; 100.0; 93.9; 93.8; 84.9; 74.8;

62.7; 62.6; 47.9; 40.2 (2C); 35.6; 35.5; 31.8 (3C); 31.2; 29.6 (3C); 29.5 (2C); 29.4 (2C); 29.3 (2C); 29.2 (3C); 29.1; 29.0; 26.9; 25.8; 22.6; 18.3; 14.1; 0.22: HRMS (APPI-TOF) m/z calcd for $C_{82}H_{132}N_2O_6Si_4[M+H]^+$: 1353.9235, found 1353.9329.

PAM3. A round bottom flask equipped with a magnetic stir bar was charged with compound **10** (380 mg, 0.28 mmol), THF (1.4 mL), MeOH (1.4 mL) and K_2CO_3 (9 mg, 0.07 mmol). The reaction mixture was stirred until complete disappearance of the starting product by TLC, diluted with CH_2Cl_2 , washed with water (3x), dried with sodium sulfate and the solvent was removed under reduced pressure. The resulting product was charged without further purification in a round bottom flask equipped with a magnetic stir bar with TBAF 1.0 M solution in THF (1.12 mL, 1.12 mmol) and THF (4.2 mL). The reaction mixture was stirred until complete disappearance of the starting product by TLC, diluted with CH_2Cl_2 , washed with water (3x), dried with sodium sulfate and the solvent was removed under reduced pressure. The resulting product was charged without further purification in a round bottom flask equipped with a magnetic stir bar with degassed pyridine (5 mL). Another round bottom flask equipped with a magnetic stir bar was charged with CuCl (1.14 g, 11.6 mmol), $CuCl_2$ (241 mg, 1.79 mmol) and degassed pyridine (23 mL) under N_2 atmosphere. The first solution was added dropwise to the catalyst solution over 4 days using a syringe pump and the reaction mixture was stirred for an additional 7 days. The reaction mixture was diluted with $CHCl_3$ and poured in water. The organic layer was extracted successively with water, 25% aqueous NH_4OH , water, 10% aqueous acetic acid, water, 10% aqueous NaOH and brine. The organic layer was dried with sodium sulfate and the solvent was removed under reduced pressure. The crude product was purified by flash chromatography on silica gel using $CHCl_3$ to 5% acetone in $CHCl_3$ as eluents to afford **PAM3** (45 mg, 16 % yield over 3 steps) as a white amorphous powder. 1H NMR and ^{13}C NMR: Due to the poor solubility of **PAM3** in common organic solvent, acquisition of clean spectrum was not afforded. The macrocycle shown strong aggregation by NMR even at 100°C in deuterated DMSO. HRMS (APPI-TOF) m/z calcd for $C_{128}H_{172}N_4O_{12}[M+H]^+$: 1958.3045, found 1958.3041.

6.7.4. Gelation properties

Table 6.1. Gelation properties of monomers where G = gel; PG= partial gelification, S = solution, I = insoluble, a= previously reported

Solvent	PAM1^a	PAM2	PAM3
Toluene	G	G	I
<i>o</i>-DCB	S	S	I
Benzene	G	G	PG
Cyclohexane	G	G	PG
Ethyl Acetate	G	G	I
MeOH	I	I	I
CHCl₃	S	S	I

6.7.5. Powder X-Ray diffraction (PXRD)

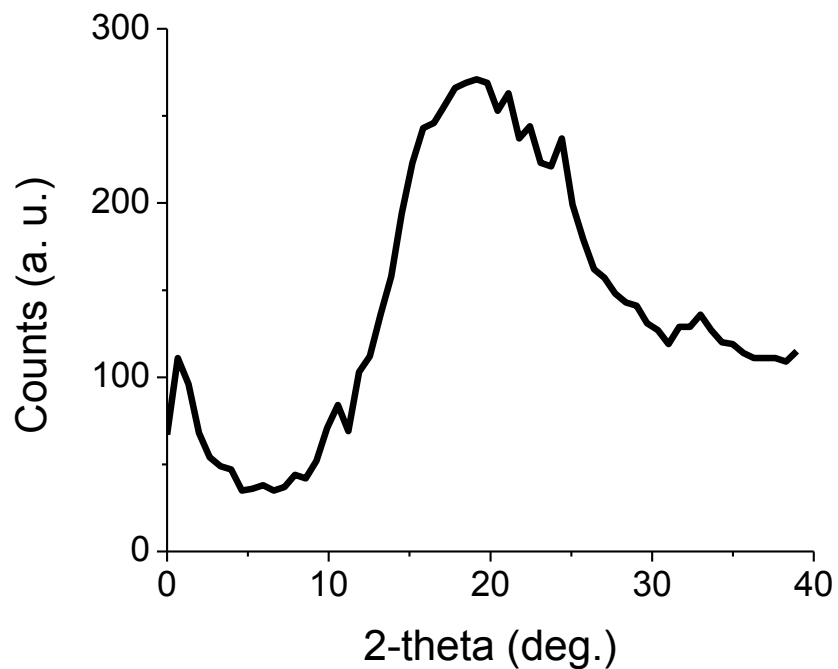


Figure 6.5. Powder X-Ray diffraction (PXRD) spectrum of a 10 mg/mL xerogel of **PAM2** in cyclohexane

6.7.6. Differential scanning calorimetry (DSC)

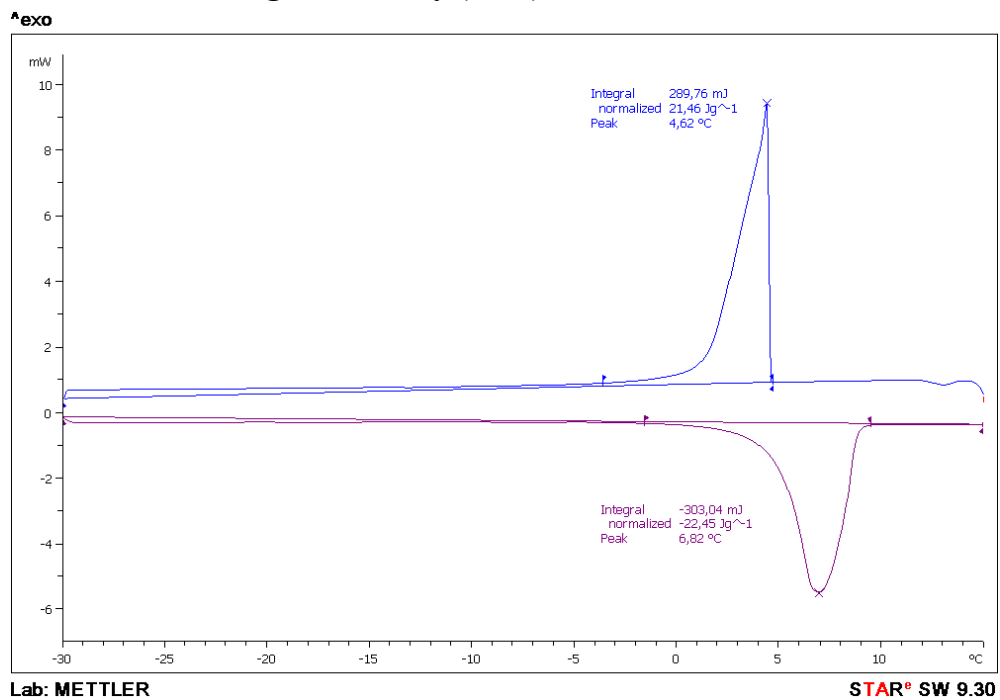


Figure 6.6. DSC curves of a gel (10 mg/mL) of **PAM1** in cyclohexane, 10°C/min.

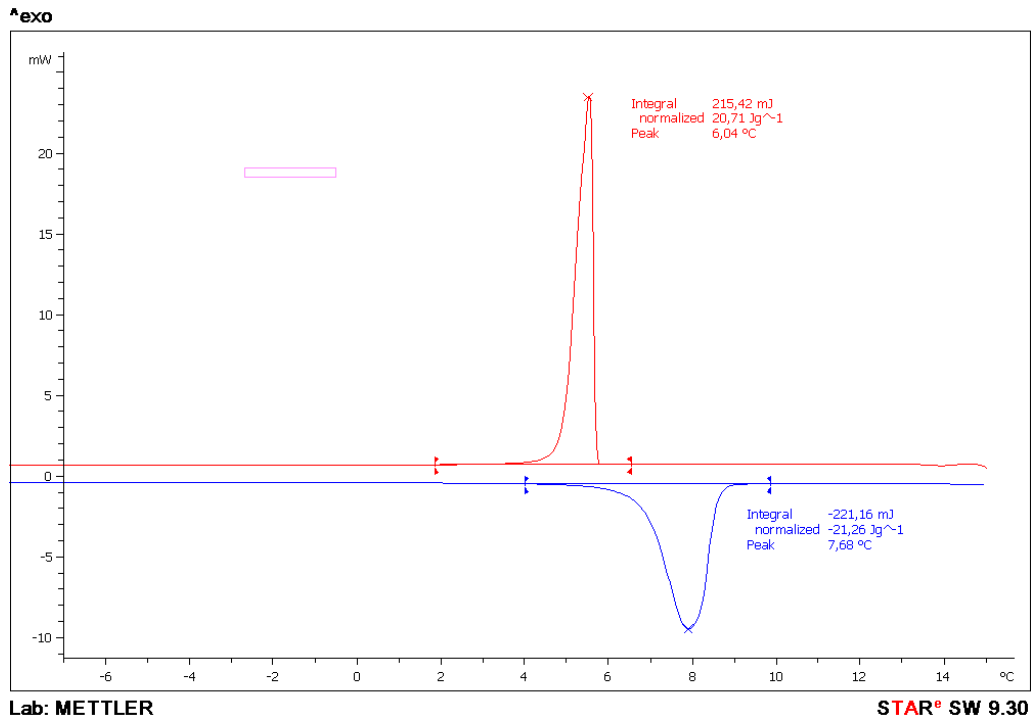


Figure 6.7. DSC curves of a gel (10 mg/mL) of **PAM2** in cyclohexane, 10°C/min

6.7.7. Transmission electron microscopy (TEM)

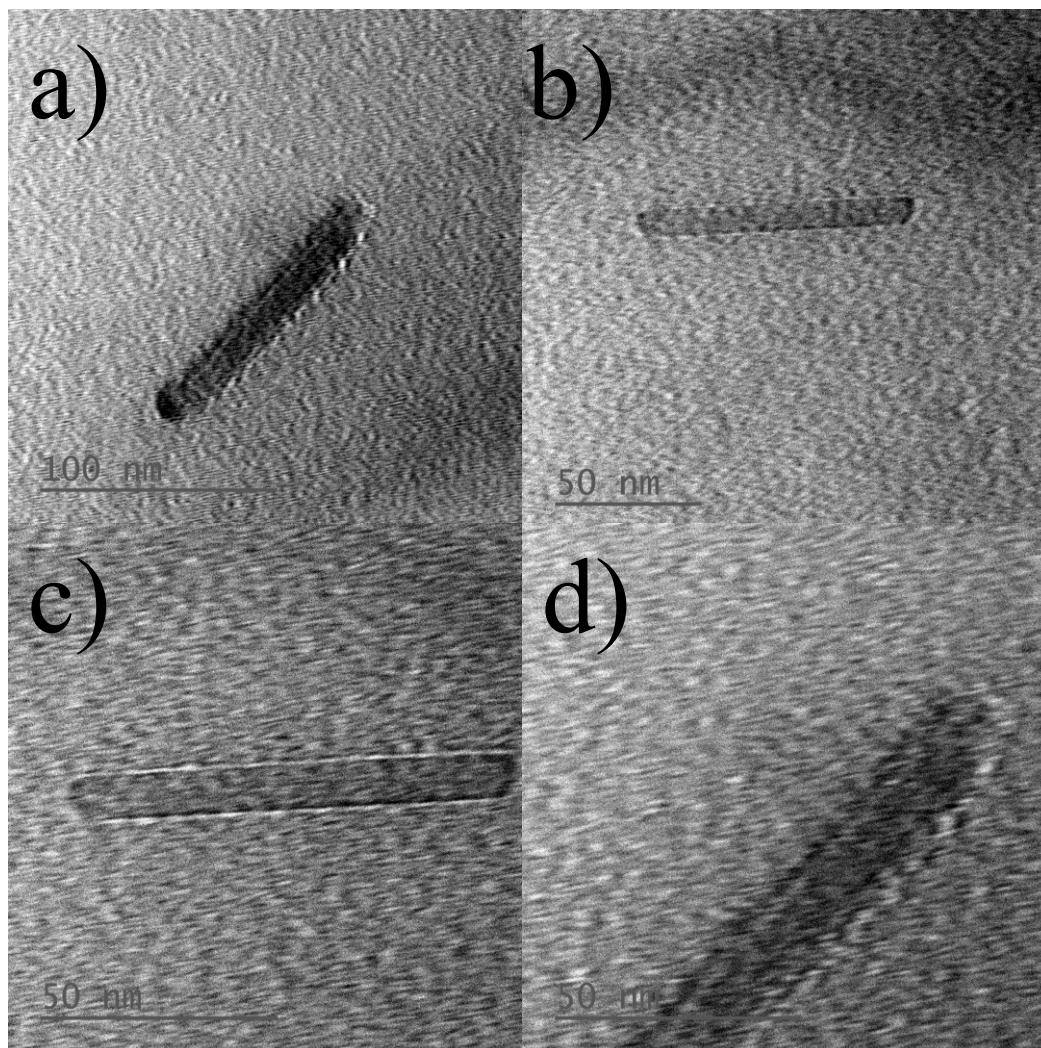


Figure 6.8. TEM imaging of PDA on carbon-coated copper grid. Scale bars are a) 100 nm and b) to d) 50 nm.

6.8 Références

- [1] For review, see: a) Zhao, Y. S.; Fu, H.; Peng, A.; Ma, Y.; Liao, Q.; Yao, J. *Acc. Chem. Res.* **2009**, *43*, 409. b) Laschat, S.; Baro, A.; Steinke, N.; Giesselmann, F.; Hägele, C.; Scalia, G.; Judele, R.; Kapatsina, E.; Sauer, S.; Schreivogel, A.; Tosoni, M. *Angew. Chem. Int. Ed.* **2007**, *46*, 4832. c) Grimsdale, A. C.; Müllen, K. *Angew. Chem. Int. Ed.* **2005**, *44*, 5592.

- [2] For review, see: a) Hasegawa, M.; Iyoda, M. *Chem. Soc. Rev.* **2010**, *39*, 2420. b) Babu, S. S.; Prasanthkumar, S.; Ajayaghosh, A. *Angew. Chem. Int. Ed.* **2012**, *51*, 1766. c) Stupp, S. I.; Palmer, L. C. *Chem. Mater.* **2013**. *In press*, dx.doi.org/10.1021/cm403028b
- [3] Bushey, M. L.; Nguyen, T.-Q.; Zhang, W.; Horoszewski, D.; Nuckolls, C. *Angew. Chem. Int. Ed.* **2004**, *43*, 5446.
- [4] For review, see: a) Hoheisel, T. N.; Schrettl, S.; Szilluweit, R.; Frauenrath, H. *Angew. Chem. Int. Ed.* **2010**, *49*, 6496. b) Rondeau-Gagné, S.; Morin, J.-F. *Chem. Soc. Rev.* **2014**, *43*, 85. c) Morin, J.-F. *Synlett* **2013**, 2032. d) Chernick, E. T.; Tykwinski, R. R. *J. Phys. Org. Chem.* **2013**, *26*, 742.
- [5] a) Wegner, G. *Natureforsch. B: Chem. Sci.* **1969**, *24*, 824. b) Wegner, G. *Makromol. Chem.* **1972**, *154*, 35.
- [6] a) Coates, G. W.; Dunn, A. R.; Henling, L. M.; Dougherty, D. A.; Grubbs, R. H. *Angew. Chem. Int. Ed.* **1997**, *36*, 248. b) Aokl, K.; Kudo, M.; Tamaoki, N. *Org. Lett.* **2004**, *6*, 4009. c) Nagasawa, J.; Kudo, M.; Hayashi, S.; Tamaoki, N. *Langmuir* **2004**, *20*, 7907. d) Fowler, F. W.; Lauher, J. W. In *Carbon-Rich Compounds*; Haley, M. M.; Tykwinski, R. R., Wiley-Vch Verlag GmbH & Co: Weinheim, **2006**. e) Dautel, O. J.; Robitzer, M.; Lere-Porte, J.-P.; Serein-Spirau, F.; Moreau, J. J. E. *J. Am. Chem. Soc.* **2006**, *128*, 16213. f) Néabo, J. R.; Tohondjona, K. I. S.; Morin, J.-F. *Org. Lett.* **2011**, *13*, 1358. g) Yarimaga, O.; Jaworski, J.; Yoon, B.; Kim, J.-M. *Chem. Commun.* **2012**, *48*, 2469.

- [7] a) Shirakawa, M.; Fujita, N.; Shinkai, S. *J. Am. Chem. Soc.* **2005**, *127*, 4164. b) Yip, H.-L.; Zou, J.; Ma, H.; Tian, Y.; Tucker, N. M.; Jen, A. K.-Y. *J. Am. Chem. Soc.* **2006**, *128*, 13042. c) Néabo, J. R.; Rondeau-Gagné, S.; Vigier-Carrière, C.; Morin, J.-F. *Langmuir* **2013**, *29*, 3446.
- [8] a) Ding, L.; Olesik, S. V. *Chem. Mater.* **2005**, *17*, 2353. b) Ding, L.; Olesik, S. V. *Nano Lett.* **2004**, *4*, 2271. c) Néabo, J. R.; Vigier-Carrière, C.; Rondeau-Gagné, S.; Morin, J.-F. *Chem. Commun.* **2012**, *48*, 10144. d) Szilluweit, R.; Hoheisel, T. N.; Fritzsche, M.; Ketterer, B.; Morral, A. F.; Demurtas, D.; Laporte, V.; Verel, R.; Bolisetty, S.; Mezzenga, R.; Frauenrath, H. *Nano Lett.* **2012**, *12*, 2573.
- [9] a) Xu, Y.; Smith, M. D.; Geer, M. F.; Pellechia, P. J.; Brown, J. C.; Wibowo, A. C.; Shimizu, L. S. *J. Am. Chem. Soc.* **2010**, *132*, 5334. b) Hsu, T. J.; Fowler, F. W.; Lauher, L. W. *J. Am. Chem. Soc.* **2012**, *134*, 142. c) Rondeau-Gagné, S.; Néabo, J. R.; Desroches, M.; Levesque, I.; Daigle, M.; Cantin, K.; Morin, J.-F. *Chem. Commun.* **2013**, *49*, 9546. d) Rondeau-Gagné, S.; Néabo, J. R.; Desroches, M.; Larouche, J.; Brisson, J.; Morin, J.-F. *J. Am. Chem. Soc.* **2013**, *135*, 110.
- [10] Levesque, I.; Néabo, J. R.; Rondeau-Gagné, S.; Daigle, M.; Vigier-Carrière, C.; Morin, J.-F. *Chem. Sci.* **2014**, *5*, 831.
- [11] a) Tobe, Y.; Nagano, A.; Kawabata, K.; Sonoda, M.; Naemura, K. *Org. Lett.* **2000**, *2*, 3265. b) Tobe, Y.; Utsumi, N.; Kawabata, K.; Nagano, A.; Adachi, K.; Araki, S.; Sonoda, M.; Hirose, K.; Naemura, K. *J. Am. Chem. Soc.* **2002**, *124*, 5350. c) Zhao, T.; Liu, Z.; Song, Y.; Xu, W.; Zhang, D.; Zhu, D. *J. Org. Chem.* **2006**, *71*, 7422. d) Zhang, L.; Che, Y.; Moore, J. S. *Acc. Chem. Res.* **2008**, *41*, 1596. e) Ide,

- T.; Takeuchi, D.; Osakada, K. *Chem. Commun.* **2012**, *48*, 278. f) Rondeau-Gagné, S.; Néabo, J. R.; Desroches, M.; Cantin, K.; Soldera, A.; Morin, J.-F. *J. Mater. Chem. C* **2013**, *1*, 2680.
- [12] Cantin, K.; Rondeau-Gagné, S.; Néabo, J. R.; Daigle, M.; Morin, J.-F. *Org. Biomol. Chem.* **2011**, *9*, 4440.
- [13] a) Vollmeyer, J.; Jester, S. S.; Eberhagen, F.; Prangenberg, T.; Mader, W.; Höger, S. *Chem. Commun.* **2012**, *48*, 6547. b) Li, J.; Zhou, W.; Yang, J.; Lang, X.; Huang, P. *Colloid Interface Sci.* **2013**, *395*, 99.
- [14] a) Zang, W.; Moore, J. S. *Angew. Chem. Int. Ed.* **2006**, *45*, 4416. b) Zhao, D.; Moore, J. S. *Chem. Comm.* **2003**, 807. c) Siemsen, P.; Livingston, R. C.; Diederich, F. *Angew. Chem. Int. Ed.* **2000**, *39*, 2632. d) Höger, S. *Chem. Eur. J.* **2004**, *10*, 1320. e) Kaushik, B.; Datar, A.; Zhang, W.; Yang, X.; Naddo, T.; Huang, J.; Zuo, J.; Yen, M.; Moore, J. S.; Zang, L. *J. Am. Chem. Soc.* **2006**, *128*, 6576. f) Finke, A. D.; Gross, D. E.; Han, A.; Moore, J. S. *J. Am. Chem. Soc.* **2011**, *133*, 14063. g) Shigemitsu, H.; Hisaki, I.; Kometani, E.; Yasumiya, D.; Sakamoto, Y.; Osaka, K.; Takur, T. S.; Saeki, A.; Seki, S.; Kimura, F.; Kimura, T.; Tohnai, N.; Miyata, M. *Chem. Eur. J.* **2013**, *19*, 15366.
- [15] a) Yu, G.; Yan, X.; Han, C.; Huang, F. *Chem. Soc. Rev.* **2013**, *42*, 6697-6722. b) Babu, S. S.; Praveen, V. K.; Ajayaghosh, A. *Chem. Rev.* **2014**, *114*, 1973- 2129.
- [16] Schott, M. *J. Phys. Chem. B* **2006**, *110*, 15864-15868.

Conclusion et perspectives

Dans le cadre des travaux présentés dans cette thèse, les objectifs initiaux ont pu être atteints. L'obtention de nanotubes rigides et covalents à partir de la réaction topochemique de polymérisation des unités diynes a pu être réalisée. Premièrement, la synthèse de monomères macrocycliques de type phénylacétylène a été effectuée par synthèse organique. Lors de cette synthèse, plusieurs dérivés ont été obtenus afin de faire varier les différents substituants périphériques influençant directement les propriétés d'auto-assemblage supramoléculaire et, par le fait même, la réactivité des monomères vis-à-vis de la photopolymérisation. Premièrement, la configuration des fonctions amides a été modifiée. En faisant varier ce paramètre, il a été possible de conclure que la configuration benzamine défavorisait l'auto-assemblage et empêchait la formation de polydiacétylènes. La configuration acétinilide est donc requise afin de favoriser les liaisons hydrogène favorisant l'auto-assemblage des macrocycles de manière optimale. Par la suite, l'incorporation d'unités diynes externes au squelette macrocyclique a été réalisée. En incorporant ces groupements diynes beaucoup plus flexibles, il a été possible d'obtenir nos premiers polydiacétylènes par photopolymérisation à l'état gel. Suite à l'obtention de ces polymères, une caractérisation complète fut effectuée. Par microscopie électronique à transmission (TEM), la présence de nanotubes de longueur et diamètre de quelques nanomètres fut confirmée, montrant l'efficacité de notre approche «hybride» pour l'obtention de nanomatériaux bien définis.

Suite à l'obtention de ces nanotubes organiques rigides de polydiacétylènes, nous avons entrepris leur modification en variant le design des monomères. Premièrement, l'augmentation de la taille des nanotubes fut entreprise par l'utilisation de macrocycles analogues aux PAMs mais possédant une cavité interne plus grande. Ainsi, la synthèse de macrocycles PBMs fut réalisée en conservant les substituants des PAMs synthétisés précédemment. Suite à l'auto-assemblage des nouveaux précurseurs à l'état gel, la polymérisation topochemique fut réalisée par irradiation au rayonnement UV. La formation de polydiacétylènes fut constatée, confirmant la réactivité des nouveaux macrocycles. Suite à une caractérisation complète par diverses méthodes spectroscopiques et microscopiques,

il a été possible de conclure à l'obtention de nanotubes organiques de polydiacétylènes possédant une cavité interne mieux définie et plus large que lors de l'utilisation de PAMs. Ce résultat démontre donc la polyvalence de notre approche et ouvre la porte au contrôle précis de la structure des nano-architectures finales.

Étant donné la nécessité d'obtenir des quantités appréciables de produits lorsque des applications sont visées, l'augmentation du rendement de polymérisation se devait d'être effectuée afin d'augmenter les quantités finales de nanotubes organiques. Il est important, cependant, de mentionner que l'approche à l'état gel permettait dès le départ, l'obtention de quantités plus importantes que par l'approche à l'état cristallin. Afin d'augmenter l'efficacité de la polymérisation topochemique des diynes, l'incorporation de chaînes périphériques polaires fut effectuée. Lors de travaux précédents, l'incorporation de ces substituants a démontré une augmentation de l'efficacité de la réticulation. De plus, la chimie bien connue des macrocycles a permis d'effectuer cet ajout au squelette macrocyclique sans grande difficulté. Ainsi, il fut possible d'incorporer dans le macrocycle, une chaîne périphérique polaire de type hydroxyethoxy. Par l'incorporation de ce groupement, la création de nouveaux sites de liaisons hydrogène et d'interactions électrostatiques devient possible, ce qui contribue à une modification du réseau supramoléculaire et, par le fait même, influe directement sur la réactivité des unités diynes internes aux macrocycles PAMs. À la suite de l'obtention des nouveaux PAMs, la photopolymérisation des macrocycles fut réalisée. Après caractérisation, l'augmentation du rendement de polymérisation fut constatée, démontrant l'efficacité des chaînes polaires pour l'augmentation des rendements de polymérisation.

Finalement, le dernier objectif du projet était de procéder à la pyrolyse des nanotubes afin d'effectuer un pas de plus vers l'obtention de nano-architectures entièrement faites de carbone. Ainsi, la pyrolyse des nanotubes fut effectuée à 500°C sous vide. Une série de caractérisation fut effectuée par la suite afin de prouver le changement de nature chimique ainsi que la rétention de configuration. Malgré la présence de matériaux graphitiques, confirmée par spectroscopie Raman, il n'a pas été possible de confirmer la rétention de la configuration tubulaire initiale. Les matériaux finaux sont insolubles dans les solvants organiques usuels ce qui complique de beaucoup leur caractérisation et rend difficile

l'observation des entités nanométriques de façon isolée par TEM. Néanmoins, le changement de nature chimique des nanotubes organiques est un résultat laissant croire à la viabilité de cette approche pour l'obtention de nanotubes de carbone de manière contrôlée.

À la lumière des résultats obtenus lors de ce projet, il est possible de conclure que les objectifs ambitieux fixés au départ de la recherche furent réalisés, même dépassés. De façon globale, notre approche, nommée approche «hybride», amène une nouvelle manière de concevoir et d'obtenir des nanomatériaux riches en carbone de façon bien contrôlée et bien définie. Comme il a été démontré précédemment dans cet ouvrage, les approches «traditionnelles» physiques et chimiques, ou ascendantes et descendantes permettent l'obtention des nanomatériaux bien définis. Cependant, les méthodes sont parfois longues et hasardeuses, permettant difficilement d'obtenir les nanomatériaux avec de bonnes puretés et en grande quantité. L'approche hybride, nécessitant moins d'étapes de synthèse et permettant l'obtention directe de nano-architecture sans réactions chimiques complexes, devient donc une alternative intéressante. Malgré les bases de cette approche, principalement mis en place par notre groupe de recherche, plusieurs phénomènes restent à expliquer et plusieurs nouveaux monomères pourraient être développés.

Premièrement, il est clair que la pyrolyse des nanotubes obtenus par polymérisation topo-chimique se doit d'être poursuivie. L'obtention de ces matériaux entièrement faits de carbone représenterait une avancée claire dans le domaine et pourrait ouvrir la porte aux nanotubes à plusieurs applications. Afin de favoriser la réaction de cycloaromatisation, il serait intéressant de procéder à une pyrolyse plus douce. Pour ce faire, la mise en solution des PDAs dans des solvants à haut point d'ébullition suivie d'un chauffage pourrait être une avenue intéressante. L'exposition à des températures plus basses (vers 150°C) pourrait également être effectuée sur de longues périodes suivit d'une purification méticuleuse afin d'enlever tous les nanotubes de polydiacétylènes non réagi. Étant donné que le problème majeur de notre étude fut la faible solubilité des architectures finales, ne permettant l'isolation par microscopie électronique, il serait intéressant d'utiliser la chimie des nanotubes de carbone. En effet, l'utilisation de surfactants utilisés dans la chimie des nanotubes de carbone serait une manière intéressante d'isoler les nanotubes pyrolysés finaux. Pour ce faire, l'utilisation de dérivés éthylèneglycol, par exemple, pourrait

permettre de briser les agglomérats et ainsi permettre la visualisation des architectures seules. Cependant, il est possible que de tels surfactants rendent la détermination des longueurs et diamètres finaux difficile. Le choix du bon surfactant sera donc primordial. L'utilisation de catalyseurs à base de métaux pourrait également être envisagée afin de favoriser la pyrolyse et la cycloaromatisation des nanotubes à base de PDA.

Lors de travaux antérieurs réalisés dans le groupe, il a été démontré la possibilité d'utiliser les polydiacétylènes pour l'obtention de matériaux entièrement graphitiques. Cependant, les mécanismes précis de la cycloaromatisation des polydiacétylènes demeurent inconnus et très peu présentés dans la littérature. Il est donc primordial de découvrir les mécanismes de cette réaction afin de pouvoir contrôler les paramètres réactionnels, déterminer les paramètres optimaux et obtenir les rendements de cycloaromatisation les plus élevés. Pour ce faire, l'étude de cycloaromatisation de molécules modèles, basées sur les motifs de base présents dans les polydiacétylènes, sera effectuée. Ces motifs de base sont le motif ène-yne-ène et yne-ène-yne, tels que représentés à la figure 7.1.

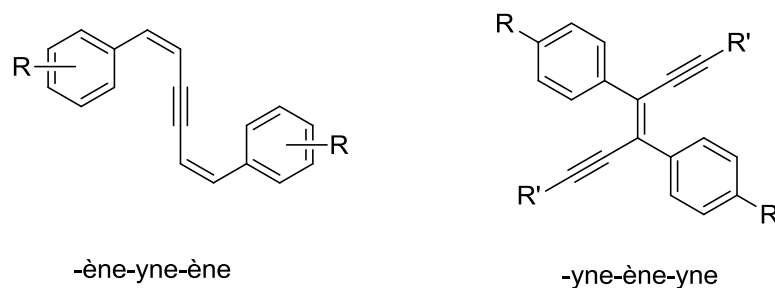


Figure 7.1. Molécules modèles inspirées des motifs de base d'un polydiacétylène pour étude de cycloaromatisation.

Grâce à ces molécules modèles, obtenues plus rapidement que les polydiacétylènes et permettant une caractérisation plus précise, il sera possible de déterminer exactement les structures finales après cycloaromatisation des polymères, et par le fait même, permettra de déterminer les paramètres optimaux pour cette réaction. Plusieurs conditions pourront être utilisées pour la cycloaromatisation. Premièrement, l'utilisation de différents catalyseurs comme le fer, l'or, le palladium ou le platine pourra être testée. Par la suite, il sera possible

d'utiliser différentes sources de lumière telles que la lumière UV-A, UV-B, la lumière blanche (avec *para*-benzoquinone) ou la lumière blanche (avec iode et oxyde de propylène). Suite à l'utilisation de ces conditions, il sera possible de vérifier la cycloaromatisation pour obtenir du chrysène ou du fulvalène. Cela constituera donc un énorme pas de franchi dans la compréhension de la réactivité de nos nouvelles architectures de polydiacétylène et pourra permettre l'obtention de nano-architectures entièrement constituées de carbone.

Finalement, une avancée majeure aux travaux présentés dans cette thèse pourra être effectué en utilisant des précurseurs moléculaires bien définis contenant des unités polyynes. En effet, comme il a été présenté pour les macrocycles de type PBMs, l'incorporation de polyynes au sein des monomères permet l'obtention de nouvelles architectures aux structures différentes et aux réactivités modifiées par rapport aux monomères contenant des unités diacétylènes. Cette approche a d'ailleurs déjà été utilisée lors de travaux antérieurs sur un monomère linéaire contenant une unité tétrayne. Lorsque le monomère a été soumis au rayonnement UV, la polymérisation topochemique de l'unité tétrayne a été constatée. Cependant, lorsque l'irradiation est prolongée, on assiste à la disparition du polydiacétylène pour former un tout nouveau matériau. Après des études plus poussées, la formation de nanoparticules de carbone a été observée, démontrant ainsi la réactivité particulière de l'unité tétrayne vis-à-vis de la polymérisation topochemique (voir figure 7.2). Inspiré par ce résultat, il sera intéressant d'incorporer une unité oligoyne au centre de macrocycles de type phénylène arylène afin d'étudier leur réactivité. Malgré le fait que la formation de nanoparticule ne sera pas favorisée, il sera intéressant de voir la réactivité de ces unités vis-à-vis de la polymérisation topochemique lorsqu'elles sont incorporées dans des monomères rigides. De plus, cette approche pourrait permettre un contrôle accru sur les diamètres et sur la rigidité des nanotubes formés.

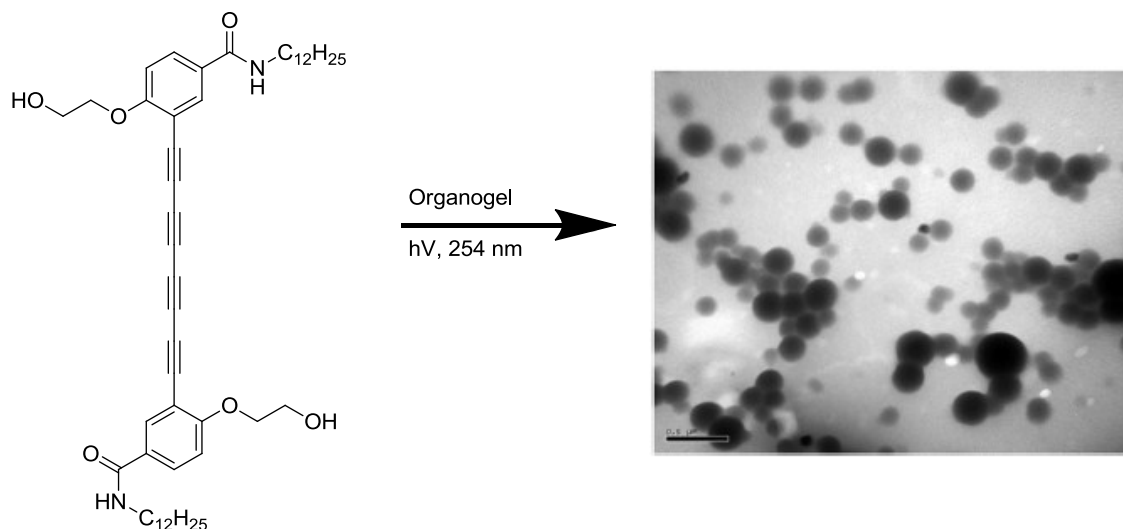


Figure 7.2. Photopolymérisation d'un précurseur tétrayne pour l'obtention de nanoparticules de carbone.

De façon plus globale, il est possible de tirer des conclusions plus générales suite à ce projet de recherche. Il est juste d'affirmer que les nouvelles nano-architectures obtenues représentent les premières vraies percées de l'approche hybride par la formation de polydiacétylène au sein de la science des matériaux modernes. Même si, présentement, l'utilité en sciences des matériaux reste inexistante, l'approche générale développée dans cette thèse constitue un pas majeur vers le contrôle des nanomatériaux à l'échelle moléculaire. Notre approche constitue donc un pas de plus vers l'élaboration de structures complexes par le contrôle moléculaire. Par l'obtention d'un tel contrôle, il sera possible d'obtenir les nano-architectures désirées simplement par design moléculaire, ouvrant la porte à l'obtention, par exemple, de système senseur ultra performant en passant par les transistors moléculaires.

D'un point de vue grande échelle, notre approche est encore loin de se distinguer. Les méthodes physiques pour la création de nanomatériaux riches en carbones utiles en électronique, en environnement, en biotechnologie et en stockage d'énergie restent les méthodes les plus efficaces. Ces méthodes, malgré un contrôle limité des nanostructures finales, permettent l'élaboration de nouveaux dispositifs performants et l'obtention de grandes quantités de produits. Comparativement à ces méthodes, l'approche hybride vers

les nanotubes, développés dans ce projet de recherche, ne permet pas encore l'obtention de grandes quantités de produits. La formation de gel, quoi qu'efficace, ne permet pas une polymérisation à haut rendement, facteur très important à optimiser pour une viabilité à long terme de l'approche hybride en synthèse de nanomatériaux. Pour régler ce problème, il faudra à coup sûr se concentrer sur les paramètres de gélification et optimiser chacun de ceux-ci, ce qui constitue un travail colossal. Par la suite, l'élaboration de nouveaux systèmes d'irradiation et de photoréaction se devra d'être effectuée. Il est important également de mentionner que la structure finale des matériaux après graphitisation reste encore à élucider, ce qui constitue, pour le moment, un frein à l'utilisation plus fréquente de l'approche hybride vers les matériaux riches en carbone.

Finalement, l'approche hybride utilisée dans ces travaux vers l'obtention de nouveaux nanotubes organiques a permis de remettre à l'avant-plan différents concepts et molécules au sein de la science des matériaux. Le meilleur exemple est les macrocycles utilisés (PAMs). Ces macrocycles étaient de moins en moins utilisés étant donné les nombreuses tentatives infructueuses de polymérisation et de synthèse de structures complexes. Nos travaux ont donc permis de donner une nouvelle vie à ces macrocycles. Les travaux présentés ici ont également servi à positionner notre laboratoire à l'avant-plan de la recherche mondiale dans ce domaine. L'approche hybride suscitera, sans aucun doute, de plus en plus d'intérêt et de questionnement au sein de la communauté mondiale ce qui contribuera à son développement futur et au progrès de la science des matériaux moléculaires.